ABSTRACT

Title of Dissertation:	PHOTOINDUCED ELECTRON TRANSFER FOR PROTECTING GROUPS AND POLYMER SYNTHESIS
	Matthew David Thum, Doctor of Philosophy, 2019
Dissertation directed by:	Professor Daniel E. Falvey Department of Chemistry and Biochemistry

Using light to drive chemical reactions affords spatial and temporal control not typically displayed in thermal chemistry. For this reason, light induced transformations have been used in the manufacturing of polymers and plastics, and in the development of systems that require precise activation, such as drug delivery. The work presented in this dissertation will involve photoinduced electron transfer (PET) and its applications in protecting groups and polymer synthesis.

Chapter 1 will discuss photoinduced electron transfer and its theory. Examples will be provided to demonstrate how it has been used as a trigger in photoremovable protecting groups, and as the mechanism of initiation in controlled radical polymerization. In Chapter 2, three different protecting groups triggered by PET will be analyzed. The analysis of key intermediates involved in the mechanism will be performed using nanosecond transient absorption spectroscopy. Chapter 3 will

discuss the adaptation of an *N*-alkyl picoloinum protecting group to be activated by stepwise absorption of two photons of visible light.

Chapter 4 will explore the photophysical properties of commonly used chain transfer agents for controlled radical polymerization. The behavior of the chain transfer agents under ultra violet and visible light photolysis, electron transfer, and energy transfer will be examined. Chapter 5 will discuss the role of the oxidation of dimethyl sulfoxide (DMSO) in the initiation of polymerization using photoredox catalysts. Our work demonstrates that, under highly oxidative conditions, an electron can be abstracted from DMSO and the resulting DMSO cation radical can degrade to for radicals capable of initiating polymerization. We explore this process for an anthraquinone-base photoredox catalyst, and apply it, along with a chain transfer agent, to the manufacturing of polymers with precise molecular weights and narrow molecular weight distributions

PHOTOINDUCED ELECTRON TRANSFER FOR PROTECTING GROUPS AND POLYMER SYTHESIS

by

Matthew David Thum

Dissertation submitted to the Faculty of the Graduate School of the
University of Maryland, College Park, in partial fulfillment
of the requirements for the degree of
Doctor of Philosophy
2019

Advisory Committee:
Professor Daniel Falvey, Chair
Professor Osvaldo Gutierrez
Professor John Fourkas
Professor Andrei Vedernikov
Professor Peter Kofinas

Dedication

This dissertation is dedicated to my grandparents.

To my grandfather, Robert Paneque: Your curiosity was infectious. I hope that I carry some of the love of life, and dedication to family, that you displayed every day. You are an example of what it means to love.

To my grandmother, Helen Paneque: You are a model of hard-work and dedication. I would not have had the strength to finish this journey if it were not for your presence in my life.

To my grandfather, Richard Thum: You have shown me that challenges are a part of life, but in the midst of the struggle, there is always time to appreciate the good fortune with which you have been blessed. I will always appreciate the small beauties in life.

To my grandmother, Cornelia Thum: The strength you display everyday is incredible. I hope that I can tap into the immeasurably deep well of dedication and love that you seem to draw from effortlessly.

You all deserve statues. However, this dissertation is on chemistry and not sculpting, so somehow I hope this small dedication will serve to remind you of how impacted I have been by our relationship. Thank you and I love you always.

Acknowledgements

My experience in the graduate program has been incredible. I have been overwhelmed by the show of support that I have received from the faculty and staff. Specifically, I would like to thank Dr. Falvey for instilling in me a sense of confidence that I will carry for the rest of my life. Research is a grind. With time, the constant failure and looming sense of dread become as familiar to graduate students as breathing. Dr. Falvey is a builder. When the day was darkest, and the NMR the messiest, he would find the sense of positivity to remind me that there is no time wasted in the lab, only learning and, hopefully at the end, a humble sense of accomplishment.

I am grateful to the current and former colleagues in the graduate school. The former members of the Falvey Group: Dr. Derek Denning and Dr. Steven Wolf both trained me, and put up with all of my stupid questions. Steven especially for listening to my daily “hot takes” about Carmelo Anthony being fat. Andrea Zeppuhar and Donald Hong for their collaborations and all of their feedback on ideas and presentations. Nipun Kottage for making me realize how fulfilling a mentorship can become. Nipun would’ve been incredible with or without me, but having the opportunity to work with him was a mentorship experience I will chase for the rest of my career.

A final thank you to my committee. Dr. Fourkas, Dr. Vedernikov, Dr. Gutierrez, and Dr. Kofinas. Although not on my committee, I would like to recognize Dr. Lyle Isaacs for believing in me enough to invite me to an on-campus interview that would lead to my becoming a graduate student and changing my life forever.

The faculty at the analytical services have been incredibly supportive. Dr. Fu Chen, and Dr. Yinde Wang, have worked tirelessly in the NMR facility to train me and keep the instruments in great condition. Thank you as well to Dr. Yue Li for running samples and training me on the various Mass Spec instruments.

To all my friends inside and outside of the department thank you for your support, and more importantly, for your distractions. Paul Toro, Adam Mahmoud, Gabe Sawhney, Leila Duman, Sam Nowak, Wes Lee, Teodora Kljaic, and many many more.

To my family. Your support made this experience possible. The example provided by my parents, Linda Paneque and Scott Thum, has made me a better brother, husband, friend, and scientist. The support and love from my brother, Douglas Thum, and my sister, Morgan Casher, made living away from home a little less isolating. I would like to thank my extended family for being legitimately interested in my graduate research despite the fact that it's mostly organic chemistry. I would also like to acknowledge my dog, Winston. He may not understand much chemistry, but he has heard me practice presentations so much he probably deserves a Bachelor's degree.

Rebecca, every word in this document was written for you. I would not be here if it were not for your never-ending support. This is a reality that you manifest, and that you have nurtured since the very beginning. You are the most incredible wife, and my best friend. Our future is bright because of the light that you bring into our lives.

Table of Contents

List of Tables

List of Figures

Chapter 1. Photoinduced Electron Transfer for Polymers and Protecting Groups

Chapter 2: Transient Absorption Spectroscopy for PRPGS

Chapter 5: RAFT Polymerization through Photocatalytic Oxidation of DMSO

Chapter 6. Supplemental Information

Chapter 1: Photoinduced Electron Transfer for Polymers and Protecting Groups

1.1 Photochemistry

Photochemistry is the reaction of a molecule initiated by the absorption of light. A major part of modern organic chemistry, photochemistry is being continually adapted with new methods developed constantly. The ability to control the rate and reaction area of a photochemical process by modulating the intensity and area of illumination is an aspect of it not found in traditional thermal reactions. Additionally, photochemistry enables for the detection of reactive intermediates, using techniques such as transient absorption spectroscopy which is paramount in the elucidation of reaction mechanisms. The goal of this chapter is to examine one important aspect of photochemistry, photoinduced electron transfer (PET), and its applications in synthetic and polymer chemistry.

Upon absorption of a photon, there is the promotion of an electron to an excited-state and there are multiple pathways available to the remediate the excess energy. Many of the pathways available are illustrated in the Jablonski diagram below. During a vertical excitation, spin is conserved and the molecule is promoted to a higher excited-state (S_n). Vibrational cooling to the lowest excited-state (usually S_1) happens on the picosecond (10^{-12} sec, ps) timescale. Once in its lowest excited-state, the excess energy can de dissipated in numerous ways. Non-radiative decay back to the ground-state involving the production of heat by dissipation of energy to the solvent competes with other photochemical processes such as fluorescence, which is

emission of a photon, and occurs on a 10^{-9} sec timescale. Alternatively, the electron can undergo a spin flip and intersystem cross (ISC) to the triplet manifold which occurs on a 10^{-9} sec timescale. Finally, the molecule can relax back to the ground-state through a radiative phosphorescence process which takes place on a $10^{-4} – 10^{-1}$ sec timescale. The majority of the chemistry that we observe happens from the lowest excited-state due to the extremely short lifetime of higher excited-states. Some reactions that take place from excited-states include, but are not limited to, energy transfer, hydrogen atom transfer (HAT), electron transfer (PET), and bond breaking. The focus of this chapter will be on the advances and applications of photoredox catalysts as they relate to PET and HAT.

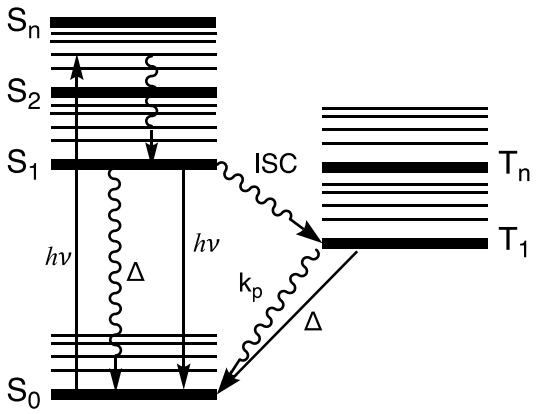

Figure 1.1. Jablonski diagram.

1.2 Photoinduced Electron Transfer

There are multiple approaches towards designing a system that involves PET as shown in Figure 1.2. The first involves the excitation of the donor (Figure 1.2, D*) resulting in PET to the ground-state acceptor while the second involves excitation of

the acceptor (Figure 1.2, A*) to initiate PET from the ground-state donor.

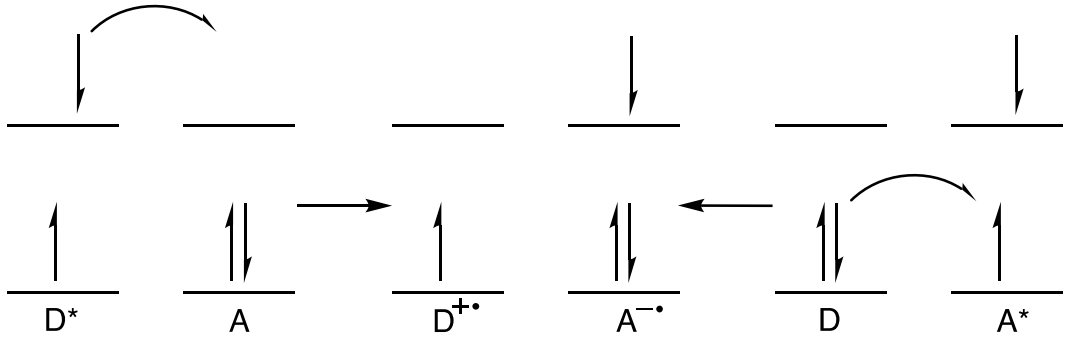

Figure 1.2. *left*: Electron transfer from an excited-state donor (D*) to a ground-state acceptor (A). *right*: Electron transfer from a ground-state donor (D) to an excited-state acceptor (A*). Both reaction pathways result in the formation of the corresponding donor cation radical ($D^{+\bullet}$) and the accepting anion radical ($A^{-\bullet}$).

An example of using PET in synthesis is given in Figure 1.3. In this case, Pandey et al. used cyanoarene photocatalysts under aerobic conditions in the oxidation annulation of silyl enol ethers[1]. In their work, the excited-state photocatalyst (DCA*, Figure 1.3.) abstracts an electron from the silyl enol ether substrate to form the cyclized radical cation product and the anion radical of the cyanoarene. The ground-state photocatayst is recovered after reaction with singlet oxygen and, after loss of a trimethylsilyl cation radical and subsequent restoration of aromaticity, the ketone adduct of the substrate is formed. Further work by Pandey used the cyclization of a silyl enol ether in the total synthesis of (+)-2,7-Dideoxypancratistatin (Figure 1.4.)[2].

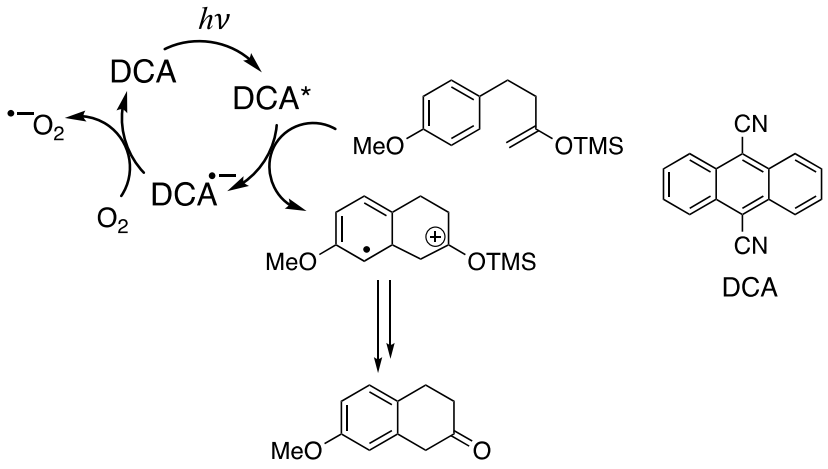

Figure 1.3. The cyclization of silyl enol ethers via oxidation using 9,10-dicyanoanthracene as the photocatalyst.

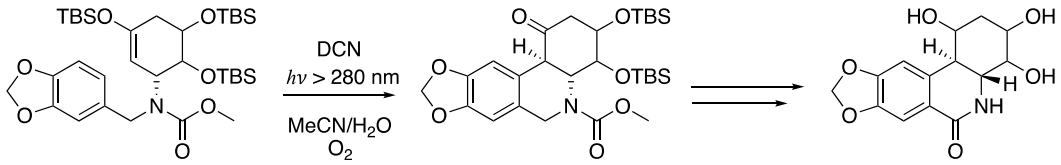

Figure 1.4. Total synthesis (+)-2,7-Dideoxypancratistatin using α-arylation of a silyl enol ether.

1.3 Mediated Electron Transfer

An alternative approach to direct PET is mediated electron transfer in which an excited-state mediator abstracts an electron from a ground-state donor and then transfers that electron to a ground-state acceptor. In a mediated electron transfer process, the mediator is recycled after electron transfer allowing for catalytic amounts of mediator to be used. Furthermore, the electron transfer happens in the ground-state which means that the excited-state life of the mediator has no effect on the efficiency of electron transfer. Additionally, when the excited-state electron transfer happens from a triplet state, the radical pair formed retains the original spin multiplicity thus

maximizing the amount of time the radical pair has to escape the solvent cage by limiting the efficiency of back electron transfer. In studies measuring the efficiency of electron transfer from 2,4,6-triphenylpyrilium to stilbene, the Tokumaru group estimated that electron transfer from the triplet state resulted in twice as many free ions in solution than the corresponding singlet state[3,4].

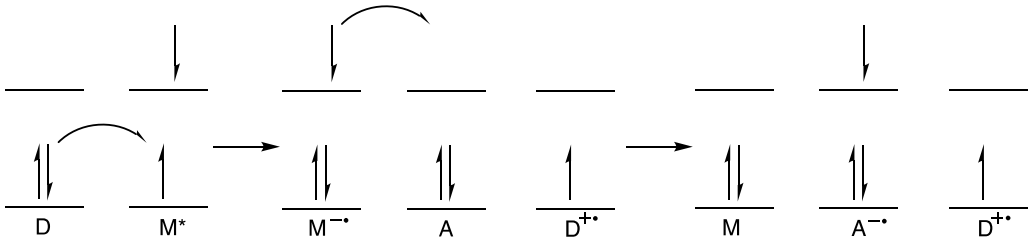

Figure 1.5. Electron transfer from a ground-state donor (D) to an excited-state mediator (M*). The newly formed anion radical (M–•) shuttles the electron to the acceptor (A) resulting in the reduced acceptor (A–•) and the recycled ground-state mediator.

An example of using mediated electron transfer is given in Figure 1.6. The Falvey group examined a series of N-alklypicolinum esters (NAP) which, when reduced, release a carboxylate anion[5–9]. Photolysis of an electron acceptor in the presence of a ground-state donor generates the anion radical of the acceptor and the cation radical of the donor. Provided that the donor is sufficiently reducing enough to transfer an electron to the NAP group (-1.1 V vs SCE), the photochemically generated anion radical of the acceptor will donate an electron to NAP group triggering release of carboxylate. An example using benzopheone as the mediator is given in Figure 1.6. The NAP group will be discussed more elaborately in chapter 3.

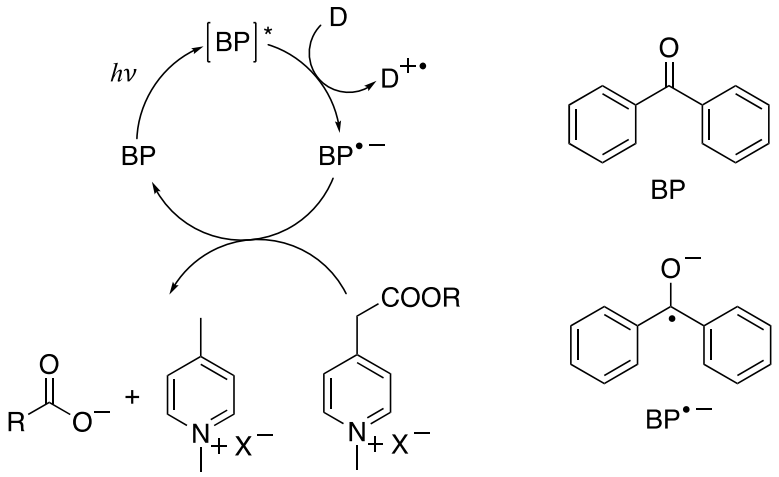

Figure 1.6. Mediated electron transfer from benzophenone (BP) to an *N*-alkylpiclinium ester (NAP) to release a carboxylate anion.

1.4 Marcus Theory and the Rhem Weller Relationship

Theoretical studies on electron transfer reactions were first examined in depth by Rudolph Marcus in the 1950's[10–12]. Marcus predicted a parabolic relationship between the free energy of the electron transfer process (ΔG_{ET}) and the and the free energy of the activation (ΔG^{**}) of the donor and acceptor (Figure 1.7.). This observation meant that as the reaction became more exergonic, the rate of the reaction should increase. However, the parabolic nature of the relationship lead to a region which came to be know as the Marcus "inverted region" which predicts that, at a certain point, making the reaction more exergonic actually decreases the overall rate of electron transfer.

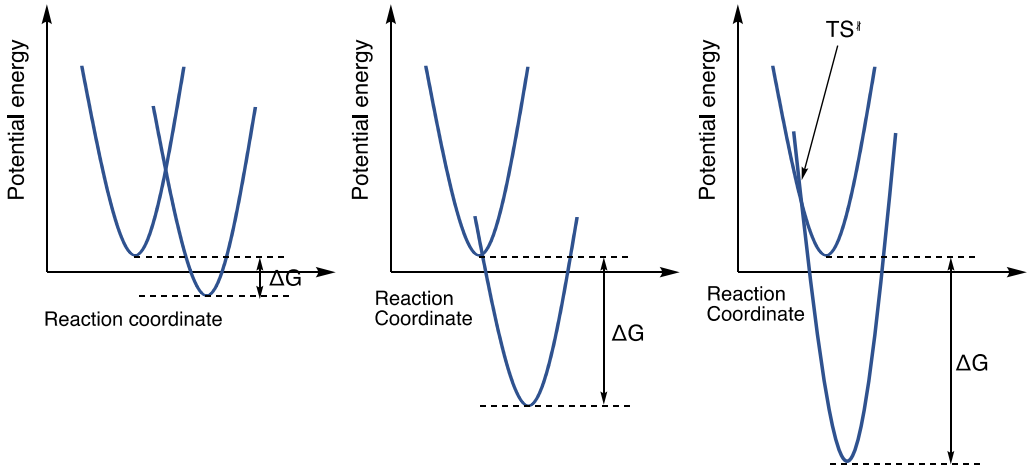

Figure 1.7. Illustration showing the return of a transition state as the exergonicity of the reaction is increased leading to the inverted region. *Left*: A reaction with a reaction barrier. *Middle*: A reaction with barrier to activation. *Right*: The reaction barrier returns when the reaction becomes more exergonic.

Much work was done to try to experimentally observe the inverted region, but attempts performed by Rehm and Weller showed that an increase in the exergonicity of the reaction led to an increase in rate, up to the diffusion limit, and Marcus' predictions could not be verified in a bimolecular system[13,14]. However, the work of Rehm and Weller in the study of the fluorescence quenching of various electron donors and acceptors led to the most important relationship in PET, as shown in equation 1.

[1] $$\Delta G_{ET} \approx 23.06 * (E_{ox}(D^{\bullet+}/D) - E_{red}(A/A^{\bullet-})) - E_{00} - \omega$$

The relationship described in Eq.1 relates the ground-state reduction potentials of the donor and acceptor (E_{ox} and E_{red}, in volts) along with the excited-state energy of the electron donor (E_{00}, in kcal/mol) as they influence the feasibility of the electron transfer process (ΔG_{ET}). Also included is a term that accounts for the influence of the

solvent (ω), but this is generally neglected in polar solvents such as alcohols or acetonitrile. This equation can easily be modified to incorporate the excited-state reduction, or oxidation, potential of the photoredox catalyst (Eq's 2 and 3)[15].

[2] $$\Delta G_{ET} \approx -23.06 * (E^*_{red}(cat^*/cat^{\bullet-}) - E_{ox}(sub^{\bullet+}/sub))$$

Where E^*_{red} refers to the excited-state reduction potential (either from a singlet or triplet), "cat" refers to the photocatalyst, and "sub" refers to the ground-state substrate.

[3] $$\Delta G_{ET} \approx -23.06 * (E_{red}(sub/sub^{\bullet-}) - E^*_{ox}(cat^{\bullet+}/cat^*))$$

Where E^*_{red} refers to the excited-state oxidation potential (either from a singlet or triplet). The excited-state redox potential can be calculated from Eq's 4 and 5. In the following equations (Eq. 4 and 5), the excited-state energy (E_{00}) is measured in Ev.

[4] $$E^*_{ox}(cat^{\bullet+}/cat^*) = E_{ox}(cat^{\bullet+}/cat) - E_{00}$$

[5] $$E^*_{red}(cat^*/cat^{\bullet-}) = E_{red}(cat/cat^{\bullet-}) - E_{00}$$

The first report experimentally observing the inverted region came when Miller et al. reported on the electron transfer rates measured in a linked donor-acceptor molecule (Figure 1.8.)[16,17]. They designed a system which involved measuring the electron transfer rate from a biphenyl electron donor to a chlorinated quinone as the acceptor with a rigid linker, 5α-androstane, between them. By keeping the distance between the donor and acceptor constant, the authors were able to measure the relationship between the driving force of the reaction and the rate of electron transfer. Much as Marcus predicted, as the reaction became more exergonic, the authors noted a marked decrease in the rate of electron transfer (Figure 1.8.).

Although previous attempts to observe the inverted region in unlinked systems failed due to the reactions being diffusion limited, the report by Miller et al. is seen as the first report that supports the existence of an inverted region. Thus, it is widely accepted that the inverted region is only observed in unimolecular electron transfer reactions, while bimolecular reactions are diffusion controlled.

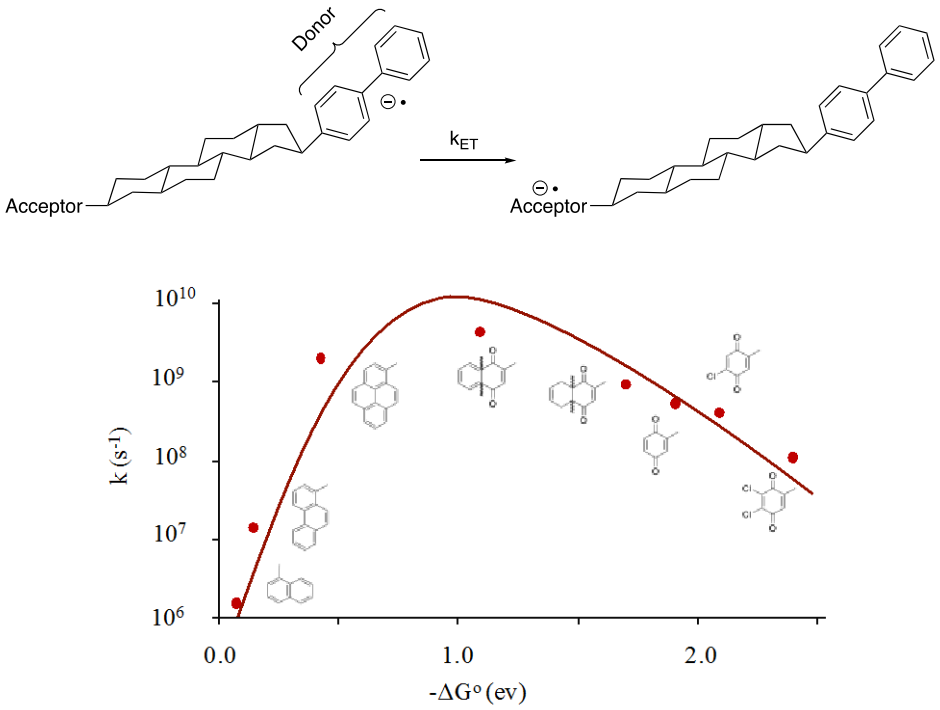

Figure 1.8. A visualization of the results demonstrating the presence of an inverted region[16,17].

1.5. Controlled "Living" Radical Polymerization - RAFT

The method of controlled radical polymerization (CRP) discussed here will specifically focus on one type of CRP, reversible activation fragmentation chain transfer polymerization (RAFT), and how it has been initiated using photoredox catalysts. Following this section, there will be specific examples of photocatalysts

that have been used to activate RAFT polymerization though a proposed PET mechanism. There are many other methods of controlled radical polymerization such as, atom transfer radical polymerization, organic atom transfer RAFT polymerization, iodine mediated polymerization, and others, which are effective methods of carrying out polymerization initiated by PET[18–22].

All methods of CRP work by limiting the concentration of propagating radicals so that all chains have the same opportunity for growth. The result is the synthesis of polymers with predictable molecular weights (MW), a narrow molecular weight distribution (as described in equation 6-8), and high end group fidelity. The three main measurements made in polymerization are the number averaged molecular weight (M_n, described in equation 7), the weight averaged molecular weight (M_w, described in equation 6), and the polydispersity (PDI, described in equation 8).

[6] $$M_w = \frac{\sum_i N_i M_i^2}{\sum_i N_i M_i}$$

Where N_i is the number of molecules of molecular weight, M_i. The weight averaged molecular weight has a larger contribution due to molecules of higher molecular mass than M_n (Eq. 7) which is strictly an just the average of all the molecular weights of all of the molecules.

[7] $$M_n = \frac{\sum_i N_i M_i}{\sum_i N_i}$$

[8] $$PDI = M_w / M_n$$

The PDI is a measure of the uniformness of the polymer chains. If all polymers grown are the same molecular weight, the PDI approaches unity, 1. Due to the fact that the contributions due to higher mass are greater in M_w than M_n, the

polydispersity will have a value greater than 1 in cases of nonuniform distribution. Normal ranges for "controlled" polymerization are between 1-1.3, with anything greater being deemed uncontrolled. Specifically, RAFT polymerization works by reversible deactivation of the growing chains through a chain transfer agent (CTA, Figure 1.10.)[23,24]. The mechanism of RAFT polymerization is given in Figure 1.10.

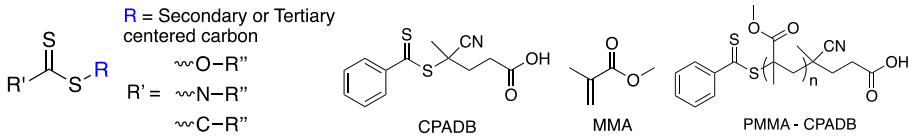

Figure 1.9. The molecular structure of a dithioester-based CTA. *Right*: Given the 4-cyanopentanic acid dithiobenzoate (CPADB) as the CTA, and methyl methacrylate (MMA) as the monomer, the resulting polymer would have the structure of PMMA-CPADB.

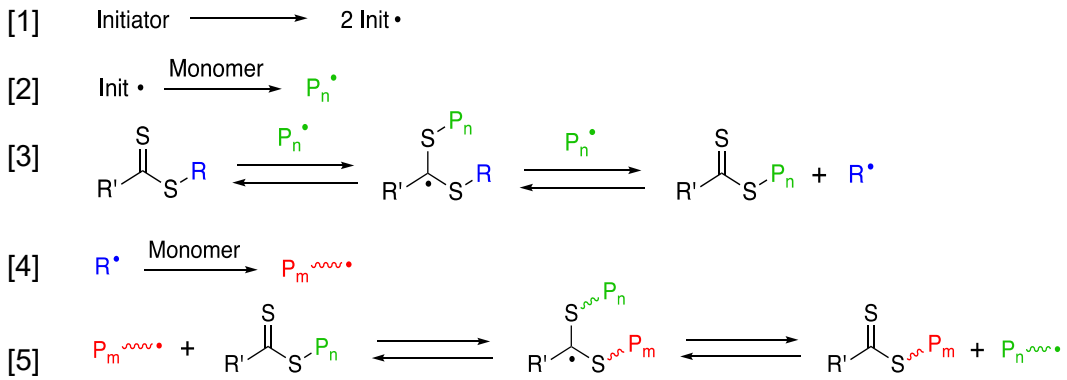

Figure 1.10. The mechanism of RAFT polymerization. [1] After initiation and polymer growth, [2], the growing chain ($P_n\bullet$), is deactivated by the CTA in step [3]. Once deactivated, the polymer chain and end group have an equal probability of elimination. Any end group eliminated will initiate chain growth as shown in step [4]. In step [5] the rapid pre-equilibrium is reached meaning that all chain growth events are being controlled by the CTA.

1.5. Photoinitiated RAFT Polymerization

There are multiple alternate methods of activating the CTA for RAFT polymerization. One method of initiating the polymerization process involving the direct photolysis of the CTA was first reported the Otsu group in 1982, however direct photolysis, known as a photoiniferter process, will be more thoroughly discussed in chapter 4[25–27]. Direct photolysis most commonly requires high energy, UV light, so, in an effort to develop visible light alternatives, Boyer, Hawker, and others developed PET-RAFT[25,28–30]. The first report of RAFT polymerization initiated by PET was reported in 2014[31]. The Boyer group developed a new method of polymerization using transition metal photocatalysts in the initiation of controlled radical polymerization (Figure 1.11). As shown in Figure 1.11, the excited-state of the photocatalyst was proposed to be involved in the activation of the CTA. The details of PET-RAFT initiated by transition metal photocatalysts will be discussed in section 1.3.

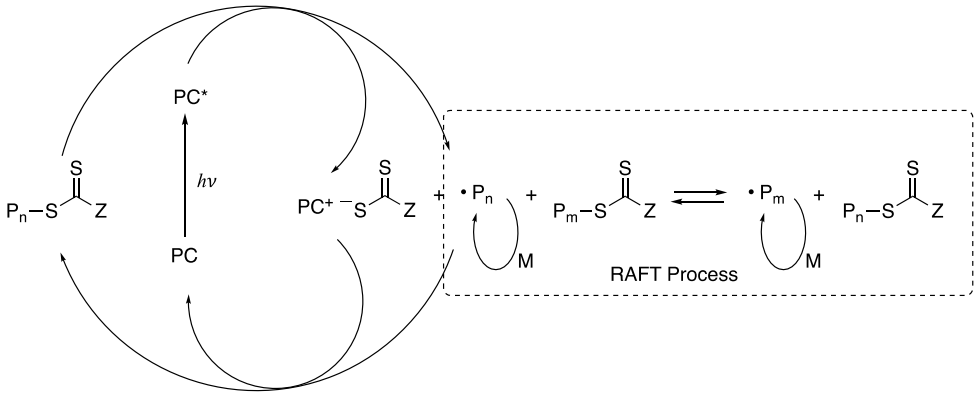

Figure 1.11. Activation of a CTA from PET from an excited-state photocatalyst.

One of the most interesting examples of PET RAFT was reported by the Boyer group involving the photolysis of chlorophyll a (ChI, Figure 1.12.) using red light (635 nm) as the photoredox catalyst[32]. Better known for its role in photosynthesis, ChI is a strong excited-state reducing agent (-1.1 V vs. SCE) capable of transferring an electron to the CTA (≈ - 0.9 V vs. SCE for dithioesters, and ≈ - 1 V vs SCE for trithioesters) for PET-RAFT. Upon photolysis with either blue (435 nm) or red (635 nm) light, they reported photo-controlled polymerization of multiple CTAs and various monomers with good control over the molecular weight were observed (table 1.1.).

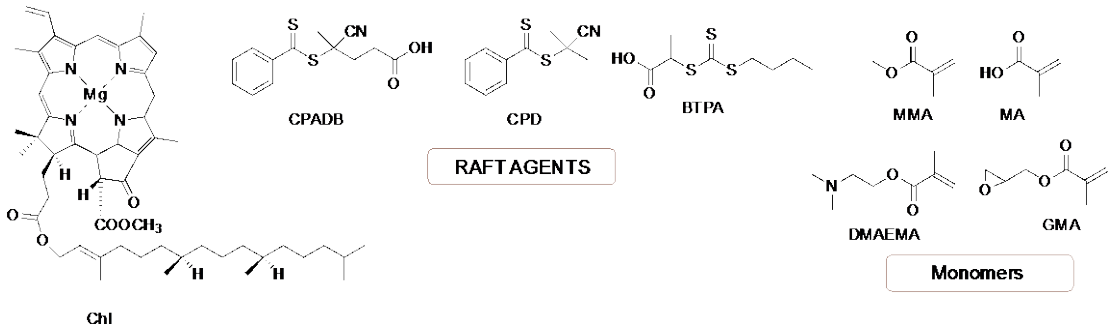

Figure 1.12. The structure of chlorophyll a (ChI). Selected CTAs and monomers used in the experiments.

Table 1.1 PET-RAFT with ChI as the photoredox catalyst under red (635 nm) light illumination

Entry	[M]:[CTA]:[ChI]	CTA	Monomer	Time, hr	Conv.	$M_{n,\,theo}$ (g/mol)	$M_{n,\,GPC}$ (g/mol)	PDI
1	200 : 0 : $8x10^{-4}$	-	MA	10	6	-	-	-
2	200 : 1 : 0	CPADB	DMAEMA	10	0	-	-	-
3	200 : 0 : $2x10^{-3}$	CPADB	MMA	25	94	19100	20420	1.16
4	200 : 0 : $8x10^{-4}$	CPD	MMA	12	33	12550	15550	1.27
5	200 : 0 : $8x10^{-4}$	BTPA	MA	8	53	9400	11500	1.07
6	200 : 0 : $8x10^{-4}$	CPADB	GMA	12	53	15330	16300	1.12
8	200 : 0 : $8x10^{-4}$	CPADB	DMAEMA	14	20	6300	9600	1.18

Selected results from the PET-RAFT polymerization using ChI are shown in Table 1.1. Under illumination with 635 nm, red LEDs, multiple methacrylate monomers formed polymers with narrow molecular weight distributions. In the absence of CTA (table 1.1, entry 1), or ChI (table 1.1, entry 2), no measurable conversion was measured. The theoretical molecular weight can be predicted using equation 9.

[8] $$M_{n,theo} = \frac{[M]_0}{[CTA]} * Mw_M * \alpha + Mw_{CTA}$$

Where $[M]_0$ is the initial concentration of the monomer, and α is the fractional conversion. The measurement of $M_{n,theo}$ assumes that all polymer chains are grown through a degenerative chain transfer mechanism resulting in each molecule having an end group. Therefore, the comparison between the measured and predicted molecular weights is a good measure of end group fidelity and living character. In the experiments performed by the Boyer group using ChI, as shown in table 1.1, there is good agreement between predicted and measured molecular weights meaning the end group was maintained throughout polymerization. This was the first report of polymerization being carried out with low-energy, red light.

In the following sections some common photoredox catalysts will be discussed as they relate to synthesis, and polymer chemistry. An example of each will be given and, in each case the proposed mechanism will involve PET from the photocatalyst as shown in one of the mechanisms previously described.

1.6 Transition Metal Based Photocatalysts

Some of the most common visible light absorbing photoredox catalysts are polypyridyl complexes of ruthenium and iridium, with the most notable being $Ru(bpy)_3^{2+}$ and *fac*-$Ir(ppy)_3$ (Figure 1.13). These compounds can absorb visible light, and their excited-states are long lived enough (up to 1 ms) to engage in electron transfer chemistry[15]. Although iridium based complexes have higher energy absorbance spectra, the tail often extends into the visible region of the spectrum, and their superior reducing properties make them popular choices for electron transfer chemistry. Although they are poor oxidants and reductants in the ground-state, the excited-state of these catalysts are effective single electron transfer reagents. Applications of transition metal based photocatalysts include the initiation of polymerization (to be discussed later in this chapter), organic synthesis, organic light emitting diodes, and photodynamic therapy[33,34].

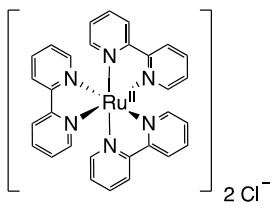

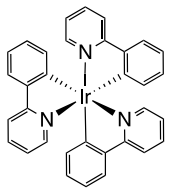

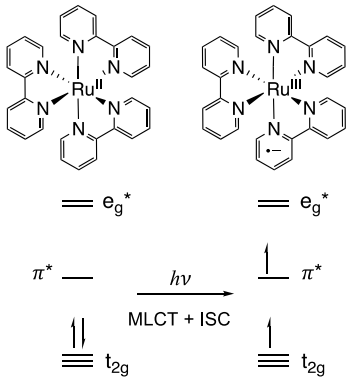

	$Ru(bpy)_3^{2+}$	*fac*-$Ir(ppy)_3$
$E_{1/2}(M^+/M^*)$	-0.81	-1.73
$E_{1/2}(M^*/M^-)$	+0.77	+0.31
λ_{max} (nm)	452	375
τ (ns)	1100	1900

Figure 1.13. *Left*: Photophysical properties of two common transition metal photocatalysts. *Right*: Photolysis of the metal to ligand charge transfer state (MLCT) leads to intersystem crossing and a long-lived triplet state. The oxidation state of the ruthenium metal center is +2 in the ground-state and +3 in the triplet state leading to its unique photophysical properties.

Upon absorption of a photon, the electrons in the t_{2g} state of the metal center are promoted to the π^* state of the ligands, increasing the oxidation state of the metal center. This metal to ligand charge transfer state (MLCT) is responsible for the photophysical properties of these transition metal based catalysts. Due to the fact that, in the excited triplet state, the ligand has undergone a one electron reduction leaving behind a hole in the t_{2g} state, the excited-state is both more oxidizing and more reducing than the ground-state.

The photochemistry of $Ru(bpy)_3^{2+}$ as a photoredox catalysts was first demonstrated in a report published by MacMillian on photocatalytic [2+2] cycloadditions, and a simultaneously published report by Yoon on α-alkylation of aldehydes[35,36]. Shortly thereafter, the Stephenson group published a similar report on the dehalogenation of alkyl halides really demonstrating three different synthetic applications of the same photocatalyst in the span of months[37]. Boncella and co-workers reported on the use of $Ru(bpy)_3^{2+}$ in the reductive cleavage of *N*-methyl picolinium carbamates in the deprotection of various amines while Falvey and coworkers used a similar system for the deprotection of carboxylic acids (Figure 1.14)[38,39]. For the deprotection of amines, the excited-state of $Ru(bpy)_3^{2+}$ was quenched by ascorbic acid to generate $Ru(bpy)_3^{+}$ and the ascorbate radical. The picolinium carbamate was quenched via one-electron reduction by $Ru(bpy)_3^{+}$, reforming $Ru(bpy)_3^{+}$ and, after bond homolysis of the reduced picolinium, and subsequent decarboxylation the free amine was formed.

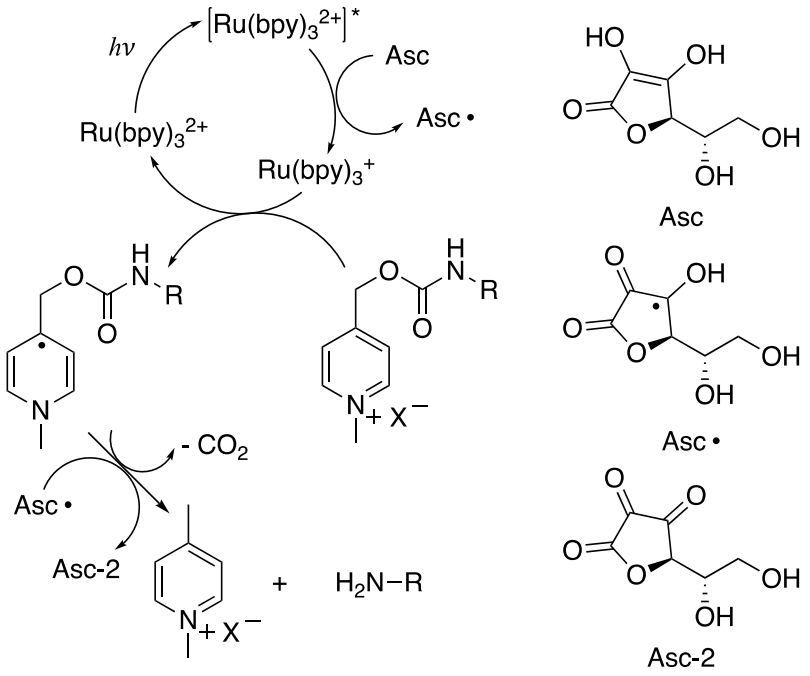

Figure 1.14. Deprotection of amines via one electron reduction of picolinium carbamate.

Recently, $Ru(bpy)_3^{2+}$ and *fac*-$Ir(ppy)_3$ have been used in the activation of dithiobenzoates, trithiocarbonates and xanthates to polymerize a broad range of monomers with good control over the molecular weights (Figure 1.15.). Under blue light illumination (435 nm), the polymerization was efficient, with only catalytic amounts of photocatalyst required, and the ability of *fac*-$Ir(ppy)_3$ to generate singlet oxygen allowed for the polymerization to be carried out in the presence of air. Selected polymerization results are given in Table 1.2.

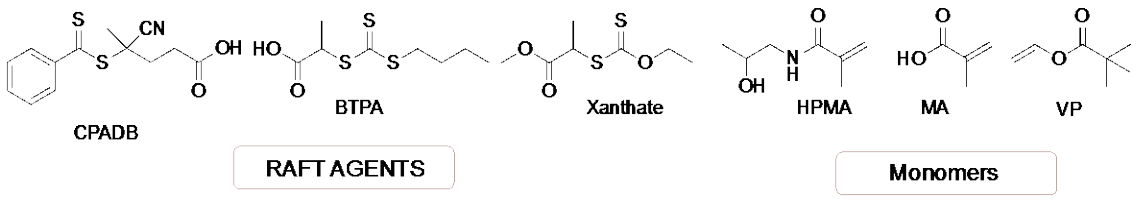

Figure 1.15. Selected CTAs and momoners used in the study.

Table 1.2 PET-RAFT with *fac*-Ir(ppy)$_3$ as the photoredox catalyst under blue light illumination

Entry	[M]:[CTA]:[Ir]	CTA	Monomer	Time, hr	Conv.	$M_{n,\ theo}$ (g/mol)	$M_{n,\ GPC}$ (g/mol)	PDI
1	200 : 1 : 10x10^{-4}	CPADB	HPMA	24	70	20300	24210	1.16
2	200 : 1 : 20x10^{-4}	CPADB	HPMA	24	72	41000	49200	1.08
3	200 : 1 : 2x10^{-4}	CPADB	HPMA	24	21	6280	6490	1.09
4	200 : 1 : 10x10^{-4}	BTPA	MA	10	99	17800	17500	1.08
5	200 : 1 : 2x10^{-4}	BTPA	MA	10	93	16170	11500	1.12
6	200 : 1 : 10x10^{-4}	xanthate	VP	24	80	20800	22000	1.38
8	100 : 1 : 10x10^{-4}	xanthate	DVP	14	41	5800	6700	1.17

In 2014, initially, the Boyer group proposed that the excited-state of the photocatalyst (either Ru(bpy)$_3^{2+}$ or *fac*-Ir(ppy)$_3$) was involved in the direct reduction of the chain transfer agent (Figure 1.11.)[31]. However, there have been numerous reports by Allonas and coworkers that suggest activation of the CTA happens, not through electron transfer, but rather is due to energy transfer the excited-state photocatalyst (Figure 1.16)[40,41]. Based on transient absorption spectroscopy and triplet quenching experiments, they propose that the excited triplet state of the photocatalyst is involved in energy transfer to the CTA and, the excited CTA, undergoes rapid C-S bond homolysis to form initiating radicals. In either case, the proposed mechanism for polymerization involves photolysis of the transition metal catalyst followed by interaction with the excited-state of the photocatalyst followed by bond scission. After bond scission, the eliminated carbon radical is free to propagate by adding to a suitable monomer before the growing chain is trapped by the CTA.

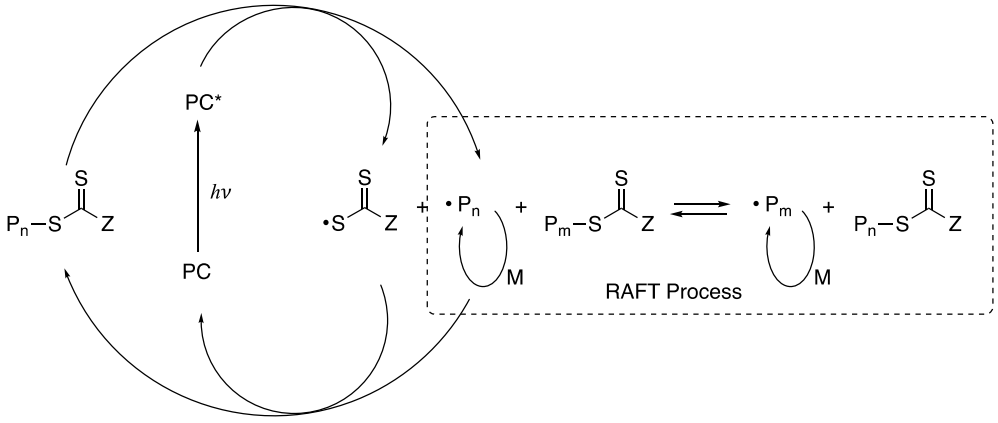

Figure 1.16. Activation of a CTA from energy transfer from an excited-state photocatalyst.

The photocatalyst plays a key role in the activation of the CTA to initiate polymerization. In chapter 4 we will consider whether the triplet state of some CTA's have enough energy to break the C-S bond efficiently as proposed in Figure 1.16. Nonetheless, the reports by Boyer and others demonstrate that transition metal based catalysts are efficient initiators in RAFT and other methods of controlled radical polymerization and allow for the reactions to be carried out with low energy visible light.

1.7 Xanthene Based Photoredox Catalysts

Xanthene based dyes are some of the most common photoredox catalysts for applications involving activation with green (~500 nm) and red (~600 nm) light. Xanthene dyes are fluorescin based, with the most common derivatives being the halogenated analogs, eosin Y and rose bengal (Figure 1.17). Although their neutral forms are colorless, the anionic forms of xanthene dyes are highly colored, and the

vast majority of the photoredox applications involve starting with the dianion and the structures that result as the dye is reduced or oxidized are shown in Figure 1.18.

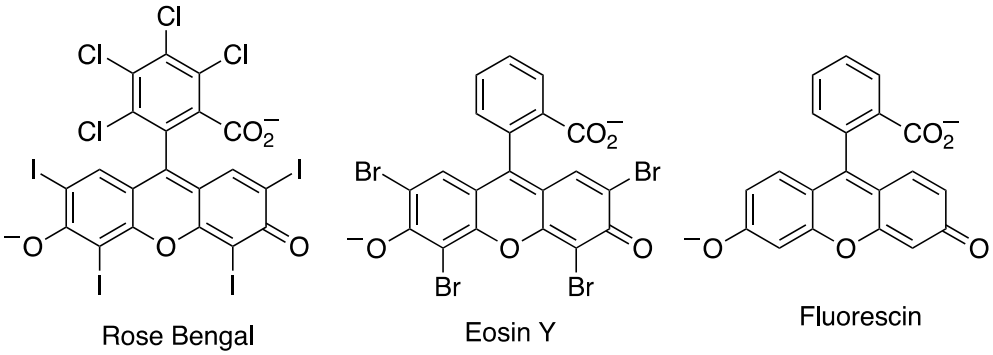

Figure 1.17. Chemical structures of some xanthene dyes.

Table 1.3 Photophysical properties of xanthene dyes[15]

	λ_{max}	Φ_{ISC}	E_{Red}	E_{Ox}	$E^*_{Red, T1}$	$E^*_{Ox, T1}$
Fluorescein	491	0.03	-1.22	+0.87	+0.77	-1.07
Eosin Y	533	0.32	-1.13	+0.76	+0.83	-1.15
Rose Bengal	499	0.77	-0.99	+0.84	+0.81	-0.96

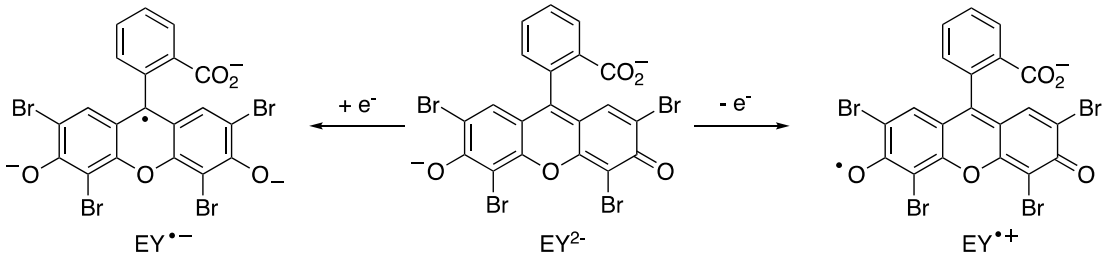

Figure 1.18. The chemical structures of eosin Y after one electron oxidation (*left*), and one electron reduction (*right*).

As discussed in an earlier section, for PET reactions, the triplet excited-state is more likely to be involved in productive electron transfer reactions due to its longer lifetime, and the reduced efficiency of back electron transfer. For this reason, fluorescein is rarely involved in PET reactions due to its low Φ_{ISC}. As shown in table 1.3, eosin Y, and rose bengal, on the other hand, undergo fast ISC ($\tau \approx 2$ ns) with

good Φ_{ISC}, with rose bengal forming the triplet most efficiently due to increased degree of halogenation causing a heavy atom effect. Coupled with their longer wavelength absorption, this makes them the most obvious choice for a given PET application. Xanthene based dyes have been used extensively in organic synthesis, and other applications include, singlet oxygen generation, photodynamic therapy, and polymer synthesis[42–44].

Eosin Y has been employed in the photochemical deprotection of alcohols via removal of the *p*-methoxybenzene (PMB) protecting group (Figure 1.19)[45]. Liu et al. demonstrated the deprotection of primary, secondary, and tertiary alcohols. The excited-state photocatalyst is proposed to abstract an electron from the aromatic system of the PMB protecting group. The newly formed cation radical can undergo C-O bond homolysis to form an alkoxy radical and benzylic cation. After protonation and oxidation using hydrogen peroxide, the deprotected alcohol is formed.

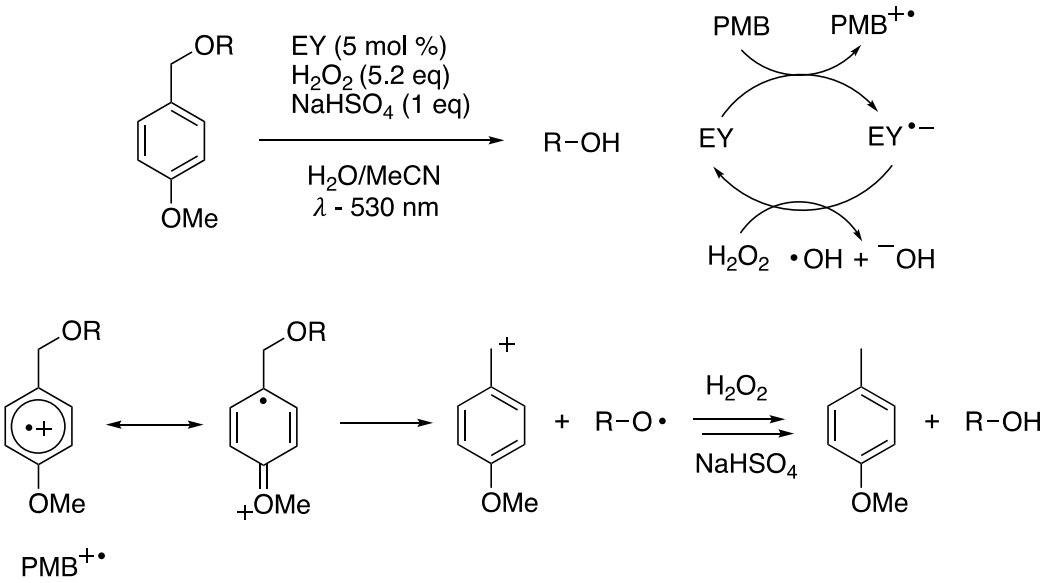

Figure 1.19. Deprotection of alcohols via oxidation of the PMB protecting group from excited-state EY.

Much like the previously described example using ChI, the low energy wavelength visible light absorption of xanthene dyes, their strong oxidizing and reducing potential, and their ability to serve as a mediator in PET processes makes them a good candidate for PET-RAFT. The first use of PET-RAFT catalyzed by organic photocatalysts was described by the Boyer group in 2015[44]. The Hawker group recently applied the approach developed by the Boyer group in the visible light (465 nm) polymerization of vinyl ketones[30]. This was particularly important because vinyl ketones are not polymerizable with other CRP techniques such as atom transfer radical polymerization, or nitroxide mediated polymerization, and RAFT polymerization of vinyl ketones previously required high temperatures and was susceptible to molecular oxygen[46].

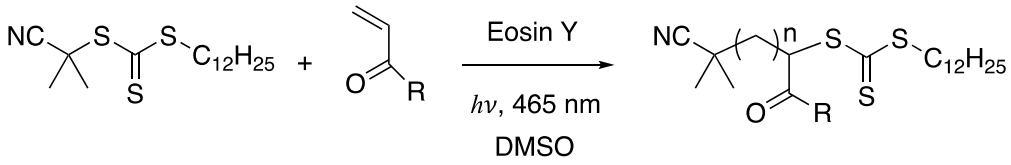

Table 1.4 PET-RAFT with Eosin Y as the photoredox catalyst under blue light illumination

Entry	[M[/[CTA]	Cat. Eq. (EY)	R	Time, hr	Conv.	$M_{n,\,GPC}$ (g/mol)	PDI
1	100	-	Me	11	-	-	-
2	100	0.02	Me	11	86	6.5k	1.11
3	200	0.02	Me	13	93	11.9k	1.15
4	200	0.02	Et	12	90	12.6k	1.14

The mechanism of polymerization was suggested to be photo-reduction of the CTA by Eosin Y and subsequent bond scission to form the capping species and the propagating species as shown in figure 1.11. The authors also found, remarking on previous reports by the Boyer group, that the addition of triethylamine, a good electron donor, sped up the polymerization process suggesting that there may be some

contribution due to a mediated electron transfer process, but other radical generation events leading to polymerization could not be ruled out.

1.9 Conclusion and Research Objectives

In this chapter the concept of photoinduced electron transfer has been introduced along with some common photoredox catalysts. Specifically, applications involving synthesis and controlled radical polymerization have been explored. PET has been used to direct the specific bond homolysis in the application of protecting groups (a topic to be coved more thoroughly in chapter 2), and in the initiation of PET-RAFT. In the proceeding chapter the identification of reactive intermediates as they relate to PET processes will be discussed. The key steps in the mechanisms of some photoremovable protecting groups (PRPGs) triggered by PET will be probed using nanosecond transient absorption spectroscopy. Following that, in chapter 3, a new PRPG which is triggered by multiphoton absorption in a stepwise process will be discussed.

Polymerization via PET-RAFT has only been recently reported, and its mechanism, although much speculated and still under investigation, will be explored in chapter 4. Although many recent publications assume that polymerization is initiated through an electron or energy transfer process, the contribution to polymerization via direct irradiation and state-specific photolysis will be explored. Finally, the contribution of the initiation process in PET-RAFT due to reactions of the photocatalyst with the solvent are discussed, and a system which is initiated via one electron oxidation of dimethyl sulfoxide, a common solvent used for PET RAFT, will be designed, and tested.

In the experiments discussed herein, an emphasis will be placed on PET. This introduction has served to demonstrate the versatility of systems triggered by PET and the many mechanisms involved.

1.10 References

(1) Pandey, G.; Karthikeyan, M.; Murugan, A. *J. Org. Chem.* **2002**, *63* (9), 2867.

(2) Pandey, G.; Murugan, A.; Balakrishnan, M. *Chem. Commun.* **2002**, *2* (6), 624.

(3) Akaba, R.; Ohshima, K.; Kawai, Y.; Obuchi, Y.; Negishi, A.; Sakuragi, H.; Tokumaru, K. *Tetrahedron Lett.* **1991**, *32* (1), 109.

(4) Kuriyama, Y.; Arai, T.; Sakuragi, H.; Tokumaru, K. *Chem. Lett.* **2006**, *17* (7), 1193.

(5) Sundararajan, C.; Falvey, D. E. *J. Org. Chem.* **2004**, *69* (17), 5547.

(6) Sundararajan, C.; Falvey, D. E. *J. Am. Chem. Soc.* **2005**, *127* (22), 8000.

(7) Sundararajan, C.; Falvey, D. E. *Photochem. Photobiol. Sci.* **2006**, *5* (1), 116.

(8) Lee, K.; Falvey, D. E. *J. Am. Chem. Soc.* **2000**, *122* (39), 9361.

(9) Sundararajan, C.; Falvey, D. E. *Photochem. Photobiol. Sci.* **2006**, *5* (1), 116.

(10) Marcus, R. A. *Pure Appl. Chem.* **2007**, *69* (1), 13.

(11) Marcus, R. A. *Annu. Rev. Phys. Chem.* **2003**, *15* (1), 155.

(12) Marcus, R. A. *J. Chem. Phys.* **1956**, *24* (5), 966.

(13) Weller, A. *Pure Appl. Chem.* **1968**, *16* (1), 115.

(14) Rehm, D.; Weller, A. *Isr. J. Chem.* **1970**, *8* (2), 259.

(15) Romero, N. A.; Nicewicz, D. A. *Chem. Rev.* **2016**, *116* (17), 10075.

(16) Miller, J. R.; Calcaterra, L. T.; Closs, G. L. *J. Am. Chem. Soc.* **1984**, *106* (10), 3047.

(17) Miller, J. R.; Beitz, J. V.; Huddleston, R. K. *J. Am. Chem. Soc.* **1984**, *106* (18), 5057.

(18) Pan, X.; Tasdelen, M. A.; Laun, J.; Junkers, T.; Yagci, Y.; Matyjaszewski, K. *Prog. Polym. Sci.* **2016**, *62*, 73.

(19) Braunecker, W. A.; Matyjaszewski, K. *Progress in Polymer Science (Oxford)*. 2007, pp 93–146.

(20) Matyjaszewski, K. *Macromolecules* **2012**, *45* (10), 4015.

(21) Theriot, J. C.; McCarthy, B. G.; Lim, C.-H.; Miyake, G. M. *Macromol. Rapid Commun.* **2017**, *38* (13), 1700040.

(22) Ni, Y.; Zhang, L.; Cheng, Z.; Zhu, X. *Polymer Chemistry*. The Royal Society of Chemistry May 21, 2019, pp 2504–2515.

(23) Hill, M. R.; Carmean, R. N.; Sumerlin, B. S. *Macromolecules*. 2015, pp 5459–5469.

(24) Perrier, S. *Macromolecules* **2017**, *50* (19), 7433.

(25) McKenzie, T. G.; Fu, Q.; Uchiyama, M.; Satoh, K.; Xu, J.; Boyer, C.; Kamigaito, M.; Qiao, G. G. *Adv. Sci.* **2016**, *3* (9), 1500394.

(26) Otsu, T.; Yoshida, M. *Die Makromol. Chemie, Rapid Commun.* **1982**, *3* (2), 127.

(27) Otsu, T. *J. Polym. Sci. Part A Polym. Chem.* **2000**, *38* (12), 2121.

(28) Corrigan, N.; Shanmugam, S.; Xu, J.; Boyer, C. *Chemical Society Reviews*., **2016**, *45*, 6165.

(29) Phommalysack-Lovan, J.; Chu, Y.; Boyer, C.; Xu, J. *Chem. Commun.* **2018**, *54* (50), 6591.

(30) Lee, I.-H.; Discekici, E. H.; Anastasaki, A.; de Alaniz, J. R.; Hawker, C. J. *Polym. Chem.* **2017**, *8*, 3351.

(31) Xu, J.; Atme, A.; Marques Martins, A. F.; Jung, K.; Boyer, C. *Polym. Chem.* **2014**, *5* (10), 3321.

(32) Shanmugam, S.; Xu, J.; Boyer, C. *Chem. Sci.* **2015**, *6* (2), 1341.

(33) Prier, C. K.; Rankic, D. A.; MacMillan, D. W. C. *Chem. Rev.* **2013**, *113* (7), 5322.

(34) Narayanam, J. M. R.; Stephenson, C. R. J. *Chem. Soc. Rev.* ***2011****, 40 (1), 102-113.*

(35) Nicewicz, D. A.; MacMillan, D. W. C. *Science* **2008**, *322* (5898), 77.

(36) Ischay, M. A.; Anzovino, M. E.; Du, J.; Yoon, T. P. *J. Am. Chem. Soc.* **2008**, *130* (39), 12886.

(37) Narayanam, J. M. R.; Tucker, J. W.; Stephenson, C. R. J. *J. Am. Chem. Soc.* **2009**, *131* (25), 8756.

(38) Edson, J. B.; Spencer, L. P.; Boncella, J. M. *Org. Lett.* **2011**, *13* (23), 6156.

(39) Borak, J. B.; Falvey, D. E. *J. Org. Chem.* **2009**, *74* (10), 3894.

(40) Christmann, J.; Ibrahim, A.; Charlot, V.; Croutxé-Barghorn, C.; Ley, C.; Allonas, X. *ChemPhysChem* **2016**, *17* (15), 1439.

(41) Corrigan, N.; Xu, J.; Boyer, C.; Allonas, X. *ChemPhotoChem* **2019**, 3, 1.

(42) Hari, D. P.; König, B. *Chem. Commun.* **2014**, *50* (51), 6688.

(43) Redmond, R. W.; Gamlin, J. N. *Photochem. Photobiol.* **1999**, *70* (4), 391.

(44) Xu, J.; Shanmugam, S.; Duong, H. T.; Boyer, C. *Polym. Chem.* **2015**, *6* (31), 5615.

(45) Liu, Z.; Zhang, Y.; Cai, Z.; Sun, H.; Cheng, X. *Adv. Synth. Catal.* **2015**, *357* (2–3), 589.

(46) Cheng, C.; Sun, G.; Khoshdel, E.; Wooley, K. L. *J. Am. Chem. Soc.* **2007**, *129* (33), 10086.

Chapter 2: Transient Absorption Spectroscopy for PRPGS

A protecting group is a compound used to mask the reactivity of a given functional group. When the appropriate trigger is applied, the protecting group is removed, restoring the original reactivity of the functional group. Protecting groups are an important aspect of organic synthesis, allowing for site specific functionalization leading to the preparation of complex natural products which would be otherwise untenable. For this reason, photoremovable protecting groups (PRPGs) have risen in popularity due to the spatial and temporal control afforded by using light as a reagent[1]. An effective PRPG should have some, or all of the following properties: [1] Absorption at wavelengths above 350 nm where light is less likely to be absorbed by other functional groups leading to undesired reactivity. [2] High quantum yield of release (Φ_{rel}). Where Φ_{rel} = number of deprotection events / number of photons absorbed. [3] High sensitivity to the trigger, and low, or no, background activity. This chapter will explore three different photoreleasable protecting groups, and the techniques used to probe their mechanism of release.

2.1 Transient Absorption spectroscopy:

Transient absorption spectroscopy, or laser flash photolysis (LFP), is an optical pump-probe technique that allows for the characterization of intermediates with lifetimes shorter than the pulse duration[2]. Specifically, this technique is useful for the identification of short-lived intermediates such as triplets, or photochemically generated radical species. Although recent advances in pulsed laser technology have allowed for the identification of intermediates on the femtosecond (10^{-15}) timescale,

most triplets and radicals live on the order of tens of nanoseconds to milliseconds making nanosecond pulsed laser photolysis ideal for their characterization[3,4]. An illustration of the laser setup used in our LFP experiments can be found in figure 2.1.

The laser system used was a neodymium-doped yttrium aluminum garnet (Nd: $Y_3Al_5O_{12}$, Nd:YAG) laser with emission wavelengths at 1064, 532, 354.7 or 266 nm respectively. The wavelength of light desired can be narrowed by choosing either the second (532 nm), third (354.7 nm), or fourth (266 nm) harmonic of the 1064 nm laser pulse using wavelength-specific dichroic mirrors. The pulsed laser (10 mJ, 5-7 ns pulse duration) is used to the excite the species being tested, and a shuttered, 350 W, xenon-arc lamp is used as the probe source. The laser pulse is focused along the z axis to spread the pulse length along the entirety of the length of the cell, while minimizing exposure outside the probe area. The probe beam offers a continuous broadband light source and is used to generate the absorption spectrum of the intermediate. The shutter is used to control the light output by blocking the probe beam shortly after the arrival of the laser pulse, and it minimizes decomposition of the substrate to be tested. The probe beam is focused through a series of lenses before the wavelength of observation is chosen by deflection off the grating of a monochromator. The light from the monochromator is focused on to a photomultiplier tube (PMT) which turns the incoming light into an amplified current measured using an oscilloscope. The laser and probe beam are set up perpendicular to one another to limit light scattering, but in cases with low signal, light scattering can still dominate at wavelengths similar to that of the excitation pulse. The samples are prepared in a quartz cuvette which, unless otherwise noted, is purged with nitrogen

prior to the experiment. Furthermore, in cases where significant decomposition of the substrate is observed or expected, the substrate will be flowed continuously under a constant stream of N_2 during the duration of the experiment.

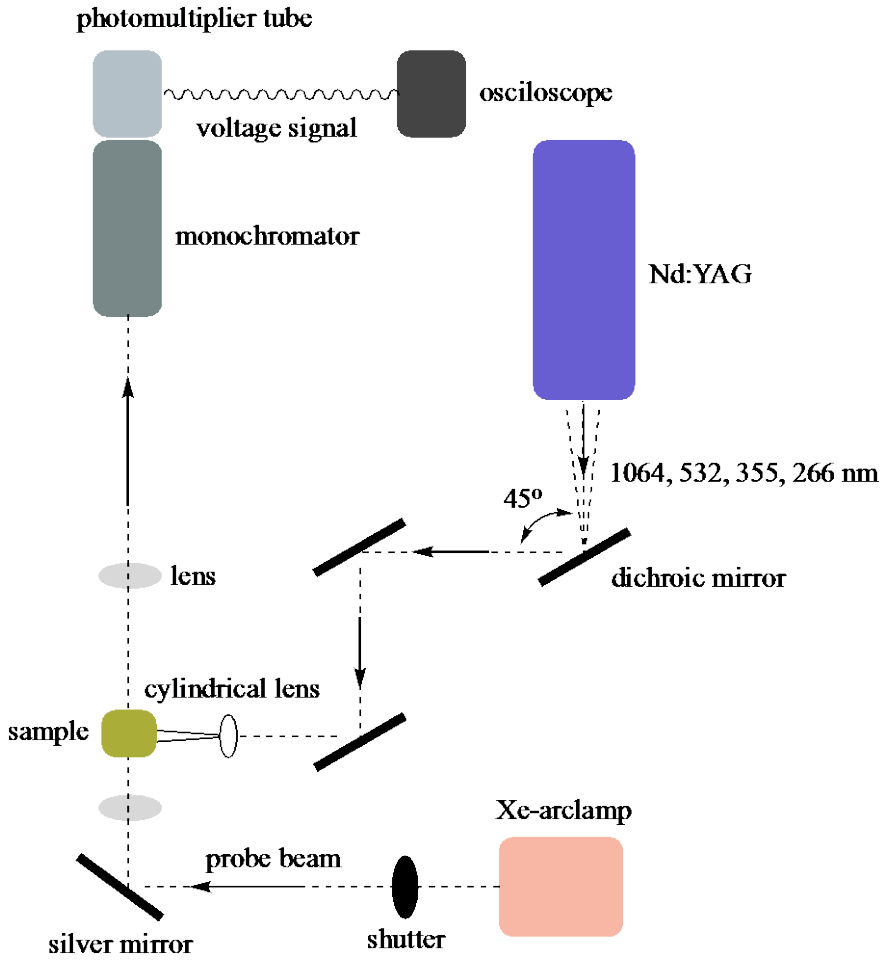

Figure 2.1. Diagram of LFP apparatus.

An example of a transient spectrum is given in figure 2.2. After photolysis, the probe beam creates a voltage deflection on the PMT which is converted into a change in optical density (ΔO.D.) using equation 1.

[1] $$\Delta O.D. = log\frac{I_0}{I_t}$$

Where I_0 is the initial voltage before the laser pulse and I_t is the voltage at time t after the laser pulse. This allows for a time-resolved measurement of the absorbance spectra of the intermediate after the laser pulse. When put in a series, a picture emerges of how the absorbance spectra evolves over time after photolysis. A positive ΔO.D. refers to an increase in the absorbance of the intermediate relative to the background and a negative ΔO.D. refers to a decrease in absorbance of the transient species relative to the background.

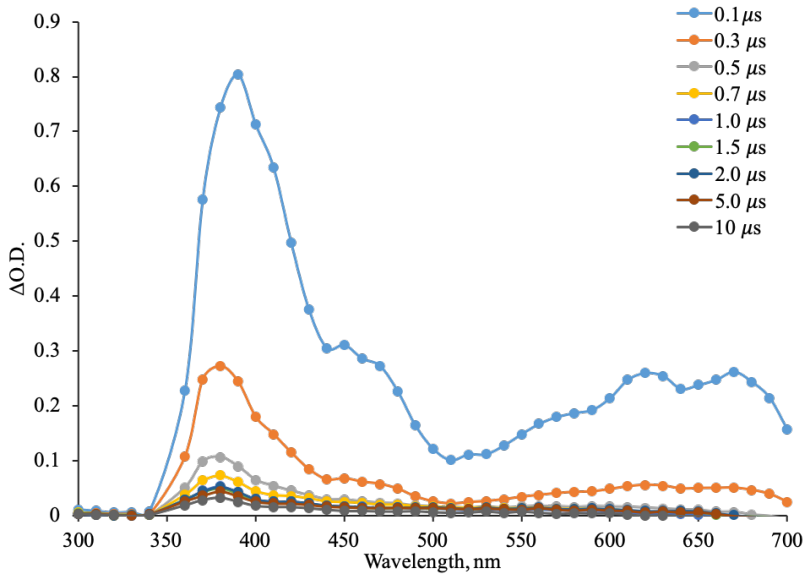

Figure 2.2. Transient absorption spectrum of 9,10-anthraquinone (AQ) in benzene from pulsed 355 nm excitation.

Immediately after the laser pulse, the transient spectra of AQ in benzene absorbs strongly, with peaks at 390 and 630 nm which, based on previously published results, can be attributed to its triplet state[5]. One of the other primary ways that triplet sates are identified is based on quenching of the signal with oxygen. Molecular oxygen is a ground-state triplet which lends itself to efficient quenching of other triplets states via energy transfer. Additionally, in figure 2.2, a long-lived species is

present at 410 nm, after the decay of the triplet, which can be assigned to the semiquinone. This forms as a result of disproportionation between the excited and ground-states[5]. In this way, based on comparison with previous literature, and various diagnostic tests such as competitive quenching, transient absorption spectroscopy can be used to identify multiple intermediates in a given photochemical reaction. This chapter will focus on the use of LFP to help elucidate the mechanism of release in three separate PRPGs: [2.2] riboflavin sensitized calcium release from EDTA, [2.5] alcohol release from a 9-phenyl-9-trytilone ether protecting group, and [2.8] CO_2 release from 1,3-dimethylimidazoylidene.

2.2 Calcium Release From EDTA:

Calcium ions are key species in multiple physiological, and environmental applications. For example, Ca^{2+} signaling is known to control muscle contractions, and the secretion of neurotransmitters and hormones[6,7]. Furthermore, calcium plays a key role in engineering processes involving biopolymers such as alginate gels[8–10]. New methods for the precise delivery of calcium have generated significant interest in the fields of microfluidics, drug delivery and more[11,12]. Specifically, caged calcium refers to a method in which Ca^{2+} is chelated in such a way so that its reactivity is diminished, or nullified. Recently, Agarwal et al. developed a nitroaromatic PRPG which releases calcium upon visible light irradiation, but there are limited examples of calcium release using visible light[13].

Our approach is to initiate calcium release via PET from oxidizing photosensitizers which can degrade EDTA-chelated Ca^{2+}. Previous work by a former graduate student demonstrated that, using the photosensitizers shown in figure 2.3,

and table 2.1, millimolar (mm) amounts of calcium can be generated. Using LFP and fluorescence spectroscopy, the mechanism of PET was probed. Additionally, experiments demonstrated that, in the case of riboflavin, the calcium generated can be used in the visible light generation of alginate hydrogels.

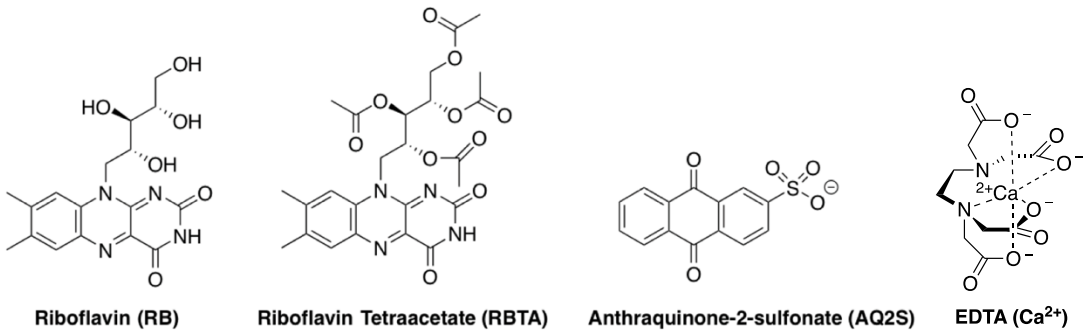

Figure 2.3. Photocatalysts used in this study, and calcium-caged EDTA

Table 2.1. Photophysical properties of photocatalysts

Sensitizer	E_{red}, V	λ_{max}, nm	$\tau_{singlet}$, ns	$\tau_{triplet}$, μs	ε, $M^{-1}s^{-1}$
AQ2S	-0.620[a,b]	330[g]	-	15[h]	5200[g]
RBTA	-1.18[c,d]	445[e]	23.8[d,j]	-	8600[e]
RB	-0.907[c,d]	450[f]	13.5[i,k]	19[j]	12200[f]

[a]Potential measured vs. SCE. [b]Reference [14]. [c]Potential measured vs. Fc/Fc^+ and converted to SCE for this work using $E^o_{1/2}(Fc/Fc+) = +0.400$ V vs. SCE. [d]Reference [15]. [e]Measured in this work. [f]Reference [16]. [g]Reference [17]. [h]Reference [18]. [i]Reference [2]. [j]Measured in MeCN. [k]Measured in water.

As shown in table 2.1, RB and RBTA absorb strongly in the visible region, and electron transfer from EDTA to the excited-state of each substrate to is expected to oxidize EDTA. Photorelease experiments were carried out as shown in Table 2.2. To aqueous buffered (pH 6.5-7.3) solutions of 2.5-25 mM Ca-EDTA the photocatalyst was added and the samples were exposed to light from a Hg-Xe arc lamp. Concentrations of calcium were determined using the spectrophotometric dye, *o*-cresolphthalein complex as described in Reference [13]. It was determined that AQ2S

was only able to release an equivalent amount of Ca^{2+}, but RB and RBTA were catalytic as demonstrated by the fact that they were able to release multiple equivalents of calcium with sub-stoichiometric amounts of sensitizer. For this reason, further mechanistic analysis was carried out on RB and RBTA.

Table 2.2. Photolytic release of Ca^{2+}

Sensitizer	[Sensitizer] (mM)	[Ca-EDTA] (mM)	λ (nm)	Time (min)	Released Ca^{2+} (mM)
2-AQDS	2.5	2.5	350[a]	60	2.1
2-AQDS	2.5	3.5	350[a]	60	2.4
RBTA	0.02	25	350[a]	60	3.9
RBTA	0.02	25	broadband[b]	60	3.7
RBTA	0.02	25	broadband[b]	120	4.9
RB	0.035	25	> 370[c]	60	4.3
RB	0.035	25	> 418[c]	60	4.0
RB	0.035	25	> 440[c]	60	2.1

[a]Phototlyzed using a 35 W, 12-bulb Rayonet photoreactor
[b]Unfiltered light from a 150 W Hg-Xe lamp
[c]Light from 150 W Hg-Xe lamp filtered with 370, 418 and 440 nm high pass filters
Calcium release determined by Romina Heymann. Please see reference [13].

2.3 Mechanistic Determination of PET from RB to EDTA:

Electron transfer from EDTA to RB and RBTA was supported by LFP and fluorescence quenching experiments (Figure 2.4.) Pulsed laser photolysis (355 nm) of RB with Ca-EDTA in aqueous solution results in an absorptions band at 510 and 660 nm with a negative bleaching event at 420 nm. These signals have been previously reported[19]. The short-lived signal at 660 nm is attributed to the triplet, RB^{3*}, and the long-lived peak at 510 nm is characteristic of the flavin radical $RB^{\bullet-}$ as a result of electron transfer from Ca-EDTA. The addition of increasing Ca-EDTA results in a

corresponding decrease in the RB^{3*} signal at 660 nm (Figure 2.4, inset), but the increased concentration of quencher has a negligible effect on the RB^{3*} decay rate suggesting that electron transfer originates from the excited singlet RB^{1*}. This result is further supported by fluorescence quenching experiments as shown in figure 2.4. Using the Stern Völmer equation (as shown in Eq. 2), along with the excited-state lifetime (τ) of RB* in table 1, the rate of RB* quenching by Ca-EDTA is 5.7×10^9 $M^{-1}s^{-1}$ which is close to the diffusion limit.

[2] $$\frac{\Phi_0}{\Phi} = 1 + k_q \tau [M]$$

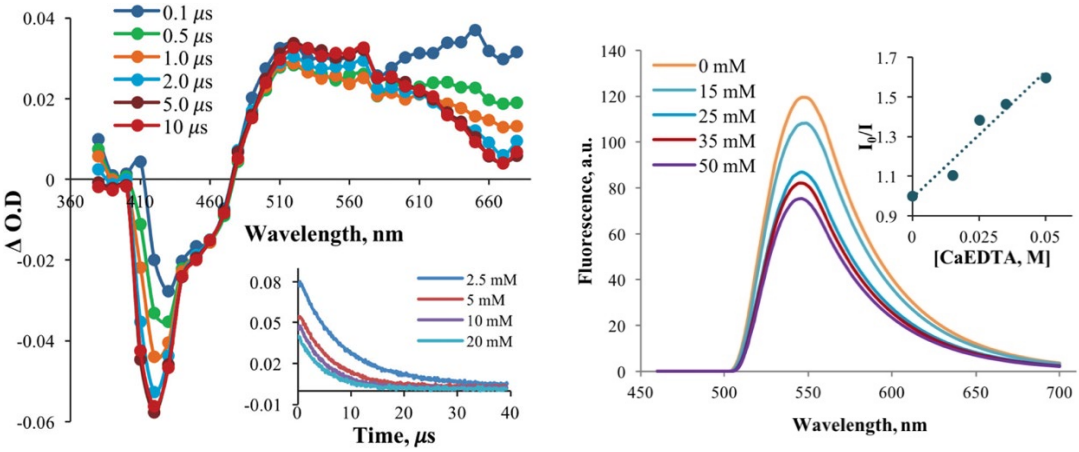

Figure 2.4. *left*: Transient absorption spectrum of RB (123 μM) with 2.5 mM Ca-EDTA in phosphate buffered water (pH = 7.4). Inset shows waveforms at 660 nm with increasing concentrations of Ca-EDTA. *Right*: Fluorescence quenching (λ_{ex} = 320 nm) of RB with varying concentrations of Ca-EDTA in phosphate buffered water (pH = 6.8). Inset, fluorescence quenching measured at 547 nm.

The proposed mechanism for calcium release is given in Figure 2.5. The excited-state of the sensitizer (singlet state in the case of the flavin derivatives and

triplet in the case of AQ2S) abstracts an electron from Ca-EDTA complex. Following decarboxylation of the aminium radical, the resulting α-amino radical may be further oxidized by a ground-state sensitizer to form a an iminium ion. Aminium ions are known to undergo decarboxylation, and given the aqueous reaction conditions, any iminium ions would hydrolyze to yield the triacetetate isomer (ED3A) and formaldehyde[20]. Further degradation would result in the loss of further chelating carboxylate arms and the loss of the ability of the isomers of diacetate (EDDA) to chelate calcium. Analysis of photolysis solutions using ^{1}H NMR showed the degradation of EDTA and the formation of formate as a peak at 8.4 ppm. These observations are consistent with previous reports on the photooxidative degradation of EDTA[21–23].

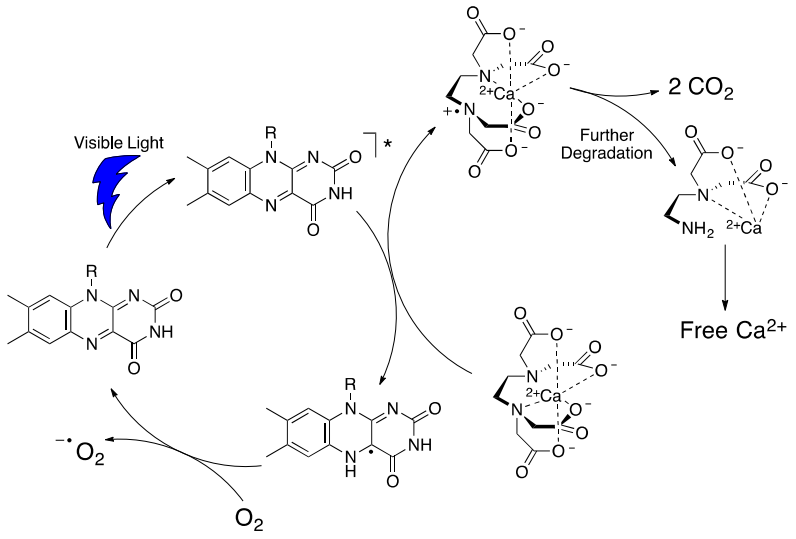

Figure 2.5. Proposed mechanism of calcium release using RB, or RBTA, as the photosensitizer.

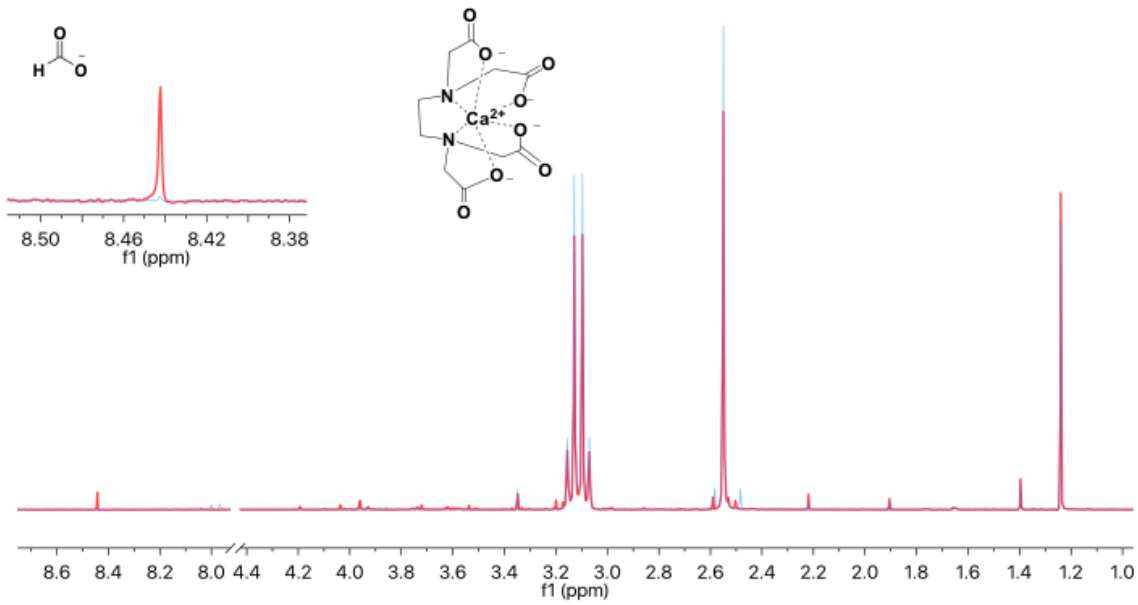

Figure 2.6. Stacked spectra showing the degradation of EDTA. Pre-irradiation (blue) and post irradiation (red) with a 1 W, CW 447 nm diode laser for 30 min. Loss of EDTA was observed as a weaker signal in red relative to blue when compared to an internal standard (tBuOH, 1.25 ppm). The Ca-EDTA complex is shown as a quartet at 3.1 and a singlet at 2.5 ppm respectively. The appearance of formate can be seen after photolysis in the magnified window as a peak at 8.44 ppm.

2.4 Release of Calcium to form Alginate Gels:

Photogeleation of alginate gels was observed from *in situ* release of Ca^{2+} after photolysis of solutions containing Ca-EDTA, RB and alginate. Stock solutions of RB (0.26 mM), Ca-EDTA (50 mM) and sodium alginate (3.75 wt%) were prepared in buffered water (pH 9.3). Unless otherwise noted, solutions were prepared by mixing 1 mL each of RB, Ca-EDTA, and sodium alginate stock solutions were mixed in a 5 mL vial with a magnetic stirbar. To this, 100 µL of 0.1M $CaCl_2$ was added. The sample was irradiated (1W, 447 nm CW diode, or 350 nm, 35 W 16 bulb Rayonet

photoreactor) for 2 hours. After photolysis, a free standing gel was observed (figure 2.7, a and b) while control experiments (Figure 2.7, c, d and e), where one or more, of the components were omitted showed no gelation.

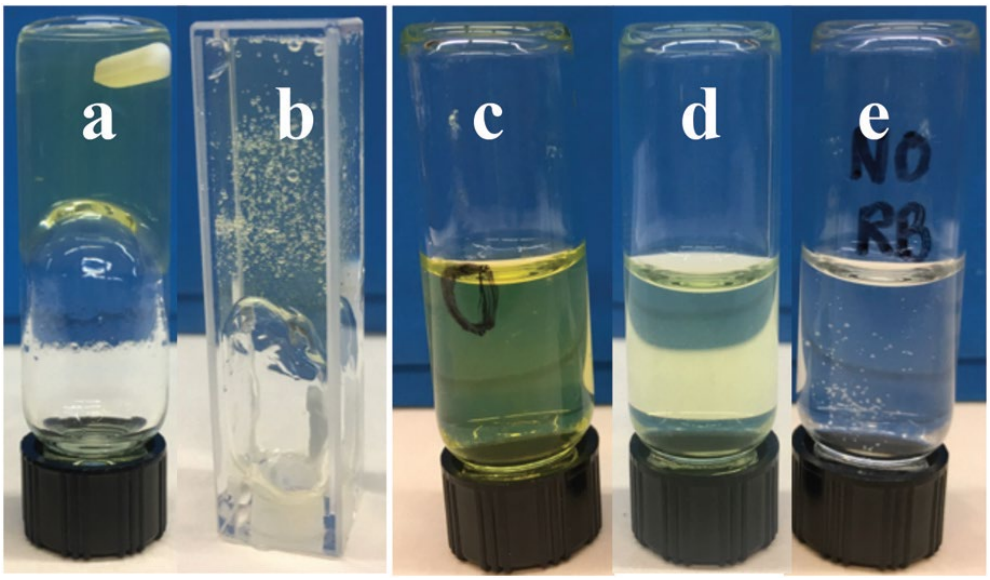

Figure 2.7. ***a.*** 350 nm photolysis ***b.*** 447 nm photolysis in an open cuvette ***c.*** dark control ***d.*** omitted Ca-EDTA ***e.*** omitted RB.

2.5 Alcohol Release from the 9-phenyl-9Tritylonyl (PTO) group:

Alcohols are one of the more difficult moieties to release using conventional PRPGs. Some approaches involve spontaneous decarboxylation of a carbonate ester and the cyclization of enol ethers (as described in Chapter 1.2), but despite being one of the most common functionalities found in natural products, the application of PRPGs for alcohols remains underdeveloped. In 2015 Denning et al. demonstrated the release of primary and secondary alcohols upon direct photolysis of a 9-phenyl-9Tritylonyl (PTO) ether in the presence of an electron donor (figure 2.8. and table 3.)[24]. The PTO group has been described as a protecting group for alcohols

previously, but this is the first attempt at triggering the release via PET. Additionally, in some cases, deprotection was initiated via photolysis of *fac*-Ir(ppy)$_3$ or Ru(bpy)$_3^{2+}$ in the presence of an electron donor, but these results will not be covered in this chapter. For additional details please see[24]. Given the previously reported reduction potential of PTO ethers (E_{red} ≈ -1.30 V vs. SCE), and assuming the PTO ether has a similar excited-state energy to benzophenone, PET from triethylamine is predicted to be exergonic by ca. 13 kcal/mol[2,25]. It was determined that the reduction of the PTO ether lead to the deprotection of alcohols (Figure 2.8 and Table 2.3) and, in this section, the mechanism was explored using transient absorption spectroscopy.

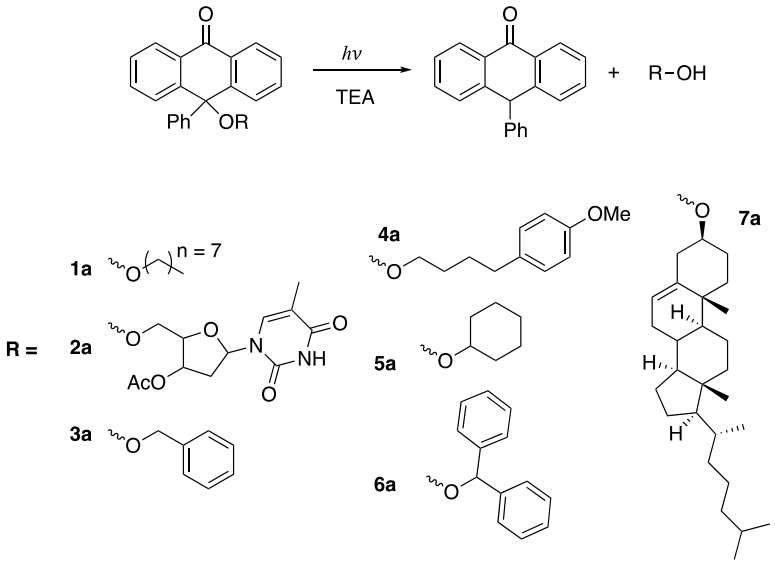

Figure 2.8. Alcohol release from direct photolysis of a PTO ether in the presence of an electron donor.

Table 2.3. Alcohol release from 350 nm photolysis[a] of various PTO ethers

Entry	[TEA], eq	Solvent	Yield, %
1a	1.9	MeOH	91 ± 2
2a	1.9	MeOH	82 ± 2
3a	3	MeOH/dioxane	92 ± 2

4a	1.8	MeOH/dioxane	32 ± 1
5a	1.8	MeOH/dioxane	82 ± 4
6a	2.5	MeOH/dioxane	64 ± 2
7a	3.1	MeOH/dioxane	77 ± 5

[a]Phototlyzed using a 35 W, 16-bulb Rayonet photoreactor for 240 min

Alcohol release determined by Derek Denning. Please see reference [24].

2.6 Mechanistic Determination of Alcohol Release Under Direct Photolysis:

To help elucidate the mechanism of release under direct photolysis, LFP was performed on select PTO ethers (Figure 2.9 and 2.11). Following pulsed laser photolysis of 3a in benzene, a species is observed with a peak at 530 nm which decays in a first order manner with rate constant of $2.63 \times 10^{-6}\ s^{-1}$. Based on comparison with benzophenone, a structurally similar compound with a well-known triplet spectrum (chapter 6), and quenching with air (figure 2.9), this signal is assigned to the triplet spectrum of PTO. With the addition of triethylamine (TEA), an electron donor, there is a long-lived signal with a peak at 530 nm and a broad tail above 550 nm. This behavior is similar to pulsed photolysis of benzophenone on the presence of triethylamine (chapter 6) in which the anion radical has an indistinct band at 650 nm which is rapidly protonated to form the ketyl radical which has an absorption band at 530 nm. Although the ketyl radical has an absorption band similar in structure and λ_{max} to the triplet, the former decays much more slowly. The signal at 650 nm decays in a biexponential manner with an initial, fast, decay having a rate constant of $4.03 \times 10^{5}\ s^{-1}$ and the second, slower, component having a rate constant of $4.75 \times 10^{4}\ s^{-1}$. Based on biexponential decay, and comparison with benzophenone, the signal at 650 nm is attributed to the anion radical, and the signal at 530 nm is

attributed to the ketyl radical. The proposed mechanism of release from direct photolysis is given in figure 2.13.

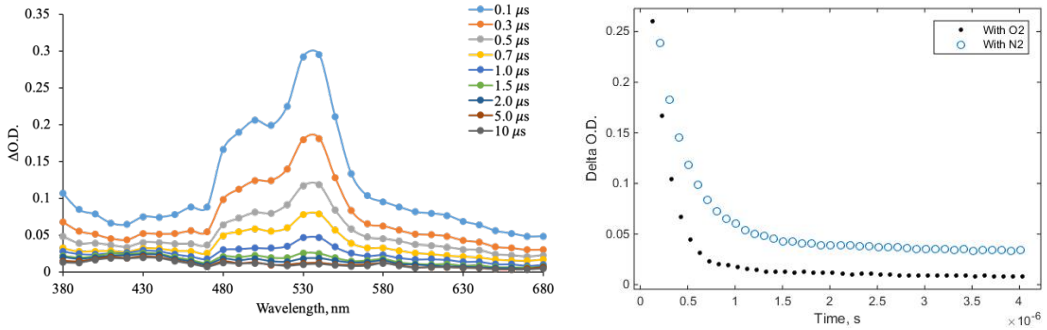

Figure 2.9. *left*: Transient absorption spectra of **3a** in benzene. The sample was flowed continuously throughout the experiment. *right*: Waveform at 540 nm showing the effect of oxygen on the triplet lifetime.

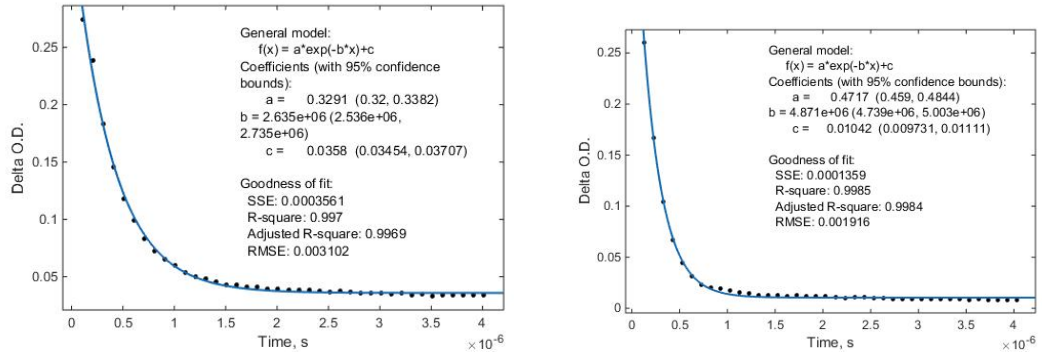

Figure 2.10. *left*: First order kinetic of the triplet decay of **3a** at 530 nm under N_2. *right*: First order kinetics of **3a** at 530 nm in an air-equilibrated sample.

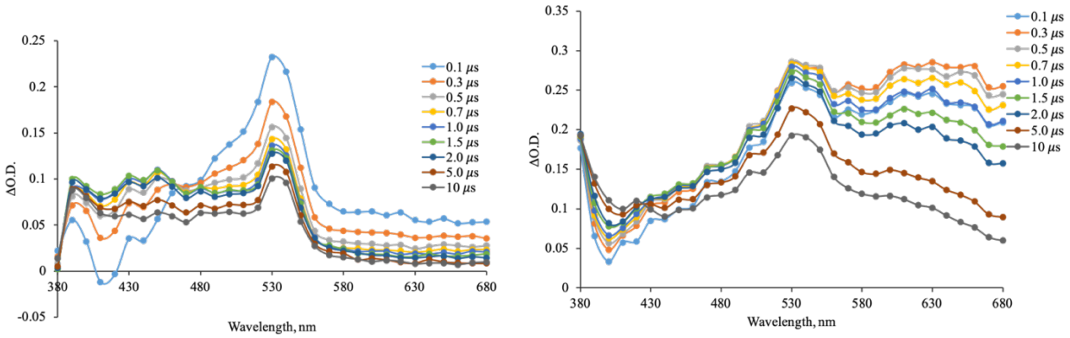

Figure 2.11. *left*: Transient absorption spectra of **3a** in MeCN *right*: Transient absorption spectra of **3a** in MeCN with TEA (50 eq.).

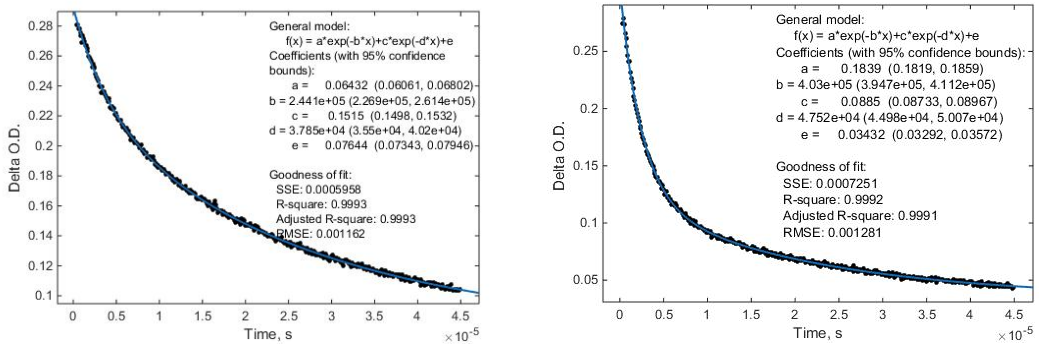

Figure 2.12. *left*: Biexponential kinetic of the triplet decay of **3a** followed by the formation of the ketyl radical at 530 nm with 50 eq. TEA. *right*: Biexponential kinetics of **3a** at 620 nm showing the formation of the anion radical and its protonation to form the ketyl radical.

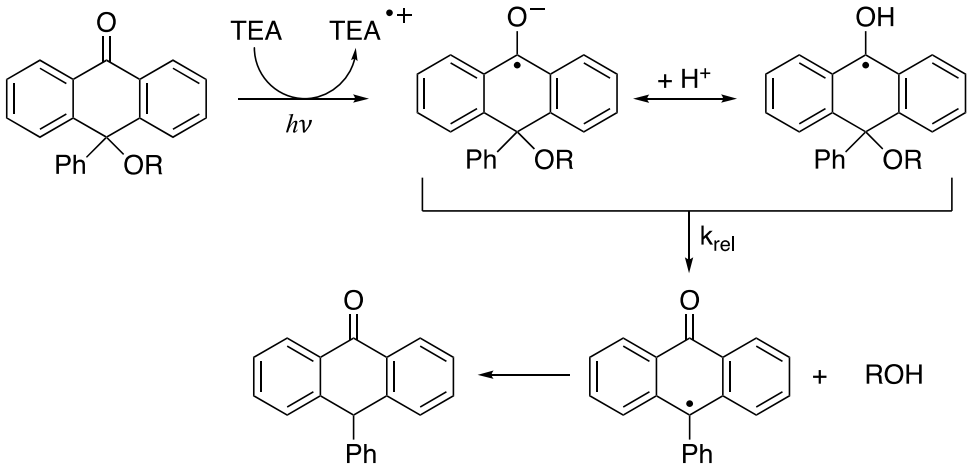

Figure 2.13. Proposed mechanism for the release of alcohols from the direct photolysis of PTO ethers in the presence of a sacrificial electron donor.

2.7 The Role of the Ketyl – Anion Radical Equilibrium:

With the information provided by the nanosecond transient absorption measurements, a picture begins to emerge of the mechanism of alcohol release. As shown in figure 2.13, direct photolysis of PTO ethers in the presence of an electron donor results in the initial formation of the triplet state, and after electron transfer, ultimately the formation of the anion radical. A complicated equilibrium then ensues between the protonated, ketyl radical, and the deprotonated, anion radical, in protic solvents. Presumably, either intermediate could lead to alcohol release, but the mechanism may vary. A recent report by Zeppuhar et al. suggested that the anion radical was the key intermediate in the release mechanism[26]. They demonstrated that photolysis of **3a** in the presence of a hydrogen atom donor did result in some alcohol formation, but the release was dominated by undesired side products. On the other hand, photolysis of **3a** in the presence of a hydrogen atom donor, but at high pH to push the equilibrium towards the anion radical, resulted in clean alcohol release. Their work indicated that, under direct photolysis conditions, while both the ketyl and anion radicals are formed, the anion radical is primarily responsible for alcohol release.

2.8 CO_2 Reduction with 1,3-dimethylimidazolylidene:

Rising levels of carbon dioxide (CO_2) in our atmosphere, and the possible global and environmental implications of large greenhouse gas concentrations, has led to innovation in the field of using CO_2 as a primary feedstock for useful materials[27,28]. Although it is possible to reduce CO_2 to yield reduction products such as carbon monoxide and formate, its stability (-2.45 V vs SCE) makes this

challenging without the help of transition metal catalysts, or highly reducing organic catalysts[27,29]. It has been shown previously that *N*-heterocyclic carbenes (NHC) can bind reversibly to CO_2 forming a stable, zwitterionic species (NHC-CO_2), and this has been used in the incorporation of CO_2 in to carboxylates and carbonates (Figure 2.14)[30,31]. Additionally, Riduan et al. demonstrated the use of NHC-CO_2 in the reduction of CO_2 to methanol[31]. Our work demonstrated that NHC-CO_2 can be photochemically reduced, and reduction of NHC-CO_2 leads to the formation of formate ions as a product from subsequent CO_2 reduction[32].

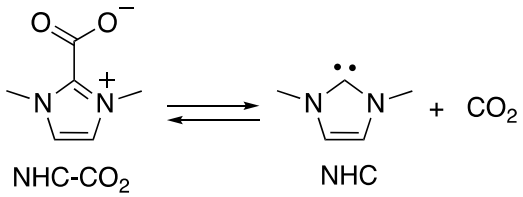

Figure 2.14. The binding of CO_2 to an NHC to the form the zwitterionic species.

2.9 Mechanism of Photochemical Reduction of CO_2:

Some of the sensitizers used in this study are given in figure 2.15. The sensitizers, *N,N,N',N'*-tetramethylbenzidine (TMB), 9-methylcarbazole (NMC), and 2-aminoanthracene (2AA) were chosen due to their relatively negative exited-state reduction potentials. The reduction potential of imidazolium cations was estimated to be -1.8V vs SCE in order to estimate the ΔG_{ET} as shown in table 4, and the singlet energy of the sensitizers was used in the calculation of E_{ox}^* according to equations 3 and 4 in chapter 1[33].

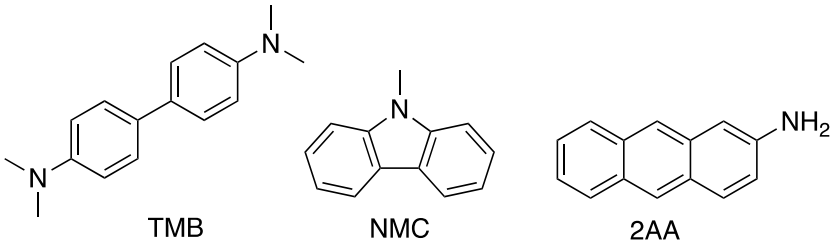

Figure 2.15. Selected sensitizers used in this study.

Table 2.4. Fluorescence Quenching of Sensitizers with NHC-CO_2 measured in 50:50 1,4-dioxane/water

Sensitizer	E_{ox}^* (V)	k_q ($M^{-1}s^{-1}$)	ΔG_{ET} (kcal/mol)[a]
TMB	-3.17	4.46×10^9	-31.6
NMC	-2.56	1.03×10^9	-17.6
2AA	-2.3	5.70×10^8	-11.4

Fluorescence quenching rates measured by Derek Denning. Please see reference [32].

Fluorescence quenching experiments (k_q, table 4) demonstrated the ability of NHC-CO_2 to quench the singlet excited-state of the sensitizers. The presence of reduced form of the NHC-CO_2 was verified by LFP. This was important because, as discussed in chapter 1, electron transfer from the singlet state leads to a contact ion pair, and due to the fact that the ion pair retains the singlet spin multiplicity, back electron transfer is efficient leading to fewer cage-escaped radical species. To try to determine if the reduced species escape the solvent cage, transient absorption spectra (355 nm) of the sensitizers in 40% H_2O / 60% 1,4-dioxane in the presence of NHC-CO_2 was measured and is given below.

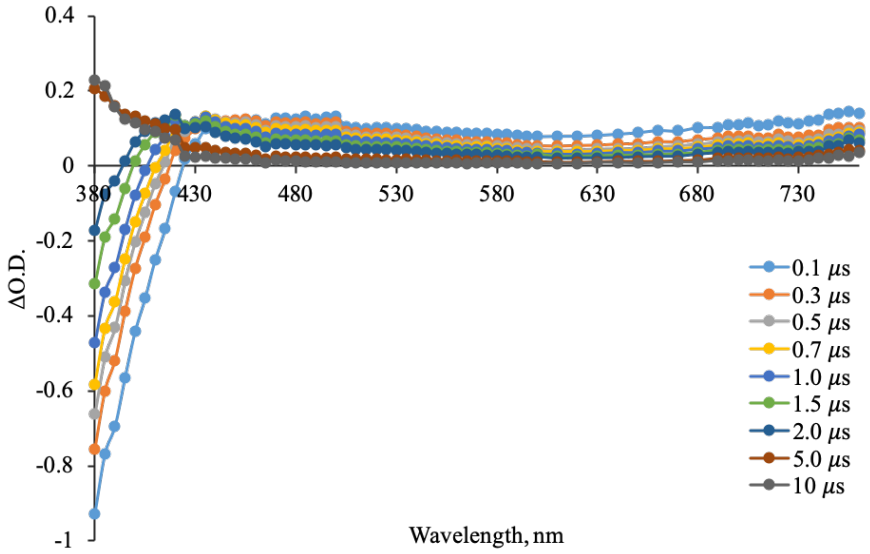

Figure 2.16. Transient absorption spectra from pulsed photolysis (355 nm) of NMC.

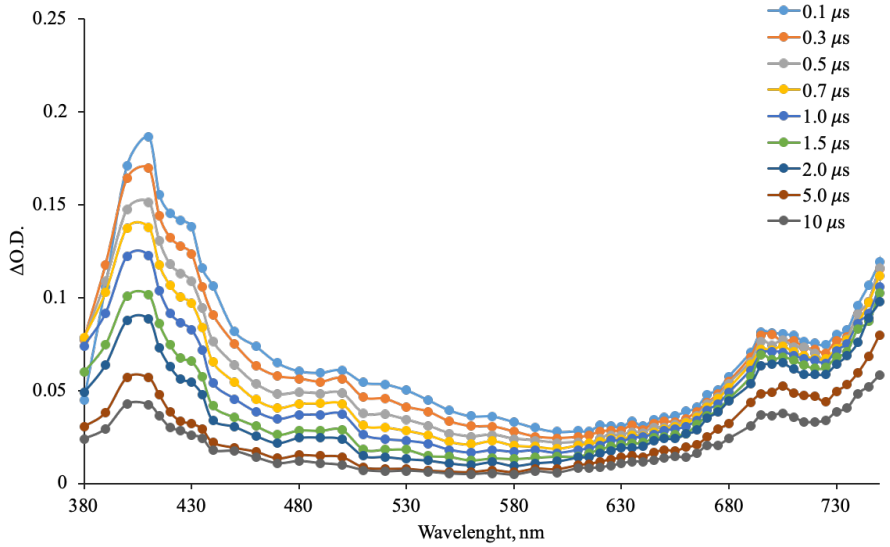

Figure 2.17. Transient absorption spectra from pulsed photolysis (355 nm) of NMC with NHC-CO_2 (10 eq.).

Figure 2.18. shows the transient absorption spectra of NMC. No distinct peaks are observed which is consistent with a low quantum yield of intersystem crossing $(\Phi_{ISC})^2$. As shown in figure 2.17, however, with the addition of NHC-CO_2, a strong

signal is observed with a lifetime of ca. 10 µs. This signal is consistent with previous reports for $NMC^{+\bullet}$ further demonstrating the ability of NMC^{1*} to reduce NHC-CO_2[34].

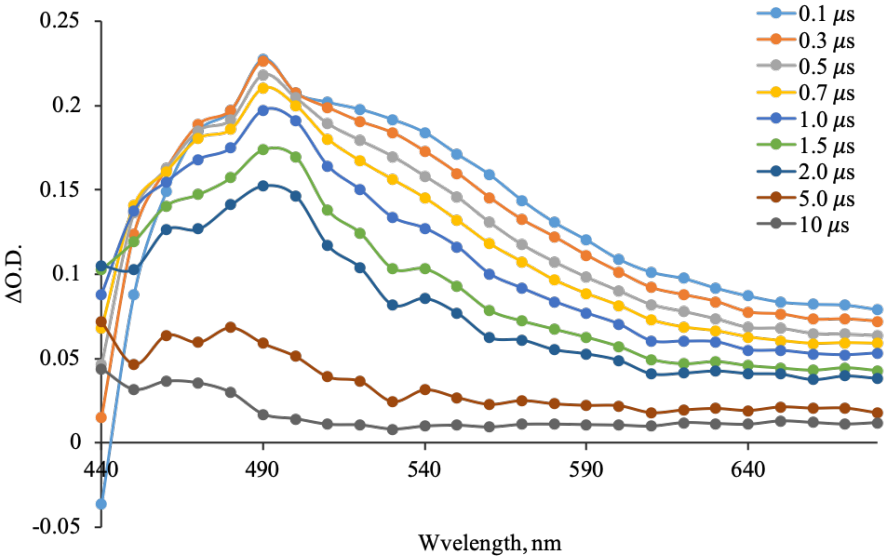

Figure 2.18. Transient absorption spectra from pulsed photolysis (355 nm) of TMB.

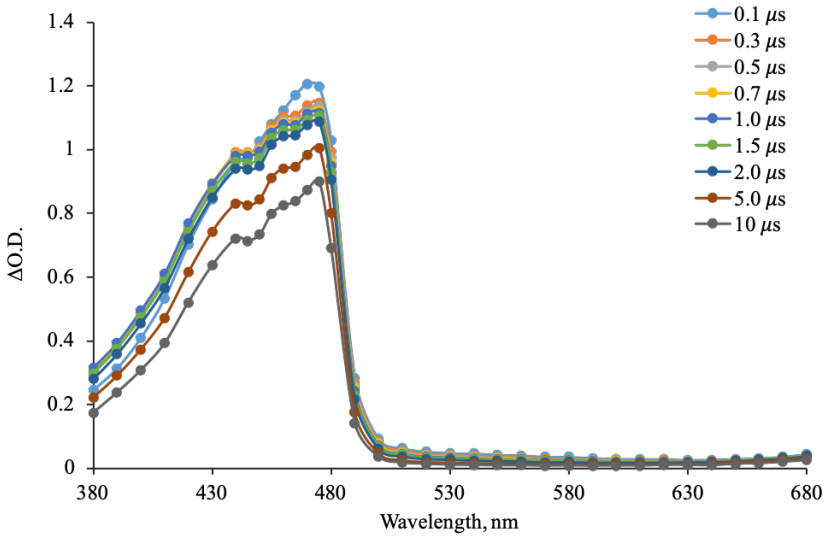

Figure 2.19. Transient absorption spectra from pulsed photolysis (355 nm) of TMB with NHC-CO_2 (10 eq.).

Figure 2.18 shows the transient absorption spectra of TMB. A signal with a peak at 490 nm with a lifetime of ca. 10 μs is observed which, based on previously reported spectra, can be assigned to the excited triplet of TMB[35]. With the addition of NHC-CO_2, a strong signal is observed with a lifetime greater than 500 μs (see figure 2.19 for the short timescale experiments and figure 2.20 for the long timescale experiments). This too, is consistent with previous reports for $TMB^{+\bullet}$ as a result of electron transfer to NHC-CO_2[35]. Nanosecond transient absorption spectra of 2AA were also collected, but will be included in chapter 6 due to the lack of proper peak assignments.

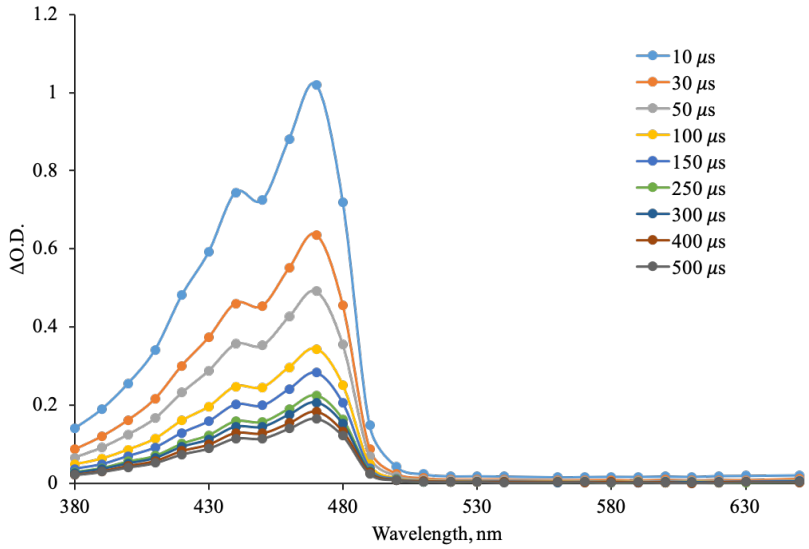

Figure 2.20. Transient absorption spectra from pulsed photolysis (355 nm) of TMB with NHC-CO_2 (10 eq.) at long timescales.

As shown in table 5, the formation of formate (a product of the reduction of CO_2) was observed upon photolysis of TMB in the presence of NHC-CO_2. It was determined that homolytic dissociation of the reduced NHC-CO_2 could result in the formation of $CO_2^{-\bullet}$ which could be further reduced to generate the observed formate.

Through a series of control experiments, reduction of $CO_2^{-\bullet}$ via hydrogen atom abstraction was found to be negligible, and it was determined that the primary source of formate was through $CO_2^{-\bullet}$ disproportionation. Given these observations along with the identification of the reactive intermediates, the proposed mechanism is given in figure 2.21.

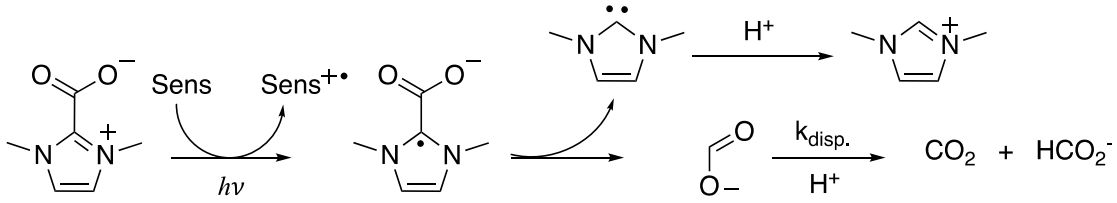

Figure 2.21. Mechanism of CO_2 reduction via PET from an excited-state sensitizer.

Table 2.5. Formation of formate from the photochemical reduction (350 nm, 60 min) of NHC-CO_2 in Dioxane/Water Mixtures

Sensitizer	[S], mM	[NHC-CO_2], mM	%H_2O	% Yield Formate
TMB	10.2	5.59	3.0	38.1
TMB	10.2	5.59	5.0	42.4
TMB	10.2	5.59	10.0	43.4

Formate production measured by Derek Denning. Please see reference [32].

2.10 The Effect of Water on the Separation of the Contact Ion Pair:

As shown in table 5, a slight increase in the amount of formate was noted with an increase in the amount of water present. As discussed previously, the reactivity of the radical species formed will depend significantly upon the probability of cage escape. Recombination of a contact ion pair, ostensibly being equivalent to an intermolecular reaction, will compete with NHC-CO_2 bond dissociation leading to a decrease in reactivity where the rate of back electron transfer dominates. Therefore the effect of the amount of water in the reaction mixture on the proportion of free ions

observed was examined below. The following experiments were performed in a mixture of 1,4-dioxane/H_2O.

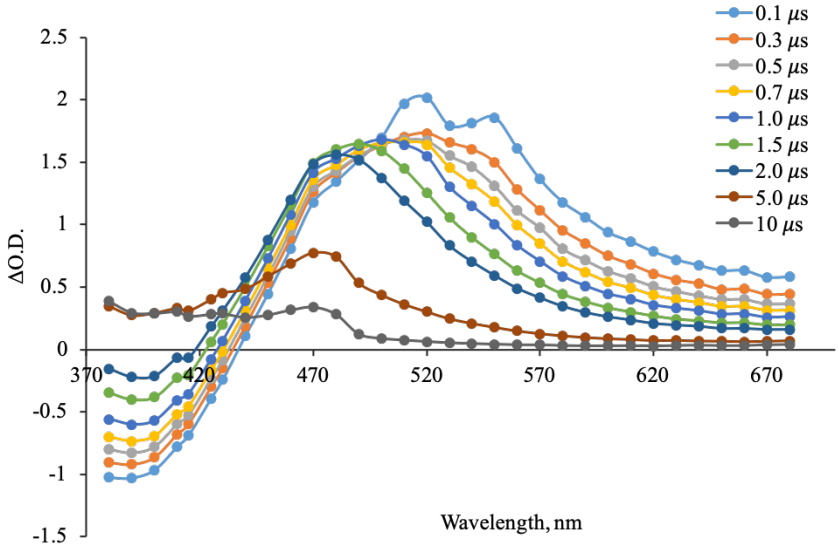

Figure 2.22. Transient absorption spectra from pulsed photolysis (355 nm) of TMB with NHC-CO_2 (1 eq.) in 10% H_2O.

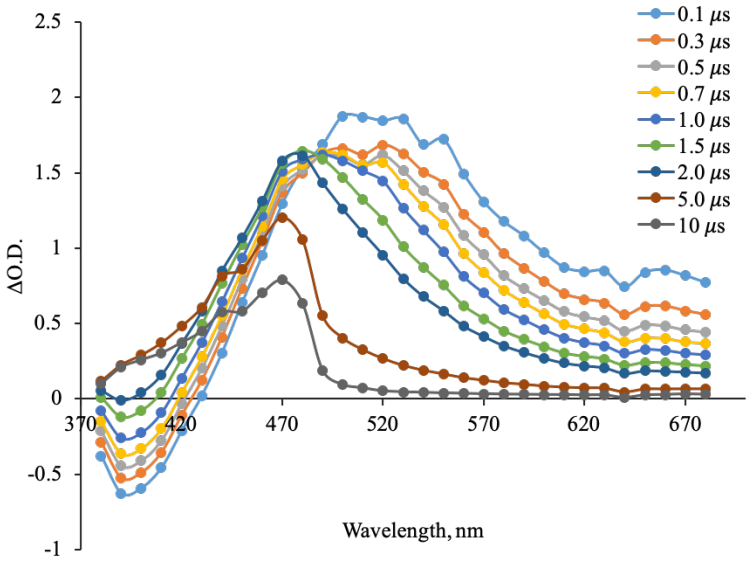

Figure 2.23. Transient absorption spectra from pulsed photolysis (355 nm) of TMB with NHC-CO_2 (1 eq.) in 20% H_2O.

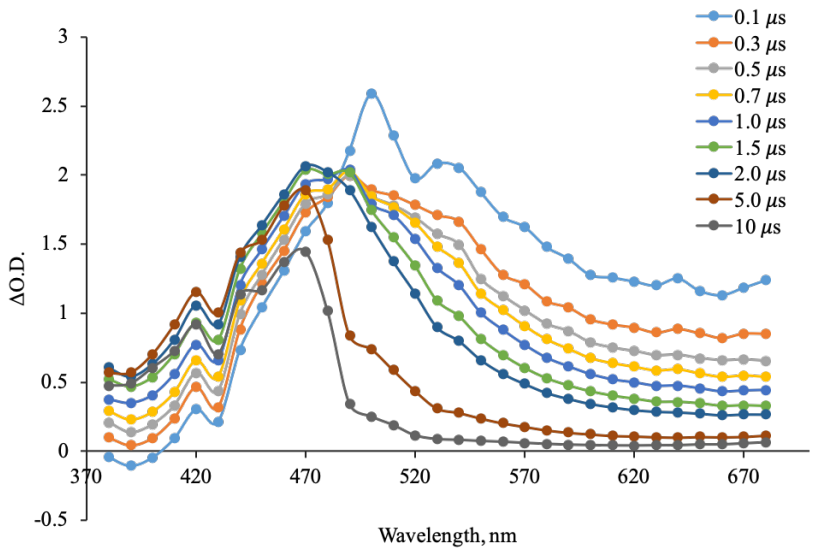

Figure 2.24. Transient absorption spectra from pulsed photolysis (355 nm) of TMB with NHC-CO_2 (1 eq.) in 40% H_2O.

Figures 2.22-2.24. show the effect of water on the ability of the formed radicals to escape the solvent cage. Immediately after the laser pulse, the triplet of TMB is seen as a peak at 490 nm. Following the decay of the triplet, the cation radical, $TMB^{+\bullet}$, can been seen as a long-lived peak at 470 nm. With increasing concentrations of water the intensity of the peak corresponding to $TMB^{+\bullet}$ also increases. This can be attributed to the formation of more free radicals in solution due to the fact that the increase in solvent polarity will lower the solvation energy of the charged radical species allowing form more efficient cage escape.

2.11 Conclusions:

The results described in this chapter demonstrate the use of LFP in the elucidation of reaction mechanisms. Additionally, in processes involving PET, it is possible to identify multiple key intermediates in a single spectrum and gain insights

into their equilibrium kinetics. The following chapters will rely heavily on nanosecond LFP as a tool to probe reactivity.

2.12 References:

(1) Klán, P.; Šolomek, T.; Bochet, C. G.; Blanc, A.; Givens, R.; Rubina, M.; Popik, V.; Kostikov, A.; Wirz, J. *Chem. Rev.* **2013**, *113* (1), 119.

(2) Murov, S. L.; Hug, G. L.; Carmichael, I. *Handbook of photochemistry*; M. Dekker, 1993.

(3) Jasny, J.; Sepit, J.; Karpiuk, J.; Gilewski, J. *Rev. Sci. Instrum.* **1994**, *65* (12), 3646.

(4) Berera, R.; van Grondelle, R.; Kennis, J. T. M. *Photosynth. Res.* **2009**, *101* (2–3), 105.

(5) Görner, H. *Photochem. Photobiol.* **2003**, *77* (2), 171.

(6) Ellis-Davies, G. C. R. *Chem. Rev.* **2008**, *108* (5), 1603.

(7) Berridge, M. J.; Lipp, P.; Bootman, M. D. *Nat. Rev. Mol. Cell Biol.* **2000**, *1* (1), 11.

(8) Javvaji, V.; Baradwaj, A. G.; Payne, G. F.; Raghavan, S. R. *Langmuir* **2011**, *27* (20), 12591.

(9) Lee, K. Y.; Mooney, D. J. *Prog. Polym. Sci.* **2012**, *37* (1), 106.

(10) Higham, A. K.; Bonino, C. A.; Raghavan, S. R.; Khan, S. A. *Soft Matter* **2014**, *10* (27), 4990.

(11) Maleki Dizaj, S.; Sharifi, S.; Ahmadian, E.; Eftekhari, A.; Adibkia, K.; Lotfipour, F. *Expert Opin. Drug Deliv.* **2019**, *16* (4), 331.

(12) Kraly, J. R.; Holcomb, R. E.; Guan, Q.; Henry, C. S. *Anal. Chim. Acta* **2009**,

653 (1), 23.

(13) Heymann, R. R.; Thum, M. D.; Hardee, A. L.; Falvey, D. E. *Photochem. Photobiol. Sci.* **2017**, *16* (6).

(14) Bechtold, T.; Burtscher, E.; Turcanu, A. *J. Electroanal. Chem.* **1999**, *465* (1), 80.

(15) König, B. *Chemical photocatalysis*; De Gruyter: Berlin, 2013.

(16) Siliprandi, N.; Bianchi, P. *BBA - Biochim. Biophys. Acta* **1955**, *16* (C), 424.

(17) Liu, C.; Zachara, J. M.; Foster, N. S.; Strickland, J. *Environ. Sci. Technol.* **2007**, *41* (22), 7730.

(18) Loeff, I.; Trelnln, A.; Llnschltz ', H. *J. Phys. Chem* **1983**, *87*, 2536.

(19) Bernt Melø, T.; Adriana Ionescu, M.; Haggquist, G. W.; Razi Naqvi, K. *Spectrochim. Acta - Part A Mol. Biomol. Spectrosc.* **1999**, *55* (11), 2299.

(20) Su, Z.; Mariano, P. S.; Falvey, D. E.; Yoon, U. C.; Oh, S. W. *J. Am. Chem. Soc.* **1998**, *120* (41), 10676.

(21) Fife, D. J.; Moore, W. M. *Photochem. Photobiol.* **1979**, *29* (1), 43.

(22) Heelis, P. F.; Parsons, B. J.; Phillips, G. O.; McKellar, J. F. *Photochem. Photobiol.* **1979**, *30* (3), 343.

(23) Babay, P. A.; Emilio, C. A.; Ferreyra, R. E.; Gautier, E. A.; Gettar, R. T.; Litter, M. I. *Int. J. Photoenergy* **2001**, *3* (4), 193.

(24) Denning, D. M.; Pedowitz, N. J.; Thum, M. D.; Falvey, D. E. *Org. Lett.* **2015**, *17* (24), 5986.

(25) Barnett, W. E.; Needham, L. L. *J. Chem. Soc. D* **1971**, *0* (3), 170.

(26) Zeppuhar, A. N.; Hill-Byrne, K.; Falvey, D. E. *Photochem. Photobiol. Sci.*

2019.

(27) Feng, D.-M.; Zhu, Y.-P.; Chen, P.; Ma, T.-Y.; Feng, D.-M.; Zhu, Y.-P.; Chen, P.; Ma, T.-Y. *Catalysts* **2017**, *7* (12), 373.

(28) Benson, E. E.; Kubiak, C. P.; Sathrum, A. J.; Smieja, J. M. *Chem. Soc. Rev.* **2009**, *38* (1), 89.

(29) La Porte, N. T.; Martinez, J. F.; Chaudhuri, S.; Hedström, S.; Batista, V. S.; Wasielewski, M. R. *Coordination Chemistry Reviews*., **2018**, *361*, 98.

(30) Tommasi, I.; Sorrentino, F. *Tetrahedron Lett.* **2005**, *46* (12), 2141.

(31) Kayaki, Y.; Yamamoto, M.; Ikariya, T. *Angew. Chemie Int. Ed.* **2009**, *48* (23), 4194.

(32) Denning, D. M.; Thum, M. D.; Falvey, D. E. *Org. Lett.* **2015**, *17* (17), 4152.

(33) de Robillard, G.; Devillers, C. H.; Kunz, D.; Cattey, H.; Digard, E.; Andrieu, J. *Org. Lett.* **2013**, *15* (17), 4410.

(34) Sundararajan, C.; Falvey, D. E. *J. Org. Chem.* **2004**, *69* (17), 5547.

(35) Alkaitis, S. A.; Grätzel, M. *J. Am. Chem. Soc.* **1976**, *98* (12), 3549.

Chapter 3: Photoreleasable Protecting Groups Triggered by Sequential Two-Photon Absorption of Visible Light

In classical photochemistry, the primary process in light absorption is a one photon process[1]. One of the most useful aspects of photochemistry is the improved spatial and temporal control over a chemical process compared to thermal chemistry. The advent of high intensity, ultra-fast femtosecond lasers, which allow for the absorption of multiple photons through a virtual state, drastically increases spatial control, however, the laser systems that are required to do so are expensive and difficult to operate. In an effort to achieve similar spatial control and threshold-like behavior, but rather using inexpensive, continuous wave (CW), lasers has been developed. This, stepwise approach, involves the absorption of a second photon via a primary state, such as a triplet or radical.

In a stepwise two-photon approach, the probability of a second photonic absorption event depends on the lifetime of the intermediate transient state. Therefore, a long lifetime of the primary state, results in a lower power threshold required to induce two-photon absorption. Practically, the primary state can be one of the following options (figure 3.1.):

(1) The singlet exited state (S_1)

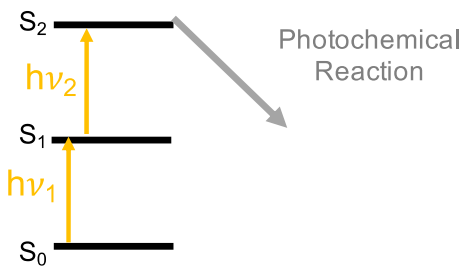

(2) The triplet excited-state (T_1)

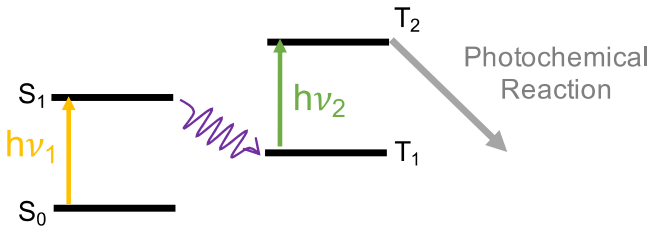

(3) The ground-state of a photoproduct

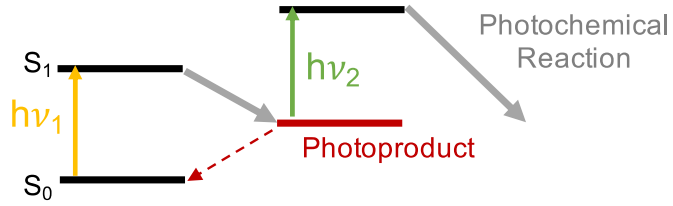

Figure 3.1. Approaches for stepwise two-photon absorption.

Approach (1) has been most notably reported as fluorescence from a higher excited-state ($S_2 \rightarrow S_1$) due to multi-photon absorption. However, due to the inherently short lifetime of excited singlet states in solution, this approach still requires pulsed photolysis and high photon density[2,3]. Similarly, approach (2) has been has been seen from two-color pulsed laser photolysis. This was most famously demonstrated by Scaiano et al. in the multiphoton bond cleavage of benzil[4–9]. Approach (3), however, involves a ground-state photoproduct which is the result of a photochemical transformation. The lifetime of the transient species is greatly increased allowing for the excitation to be performed with low power lasers, or even LEDs[10]. This approach has been used in photoacid generation, 3-D holography and more[11–19]. Our work involves the development of a stepwise photoremovable protecting group triggered by PET through sequential absorption of visible light photons through a photochemically-reduced chromophore.

3.1 Reduction of Aryl Halides Using Stepwise Two-Photon Absorption:

In the last two decades, two-color laser flash photolysis studies have been used successfully to irradiate short lived (ca. ms) radical anion species to allow for excited-state electron transfer[20–22]. Because redox potentials of radical ions in the excited-state are different than those in the ground state, reactions that are not possible in the ground-state may proceed readily in the excited-state[23]. In most cases, the limiting factor is the lifetime of the excited-state of the radical ion and not their excited-state reduction potential[24]. With this in mind, The König group developed multiple strategies using stepwise photochemical absorption in the reduction of aryl halides[25,26]. The first example involves the photolysis of a photochemically generated perelyene bismide (PDI) anion radical to trigger PET to an aryl halide resulting in the eventual formation of new C-C bonds (figure 3.2).

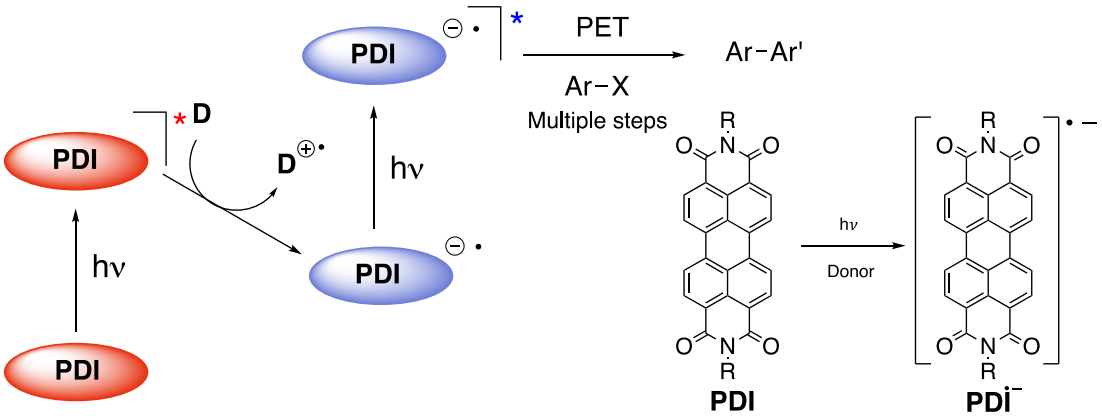

Figure 3.2. Stepwise two photon reduction of aryl halides.

Although, in principle, this system should work using visible and NIR light, a recent study by Marchini et al. cast some doubt on the role of the anion radical in the second photon absorption event[24]. They suggest the active species is some, as of yet unidentified, photoproduct which is responsible for the PET, based on the observation

that the lifetime of the excited-state anion radical of PDI is ≈ 145 ps which is much too low for an excited- state intramolecular electron transfer event. Although reported products of the König study are undeniable, the fact that their only published experiments are carried out with blue light irradiation, and not a mixture of visible and NIR light may suggest that the excited-state of the anion radical is not the primary reductant in their experiments. Preliminary polymerization results in our lab seem to agree with their observation, but additional work needs to be done to determine if there are ways to interact with the short-lived anion radical. These results will be discussed further in Chapter 6.3.

A second example of stepwise two-photon PET for synthesis, as described by the König group, involves a mechanism where a substituted anthraquinone first is photochemically reduced to its anion radical, or semiquinone, and subsequent photolysis of the latter resultes in PET to an aryl halide and eventual new C-C bond formation (figure 3.3.)[26]. Although reports by Eggins et al. and Nelleborg et al. demonstrated that the excited-state of the colored radical anions of quinones are very good reductants, this is the first report on the use of an excited-state anthraquinone radical in catalytic reductive synthesis[27,28]. This report by the König group is the first piece of evidence that suggests the excited-state of quinone radicals can be used as an alternative to the more commonly used transition metal-based systems.

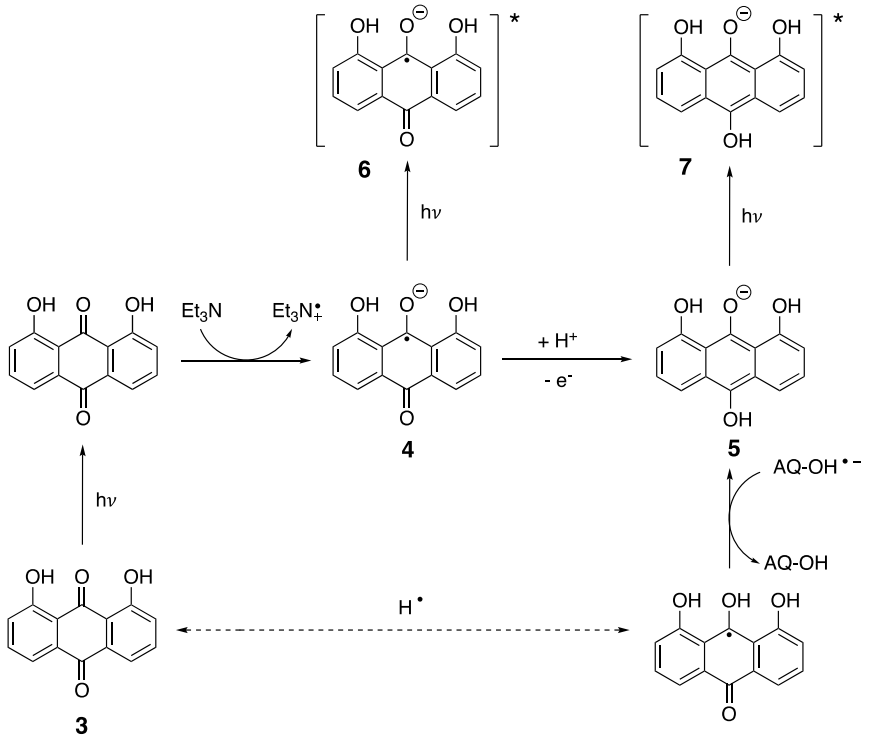

Figure 3.3. Photolysis of **3** in the presence of a suitable electron donor results in the formation of **4**, and after disproportionation, the hydroquinone, **5**. Compounds **4** and/or **5** are photolyzed, and their excited-states, **6** and **7** respectively, are able to reduce an aryl halide.

3.2 PRPGs Triggered by Stepwise Two-Photon Absorption:

Our studies will focus on the electron transfer from the excited-state of a photochemically reduced anthraquinone chromophore as a means for triggering release of a carboxylic acid from a PRPG. There are few examples of PRPGs triggered by stepwise, two-photon absorption, but one notable example by Pirrung et al. combines an *o*-nitrobenzyl group with a thermally reversible cis/trans isomerization of a cinnamate ester to release an alcohol (figure 3.4)[29]. In their proposed mechanism, the first photon absorption event triggered the conformational

cis-trans isomerization, which allowes the ester to be in a better position for the intramolecular trans esterification. The alcohol release was initiated after absorption of a second photon triggered the release of the *o*-nitrobenzyl group.

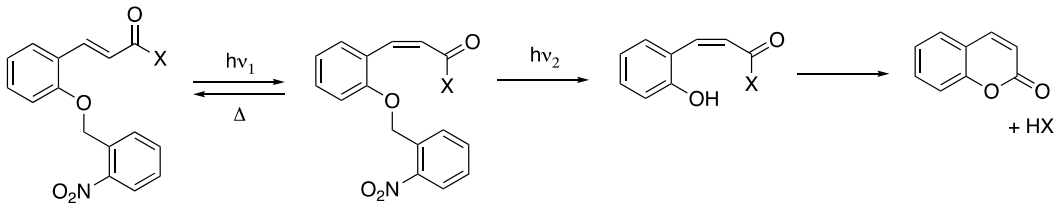

Figure 3.4. Stepwise two-photon deprotection of alcohols.

Although they were able to successfully achieve the desired two-photon release, their system has only been applied to the release of methanol and ethanol. Furthermore, it is difficult to further extend the activation wavelength into the visible region using an *o*-nitrobenzyl protecting group, and the isomerization of a cinnamate ester is a limited to UV light absorption. This leaves little hope to achieve orthogonal absorption between the initial species and the activated species, effectively limiting the spatial control of these systems.

3.3 The N-alkyl picolinium (NAP) protecting group:

The last chapter discussed various applications of PET in synthesis and polymerization. Using the same approach, PET can be applied to trigger release of a substrate. The *N*-alkyl picolinium (NAP) group is an example of a protecting group for carboxylic acids, phosphates and amines which can be reduced to release the free substrate. In its first iteration, Falvey and co-coworkers demonstrated that 4-pyridinemethyl group could be used as a protecting group for carboxylic acids. However, the highly negative reduction potential (-2.62 vs SCE) makes it difficult to

reduce with common sensitizers. Therefore, the pyridine ring was alkylated to form the basis of the NAP group. Alkylation of the ring increased the reduction potential to -1.1 vs SCE allowing for its reduction by an large number of sensitizers[30]. The NAP group has been applied to the protection of amines, carboxylate, and phosphates[31–35]. Furthermore, deprotection has been triggered by, direct and mediated electron transfer, stepwise two-photon PET, transition metal photocatalysis, gold nanoparticles and more[36–38]. The current chapter will discuss a study of the stepwise two-photon activation of the NAP group to trigger release of a model carboxylic acid.

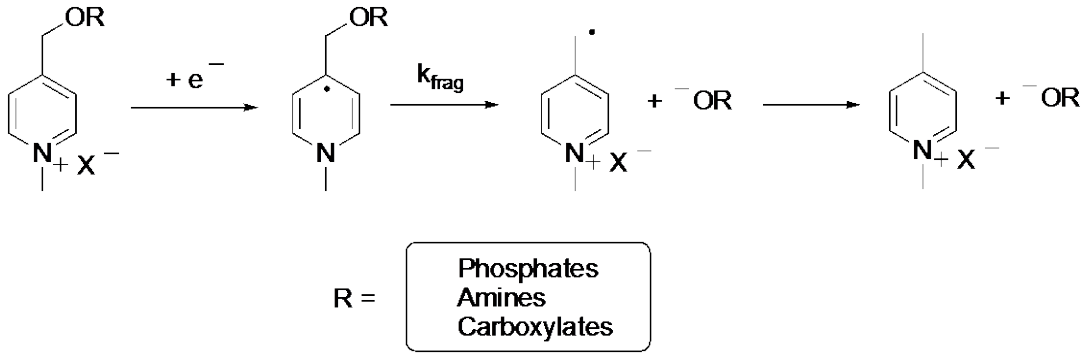

Figure 3.5. A general description of the NAP protecting group.

3.4 Design and Synthesis:

As discussed previously, single-photon release of a carboxylate anions using an *N*-alkylpicolinium (NAP) ion covalently attached to a mediator was achieved via a PET mechanism[30,32,39–41]. This work describes a method in which, by tuning the system in such a way that electron transfer from the photochemically generated mediator to the NAP group be endergonic, stepwise, two-photon release of a carboxylate can be achieved. As shown in figure 3.6, upon photolysis the mediator will abstract and electron and/or hydrogen atom from a sacrificial electron donor to

form its reduced species. If electron transfer to the NAP group is endergonic, the anion radical will persists until a second photon triggers PET, or it undergoes back electron transfer (k_{BET}). To do this we propose to use a derivative of 9,10-anthraquinone as a mediator.

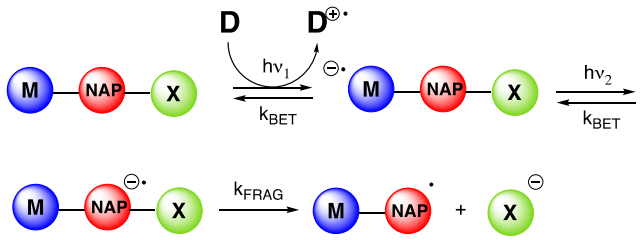

Figure 3.6. Sequential two-photon release of a substrate, X, using two photochemical electron transfer steps.

Quinones are some of the more common chromophores in photoredox chemistry[42,43]. They have been used extensively in electron transfer studies, organic flow batteries, synthesis and more[44–48]. For a more extensive list of recent examples, please see the review by Romero et al[49]. One of the advantages afforded by anthraquinone is the presence of many reductive pathways leading to reactive intermediates with varying properties.

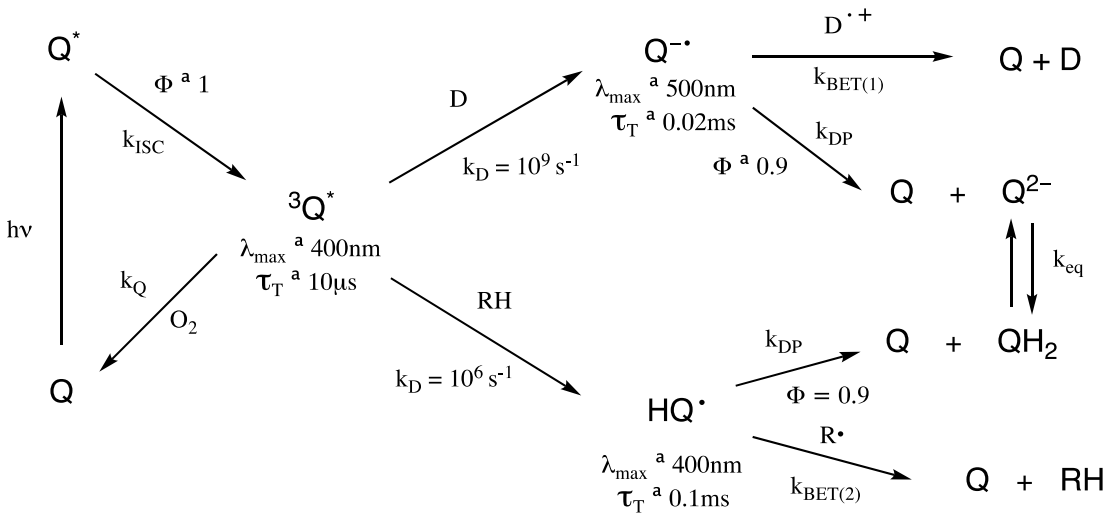

Figure 3.7. Photochemical processes of anthraquinone derivatives. Values shown are typical of the reactivity of 9,10-anthraquinone.

An anthraquinone chromophore was chosen as the mediator in our system for several reasons. First of all, with proper substitution, they are known to absorb in the visible light region of the spectrum and, in most cases, as shown in Figure 3.7., photolysis results the efficient formation of excited triplet states $^3Q^*$[50]. In the presence of a suitable electron, or hydrogen atom donating species, $^3Q^*$ is known to undergo reduction to generate three species that may serve as a suitable intermediate in a step-wise photochemical process[50]. One electron reduction results in the formation of the anion radical, $Q^{\bullet-}$, and/or its conjugate acid $QH^{\bullet}$. Disproportionation, or subsequent HAT of the latter radicals, can result in the formation of hydroquinones, QH_2. Anthraquinone species have varying reduction potentials, but the specific chromophore used in this study has a value of E_{red} = -0.62 V vs SCE (chapter 6) which is less negative than that of the NAP group (-1.1 V vs SCE)[39]. Consequently, electron transfer from $Q^{\bullet-}$ to the NAP group should be disfavored, and the protonated species, $QH^{\bullet}$ and QH_2 should even less susceptible to electron transfer. Therefore, any of the reduced species described above could serve as the initially prepared state in a stepwise, two-photon process. Our system is described in figure 3.8.

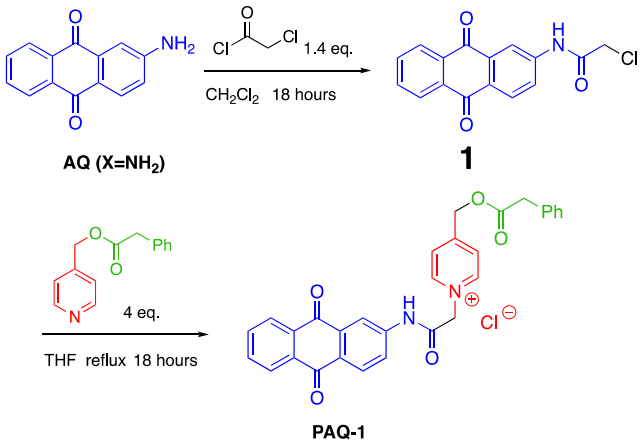

Figure 3.8. Synthesis of PAQ-1

In brief, 2-chloroactyl chloride in a dichloromethane (DCM) was added dropwise to a solution of 2-amino-9,10-anthraquionoe in DCM over an ice bath followed by stirring at room temperature overnight to yield **1**. The final linked chromophore was prepared by heating **1** and picolyl phenyl acetate in THF for 18 hr at reflux to yield PAQ-1.

3.5 Photochemical Deprotection:

Photolysis of PAQ-1 in isopropyl alcohol (iPrOH), or methanol (MeOH) resulted in the clean release of phenylacetic acid. The photolysis could be carried out with high intensity visible light (447 nm, 1 W diode laser), or with subsequent broadband 350 nm light followed by 447 nm irradiation. Both MeOH and iPrOH can serve as a hydrogen atom donor, and thus produce the semiquinone which could then be photolyzed to initiate release of the carboxylate from the NAP group.

The release was followed by ^{1}H NMR (figures 3.10-3.11.). A stock solution of PAQ-1 was filtered through a 0.45 μm syringe filter prior to photolysis in a quartz cuvette. The sample was purged with N_2 for 10 minutes in the solution and an

additional 5 minutes in the headspace before exposure. After photolysis, the solvent was removed under reduced pressure and CD_3OD was added before analysis by ^1H NMR. Additionally, the photolysis of the samples was followed by mass spectrometry (ESI^+, only timepoints 0, 10 and 50 minutes shown).

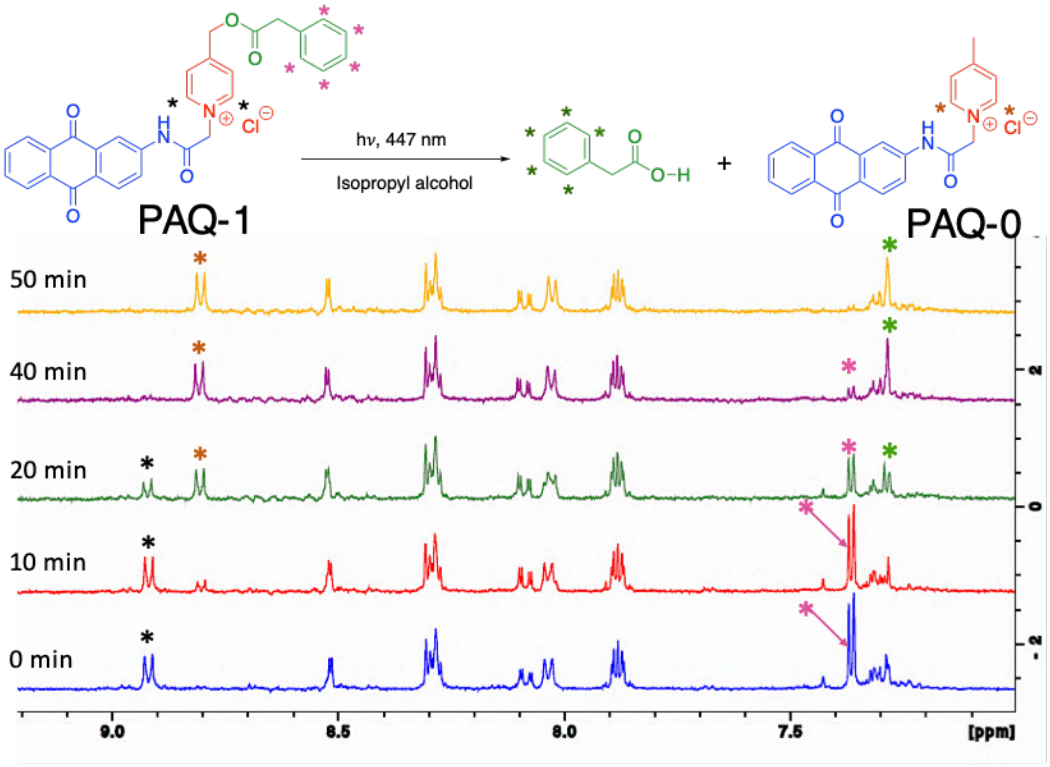

Figure 3.10. ^1H NMR spectra from photolysis of PAQ-1 in isopropyl alcohol at 447 nm.

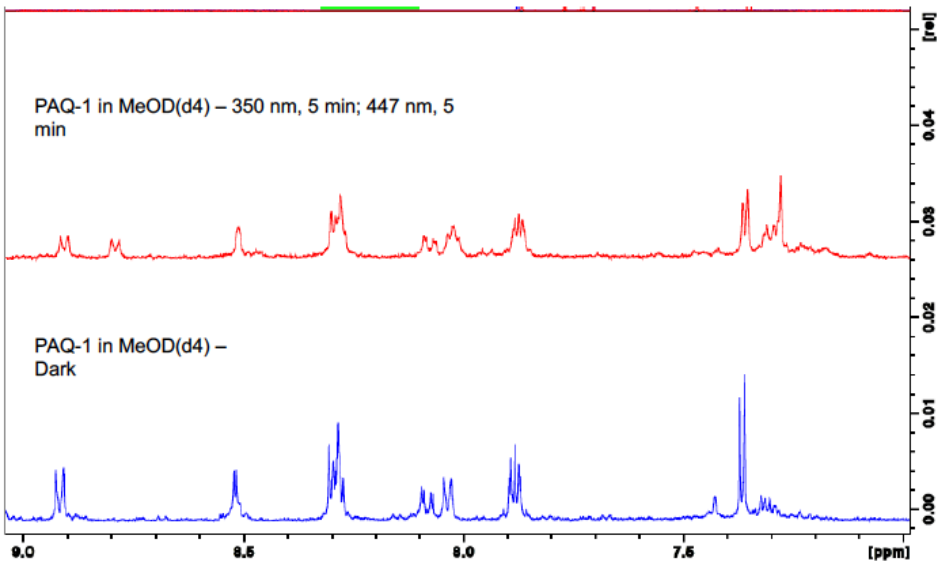

Figure 3.11. Photolysis of PAQ-1 in isopropyl alcohol at 350 nm for 5 minutes followed by 447 nm photolysis for 5 minutes.

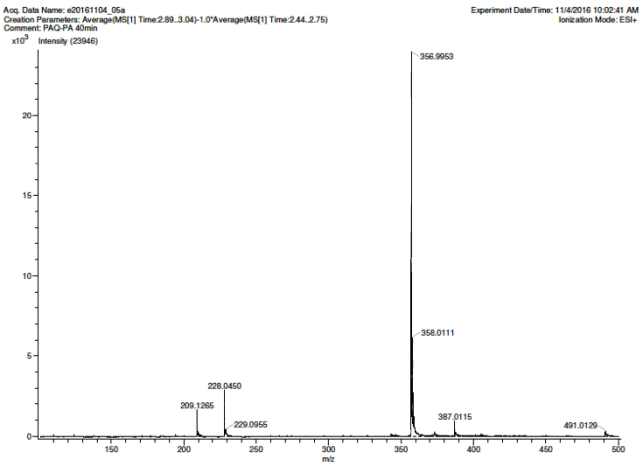

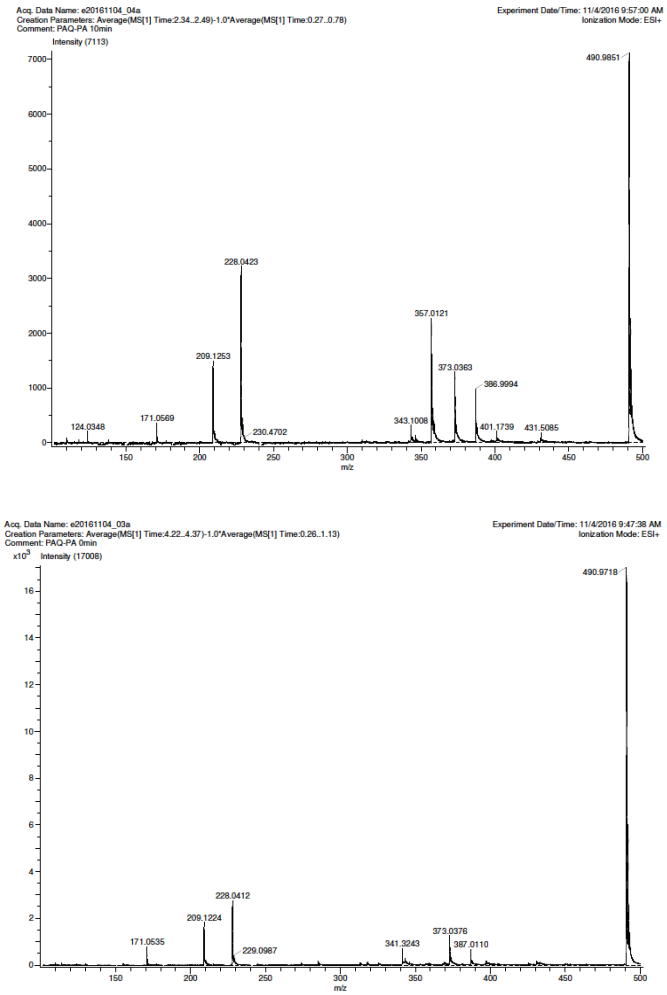

Figure 3.12. Mass spectra (ESI+) from photolysis of PAQ-1 at 447 nm in isopropyl alcohol at 0 (top), 10 (middle) and 50 (bottom) minutes respectively.

Photoproduct PAQ-0 appears after 10 minutes of photolysis and, at 50 minutes, is the only major product. Formation of free phenyl acetic acid is shown in Figure 3.11. By monitoring the changes in their relative peak intensities, it was shown that the peak corresponding to the ester at 7.4 ppm is replaced by a new peak at 7.2 ppm corresponding to free phenylacetic acid. Unfortunately, the exact amount of acid formed could not be quantified due to the loss of product during the solvent removal step. The formation of PAQ-0 can be followed by ^{1}H NMR and mass spectrometry

(figure 3.11-3.12). The peaks corresponding to the pyridinium ring in PAQ-1 at 8.95 ppm shift upfield to 8.8 ppm which corresponds to the formation of PAQ-0 as the major photoproduct. This is further substantiated by the UV/Vis spectra as shown in figure 3.14. After 10 minutes of photolysis, PAQ-0 is formed with a M/Z of 356.99 and, after 50 minutes of photolysis, PAQ-0 is the only major product observed. The presence of PAQ-0 was further demonstrated by comparing ^{1}H NMR spectra of photolysis mixtures to those of an independently synthesized standard (Figure 3.13.)

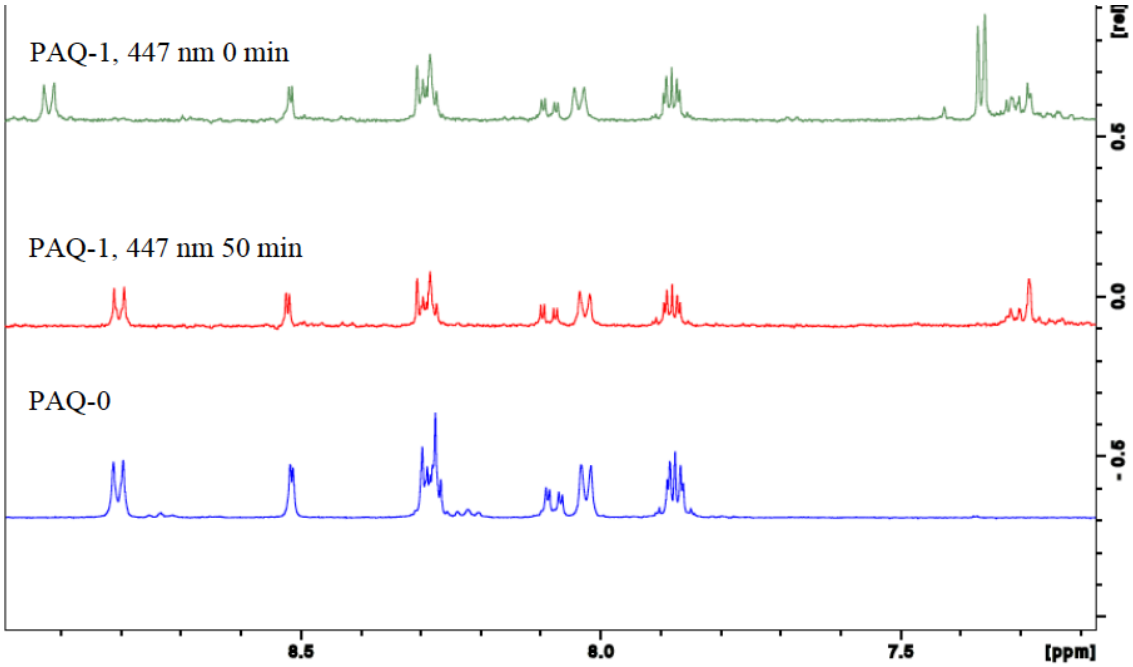

Figure 3.13. Confirmation of formation of PAQ-0 upon photolysis of PAQ-1 in iPrOH.

3.6 Characterization and Identification of Reactive Intermediates:

Laser flash photolysis of PAQ-1 in iPrOH is given in figure 3.15. The transient absorption spectrum from pulsed photolysis (354.7 nm, 10 mJ, 5-7 ns)

shows, immediately following excitation, a short-lived species with an absorption at 490 nm which is assigned to the triplet of PAQ-1. This assignment is made on the basis of oxygen quenching experiments and the spectra of structurally similar anthraquinone derivatives (Chapter 3 figure 3.19 and chapter 6)[50]. The donor at the 2 position limits, but does not prevent HAT from the solvent to form the semiquinone. Furthermore, the lifetime of the triplet suggests that energy transfer from triplet of PAQ-1 to the NAP group is not significant. Based on this observation, and experiments performed on unlinked compounds, we conclude that the triplet state of the AQ either abstracts a hydrogen atom from the solvent, or relaxes back to the ground-state.

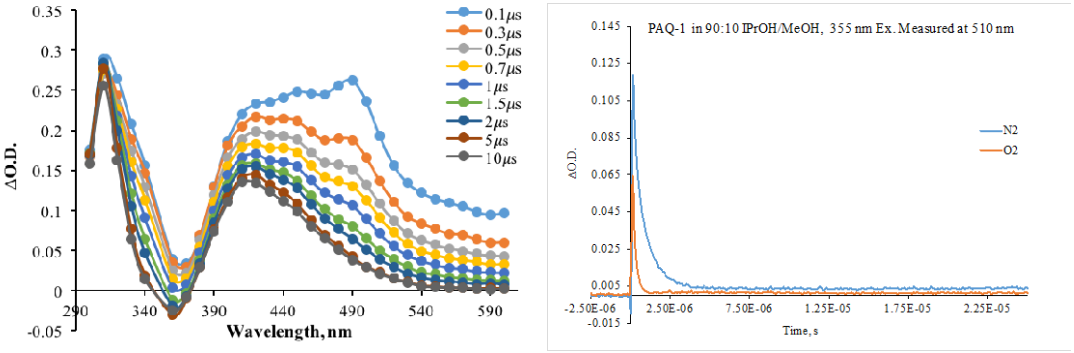

Figure 3.14. *left*: Transient absorption spectrum of PAQ-1 in 90:10 iPrOH/MeOH. *Right*: Waveforms showing the oxygen quenching of the triplet at 510 nm.

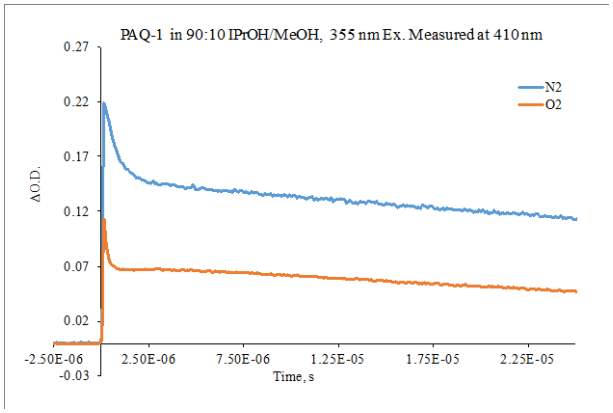

Figure 3.15. Kinetic traces (410 nm) from LFP experiments showing the oxygen quenching of the semiquinone at 410 nm.

Following the decay of the triplet, a new peak at 410 nm is shown which is assigned to the semiquinone. The lifetime of the semiquinone is too long to be accurately measured by LFP ($t_{1/2}$ ca. >1 ms). The long lifetime of the semiquinone suggests that there is no ground-state electron transfer to the NAP group. To characterize the intermediates generated over long timescales, a sample of PAQ-1 in IPrOH was photolyzed at 447 nm and the products were characterized by UV/Vis spectroscopy (Figure 3.16). A new absorption is generated with a λ_{max} at 390 nm which is attributed to the hydroquinone[51,52]. The latter, which is formed with a quantum yield of 0.2 (See chapter 6) is persistent for more than one day. However, upon bubbling with O_2, this species reverts back to the original spectrum of the starting quinone. Given that the anthraquinone chromophore, and its reduced semiquinone radical do not have the reduction potential necessary to transfer an electron to the NAP group, two possible mechanisms can be conceived. (1) Electron transfer from the excited-state of the semiquinone, or (2) electron transfer from the excited-state of the hydroquinone. Although it cannot be ruled out, electron transfer from the excited-state of the semiquinone is unlikely do its relatively short lifetime (ca. 0.1 ms, Figure 3.14).

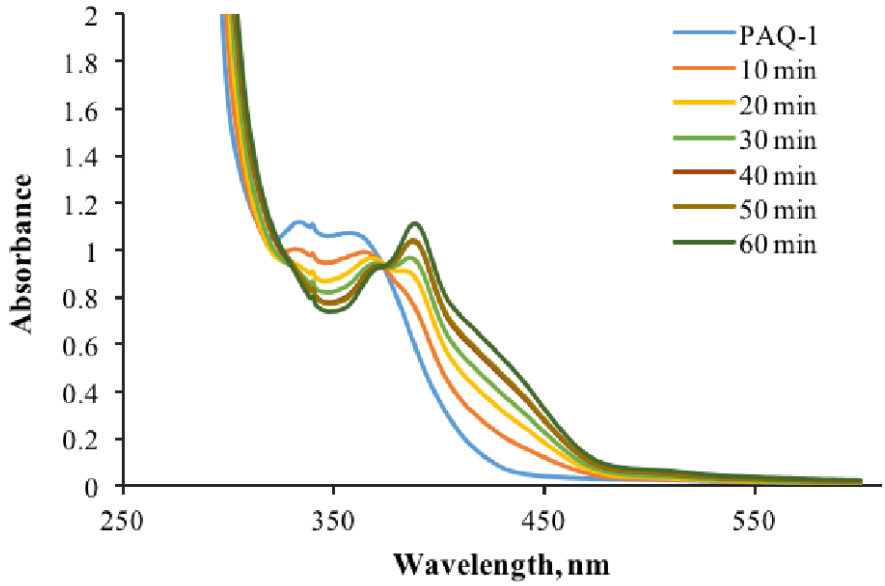

Figure 3.16. Steady-state UV-Vis spectra from photolysis of PAQ-1 in iPrOH.

3.7 Formation of the Hydroquinone by Chemical Reduction:

To test if photolysis of the hydroquinone would lead to formation of free phenylacetic acid, the linked hydroquinone was also prepared by chemical reduction using sodium dithionite. The linked compound, PAQ-1, was reduced using sodium dithionite in a mixture of D_2O/CD_3OD. Quantitative formation of the hydroquinone was confirmed by UV/Vis. Two identical samples were prepared. In the first, PAQ-1 was chemically reduced followed by photolysis at 447 nm, while in the second, the sample was kept dark. After 60 minutes of photolysis, clean conversion to PAQ-0 and the resulting carboxylic acid was observed while the dark control showed no conversion. The results serve to further establish the hydroquinone as the active transient species in a stepwise two-photon system.

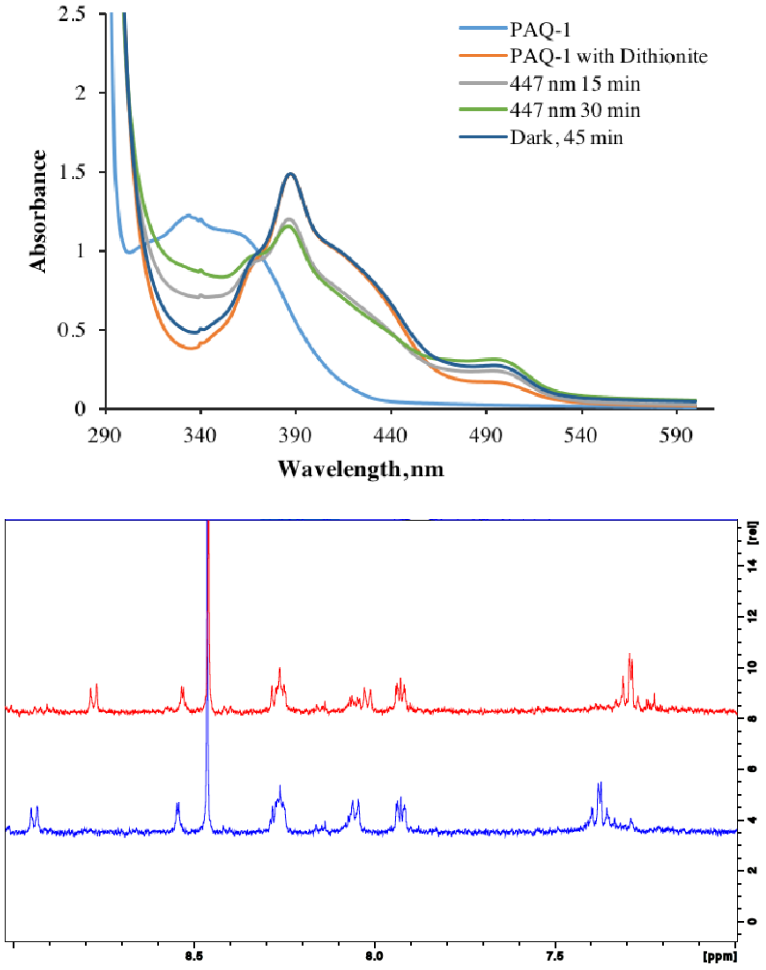

Figure 3.17. *Top*: UV/Vis spectra showing PAQ-1 was converted to the hydroquinone (as shown as a peak at 390 nm) with sodium dithionite as seen in orange. *Bottom*: ^{1}H NMR spectra *Red:* PAQ-1 chemically reduced with sodium dithionite followed by 447 nm photolysis. PAQ-0 can be seen as an upfield shift in the peak at 8.8 ppm and free phenylacetic acid can be seen as a shit upfield in the peaks at 7.4 ppm. *Blue:* PAQ-1 chemically reduced with sodium dithionite kept dark for one hour.

3.8 Mechanistic Studies Using an Unlinked System:

To further substantiate the mechanism, a series of experiments were performed on unlinked compounds **2** and **3** (Figure 3.18).

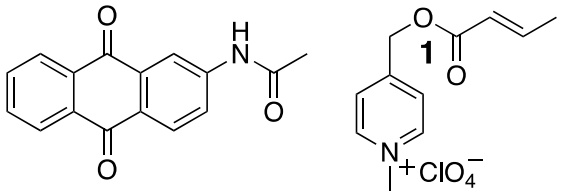

Figure 3.18. Model compounds used in this study.

Transient absorption spectroscopy of **2** in iPrOH is given in Figure 3.19. As with the linked system, following excitation, a peak is seen with an absorption at 510 nm which is attributed to the triplet and a long-lived peak is seen at 410 nm which is attributed to the semiquinone. Figure 3.19 shows that neither the lifetime of the triplet, or that of the semiquinone were affected by the presence of **3** up to its saturation in iPrOH (1 mM). This further excludes the possibility of triplet energy transfer, or ground-state electron transfer from the intermediate species to the NAP group.

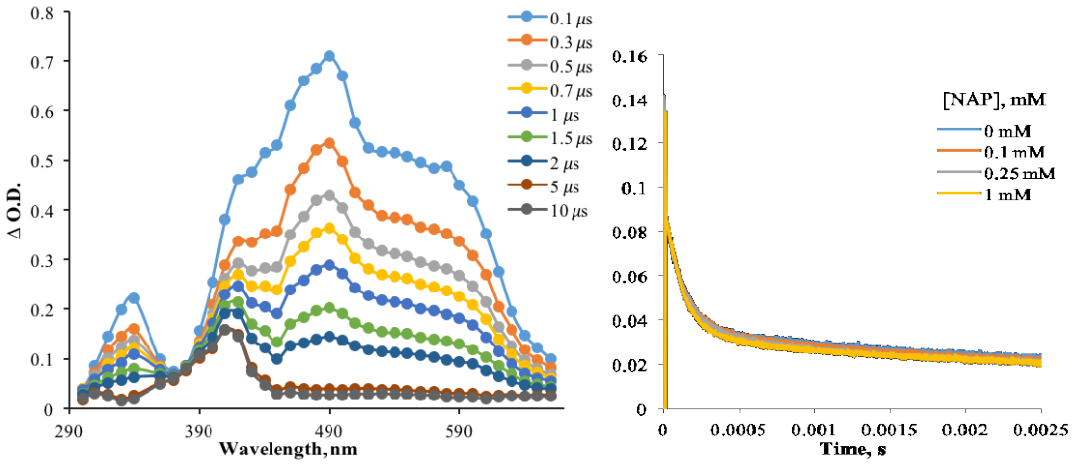

Figure 3.19. *left*: Transient absorption spectra of **2** in iPrOH. *Right*: Waveforms at 410 nm with increasing concentrations of **3**.

Additional experiments were performed to demonstrate that photolysis of the hydroquinone would result in release of carboxylic acid (figure 3.20). First,

compounds **2** and **3** were treated with a mild reducing agent, sodium dithionite, in CD_3OD to form the corresponding hydroquinone. The presence of the hydroquinone was confirmed by UV/Vis (Figure 3.17.). Photolysis of the thermally generated hydroquinone in the presence of **3** results in clean release of the carboxylic acid while control experiments showed no change. (Figure 3.17). Control experiments showed that the formation of free carboxylate requires the presence of the reducing agent and light. Omitting either component leaves the materials unchanged.

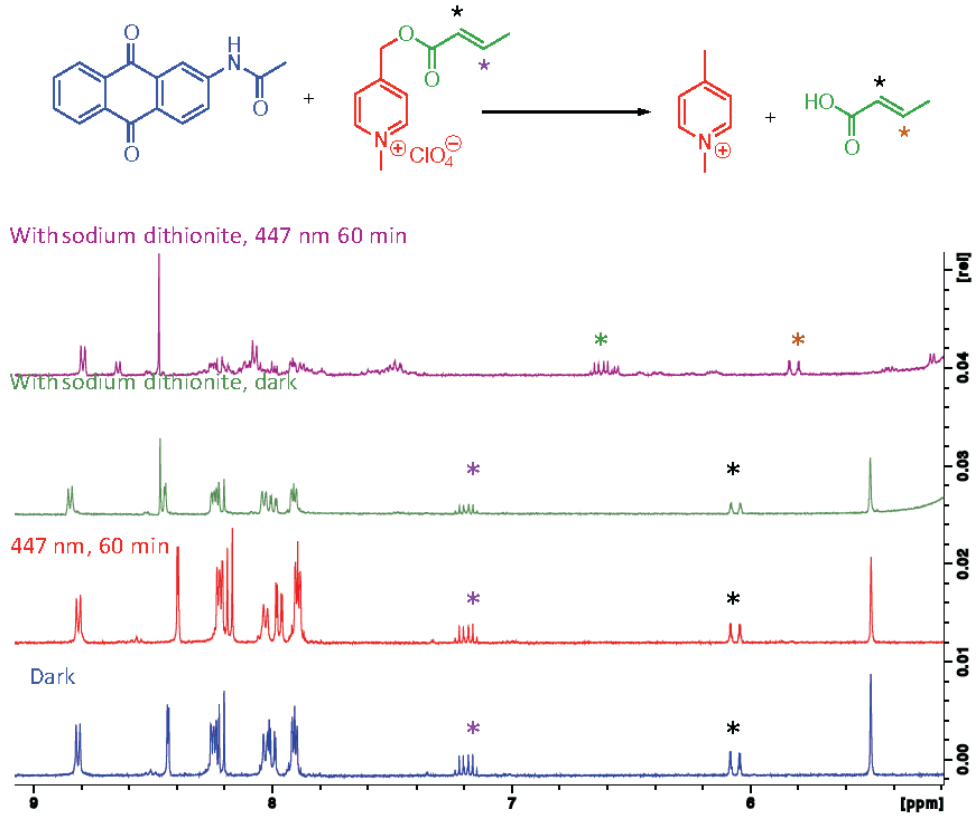

Figure 3.20. ^{1}H NMR spectra showing control experiments preformed with unlinked compounds **2** and **3**. *Blue*: A solution of the two compounds in 2:1 CD_3OD/D_2O in the dark for 60 minutes. *Red*: Photolysis at 447 nm for 60 minutes. *Green*: the hydroquinone was formed by purging the in CD_3OD for 5 minutes with N_2 before adding 0.5 mL of 39 mM sodium dithionite in D_2O via cannula. The solution was

then kept dark for 60 minutes. *Purple*: After reduction with sodium dithionite, the sample was photolyzed at 447 nm for 60 minutes.

3.9 Proposed Mechanism:

A proposed mechanism detailing the stepwise two-photon release of a carboxylic acid is given in figure 3.21. The first photon excites the AQ chromophore to form its first triplet state, PAQ-1^3*, and after hydrogen atom abstraction from the solvent, forms the semiquinone PAQ-1H•. After disproportionation, hydroquinone PAQ-$1H_2$ is formed as the active intermediate. Absorption of a second photon initiates PET to the NAP group and subsequent release of the carboxylate. In the presence of oxygen, PAQ-$1H_2$ is reduced back to the starting material.

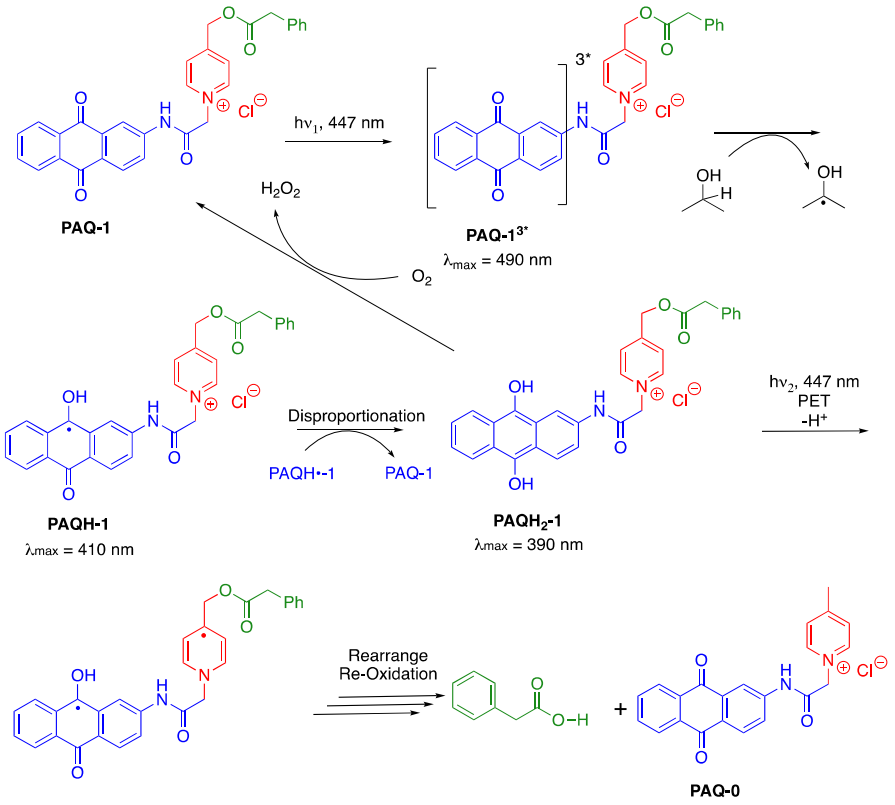

Figure 3.21. Proposed mechanism for photochemical release.

3.10 Conclusions and Future Work:

The results described demonstrate our efforts in the synthesis and characterization of a PRPG based on the well-developed NAP group for carboxylic acids, amines and phosphates. In order to trigger release of a substrate, the NAP group needs to accept an electron from a donor or mediator. By covalently attaching a mediator to the NAP group from which electron transfer is endergonic, a system that requires the stepwise two-photon activation is realized. An anthraquinone-based mediator was chosen because it allows for the reduction of the chromophore with one photon, and subsequent irradiation results in PET to the NAP group and the release of the protected substrate. Control experiments demonstrated that, after absorption of a photon, anthraquinone abstracts an hydrogen atom from the solvent to form semiquinone. The semiquinone is then involved in a disproportionation reaction to form hydroquinone which, upon photolysis can donate an electron to the NAP group to trigger release of a model carboxylic acid. The photolysis was triggered with two-photons of 447 nm light.

Although the system described in this chapter achieved the goal of a step-wise two-photon PRPG, there are numerous areas for improvement. Primarily, although the absorption spectra of anthraquinone and hydroquinone are different, there is no wavelength of light that is able to activate the anthraquinone without also photolyzing the hydroquinone. In order for 3-D control to be achieved, the absorption spectra of the two species must be orthogonal. One possible approach for this could be realized by adapting the system described by the König group in Figure 3.2. The perylene bisimide (PDI) group is unique in that its persistent anion radical has absorption

bands in solution that stretch out into the NIR region of the spectrum. Additionally, its absorption is almost completely orthogonal to the neutral form at high wavelengths (figure 3.22.).

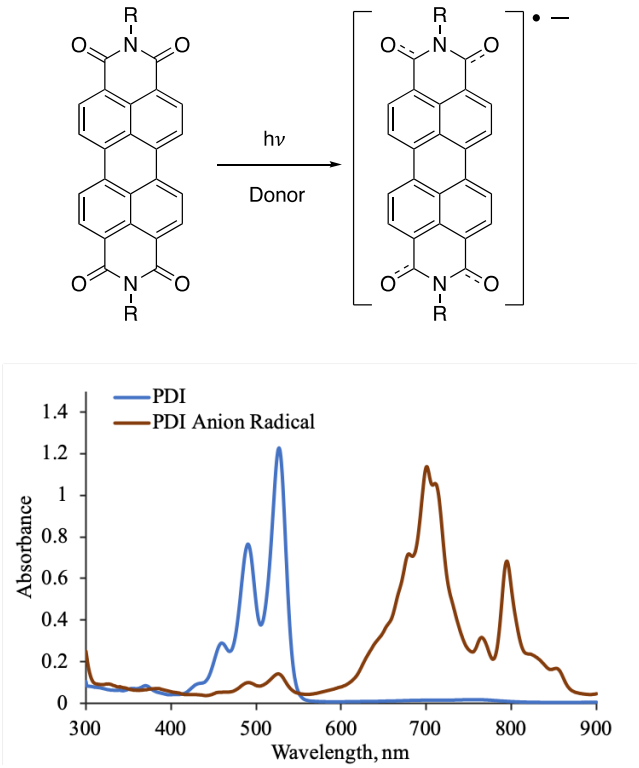

Figure 3.22. The absorption spectra of PDI (*blue*) in DMF. Under N_2, after photolysis at 532 nm for 60 sec (*orange*) in the presence of TEA (20 eq.).

The reduction potential of PDI (-0.43 V vs SCE) is not negative enough to make electron transfer from the anion radical ($PDI^{\bullet-}$) exergonic, and the excited-state redox potential of $PDI^{\bullet-}$, based on the work by König is estimated to be -1.6 V vs SCE which would result in PET to the NAP group (-1.1 V vs SCE)[25,53]. One foreseeable issue is that the excited-state lifetime of $PDI^{\bullet-}$ was estimated to be ca. 145 ps which is not long-lived enough to facilitate intermolecular electron transfer[24].

Therefore, a system would need to be designed in which PDI and the NAP group were covalently attached. Such a system is proposed in figure 3.24.

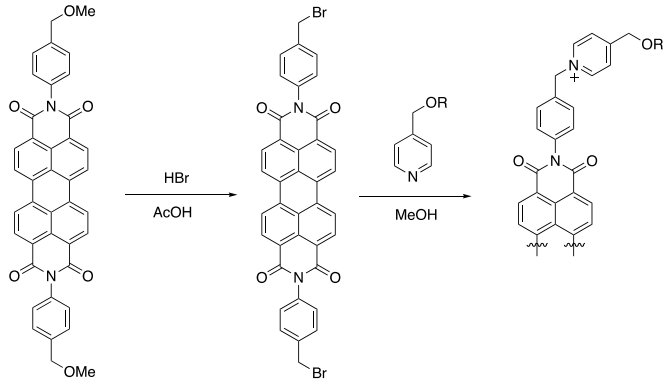

Figure 3.23. Proposed synthesis for a linked PDI-NAP system.

In the proposed system, photolysis of the linked-compound at 532 nm in the presence of an sacrificial electron donor would result in the formation of the reduced chromophore which would persist in the absence of oxygen. Photolysis of the reduced compound at ca. 800 nm would result in electron transfer and eventual release of the substrate. The use of visible and NIR would make competing absorption negligible and allow for a system with precise 3-D control over the reaction area.

3.11 References:

(1) Murov, S. L.; Hug, G. L.; Carmichael, I. *Handbook of photochemistry*; M. Dekker, 1993.

(2) Huppert, D.; Jortner, J.; Rentzepis, P. M. *Chem. Phys. Lett.* **1972**, *13* (3), 225.

(3) Müller, A.; Pflüger, E. *Chem. Phys. Lett.* **1968**, *2* (3), 155.

(4) Scaiano, J. C.; Tanner, M.; Weir, D. *J. Am. Chem. Soc.* **1985**, *107* (15), 4396.

(5) Scaiano, J. C.; Johnston, L. J. *Pure Appl. Chem.* **1986**, *58* (9), 1273.

(6) McGimpsey, W. G.; Scaiano, J. C. *J. Am. Chem. Soc.* **1987**, *109* (7), 2179.

(7) Scaiano, J. C.; Johnston, L. J.; McGimpsey, W. G.; Weir, D. *Acc. Chem. Res.* **1988**, *21* (1), 22.

(8) Wintgens, V.; Johnston, L. J.; Scaiano, J. C. *J. Am. Chem. Soc.* **1988**, *110* (2), 511.

(9) Turro, N. J.; Ramamurthy, V.; Cherry, W.; Farneth, W. *Chem. Rev.* **1978**, *78* (2), 125.

(10) Kobayashi, Y.; Mutoh, K.; Abe, J. *J. of Photochem. and Photobiol. C: Photochem. Rev*. **2018**, *34*, 2.

(11) O'Connor, N. A.; Berro, A. J.; Lancaster, J. R.; Xinyu, G.; Jockusch, S.; Nagai, T.; Ogata, T.; Lee, S.; Zimmerman, P.; Willson, C. G.; Turro, N. J. *Chem. Mater.* **2008**, *20* (24), 7374.

(12) Tasdelen, M. A.; Kumbaraci, V.; Jockusch, S.; Turro, N. J.; Talinli, N.; Yagci, Y. *Macromolecules* **2008**, *41* (2), 295.

(13) Yagci, Y.; Jockusch, S.; Turro, N. J. *Macromolecules* **2010**, *43* (15), 6245.

(14) Jeudy, M. J.; Robillard, J. J. *Opt. Commun.* **1975**, *13* (1), 25.

(15) Mutoh, K.; Nakagawa, Y.; Sakamoto, A.; Kobayashi, Y.; Abe, J. *J. Am. Chem. Soc.* **2015**, *137* (17), 5674.

(16) Kobayashi, Y.; Katayama, T.; Yamane, T.; Setoura, K.; Ito, S.; Miyasaka, H.; Abe, J. *J. Am. Chem. Soc.* **2016**, *138* (18), 5930.

(17) Yamaguchi, T.; Kobayashi, Y.; Abe, J. *J. Am. Chem. Soc.* **2016**, *138* (3), 906.

(18) Kobayashi, Y.; Okajima, H.; Sotome, H.; Yanai, T.; Mutoh, K.; Yoneda, Y.; Shigeta, Y.; Sakamoto, A.; Miyasaka, H.; Abe, J. *J. Am. Chem. Soc.* **2017**, *139* (18), 6382.

(19) Inagaki, Y.; Kobayashi, Y.; Mutoh, K.; Abe, J. *J. Am. Chem. Soc.* **2017**, *139* (38), 13429.

(20) Fujita, M.; Ishida, A.; Majima, T.; Takamuku, S. *J. Phys. Chem.* **1996**, *100* (13), 5382.

(21) Sakamoto, M.; Cai, X.; Kim, S. S.; Fujitsuka, M.; Majima, T. *J. Phys. Chem. A* **2007**, *111* (2), 223.

(22) Cai, X.; Sakamoto, M.; Fujitsuka, M.; Majima, T. *J. Phys. Chem. A* **2007**, *111* (10), 1788.

(23) Breslin, D. T.; Fox, M. A. *J. Phys. Chem.* **1994**, *98* (2), 408.

(24) Marchini, M.; Gualandi, A.; Mengozzi, L.; Franchi, P.; Lucarini, M.; Cozzi, P. G.; Balzani, V.; Ceroni, P. *Phys. Chem. Chem. Phys.* **2018**, *20* (12), 8071.

(25) Ghosh, I.; Ghosh, T.; Bardagi, J. I.; König, B. *Science* **2014**, *346* (6210), 725.

(26) Bardagi, J. I.; Ghosh, I.; Schmalzbauer, M.; Ghosh, T.; König, B. *European J. Org. Chem.* **2018**, *2018* (1), 34.

(27) Eggins, B. R.; Robertson, P. K. J. *J. Chem. Soc. Faraday Trans.* **1994**, *90* (15), 2249.

(28) Nelleborg, P.; Lund, H.; Eriksen, J. *Tetrahedron Lett.* **1985**, *26* (14), 1773.

(29) Pirrung, M. C.; Pieper, W. H.; Kaliappan, K. P.; Dhananjeyan, M. R. *Proc. Natl. Acad. Sci. U. S. A.* **2003**, *100* (22), 12548.

(30) Falvey, D. E.; Sundararajan, C. *Photochem. Photobiol. Sci.* **2004**, *3* (9), 831.

(31) Falvey, D. E.; Sundararajan, C. *Photochem. Photobiol. Sci.* **2004**, *3* (9), 831.

(32) Sundararajan, C.; Falvey, D. E. *Photochem. Photobiol. Sci.* **2006**, *5* (1), 116.

(33) Kunsberg, D. J.; Kipping, A. H.; Falvey, D. E. *Org. Lett.* **2015**, *17* (14), 3454.

(34) Cape, J. L.; Edson, J. B.; Spencer, L. P.; Declue, M. S.; Ziock, H.-J.; Maurer, S.; Rasmussen, S.; Monnard, P.-A.; Boncella, J. M. *Bioconjug. Chem.* **2012**, No. 23, 2014.

(35) Edson, J. B.; Spencer, L. P.; Boncella, J. M. *Org. Lett.* **2011**, *13* (23), 6156.

(36) Borak, J. B.; Falvey, D. E. *J. Org. Chem.* **2009**, *74* (10), 3894.

(37) Borak, J. B.; Falvey, D. E. *Photochem. Photobiol. Sci.* **2010**, *9* (6), 854.

(38) Thum, M. D.; Falvey, D. E. *J. Phys. Chem. A* **2018**, *122* (12), 3204.

(39) Lee, K.; Falvey, D. E. *J. Am. Chem. Soc.* **2000**, *122* (39), 9361.

(40) Sundararajan, C.; Falvey, D. E. *Org. Lett.* **2005**, *7* (13), 2631.

(41) Kunsberg, D. J.; Kipping, A. H.; Falvey, D. E. *Org. Lett.* **2015**, *17* (14), 3454.

(42) Griesbeck, A. G.; Oelgemöller, M.; Ghetti, F. *CRC handbook of organic photochemistry and photobiology*; Taylor & Francis, 2012.

(43) Patai, S.; Rappoport, Z. *Chem. Funct. groups* **1988**, *I*, 878 blz.

(44) Kuss-Petermann, M.; Orazietti, M.; Neuburger, M.; Hamm, P.; Wenger, O. S. *J. Am. Chem. Soc.* **2017**, *139* (47), 5225.

(45) Goulet, M.-A.; Tong, L.; Pollack, D. A.; Tabor, D. P.; Kwan, E. E.; Aspuru-Guzik, A.; Gordon, R. G.; Aziz, M. J. *J. Am. Chem. Soc.* **2019**, jacs. 8b13295.

(46) Zhang, J.; Hill, N.; Lalevée, J.; Fouassier, J.-P.; Zhao, J.; Graff, B.; Schmidt, T. W.; Kable, S. H.; Stenzel, M. H.; Coote, M. L.; Xiao, P. *Macromol. Rapid Commun.* **2018**, *39* (19), 1800172.

(47) Kuss-Petermann, M.; Wenger, O. S. *J. Am. Chem. Soc.* **2016**, *138* (4), 1349.

(48) Lerch, S.; Unkel, L.-N.; Brasholz, M. *Angew. Chemie* **2014**, *126* (25), 6676.

(49) Romero, N. A.; Nicewicz, D. A. *Chem. Rev.* **2016**, *116* (17), 10075.

(50) Görner, H. *Photochem. Photobiol.* **2003**, *77* (2), 171.

(51) Ly, D.; Kan, Y.; Armitage, B.; Schuster, G. B. *J. Am. Chem. Soc.* **1996**, *118* (36), 8747.

(52) Breslin, D. T.; Schuster, G. B. *J. Am. Chem. Soc.* **1996**, *118* (10), 2311.

(53) Sundararajan, C.; Falvey, D. E. *J. Org. Chem.* **2004**, *69* (17), 5547.

Chapter 4: Photophysical Properties of Dithioester and Trithiocarbonate RAFT Agents

Reversible addition fragmentation chain transfer (RAFT) polymerization is a method of controlled radical polymerization that works using dithioester, or trithiocarbonates-based compounds to cap the growing radicals chains and limit termination. For a more complete discussion of RAFT please see chapter 1. This chapter will focus on the photophysical properties of a series of RAFT, or chain transfer (CTA), agents and how they react under direct illumination.

Disulfides were first proposed as iniferters for CRP by Otsu et al. in 1982[1]. In an iniferter, or photoRAFT, mechanism, the CTA is both the source of the propagating radical species as well as the capping agent (Figure 4.1). Since these processes require only CTA and monomer, they are valued due to their simplicity. Photolysis of the CTA is proposed to induce C-S bond homolysis resulting in the formation of a propagating, Z group, radical, and a capping, sulfur-centered radical. Initial reports described photoRAFT carried out under UV irradiation, but the high energy light resulted in unwanted degradation of the CTA, and loss of end group fidelity[2–5]. Attempts to recover relevant photoproducts suggested the formation of CS_2 as a possible degradation pathway, but there is a lack of evidence to support any one decomposition mechanism[5].

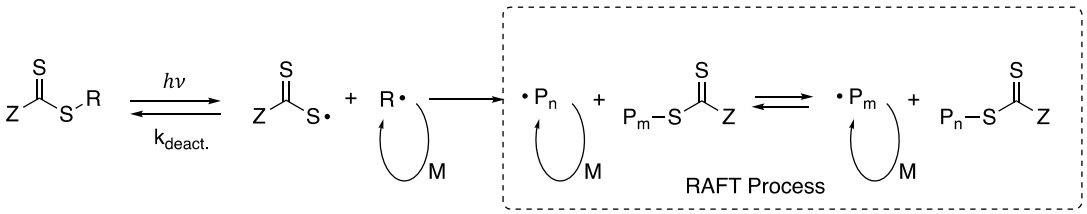

Figure 4.1. Proposed mechanism for the direct photolysis of the RAFT agent to generate well-controlled polymers.

Recently, in an attempt to use lower-energy visible light, trithiocarbonates and some xanthates have emerged as efficient CTAs for visible light photoRAFT. Examples have shown the polymerization of acrylates, acrylamides, and methacrylates mediated by blue light irradiation of trithiocarbonates, and one example of vinyl acetate polymerization mediated by blue light irradiation of xanthates (Z = OR) [6–9].

4.1 Photolytic Stability of CTAs under Visible light Illumination:

Previous studies have attempted to probe the iniferter mechanism by measuring the decomposition rate of various trithio-based CTAs. Qiao et al. determined that the photolytic stability of the RAFT agents was regulated by the nature of the X group as shown in figure 4.2[10]. For example, they demonstrated that a CTA which would form a tertiary X radical could decompose measurably, while one which could form a secondary X radical was unchanged. Interestingly, however, the only dithio-based CTA they studied was found to be photochemically stable under visible light illumination, and, some of the cases where degradation was not observed, such as a case in which a benzyl group was the X group, are known to undergo visible light photo-RAFT polymerization. This suggests that although the compounds appeared to be stable under visible light, it may be those cases are dominated by recombination of the formed radical species and, measuring the degradation in the absence of a trap for the propagating radicals may be misleading. Our work demonstrates that while trithiocarbonates are mildly stable under visible light

illumination, there is a significant solvent cage effect and, in the presence of a monomer to trap the X radical, the observed rate of decomposition increases drastically.

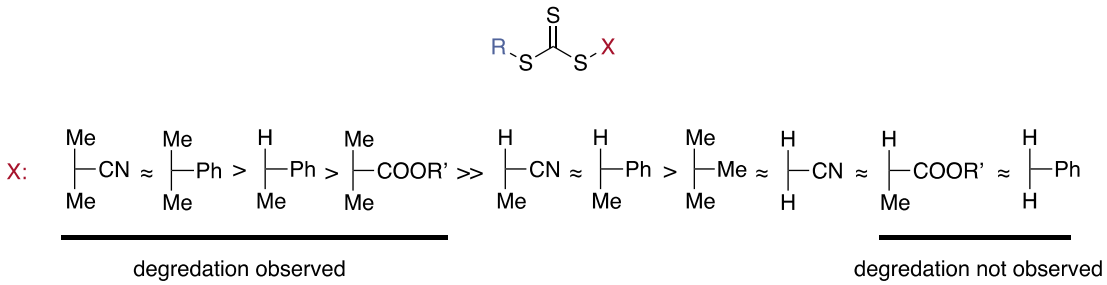

Figure 4.2. Trends of visible light degradation of trithio-based RAFT agents as they relate to the X group.

The first sections of this chapter describes the photophysics of various CTAs as they relate to an iniferter mechanism. The later sections discuss their photophysics as they relate to PET-RAFT as discussed in Chapter 1.

4.2 Absorption and Fluorescence

According to Kasha's rule, fluorescence for organic compunds occurs from the S_1 state, and phosphorescence from the T_1 state. This process is independent of whichever excited-state is initially created. This leads to the general observation that the photophysical properties of most compounds in solution are independent of the wavelength of activation. However, there are some important exceptions. In cases where the $S_2 - S_1$ energy difference is large relative to that of the $S_0 - S_1$ energy difference (or comparable cases involving triplet states) it is possible to observe fluorescence, or phosphorescence, from higher excited-states. Thioketones and azulenes are two well-known examples of S_2 emission, and some anthracenes are

known to phosphoresce from T_2[11–14]. A recent review of chemistry from higher excited-states can be found here[15]. Previous work done by Steven Wolf in our group demonstrated that, using TD-DFT methods on model compounds at the B3LYP/6-311G(d,p) level, there is a significant $S_2 - S_1$ energy gap; 36 kcal/mol and 23 kcal/mol for the dithioesters and trithiocarbonates respectively. To determine if these effects could be seen in various CTAs, computational and spectroscopic measurements were performed. The computational work was done by Steven Wolf on model CTA's and will be referenced extensively in this chapter. For more information, please see the following reference[16].

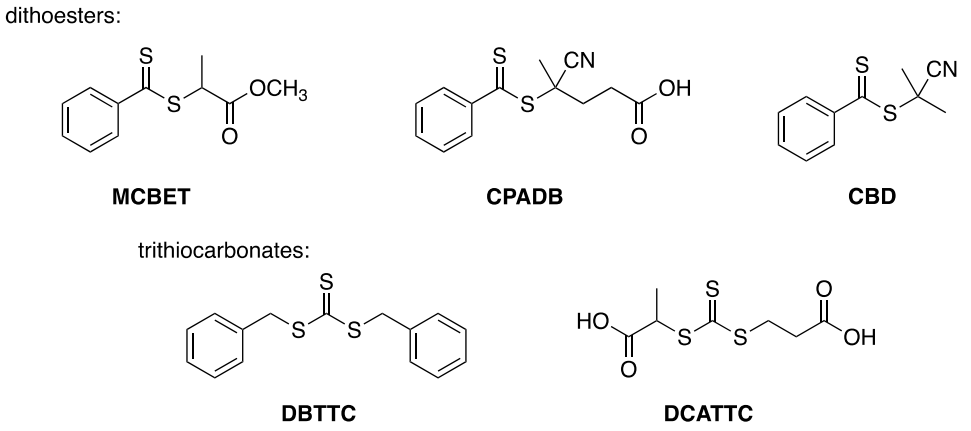

Figure 4.3. Selected CTA's to be studied in this work.

The UV/vis absorption spectra of the dithioester CPADB and the trithiocarbonate DBTTC are given in figure 4.4. Dithioesters show a weak ($\varepsilon = 120$ $M^{-1}cm^{-1}$) n-π* absorption band at ca. 520 nm and a strong ($\varepsilon = 13000$ $M^{-1}cm^{-1}$) π-π* band at 300 nm. Similarly, the trithiocarbonates have weak ($\varepsilon = 100$ $M^{-1}cm^{-1}$) visible light absorption band at 450 nm, and a much stronger ($\varepsilon = 20000$ $M^{-1}cm^{-1}$) band at 300 nm.

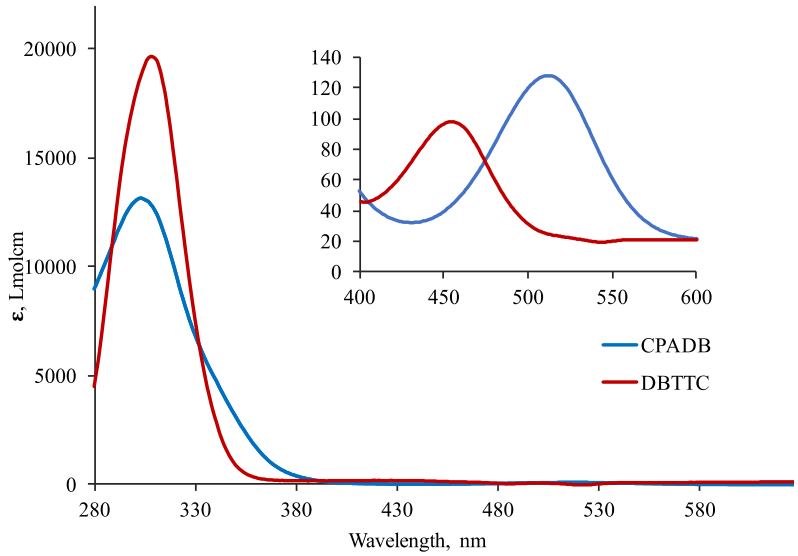

Figure 4.4 Absorption spectra of CPADB and DBTTC in EtOH.

Both the dithioesters and the trithiocarbonates exhibit weak fluorescence from S_2. The fluorescence spectra of the CTA's are shown in figure 4.5. For CPADB and MCEBT (both dithioesters), upon excitation at 300 nm (into S_2), a weak emission is seen with a λ_{max} at 460 and 440 nm respectively. In case of the trithiocarbonates, DBTTC and DCATTC, excitation into S_2 at 300 nm results in a weak emission at 348 and 343 nm respectively. For each CTA studied, excitation into S_1 (512 and 470 nm for the dithioesters and trithiocarbonates respectively) results in no measurable emission. As shown in Table 4.1, when compared with an acridine standard, the emission intensities were found to be very weak, with Φ_{em} all $<10^{-4}$. These results are consistent with a previous report by Steer et al who measured the Φ_{em} of CPDB to be 0.00069[17].

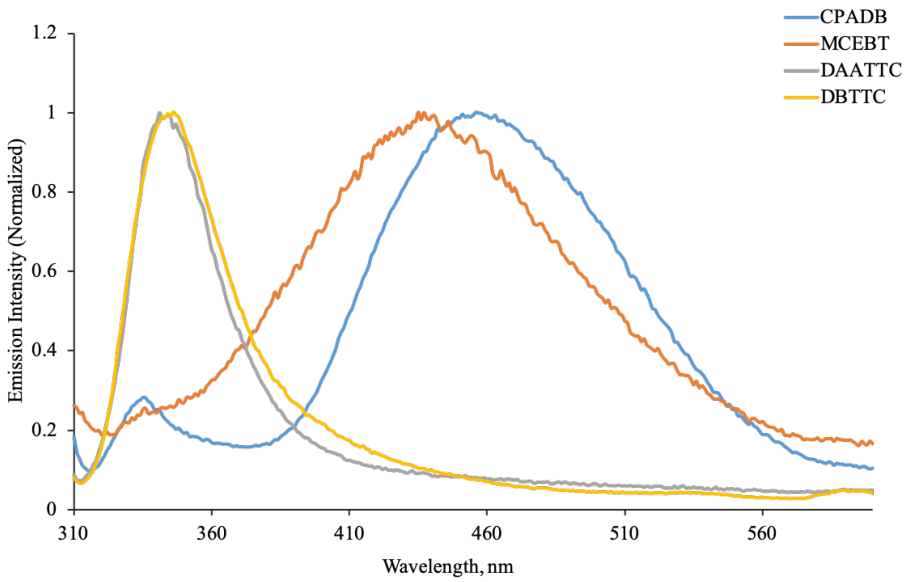

Figure 4.5 Emission of CTA's after 300 nm excitation.

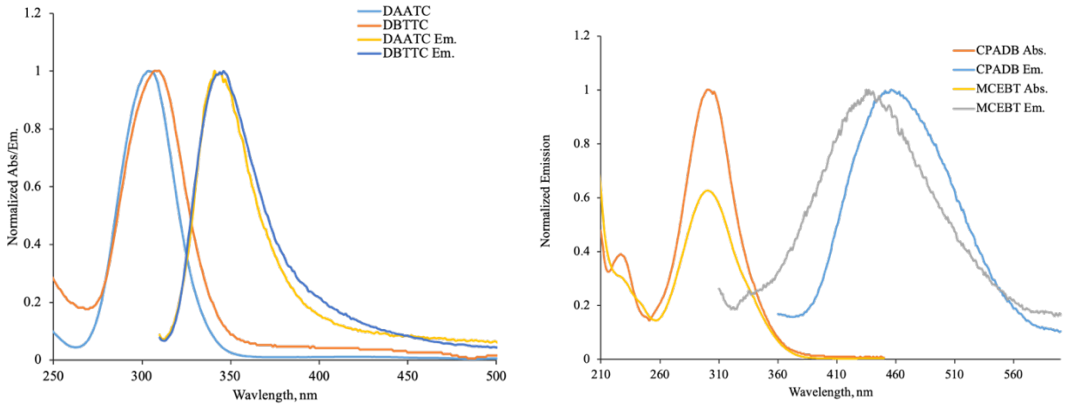

Figure 4.6. *left*: Normalized absorption and emission of trithiocarbonates. *right*: Normalized absorption and emission of dithioesters.

Table 4.1. Experimental Photophysical parameters of CTA's

	CPADB	MCEBT	DBTTC	DCATTC
$\lambda_{max,\ S2}$ (nm)	303	301	308	304
ε_{S2} ($L*mol^{-1}cm^{-1}$)	13,134	11,109	19,624	14,544
E_{S2} (kcal/mol)	82.3	85.3	86.9	87.9
$\lambda_{max,\ S1}$ (nm)	512	494	433	431

ε_{S1} (L*mol^{-1}cm^{-1})	120.5	101.1	53.4	37.8
E_{S2} (kcal/mol)	51.2	52.8	61.2	60.6
$\lambda_{Em,\ max}$ (nm)	435	456	344	341
Φ_{em}[a]	6.4x10^{-4}	3.7x10^{-5}	7.5x10^{-5}	1.4x10^{-4}

[a]Relative quantum yields measured against acridine (Φ_{em}= 0.0047), in EtOH

4.3 Degradation Under Direct Photolysis:

As discussed earlier, the photoiniferter process involves direct irradiation of the CTA resulting in C-S bond cleavage and the formation of a propagation radical species and a deactivating end group. Although, as discussed in section 4.1, the photolytic stability of the CTA's under visible light illumination are determined primarily by the Z-group, little work has been done on the contribution of higher excited-states to the photochemical degradation of CTA's. Our work demonstrates that, in the case of dithioesters, excitation into S_2, but not S_1, is the primary pathway for decomposition, and contributions due to S_1 are minor.

The degradation of CPADB in CD_3CN was monitored by ^{1}H NMR. The ^{1}H NMR spectrum, shown in figure 4.8 and 4.9, of a solution of CPADB was photolyzed under broadband irradiation at 350 nm (16 bulb, 35 W) or 532 nm (CW diode, 100 mW). Irradiation into S_2 using 350 nm light results in complete decomposition of the RAFT agent after an hour of photolysis while no change was observed after 4 hrs of photolysis at 532 nm and little change is noticed after 16 hrs of photolysis.

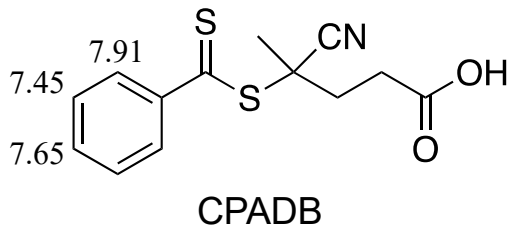

Figure 4.7. ^{1}H NMR assignments (in ppm) for degradation experiments shown in this study.

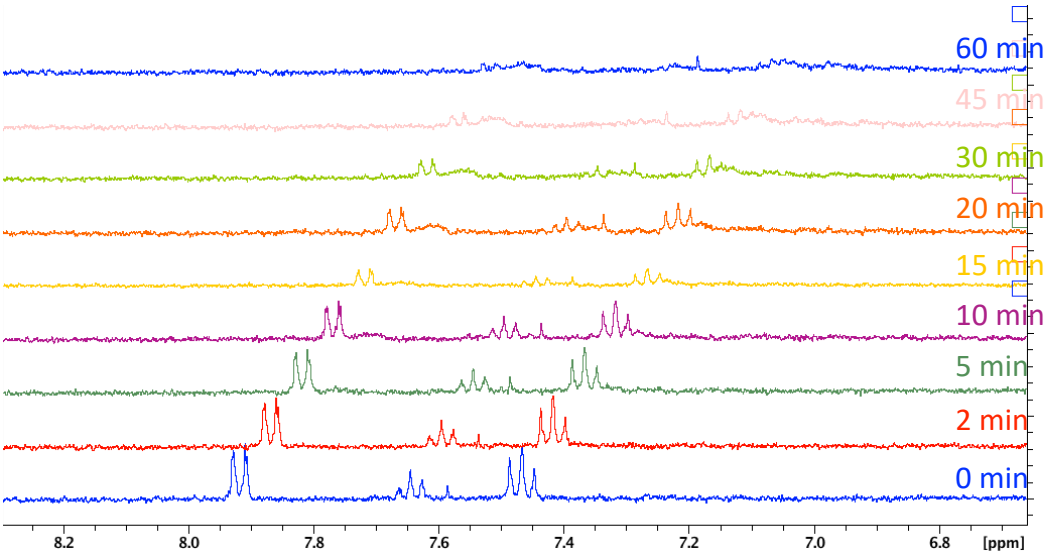

Figure 4.8. ^{1}H NMR of CPADB in CD_3CN photolyzed at 350 nm for the illustrated amount of time.

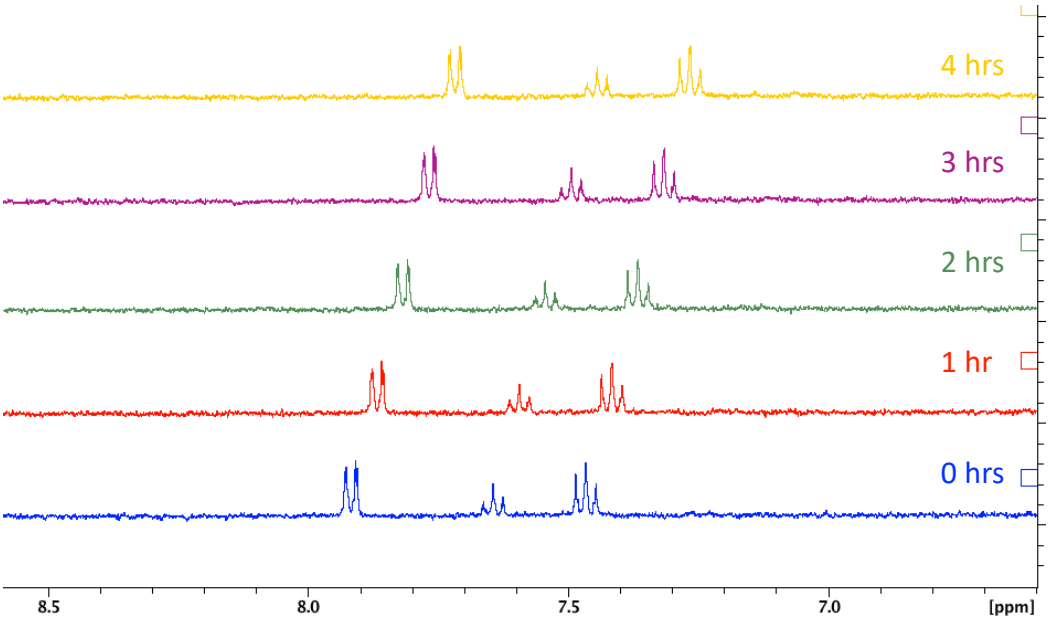

Figure 4.9. ^{1}H NMR of CPADB in CD_3CN photolyzed at 532 nm for the illustrated amount of time.

In order to examine multiple wavelengths of irradiation, photolysis of CPADB was performed using a variable power Ti:Sapphire laser, and its conversion was monitored using high pressure liquid chromatography (HPLC) against a calibration curve (See chapter 6). An N_2 purged solution of CPADB in MeCN was photolyzed at 10 Hz and the laser power was attenuated to output a similar total laser dose at each wavelength. After photolysis, conversion was measured by HPLC. Irradiation with visible light, despite CPADB having a measurable absorbance, showed very little degradation. However, UV photolysis at 380 nm showed significant loss of substrate, and photolysis at 300 nm resulted in almost complete decomposition.

Table 4.2 Wavelength Dependent Photolysis of CPADB in MeCN

Wavelength, nm	[CPADB], M	ε, $L*mol^{-1}cm^{-1}$	Absorbance	[a]Laser Dose, J	[b]Conversion
540	0.0057	94	0.353	10.86	3.4%
500	0.0057	103	0.549	11.93	3.1%
450	0.0057	43	0.097	13.54	3.8%

380	0.0057	421	0.542	10.54	19.7%
300	0.00114	12962	1.475	11.84	99.0%

[a]Photolysis performed with a variable power Ti:Sapphire Laser [b]Conversion followed by HPLC

4.4 Free Radical Cage Effect and Photodissociation Quantum Yields:

One observation that supports the idea of C-S bond dissociation is the presence of a free radial cage effect. As shown in figure 4.10, the degradation of CPADB in MeCN alone is an order of magnitude slower than experiments performed with added methyl methacrylate (MMA). The monomer acts as a radical scavenger for the alkyl radicals forming PMMA. Figure 4.12 shows photolysis in the presence of a monomer (methyl methacralate, MMA) resulted in the formation of polymer as a broad peak at 3.6 ppm (poly-methyl mehtacrylate, PMMA), while no such obervation was made under visible light photolyisis.

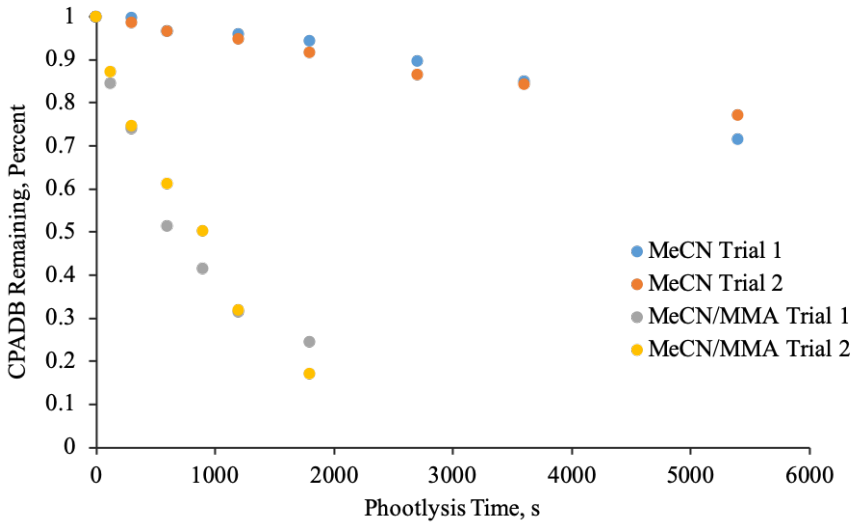

Figure 4.10. Comparison of decomposition of CPADB in MeCN and MeCN/MMA under 350 nm irradiation.

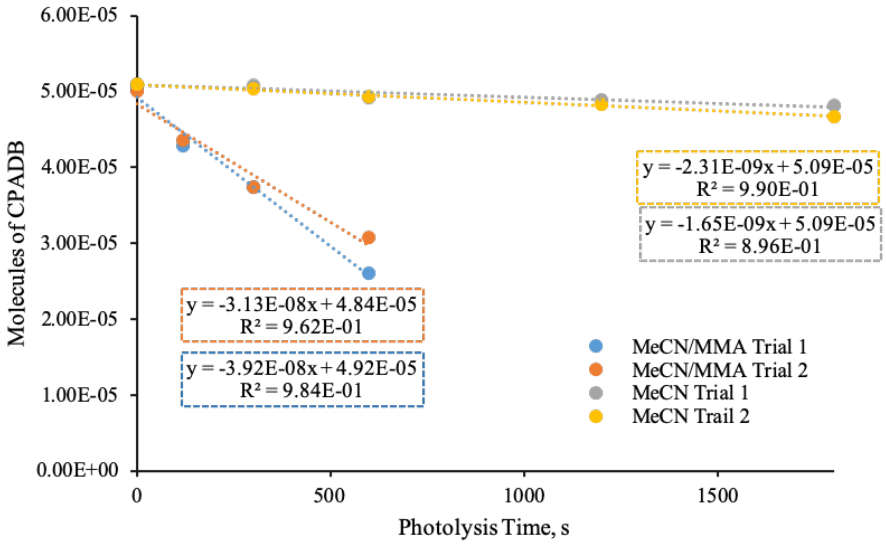

Figure 4.11. Initial decay rates of CPADB in MeCN and MeCN/MMA

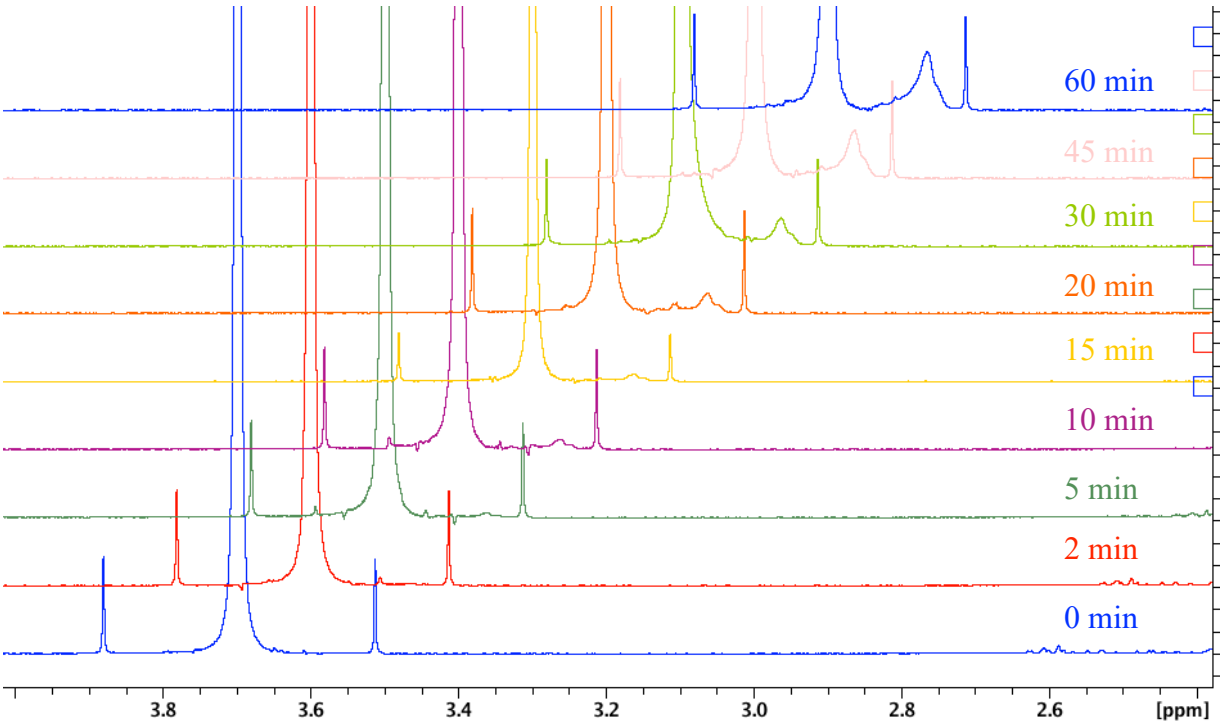

Figure 4.12. ^{1}H NMR of CPADB in CD_3CN photolyzed at 350 nm for the illustrated amount of time showing the conversion of MMA (at 3.7 ppm) to PMMA (at 3.6 ppm)

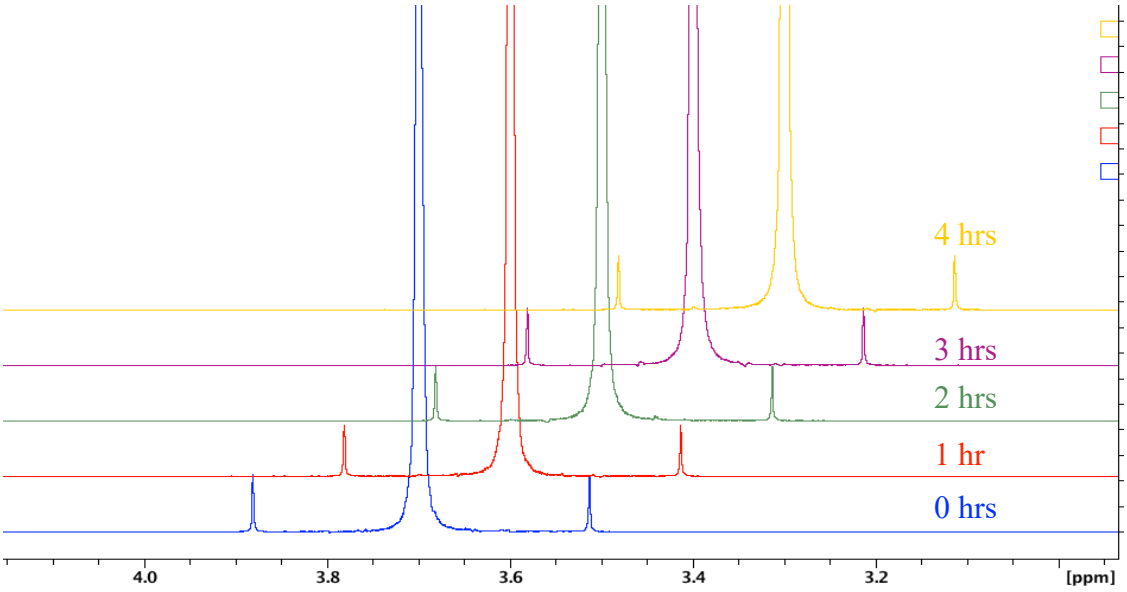

Figure 4.13. ^{1}H NMR of CPADB in CD_3CN photolyzed at 532 nm for the illustrated amount of time showing no conversion of MMA (at 3.7 ppm) to PMMA (at 3.6 ppm)

The decomposition under UV irradiation of selected CTA's is given below. Unless otherwise noted, the decomposition experiments for all of the CTA's discussed below were performed as follows: A 3 mL solution (in a vial for the Rayonet photolysis and a quartz cuvette for the laser photolysis) of the CTA, 17 mM in a 1:1 MeCN/MMA mixture with t-butyl alcohol as an internal standard, was purged with N_2 for 10 min in the solution and an additional 5 min in the headspace. The vial was then photolyzed for the appropriate amount of time when, while purging, a 50 µL aliquot was removed. This aliquot was measured in one of two ways. For ^{1}H NMR analysis: From this aliquot, 10µL was added to 0.5 mL of CD_3CN before measuring the sample on a 400 mHz NMR. For HPLC analysis: From this aliquot, HPLC (C18 column, 85:15 MeCN/H_2O, 1.5 mL/min) was performed and compared to a calibration curve. Figure 4.14 compares the decomposition rates of CTA's in the under UV photolysis (350 nm) in a mixture of MMA/MeCN. Based on

the decomposition data, the quantum yields for decomposition (Φ_D) of the RAFT agents were measured as shown in table 4.3. Azobenzene actinometry was used to calibrate the light output.

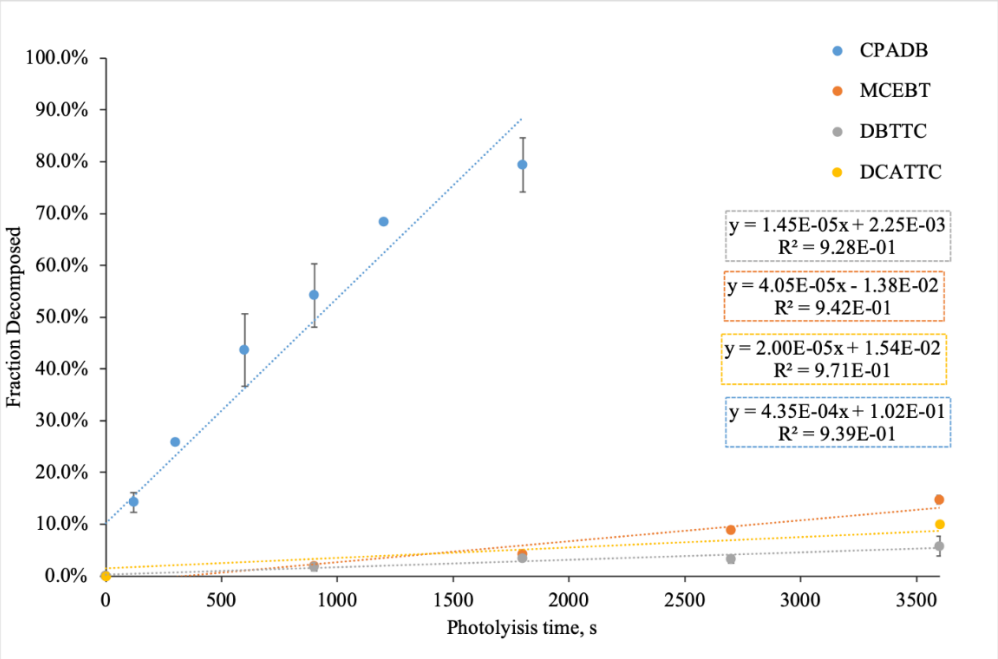

Figure 4.14. Decomposition rates of CTAs under 350 nm photolysis.

Table 4.3 Quantum Yield of Decomposition (Φ_D) at 350 nm (S2 Irradiation)[a]

Compound	Φ_D
CPADB	0.003[b,c], 0.004[b,d]
CPADB	0.050[c,e]
MCEBT	0.004[d,e]
DBTTC	0.0001[d,e]
DCATTC	0.0002[c,e]

[a]Quantum yields calculated with respect to Azobenzene ($\Phi_{D,UV} = 0.11$)
[b]in MeCN, [c]Measured by ^{1}H NMR, [d]Measured by HPLC [e]in MeCN/MMA

All CTA's studied show measurable decomposition upon UV light photolysis. Much like previous reports on dithiocarbonates, The stability of the Z radical plays a role in the photolytic stability. For the dithioesters, CPADB decomposes more readily than MCEBT because the Z radical formed is tertiary for CPADB and secondary in the case of MCEBT. The trithiocarbonates explored in this study were not measurably different from one another, but all decomposed at least an order or magnitude slower than the dithioesters.

4.5 Photoproduct Analysis:

Photoproducts from CTA degradation have never been fully explored[18]. Our work used photoproduct analysis in the characterization of the dimeric product, DTBDS, which is a result of the coupling of two dithiobenzoate radicals (Figure 4.15). This was observed by HPLC and ^{1}H NMR upon 350 nm photolysis of CPADB in MeCN (Figure 4.15). As a photoproduct, DTBDS was never observed in excess of 25% yield, but control experiments on an independently synthesized sample show that DTBDS degrades under the photolysis conditions.

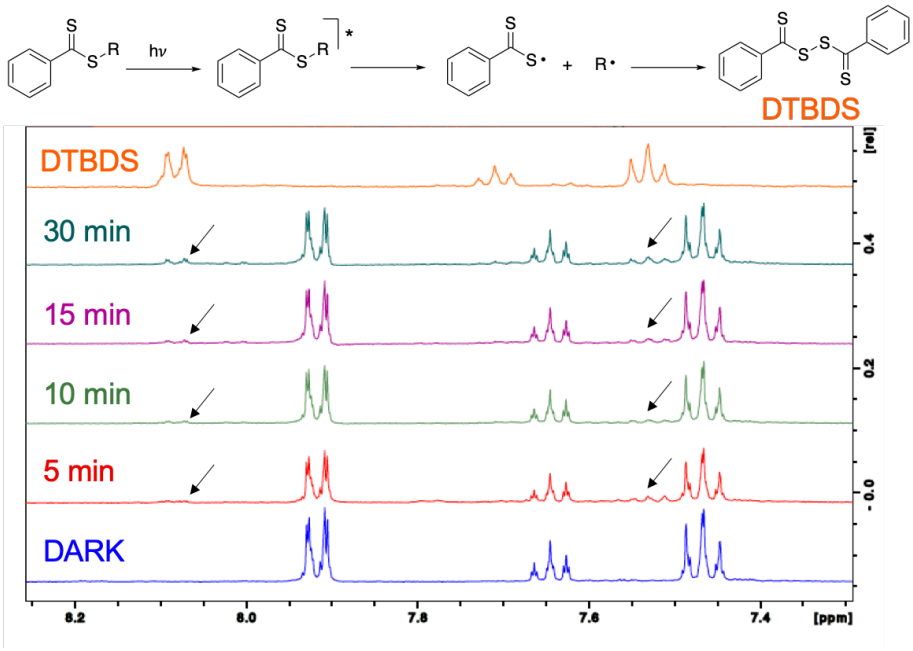

Figure 4.15. ^{1}H NMR showing photolysis of CPADB in MeCN at 350 nm for the allotted amount of time. The formation of DTBDS can be seen as a peak at 8.09 and 7.55 ppm.

4.6 Calculated BDEs for Model CTA's:

Previous work done by our group used DFT calculations to estimate the bond dissociation energies associated with C-S bond homolysis for trithiocarbonates and dithioesters[16]. These results are summarized in Figures 4.16 and 4.17. Previous attempts at predicting the stability of sulfur centered radicals have similarly shown the effect of the substituted as shown below[19].

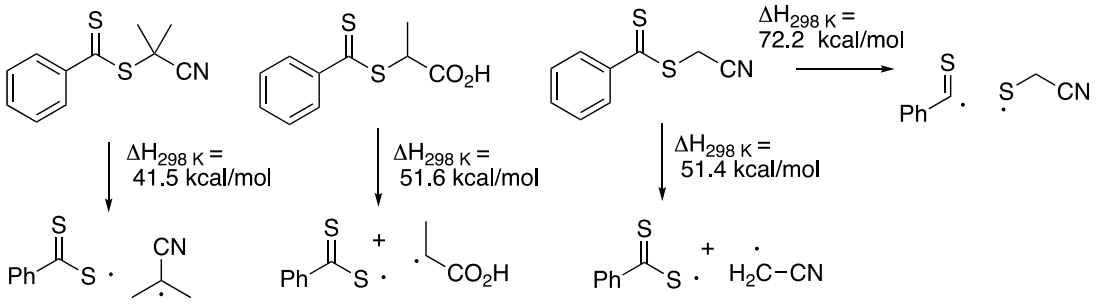

Figure 4.16. S-C BDEs for dithioesters calculated at the MN12SX/6-311++G(d,p) level. Computations performed by Steven Wolf.

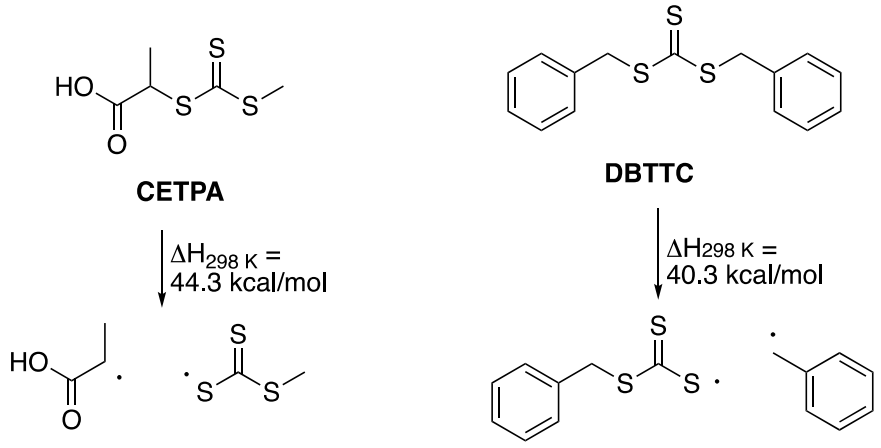

Figure 4.17. S-C BDEs for trithiocarbonates calculated at the MN12SX/6-311++G(d,p) level. Computations performed by Steven Wolf.

4.7 Triplet Energy Transfer:

As discussed in the Chapter 1, one of the main mechanisms proposed for the activation of the CTA in PET-RAFT is triplet energy transfer from the excited-state sensitizer to the CTA resulting C-S bond dissociation. Calculations on model compounds predict low-lying T_1 states at 33 and 44 kcal/mol for the model dithioester and trithiocarbonate respectively as shown in Figure 4.18.

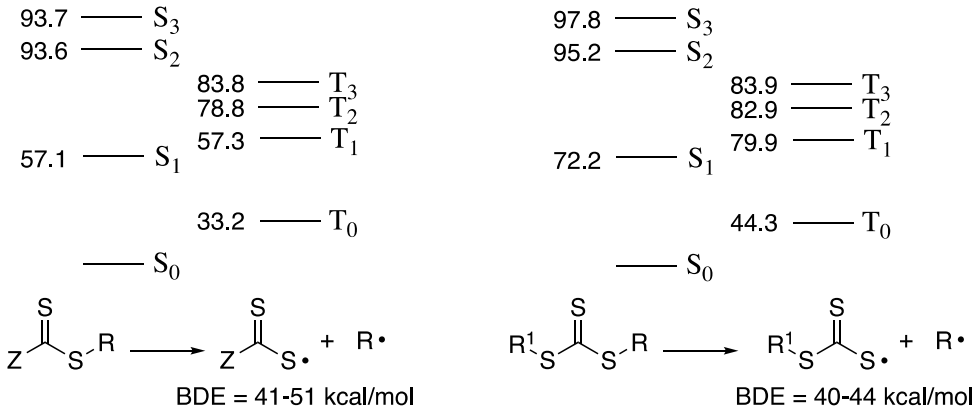

Figure 4.18. Excited-state energies of a model dithioester (left) and dithiocarbonate (right). Calculations performed at the (u)MN12SX/6-311G++(d,p)//(u)MN12SX/6-31G(d) level by Steven Wolf.

In order to determine if C-S bond dissociation from the triplet of common CTAs would be exergonic, LFP measurements were carried out to estimate their triplet excited-state energy. Figure 4.19 shows the spectra from pulsed photolysis (532 nm, 80-90 mJ/pulse, 5-7 ns) of Eosin Y, a common photosensitizer, in 3:2 Water/EtOH. The spectrum is assigned to the triplet state on the basis of previous reports[20]. Figure 4.20 shows a waveform at 570 nm assigned to the triplet of Eosin Y with increasing concentrations of CPADB and the dependence of the psudeo-first order decay rate constant on the concentration of CPADB gives a rate of energy transfer of 3.31×10^8 s^{-1}. The results for all photosensitizers studied are shown in table 4.4 for CPADB and table 4.5 for DBTTC. Unless noted otherwise triplet energies of sensitizers were previously reported[21,22].

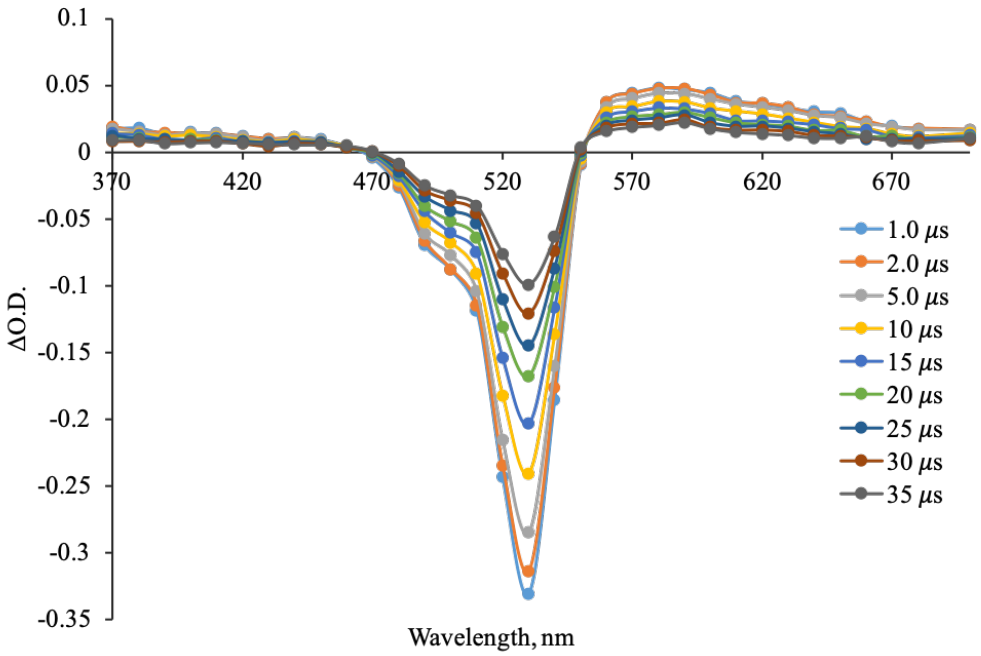

Figure 4.19. Transient absorption spectra of Eosin Y in 3:2 H_2O/EtOH, 532 nm photolysis.

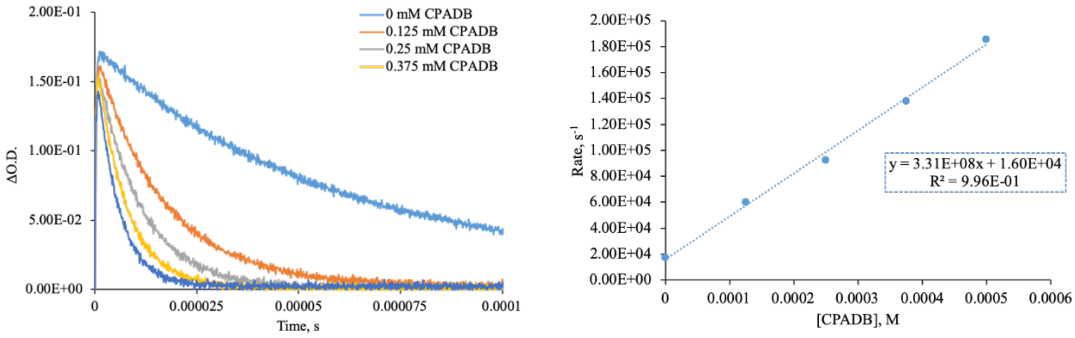

Figure 4.20. *left*: Waveforms at 570 nm of Eosin Y with increasing concentrations of CPADB (0 to 0.375 mM). *right*: Rate constants from pseudo-first order analysis to determine the rate of energy transfer.

Table 4.4. Benchmarking the triplet energy of CPADB

Photosensitizer	Triplet Energy (kcal/mol)	Rate, $M^{-1}s^{-1}$

Thioxanthone[a]	63.3	7.86E+09
Anthraquinone-2 acetanaline[a]	63.7[d]	3.42E+09
Acridine[c]	45.0	1.93E+09
Eosin Y[b]	42.3	3.31E+08
Rose Bengal[c]	41.5	5.31E+08
Zinc-Tetraphenyl Porphine[c]	36.6	1.40E+08
Methylene Blue[c]	33.0	<1E+06

[a]Measured in Benzene. [b]Measured in 3:2 EtOH/H_2O. [c]Measured in MeCN [d]Energy calculated using (U)MO62X/6-311+G(d,p)

Table 4.5. Benchmarking the triplet energy of DBTTC

Photosensitizer	Triplet Energy (kcal/mol)	Rate, $M^{-1}s^{-1}$
Thioxanthone[a]	63.3	1.61E+10
Benzil[a]	54.3	1.44E+08
Pyrene[a]	48.4	7.13E+07
Acridine[a]	45.0	<1E+06
Eosin Y[b]	42.3	<1E+06
Rose Bengal[a]	41.5	<1E+06

[a]Measured in MeCN. [b]Measured in DMSO.

The behavior reported in Tables 4.4 and 4.5 is consistent with the calculated values of the triplet energy of model compounds. For CPADB, there is measurable quenching for sensitizers with E_T above 33.0 kcal/mol, and for DBTTC, there is measurable quenching for sensitizers with E_T above 48.4 kcal/mol. Although exact triplet energies cannot be calculated with the data presented, the onset of measurable quenching is near the predicted values of 33 and 44 kcal/mol for the model dithioester and trithiocarbonate respectively.

In the case of a dithioester, the value predicted for T_1, 33 kcal/mol, is lower in energy than the predicted BDE of 41.6 kcal/mol given in figure 4.16. Conversely, the predicted T_1 for the model trithiocarbonate, 44 kcal/mol, has more than enough energy to break the C-S bond (40.3 kcal/mol) as shown in figure 4.17. To further examine the extent to which T_1 plays a role in the photodissociation, a series of experiments were performed where the decomposition was measured after T_1 was generated indirectly through energy transfer from a photosensitizer. As shown in figure 4.21, photolysis of Rose Bengal ($E_T = 41.5$ kcal/mol, $k_{q,\,CPADB} = 5.31 \times 10^8\ s^{-1}$) at 532 nm in the presence of CPADB results in negligible decomposition when compared to a control experiment without sensitizer.

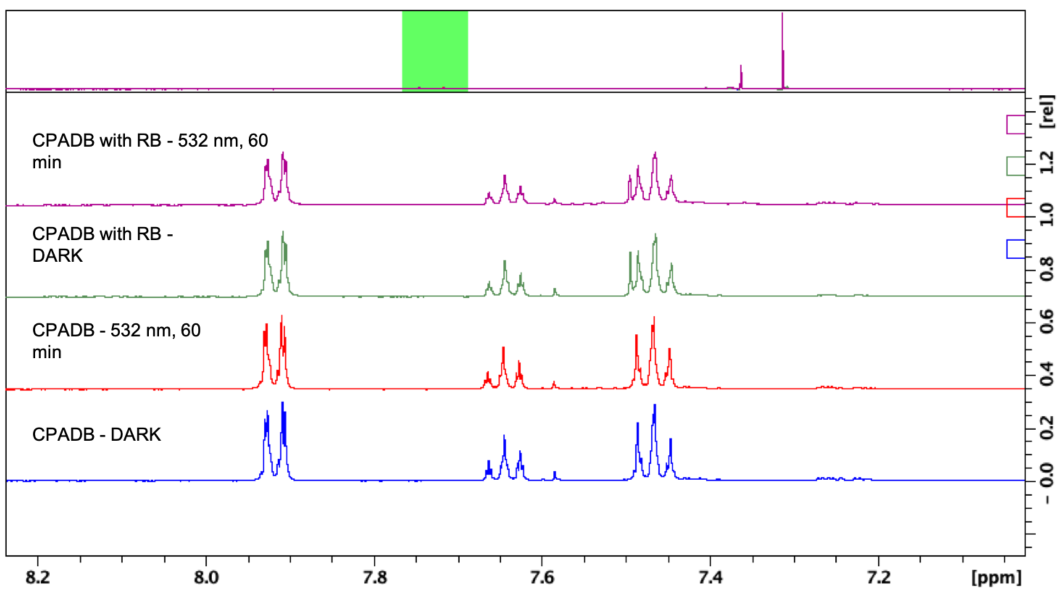

Figure 4.21. *Red and Blue*: H^1 NMR Spectra from photolysis of CPADB in CD_3CN at 532 nm under N_2. *Green and Purple*: H^1 NMR Spectra from photolysis of CPADB in CD_3CN with RB at 532 nm under N_2.

Trithiocarbonates, on the other hand have a predicted triplet energy (44.3 kcal/mol) greater than that of the predicted BDE (40-44 kcal/mol). This suggests that

BDE from the excited CTA may be exergonic. In fact, as discussed in section 4.1, trithiocarbonates are well known to initiate polymerization via an iniferter mechanism when photolyzed with visible light. In order to examine whether triplet sensitization lead to a greater degree of dissociation of the CTA, the decomposition of DBTTC was measured after visible light photolysis in the presence of a thioxanthone (E_T = 63.3 kcal/mol, $k_{q,\ DBTTC} = 1.61x10^{10}\ s^{-1}$). As shown in figure 4.22, sensitized photolysis of thioxanthone and DBTTC in CD_3CN does not result in increased CTA decomposition. Additionally, in a separate experiment, when monomer was added (Table 4.6), no increase in monomer conversion was observed. This suggests that, although the trithiocarbonates are capable of C-S bond dissociation from T_1, the quantum yield from T_1 is too low to result in a meaningful difference in the direct and sensitized experiments.

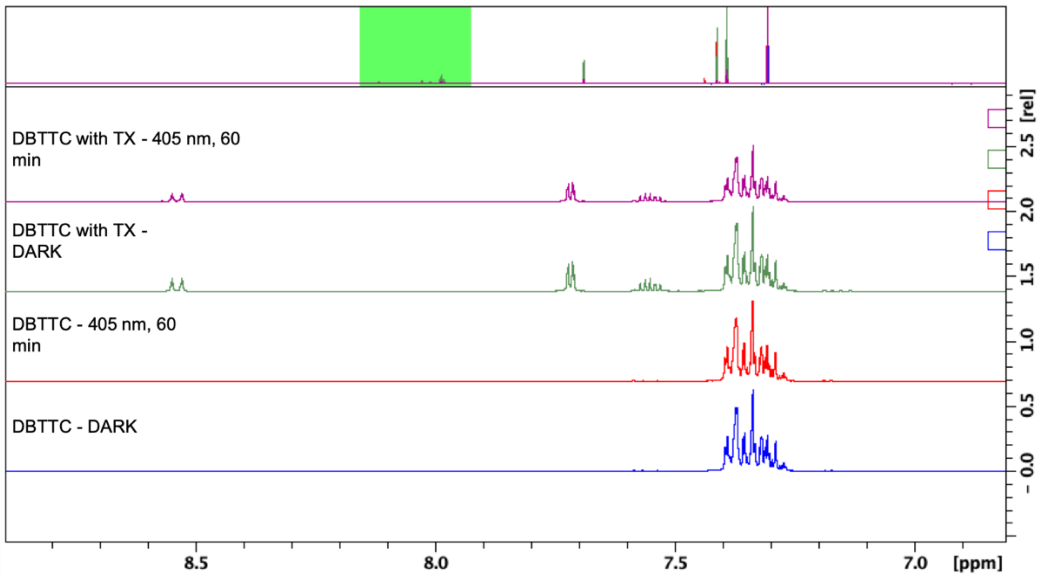

Figure 4.22. *Red and Blue*: H^1 NMR Spectra from photolysis of DBTTC in CD_3CN at 405 nm under N_2. *Green and Purple*: H^1 NMR Spectra from photolysis of DBTTC in CD_3CN with TX at 405 nm under N_2.

Table 4.6 Polymerization of MMA Under Direct and Sensitized Photolysis of DBTTC

MMA[a]/DBTTC/TX	Photolysis time, hrs[b]	Conv.
200/1/0	5	27.6%
200/1/0.5	5	30.7%

[a]Reactions performed in 1/1 MeCN/MMA. [b]100 mW 405 nm CW Diode laser

4.8 Evidence for Chemistry from T2 in Dithioesters:

Fluorescence and decomposition experiments using dithioesters demonstrate the participation of higher excited-states in the photophysics. As discussed earlier, T_1 sensitization and visible light photolysis (population of S_1), of a dithioester does not result in significant decomposition. This is presumably due to the low energy T_1 relative to C-S BDE. In an attempt to determine if higher triplet states contribute to decomposition, the degradation of CPADB was measured after sensitization to either T_1, or T_2, using different sensitizers (Table 4.7). The triplet state of acridine was shown to be quenched by CPADB near the diffusion limit, but excited-state acridine only has enough energy to sensitize T_1 of the CTA. Similarly, the triplet state of thioxanthone was shown to be quenched by CPADB, but excited-state thioxanthone has enough energy to sensitize T_2.

Table 4.7. Quenching T_1 of various sensitizers with CPADB

Photosensitizer	Triplet Energy (kcal/mol)	k_q, s^{-1}
Thioxanthone[a]	63.3	7.86E+09
Acridine[b]	45.0	1.93E+09
CPADB, T_1	37.3	-
CPADB, T_2	57.2	-

[a]Measured in Benzene. [b]Measured in MeCN

Solutions of sensitizer in MeCN were made so that their absorbance at 355 nm was greater than 4 in order to limit background absorption by the CTA in the sensitized experiments. Samples of CPADB and sensitizer were photolyzed with a pulsed 355 nm laser (90 mJ, 5-7 ns) for 60 sec. The decomposition of CPADB, and the formation of the dimer, DTBDS, was measured by HPLC (Table 4.8). Significant background degradation of CPADB and formation of DTBDS was observed in the absence of a sensitizer as shown in entries 2 and 3. With the addition of acridine (a T_1 sensitizer), the extent of decomposition drops significantly and there is no noticeable formation of dimer. Indeed, in the presence of air (Table 4.8, entry 4), there is almost no degradation observed suggesting that T_1 of CPADB is unable to undergo C-S bond homolysis efficiently. On the other hand, with the addition of thioxanthone (a T_2 sensitizer) the conversion and dimer formation is comparable to background despite a significant portion of the light being absorbed by the sensitizer.

Table 4.8. Quenching T_n of various sensitizers with CPADB

Entry	Photosensitizer	Atmosphere	Conversion[a,b]	Yield, DTBDS[a,b]
1	Dark	Air	<1%	<1%
2	None	Air	41.0%	20.6%
3	None	N_2	31.6%	32.6%
4	Acridine	Air	1.3%	<1%
5	Acridine	N_2	11.5%	<1%
6	Thioxanthone	Air	20.0%	<1%
7	Thioxanthone	N_2	33.1%	30.3%

[a]Measured in MeCN, [b]Measured by HPLC, *Photolysis with 355 nm Nd:YAG Laser for 60 sec.

These results demonstrate that, for the dithioesters, much like on the singlet manifold, it is higher excited-states which are primarily responsible for the observed degradation and C-S bond homolysis. Sensitization to T_1 with rose bengal, or acridine, does not result in significant decomposition while degradation is observed when using high energy triplets capable of sensitizing T_2.

4.9 Chemical Reduction:

An alternatively proposed strategy in PET-RAFT is through reduction of the CTA resulting in bond C-S bond homolysis as discussed in Chapter 1. In order to predict the likelihood of PET, the ground-state reduction potential of the CTAs must be accurately determined. There has been some confusion in the literature as to the value of the reduction potentials, with initial reports citing it as low as -0.4V vs. SCE for CPADB[23–26], but the experiments discussed herein agree with a very recent report by Allonas et al. in which they were measured by cyclic voltammetry (CV) to be >-0.9 V vs SCE[27]. Solutions of the CTAs were examined by CV, in the presence of ferrocene for calibration, and the results are compiled in table 4.9. Figure 4.23 shows the CV of varying concentrations CPADB in MeCN.

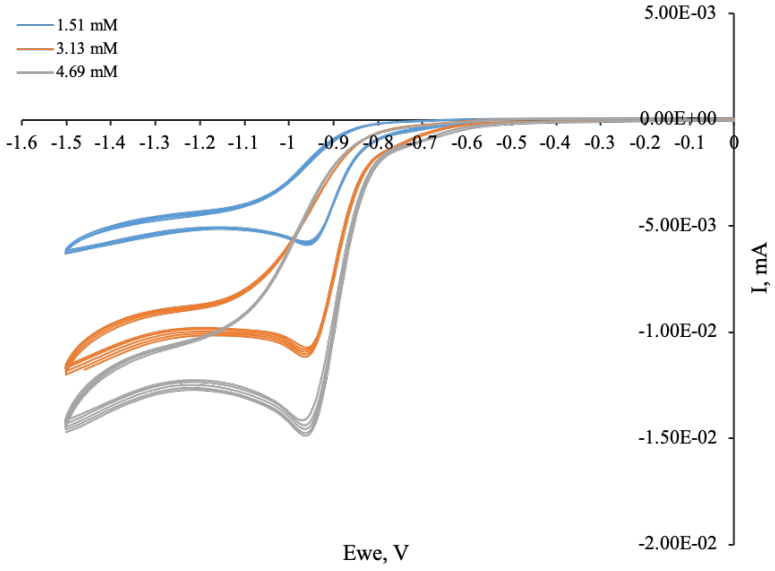

Figure 4.23. CV of CPADB in MeCN with ferrocene at varying concentrations.

Table 4.9 Reduction Potential of CTAs measured in this work

CTA	E_{red}, V (vs. SCE)
CPADB	-0.92
MCEBT	-1.11
DBTTC	-1.00
DCATTC	-0.99

All potentials measured in MeCN vs. Ag/AgCl and converted to SCE by adding 0.045 V

The CTA's measured in this study have reduction potentials varying from -0.9 to -1.1 V vs SCE. This suggests that it is possible for them to be reduced via PET from a photosensitizer. To determine the viability of the PET electron transfer mechanism, the likelihood of electron transfer was measured using transient absorption spectroscopy. In a typical experiment, a mediator was excited in the

presence of a sacrificial electron donor, such as triethylamine, to generate the corresponding reduced mediator. The decay rate constant of the reduced mediator was monitored with respect to the amount of CTA added to determine a rate of electron transfer (k_q, table 4.10). The results for CPADB are compiled in table 4.7. The reduction potentials of AQNOC was measured in this work (see chapter 6), and the others were compiled from the following review[22].

Table 4.10. Observed quenching rate constants for PET to CPADB

Mediator	Donor	E_{red}[a]	k_q, $M^{-1}s^{-1}$	R^2
AQNOC	TEA	-0.62	$<10^5$	0.88
9,10-DCA	TEA	-0.91	$5.17x10^7$	0.95
Anthraquinone	TEA	-0.96	$9.26x10^5$	0.88
Rose Bengal[b]	TEA	-0.99 -0.78	$1.12x10^8$	0.95
Fluorenone	TEA	-1.17 -1.22	$1.58x10^7$	0.65
Xanthone[c]	TEA	-1.62	$4.14x10^8$	0.98
Benzophenone	DABCO	-1.72	$1.36x10^8$	0.98

[a]Potentials shown measured vs. SCE. [b]Excitation with 532 nm ND:YAG. [c]Only fit to biexponential decay profile

Electron transfer to CPADB leads to its rapid decomposition. As shown in Figure 4.24, photolysis of the triplet sensitizer Rose Bengal ($k_{q, ET} = 1.12x10^8$ s^{-1}) in the presence of CPADB and an electron donor leads to ca. 65% conversion in 45 minutes as measured by ^1H NMR. Photolysis in the absence of the donor resulted in ca. 15% conversion while direct photolysis of CPADB lead to >5% conversion. Similar results were observed for MCEBT. Analysis was performed by measuring the loss of the peak corresponding to the CTA at 7.8 ppm with respect to tBuOH as an

internal standard (chapter 6). A solution of 3 mL CTA, 5.37 mM, Rose Bengal, 1 mM, and tBuOH in CD_3CN was purged with N_2. Aliquots of 0.5 mL were removed at the indicated time and were analyzed by ^1H NMR. The decomposition was measured in the absence of a radical trap to eliminate the likelihood of decomposition due to radical addition chain transfer pathways.

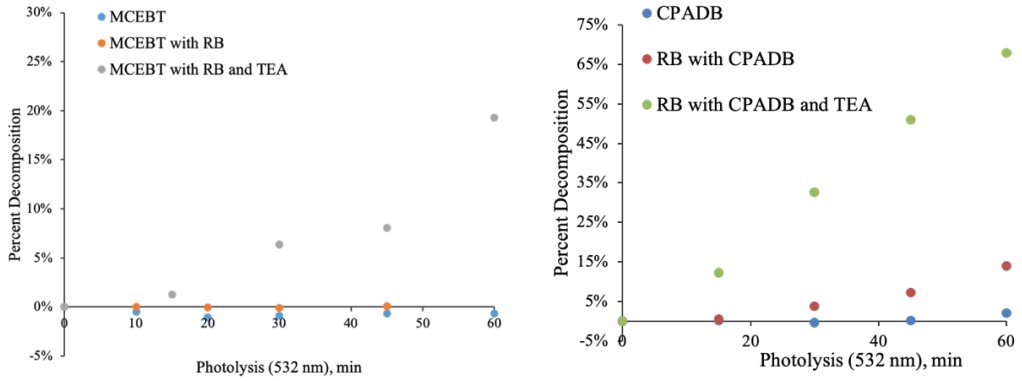

Figure 4.24. Sensitizer decomposition of a dithioester. *left*: MCEBT decomposition with 532 nm irradiation under direct (blue), triplet sensitized (orange), and PET sensitized (grey). *right*: CPADB decomposition with 532 nm irradiation under direct (blue), triplet sensitized (red), and PET sensitized (green).

Similarly, electron transfer to trithiocarbonates results in rapid decomposition. As discussed in Figure 4.22, photolysis of the triplet sensitizer thioxanthone in the presence of DBTTC results in negligible decomposition, but, as shown in Figure 4.5, the addition of an electron donor (triethylamine) leads to ca. 85% conversion in 60 minutes as measured by ^1H NMR. A solution of 3 mL CTA, 5.0 mM, thioxanthone, 1 mM, TEA, 25mM, and tBuOH in CD_3CN was purged with N_2. Aliquots of 0.5 mL were removed at the indicated time and were analyzed by ^1H NMR.

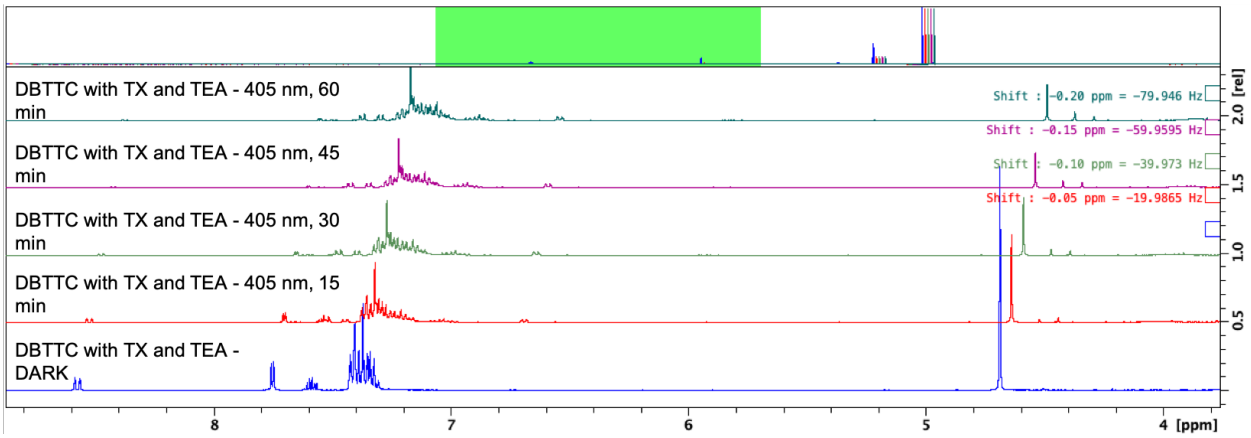

Figure 4.24. H^1 NMR Spectra from photolysis of TX with DBTTC and TEA in CD_3CN at 405 nm under N_2.

4.10 Conclusions and Future Work:

Dithioesters: It has long been observed that, for dithioesters, UV wavelengths are required for direct activation. Our work demonstrates that it is the higher excited-states, S_2 and/or T_2, that are primarily responsible for C-S bond dissociation. Although dithioesters exhibit a weak n-π* visible light absorption band, no decomposition is observed after photolysis of this band and population of S_1 and/or T_1 states. Calculations predict that the C-S bond dissociation energy is above the predicted T_1 state energy. Population of higher excited-states, however, results in rapid decomposition of the CTA and measurable formation of the dimer from radical recombination. This suggests that, when performing PET energy transfer RAFT, the selection of the sensitizer is important. Triplet energy transfer with sensitizers having excited-state energies lower than 60 kcal/mol will not result in efficient C-S bond dissociation and subsequent polymer formation. Future work will involve examining the effect of the triplet energy of the sensitizer on the polymerization efficiency.

Conversely, electron transfer to dithioesters does result in rapid decomposition, and it is possible to transfer an electron to the CTA from a variety of mediators. PET electron transfer RAFT can result from C-S bond homolysis from the CTA, but more work needs to be done to identify the CTA anion radical formed as a result of PET from a mediator. Furthermore, future research will involve attempting to measure the rate of C-S bond homolysis from the anion radical.

Trithiocarbonates: Irradiation of trithiocarbonates at UV, or visible wavelengths results in slow decomposition as demonstrated in the many examples of trithiocarbonates being used as an iniferter in RAFT processes. Calculations predict that C-S bond dissociation should be exergonic from S_1 and T_1. It is possible to populate the T_1 of a trithiocarbonates via triplet energy transfer from an excited-state photosensitizer, but formation of T_1 of the trithiocarbonates in this way does not result significantly more degradation, or polymer formation, suggesting that photodissociation from T_1 is no more efficient than direct activation.

Much like the dithioesters, electron transfer to trithiocarbonates results in rapid decomposition of the CTA. Future work will involve attempts at identification of the reduced trithiocarbonate and measurement of C-S bond dissociation rate constant.

4.11 References:

(1) Otsu, T.; Yoshida, M. Role of Initiator-Transfer Agent-Terminator (Iniferter) in Radical Polymerizations: Polymer Design by Organic Disulfides as Iniferters. *Die Makromol. Chemie, Rapid Commun.* **1982**, *3* (2), 127–132.

(2) McKenzie, T. G.; Fu, Q.; Wong, E. H. H.; Dunstan, D. E.; Qiao, G. G. Visible

Light Mediated Controlled Radical Polymerization in the Absence of Exogenous Radical Sources or Catalysts. *Macromolecules* **2015**, *48* (12), 3864–3872.

(3) Otsu, T. Iniferter Concept and Living Radical Polymerization. *J. Polym. Sci. Part A Polym. Chem.* **2000**, *38* (12), 2121–2136.

(4) Quinn, J. F.; Barner, L.; Barner-Kowollik, C.; Rizzardo, E.; Davis, T. P. Reversible Addition - Fragmentation Chain Transfer Polymerization Initiated with Ultraviolet Radiation. *Macromolecules* **2002**, *35* (20), 7620–7627.

(5) Lu, L.; Zhang, H.; Yang, N.; Cai, Y. Toward Rapid and Well-Controlled Ambient Temperature RAFT Polymerization under UV - Vis Radiation: Effect of Radiation Wave Range. *Macromolecules* **2006**, *39* (11), 3770–3776.

(6) Khan, M. Y.; Cho, M.-S.; Kwark, Y.-J. Dual Roles of a Xanthate as a Radical Source and Chain Transfer Agent in the Photoinitiated RAFT Polymerization of Vinyl Acetate. *Macromolecules* **2014**, *47* (6), 1929–1934.

(7) McKenzie, T. G.; Fu, Q.; Uchiyama, M.; Satoh, K.; Xu, J.; Boyer, C.; Kamigaito, M.; Qiao, G. G. Beyond Traditional RAFT: Alternative Activation of Thiocarbonylthio Compounds for Controlled Polymerization. *Adv. Sci.* **2016**, *3* (9), 1500394.

(8) Jiangtao, X.; Sivaprakash, S.; Nathaniel Alan, C.; Cyrille, B. Catalyst-Free Visible Light-Induced RAFT Photopolymerization. *Control. Radic. Polym. Mech.* **2015**, *1187* (1187), 247–267.

(9) Ding, C.; Fan, C.; Jiang, G.; Pan, X.; Zhang, Z.; Zhu, J.; Zhu, X. Photocatalyst-Free and Blue Light-Induced RAFT Polymerization of Vinyl Acetate at

Ambient Temperature. *Macromol. Rapid Commun.* **2015**, *36* (24), 2181–2185.

(10) Mckenzie, T. G.; Da, L. P.; Costa, M.; Fu, Q.; Dunstan, D. E.; Qiao, G. G. Investigation into the Photolytic Stability of RAFT Agents and the Implications for Photopolymerization Reactions. *Polym. Chem.* **2016**, *7*, 4246.

(11) Huppert, D.; Jortner, J.; Rentzepis, P. M. S2 → S1 Emission of Azulene in Solution. *Chem. Phys. Lett.* **1972**, *13* (3), 225–228.

(12) Murata, S.; Iwanaga, C.; Toda, T.; Kokubun, H. Fluorescence Yields of Azulene Derivatives. *Chem. Phys. Lett.* **1972**, *13* (2), 101–104.

(13) Gillispie, G. D.; Lim, E. C. Further Results on the Triplet—Triplet Fluorescence of Anthracenes. *Chem. Phys. Lett.* **1979**, *63* (2), 355–359.

(14) Eaton, D. F.; Evans, T. R.; Leermakers, P. A. No Title. *Mol. Photochem.* **1969**, *1*, 347.

(15) Demchenko, A. P.; Tomin, V. I.; Chou, P. T. Breaking the Kasha Rule for More Efficient Photochemistry. *Chem. Rev.* **2017**, *117* (21), 13353–13381.

(16) Wolf, S. Applied Photochemistry for Multicolor Photolithography, University of Maryland, 2018.

(17) Kitchin, A. D.; Velate, S.; Chen, M.; Ghiggino, K. P.; Smith, T. A.; Steer, R. P. Photophysics of a Dithioester RAFT Polymerization Agent and the Acenaphthenyl Model Light-Harvesting Chromophore. *Photochem. Photobiol. Sci.* **2007**, *6* (8), 853.

(18) Quinn, J. F.; Barner, L.; Barner-Kowollik, C.; Rizzardo, E.; Davis, T. P. Reversible Addition - Fragmentation Chain Transfer Polymerization Initiated with Ultraviolet Radiation. *Macromolecules* **2002**, *35* (20), 7620–7627.

(19) Degirmenci, I.; Coote, M. L. Effect of Substituents on the Stability of Sulfur-Centered Radicals. *J. Phys. Chem. A* **2016**, *120* (37), 7398–7403.

(20) Shen, T.; Zhao, Z.-G.; Yu, Q.; Xu, H.-J. Photosensitized Reduction of Benzil by Heteroatom-Containing Anthracene Dyes. *J. Photochem. Photobiol. A Chem.* **1989**, *47* (2), 203–212.

(21) Murov, S. L.; Hug, G. L.; Carmichael, I. *Handbook of Photochemistry*; M. Dekker, 1993.

(22) Romero, N. A.; Nicewicz, D. A. Organic Photoredox Catalysis. *Chem. Rev.* **2016**, *116* (17), 10075–10166.

(23) Xu, J.; Jung, K.; Boyer, C. Oxygen Tolerance Study of Photoinduced Electron Transfer-Reversible Addition-Fragmentation Chain Transfer (PET-RAFT) Polymerization Mediated by Ru(Bpy)3Cl2. *Macromolecules* **2014**, *47* (13), 4217–4229.

(24) Xu, J.; Shanmugam, S.; Duong, H. T.; Boyer, C. Organo-Photocatalysts for Photoinduced Electron Transfer-Reversible Addition-Fragmentation Chain Transfer (PET-RAFT) Polymerization. *Polym. Chem.* **2015**, *6* (31), 5615–5624.

(25) Shanmugam, S.; Xu, J.; Boyer, C. Exploiting Metalloporphyrins for Selective Living Radical Polymerization Tunable over Visible Wavelengths. *J. Am. Chem. Soc.* **2015**, *137* (28), 9174–9185.

(26) Shanmugam, S.; Xu, J.; Boyer, C. Utilizing the Electron Transfer Mechanism of Chlorophyll a under Light for Controlled Radical Polymerization. *Chem. Sci.* **2015**, *6* (2), 1341–1349.

(27) Corrigan, N.; Xu, J.; Boyer, C.; Allonas, X. Exploration of the PET-RAFT Initiation Mechanism for Two Commonly Used Photocatalysts. *ChemPhotoChem* **2019**, 3, 1.

Chapter 5: RAFT Polymerization through Photocatalytic Oxidation of DMSO

Controlled radical polymerization (CRP) is a method of preparing polymers with narrow molecular weight distributions and specific architectures. Specifically, photomediated-CRP has been popularized due to its mild reaction conditions, and spatial and temporal control[1]. The ability of light to switch the polymerization process 'on' and 'off' is advantageous in the manufacturing of polymers with exact control over the monomer conversion. As discussed in previous chapters, reversible addition fragmentation chain transfer (RAFT) polymerization, one of the more popular methods of CRP, can be initiated with light in multiple ways[1–6]. Photo-RAFT is traditionally carried out under UV illumination through direct activation of the CTA, but concerns about competing absorption of other substrates in addition to unwanted degradation lead to the development of visible light alternatives[7–13].

Most popular among the alternatives is PET-RAFT as developed by the Boyer group[14–22]. This approach uses photosensitizers, or photocatalysts, which are excited-state oxidants or reductants, to trigger the initiation step (Figure 5.1). The general scheme assumes the radical generation is a result of the direct interaction between the photocatalyst and the CTA. The photocatalytic approach has been successful due the lack of degradation of the CTA, however, these systems are more complex; often requiring photocatalyst, a ground-state donor, monomer and CTA. In an attempt to understand the variables, in addition to providing some mechanistic insight into the initiation step, our work has focused on the ability of an excited-state photocatalyst to

initiate polymerization through interaction with the solvent, not the CTA as is commonly suggested.

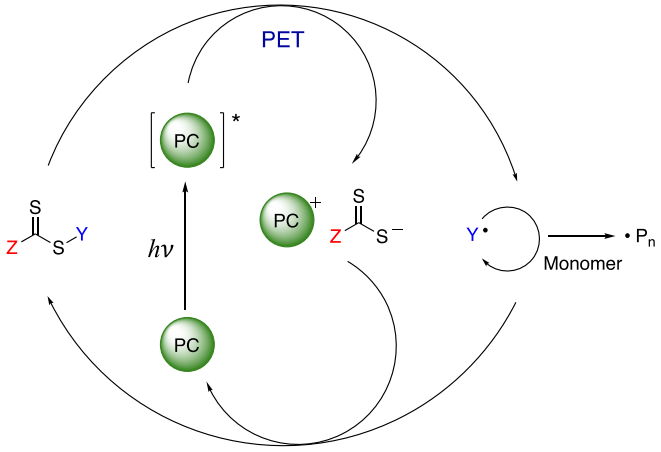

Figure 5.1. A general description of the initiation step in PET-RAFT where the CTA is activated by reduction.

5.1 Solvent-Assisted Polymerization using N-methyl-2-pyrrolidone:

Currently, the only example of using the solvent as a means of generating radicals to initiate RAFT polymerization was reported by the Boyer group[23]. They developed a method in which metal phthalocyanines, activated by NIR irradiation, were used in the controlled polymerization of acrylate monomers (Figure 5.2). Interestingly, the initiation step did not involve photoreduction of the RAFT agent, rather, the excited photocatalyst reacts with the solvent, *N*-methyl-2-pyrrolidone, to generate initiating radicals.

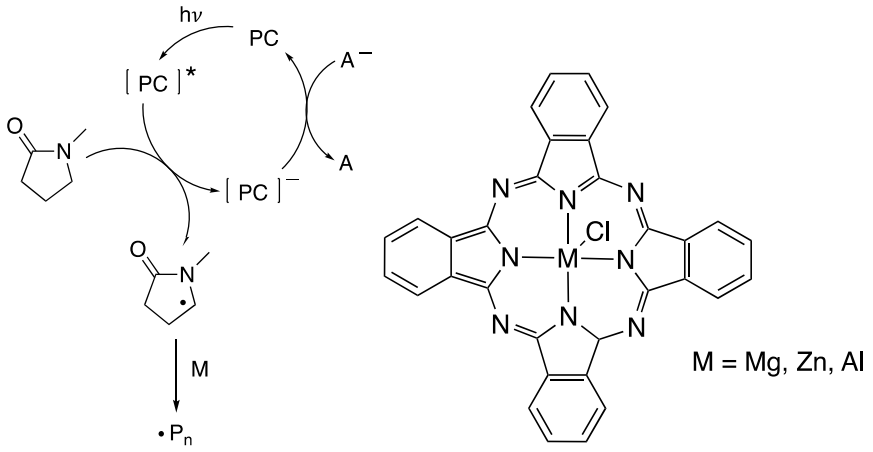

Figure 5.2. RAFT polymerization triggered by the oxidation of *N*-methyl-2-pyrrolidone.

Most notably, the use of metallic phthalocyanines allowed for the polymerization to be carried out using visible, or NIR light and the high molar extinction coefficient of phthalocyanines allowed for polymerization using low (5 ppm) concentrations of catalyst. Furthermore, they demonstrated high oxygen tolerance, temporal control, and the controlled/ "living" behavior expected of RAFT polymerization.

5.2 Oxidation of DMSO to Generate Methyl Radicals:

Dimethylsulfoxide (DMSO), is a commonly used solvent in polymerization reactions. Although it is widely assumed to function as an inert solvent, some reports have shown that DMSO can produce radicals under highly oxidation conditions. Kishore and Asmus estimated the oxidation potential of DMSO as ca. +1.55 to +1.75 V (vs. SCE) and the solvent window for measuring oxidation potentials in DMSO is reported as +1.3 V (vs. SCE)[24,25]. Furthermore, it is assumed that the oxidation of DMSO in the presence of water results in the formation of methyl radicals (Figure

5.3). This approach was later used by Crean et al. for the free radical methylation of 2'-deoxyguanosine[26].

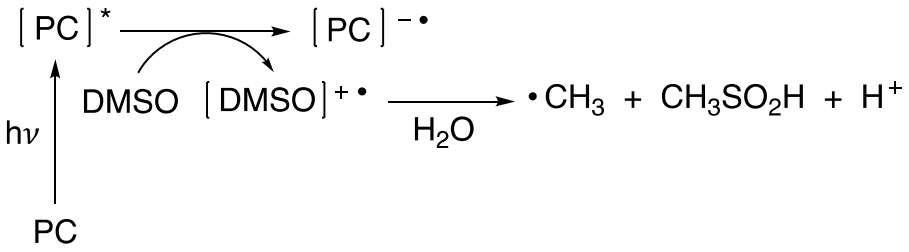

Figure 5.3. The photochemical oxidation of DMSO. The excited-state of the photocatalyst (PC), abstracts an electron from ground-state DMSO resulting in the formation of the cation radical ($DMSO^{\bullet+}$) which can be trapped by water to yield sulfinic acid, a methyl radical and a proton.

As discussed earlier in Chapter 3, excited-state quinones have been used extensively as oxidants as well as electron shuttles in mediated electron transfer processes[27–33]. A previous report by Görner established, using transient absorption spectroscopy, that the triplet state of 9,10 anthraquinone derivatives reacts with DMSO at or near the diffusion limit and that this quenching is the result of the one electron oxidation of DMSO[34]. Some results from the Görner study are shown in Table 5.1.

Table 5.1: Rate constant for triplet quenching of quinones in DMSO

Quinone[a]	k_q:DMSO/MeCN[b], $M^{-1}s^{-1}$	k_q:DMSO/MeCN-H_2O[c], $M^{-1}s^{-1}$
Me_2BQ	3×10^9	2×10^9
Cl_4BQ	3×10^9	2×10^9
NQ	6×10^9	5×10^9
MeNQ	8×10^9	6×10^9
AQ	3×10^9	2×10^9
MeAQ	1×10^9	6×10^8
Me_2AQ	3×10^8	1×10^8

[a]abbreviations: Me_2BQ: 2,6-dimethyl-1,4-benzoquinone; Cl_4BQ: chloranil; NQ: 1,4-napthoquinone; MeNQ: 2-methyl-1,4-

nathpthoquinone; AQ: 9,10-anthraquinone; MeAQ: 2-methyl-9,10-anthraquinone; Me_2AQ: 2,6-dimethyl-9,10-anthraquinone.
[b]1:1 MeCN/DMSO [c]2:1:1 DMSO/MeCN/H_2O

The studies described herein aim to determine if a similar DMSO oxidation reaction would be operative in the initiation of radicals for a photoRAFT process. We examined the ability of a visible-light absorbing quinone (Figure 5.4) to initiate polymerization through photochemical oxidation of DMSO. Product analysis, transient absorption spectroscopy, and chemical trapping demonstrate the oxidation of DMSO leading to the formation of methyl radicals and the production of methacrylate polymers with photochemical control, high end group fidelity and narrow molecular weight distributions.

5.3 Polymerization of Methacrylate Monomers:

Polymerization reactions were carried out at 419 nm under broadband irradiation in a 35 W, 16 bulb Rayonet photoreactor with an operating temperature of 35ºC. Initial polymerization reactions are given in Table 5.2. Photolysis of AQ-1 in a mixture of DMSO/MMA results in formation of p-MMA (Table 5.2, Entry 1). This demonstrates the formation of initiating radicals in the absence of a co-sensitizer. The polymerization process was able to be controlled with the addition of CPADB resulting in low polydispersity and good agreement between predicted and measured molecular weights (Table 5.2. Entries 2-18.). The presence of the dithiobenzoate end group was confirmed by ^{1}H NMR and UV/VIS (Figures 5.6-5.8).

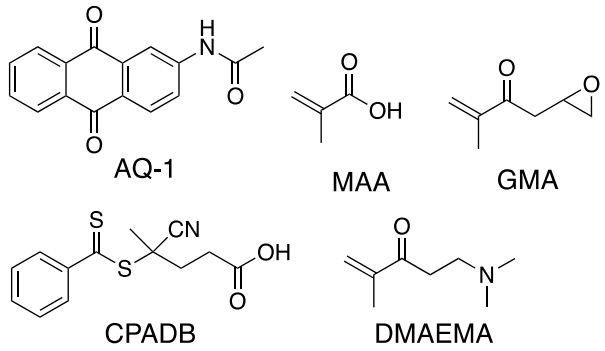

Figure 5.4. Compounds used in this study. The synthesis of AQ-1 is given in chapter 6. MAA, DMAEMA, GMA, stand for methacrylic acid, *N,N*-diaminoethyl methacrylate, glycidyl methacrylate, respectively.

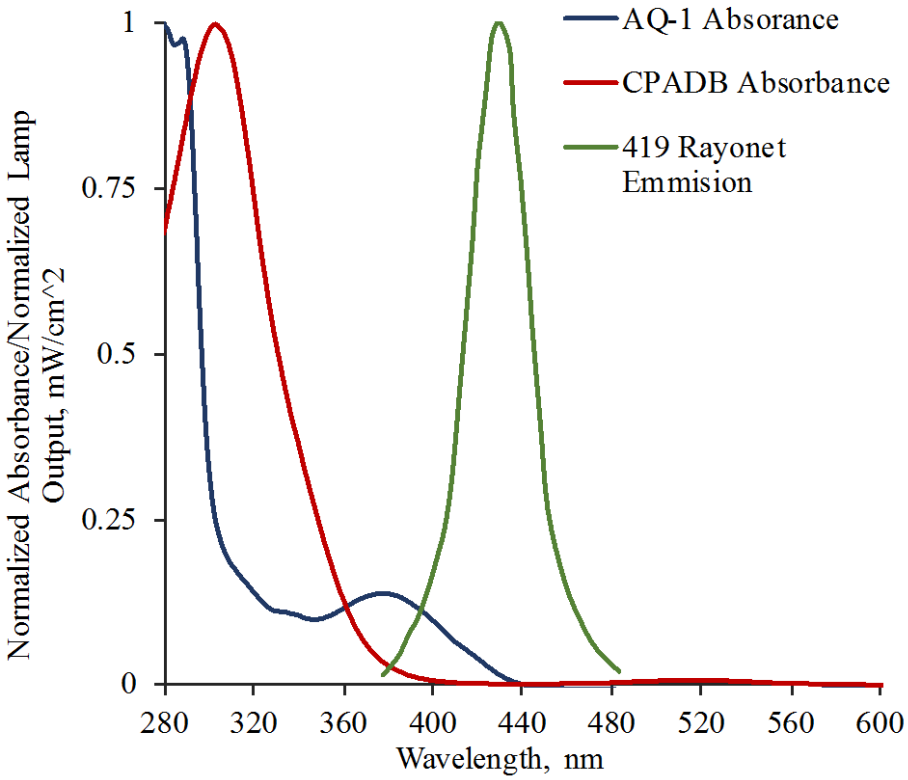

Figure 5.5. Normalized absorption spectra of AQ-1 and CPADB in MeCN. Normalized emission spectrum of the 419 nm bulbs from the Rayonet photoreactor.

Encouragingly, all experiments showed an increase in conversion and molecular weight relative to background polymerization while maintaining control

over the polymerization process. Examples where the solution was left unexposed to light showed no conversion, and although control experiments confirm the polymerization to be photocatalytically initiated, some background photolysis of the CTA is observed (Table 5.2. Entries 2-3.). One possible explanation for the observed background polymerization is due to contributions from a photoiniferter mechanism involving the UV edge of the broadband emission of 419 nm bulbs. To assess the feasibility of the photocatalyst in low concentrations, polymerizations were carried out using sub-mM amounts of AQ-1 (Table 5.2, entries 5-8. Figure 5.9).

Table 5.2: RAFT Polymerization with AQ-1 in a DMSO/Monomer mixture in the presence of Air

Entry	M/CTA	[AQ-1][a], equiv.	Monomer	Photolysis Time, hrs	$M_{n,GPC}$[b]	$M_{n,theo}$[c]	PDI	Conv.[d]
1	0	0.1	MMA	4	42.1k	-	1.61	21%
2	200	0	MMA	8	7.6k	5.6k	1.03	26%
3	200	0	MMA	16	9.8k	12.2k	1.05	59%
4	200	0.1	MMA	DARK	-	-	-	0%
5	200	0.01	MMA	8	10.8k	7.8k	1.16	37%
6	200	0.02	MMA	8	8.7k	9.5k	1.06	45%
7	200	0.03	MMA	8	8.7k	10.5k	1.02	50%
8	200	0.04	MMA	8	9.1k	10.9k	1.03	52%
9	200	0.05	MMA	8	9.9k	12.3k	1.14	59%
10	200	0.05	MMA	16	13.1k	19.2k	1.23	93%
11[e]	200	0.05	MMA	6	15.1k	14.1k	1.30	87%
12	200	0.1	MMA	8	9.1k	9.5k	1.06	45%
13	200	0.1	MMA	16	10.1k	15.7k	1.03	76%
14	200	0.25	MMA	16	10.4k	12.6k	1.06	61%
15[f]	200	0.1	MMA	1	-	-	-	<5%
16	230	0.1	GMA	8	35.4k[g]	29.0k	-	95%
17	220	0.1	MAA	8	11.0k[g]	13.0k	-	74%
18	205	0.1	DMAEMA	5	43.8k	19.3k	1.64	65%

[a] Relative to the amount of CTA-1. [b] Measured by GPC using THF as the solvent and calibration using polystyrene standards. [c] Calculated according to the following equation: $M_{n,theo} = [M]_0/[CTA]_0 \bullet MW_M \bullet conv. + MW_{CTA}$. Where $[M]_0$, $[CTA]_0$, MW_M, conv., MW_{CTA}, correspond to initial concentration of monomer, M, the initial concentration of RAFT agent, the molecular weight of the monomer, the fraction of monomer converted into polymer and the molecular weight of the RAFT agent respectively. [d] Determined using ^{1}H NMR. [e] Photolysis performed with a 1.0 W, 447 nm CW diode laser. [f] Sample was photolyzed for 1 hour and then kept dark for 20 hours. [g] Polymer analysis performed by ^{1}H NMR.

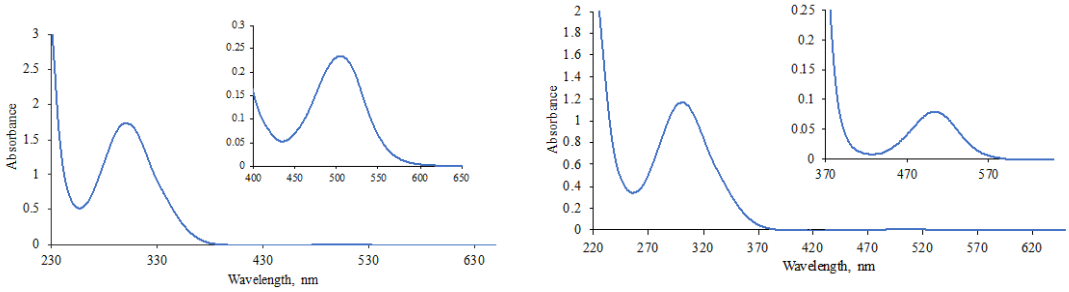

Figure 5.6. *Left*: UV/Vis of Table 5.2, Entry 12. *Right*: UV/Vis of Table 5.2, Entry 4.

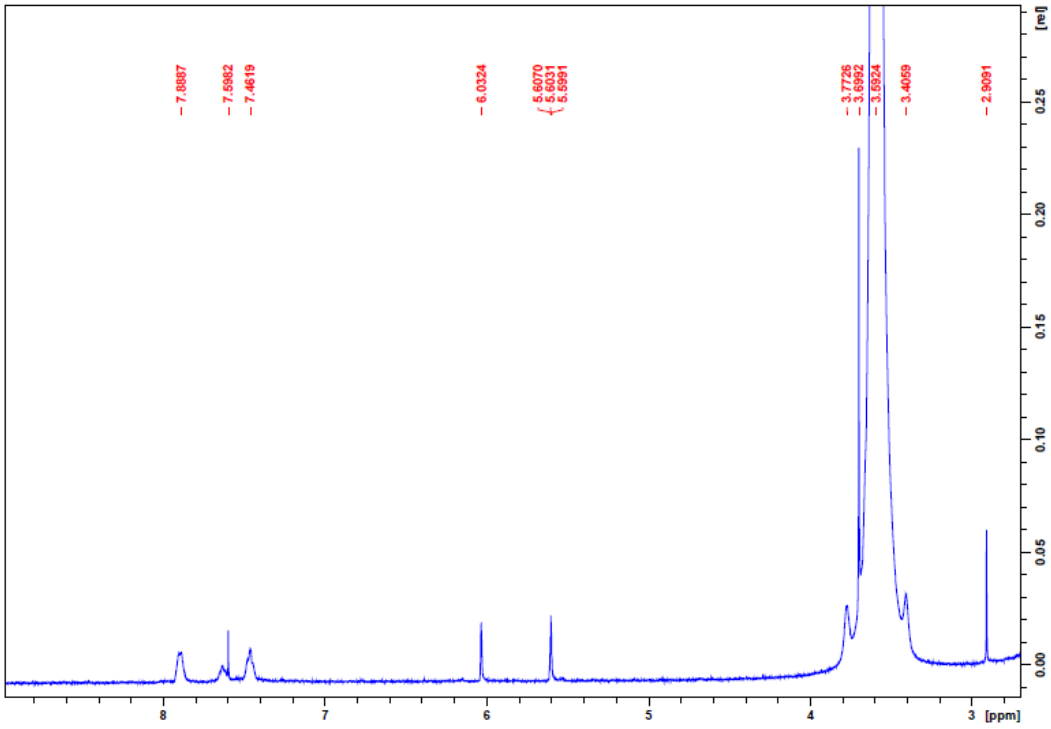

Figure 5.7. ^{1}H NMR of Table 5.2, entry 12.

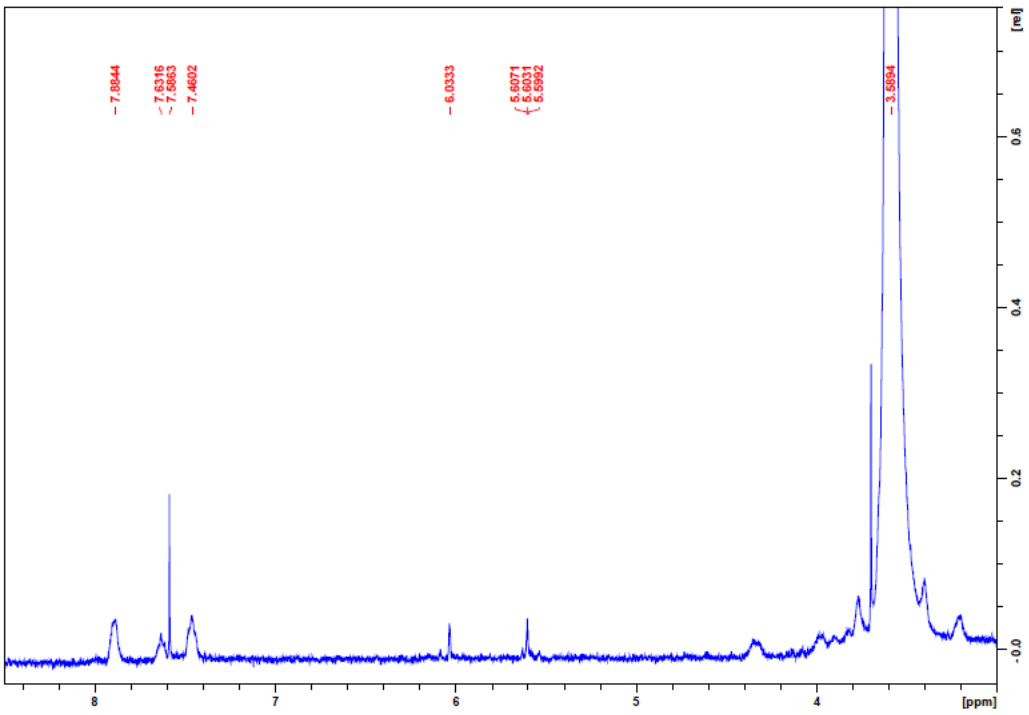

Figure 5.8. ^{1}H NMR of Table 5.2, entry 4.

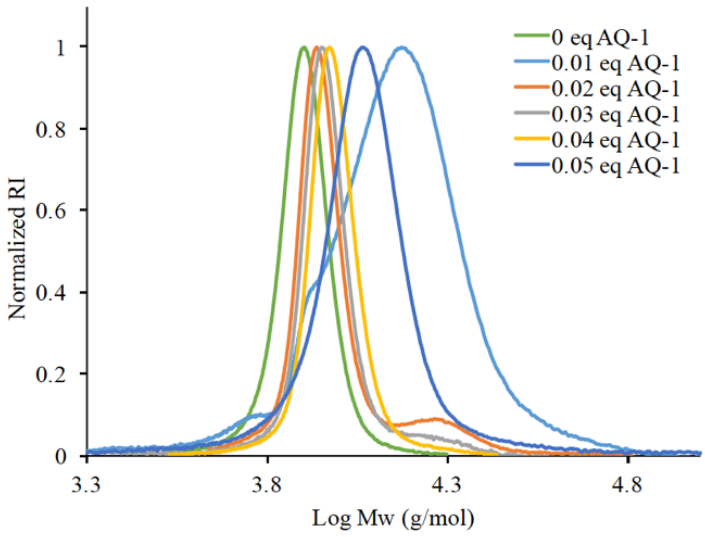

Figure 5.9. GPC traces showing narrow molecular weight distributions and an increasing in the M_n with increasing concentrations of photoinitiator used.

In an attempt to limit the direct irradiation of the CTA, an experiment was carried out with illumination from a 1 W, 447 nm CW diode laser (Table 5.2, entry

11). Although high conversions are reached more quickly than with broadband irradiation, some control over the polymerization process was lost when approaching high conversions. However, end group fidelity is preserved as is shown by the agreement with the predicted and observed molecular weights. Therefore, the loss control which is observed is, most likely, due to rapid initiation under intense illumination resulting in an increase in termination due to the growth of more chains than the CTA can deactivate at any one time.

The polymerizations were applied to multiple methacrylate monomers. Polymerization of GMA, DMAEMA, and MAA were carried out as described in Table 5.2 (entries 16-18.). Well-defined polymers with good agreement between predicted and measured molecular weights were achieved for both MAA and GMA, but DMAEMA showed significant degradation of the CTA and, consequently, poor control over the molecular weight. As shown in Figure 5.4, DMAEMA has an alkyl amino substituent at one of the terminal positions. Anthraquinones are well known to act as excited-state oxidants of alkyl amines and substituted amines are commonly used as sacrificial electron donors in photoinduced electron transfer process[30]. The reaction of the excited-state AQ-1 with DMAEMA likely results in unwanted radical formation and redox process which, in turn, may be responsible for the poor polymer properties.

Moving forward, based on the optimization data in Table 5.2, polymerizations were carried out using either 0.05 or 0.1 equivalents of AQ-1, and photolysis at 419 nm in order to main high conversions without sacrificing end group fidelity. Although purging the solution with nitrogen prior to photolysis resulted in slightly higher

conversions than those carried out in air, the effect was minimal. Therefore polymerizations were carried out without prior deoxygenation (Table 5.3).

Table 5.3: RAFT Polymerization of MMA with AQ-1 in DMSO under Nitrogen

Entry	CTA/I	[AQ-1][a], equiv.	Atmosphere	Photolysis Time, hrs	M_n[b]	PDI[b]	Conv.[c]
1	200	0	N_2	8	6.1k	1.03	32%
2	200	0.05	N_2	8	10.3k	1.09	77%
3	200	0.05	N_2	16	12.2k	1.32	94%
4	200	0.1	N_2	8	7.4k	1.10	48%
5	200	0.5	N_2	8	-[d]	-[d]	24%

[a] Relative to the amount of CTA-1. [b] Measured by GPC using THF as the solvent and calibration using polystyrene standards. [c] Determined using ^{1}H NMR. [d] Not enough polymer was available for analysis.

Figure 5.10 illustrates 'On'/'Off' experiments that were performed to demonstrate the temporal control over the reaction process. To assess the spatial control, a sample of AQ-1 in DMSO/MMA was irradiated at 419 nm for the appropriate amount of time. Afterwards, the sample was opened and a 10 μL sample was removed and added to 0.5 mL of CD_3CN to measure the conversion by ^{1}H NMR . Although it is possible that the introduction of air into the system by opening the vial halted the polymerization process, a sample (Table 5.2., entry 15) which was photolyzed for one hour followed by an extended (24 hr) incubation period showed low conversion which further illustrates the need for light to initiate the polymerization process and rules out "dark" polymerization as has been previously reported[35].

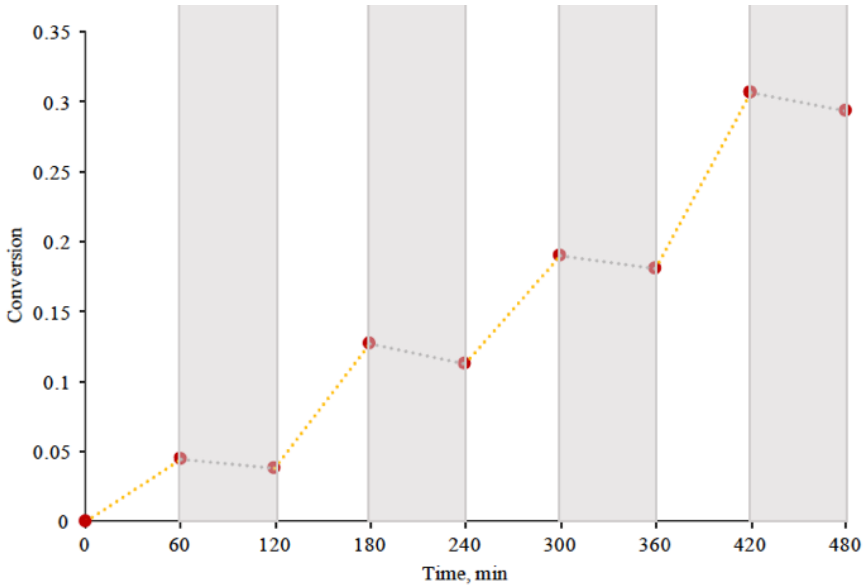

Figure 5.10. Reaction process was monitored by ^{1}H NMR. During photolysis (white regions) noticeable amounts of monomer were consumed while, in the dark (grey regions), no conversion was noted.

5.4 Solvent Dependence:

Photopolymerizations were carried out in different solvents to examine the versatility of the polymerization process, and asses the necessity of DMSO in the initiation mechanism. To perform the analysis, a sample of AQ-1 and CPADB in a 1/1 mixture of MMA and different solvents was irradiated at 419 nm for 16 hrs. Polymerization was observed irrespective of the solvent used, but with DMSO having the highest conversion. Polymerization in other solvents all resulted in lower conversion suggesting that AQ-1 is unable to efficiently initiate polymerization and the polymer observed is resultant of a photo-iniferter mechanism. However, interestingly methanol (Table 5.4., entry 3), which is known to be a weak H atom donor, showed very poor control over the molecular weight and very low conversions

which indicates that any semiquinone that is formed during the polymerization process is not operable in the initiation process.

Table 5.4: Solvent dependence on the RAFT polymerization of MMA with AQ-1

Entry	CTA/I	[AQ-1][a], equiv.	Solvent	Photolysis Time, hrs	M_n[b]	PDI[b]	Conv.[c]
1	200	0.05	DMSO	16	13.1k	1.23	93%
2	200	0.05	Toluene	16	11.0k	1.30	34%
3	200	0.05	MeOH	16	8.4k	2.09	21%
4	200	0.05	MeCN	16	11.9k	1.12	40%
5	200	0.05	THF	16	9.0k	1.06	32%

Photolysis at 419 nm. [a] Relative to the amount of CTA-1. [b] Measured by GPC using THF as the solvent and calibration using polystyrene standards. [c] Determined using ^{1}H NMR.

5.5 Transient Absorption Spectroscopy:

To provided further evidence of electron transfer from DMSO, transient absorption spectroscopy was performed on AQ-1 in DMSO. Pulsed photolysis (354.7 nm, 10 mJ, 5-7 ns) of AQ-1 in DMSO in the presence of air initially generates an absorption band with peaks at 480 and 620 nm respectively which is assigned to the triplet of AQ-1 (AQ-1^3*) based on previous reports and other work described in this dissertation (chapter 5, Figure 5.11.)[30]. Following the decay of the triplet, there is a longer-lived species with absorption bands at 550 nm which is assigned to the anion radical of AQ-1 (AQ-1$^{\bullet-}$) formed after oxidation of DMSO[34]. As shown in figure 5.11, the addition of air has little effect on the lifetime of the triplet, however, the lifetime of the signal corresponding to AQ-1$^{\bullet-}$ decreases significantly due to quenching by molecular oxygen.

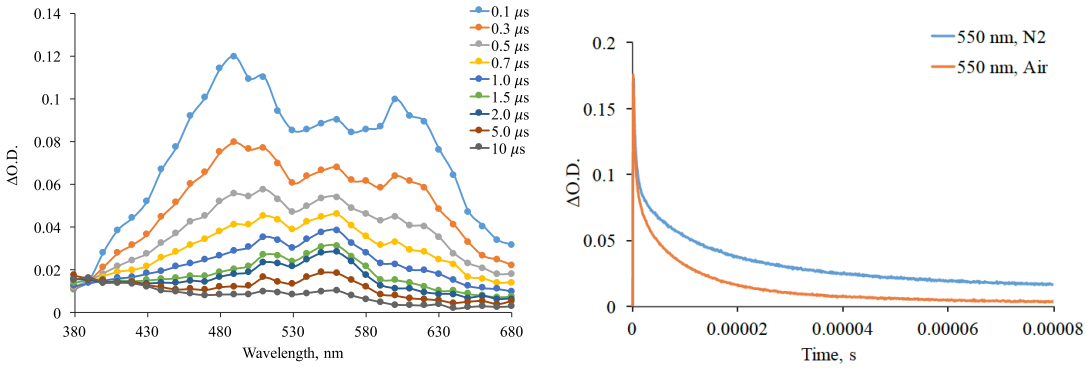

Figure 5.11. *Left*: Transient absorption spectra of AQ-1 in DMSO in the presence of air. *Right*: Waveforms showing the effect of oxygen on the lifetime of the triplet and radical species.

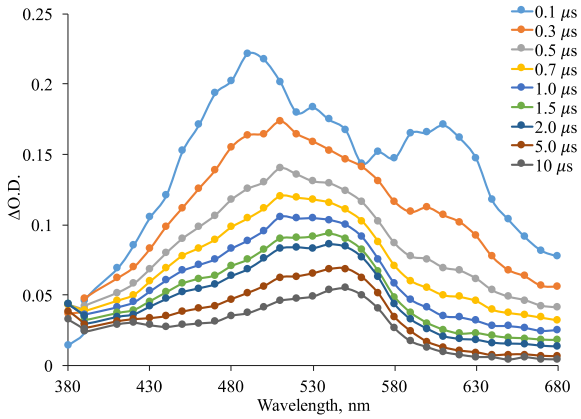

Figure 5.12. Transient absorption spectra of AQ-1 in DMSO under N_2. The anion radical, AQ-1$^{\bullet-}$, can be see much more clearly as a long-lived signal at 550 nm.

As discussed in Chapters 1 and 4, one plausible mechanism in PhotoRAFT is electron transfer from the reduced photocatalyst to the CTA. The anion radical was generated from pulsed photolysis of AQ-1 in MeOH with TEA (Figure 5.13). To test this, the lifetime of AQ-1$^{\bullet-}$ was monitored with increasing amounts of CPADB as shown in Figure 5.13. With increasing amounts of CTA, the initial signal was observed to decrease, but no change in the lifetime of AQ-1$^{\bullet-}$ was observed. Stern

Völmer analysis demonstrated that, as shown in Chapter 4, CPADB quenches the triplet of AQ-1 at the diffusion limit. The analysis was performed by averaging the signal corresponding to AQ-1$^{\bullet-}$ over 1 μs (Figure 5.14, grey area) and the change in signal was plotted with respect to the concentration of quencher. A linear relationship was observed which is consistent with quenching of AQ^3*.

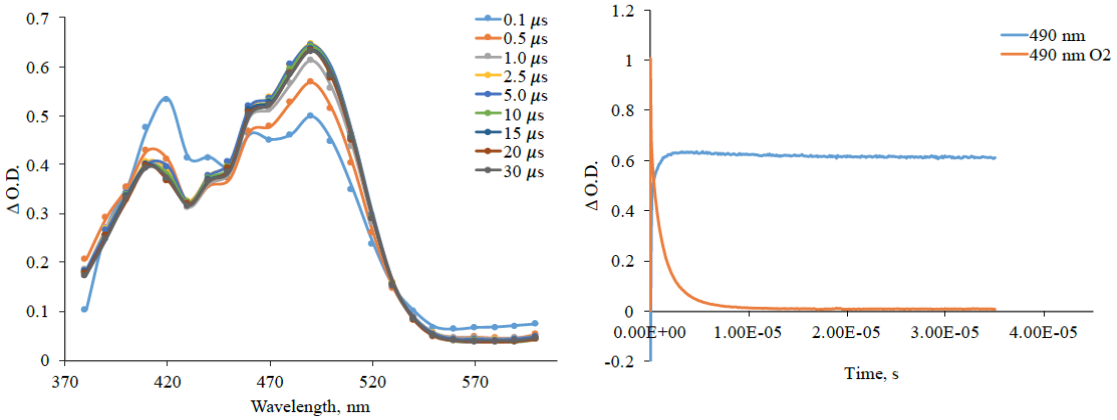

Figure 5.13. *Left*: Transient absorption spectrum of AQ-1 in MeOH with 25 mM TEA under N_2. The sample was continuously flowed to avoid the buildup of photoproducts. A very long-lived peak at 490 nm is assigned to AQ-1$^{\bullet-}$. Also notable is the semiquinone which can be seen at 410 nm. *Right*: Waveforms illustrating the quenching of AQ-1$^{\bullet-}$ by molecular oxygen.

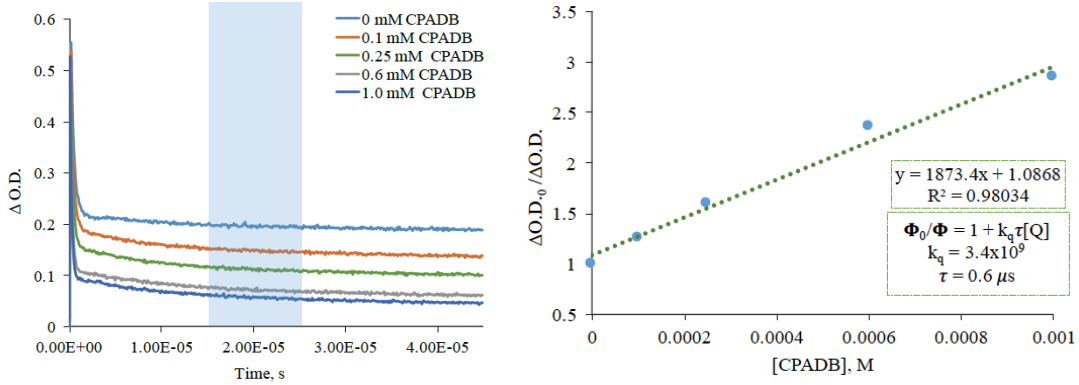

Figure 5.14. *Left*: Waveforms at 490 nm of AQ-1-• generated by pulsed photolysis of AQ-1 in MeOH with TEA under N_2. The addition of increasing concentrations of CPADB resulted in a smaller magnitude for signal for AQ-1-• due to competitive quenching between CPADB and TEA. *Right*: Stern Völmer analysis. The value of τ was estimated from the transient spectra of AQ-1 in benzene (chapter 6).

As discussed earlier in chapter 4, although it was observed that AQ-1^3* is quenched by CPADB, given that AQ-1 can only populate T_1 of the former, it is unlikely that triplet energy transfer results in meaningful radical generation and polymer formation. Furthermore, the high concentration of DMSO with respect to CTA, and the fact that the polymerization was carried out in the presence of air suggests PET-energy transfer RAFT can be further ruled out as a contributing mechanism.

5.6 Proposed Mechanism of Solvent Assisted RAFT Polymerization:

The proposed mechanism of initiation leading to controlled polymerization is given in Figure 5.15. The photocatalyst, AQ-1, absorbs a photon, and after rapid intersystem crossing, forms its triplet state AQ-1^3*. The latter can oxidize DMSO leading to the formation of AQ-1-• and the cation radical of DMSO. The cation radical can be trapped by water eventually leading to the formation of a methyl radical and sulfinic acid. The methyl radical can react with a monomer to initiate polymerization and enter into the RAFT process. The photocatalyst can be recycled by the reaction of AQ-1-• with air to generate superoxide and reform the starting photocatalyst. Not shown is the background iniferter initiation from direct irradiation of CPADB.

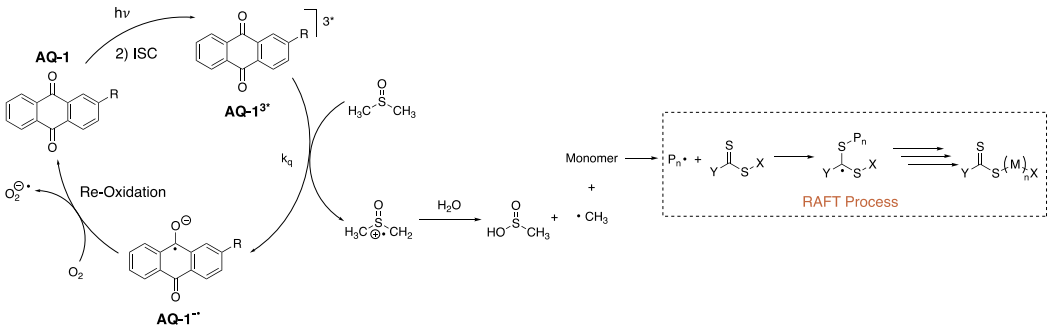

Figure 5.15. Proposed mechanism of initiation leading to controlled polymerization.

5.7 Chemical Trapping of the Methyl Radical formed from DMSO Oxidation:

To provide further evidence for the formation of methyl radicals during photolysis, chemical trapping experiments were performed. As shown in figure 5.16, the methyl radical formed from photo-oxidation of DMSO is expected to add to CPADB to form the methyl adduct, methyl benzodithioate. A solution of AQ-1 (4.7 mM), and CPADB (47 mM) in DMSO was photolyzed at 419 nm for 45 minutes. The sample was analyzed by mass spectrometry (DART -) after photolysis. A peak with signals corresponding to, the independently synthesized (chapter 6), methyl benzodithioate was found. Evidence for the formation of methyl radicals during photolysis suggests, along with literature precedent, that DMSO oxidation can lead to the formation of radicals reactive enough to initiate polymerization.

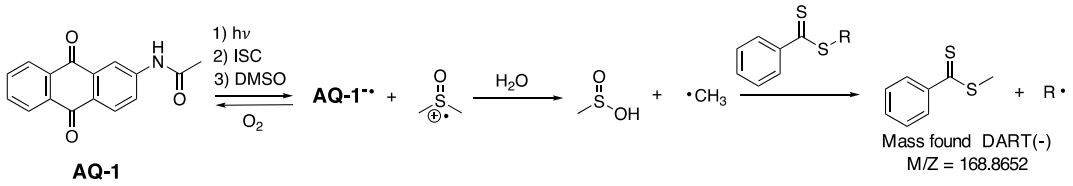

Figure 5.16. Chemical trapping of methyl bezodithioate.

5.8 Conclusions and future work.

Our work has shown that DMSO can be used a reactive solvent and a source of initiating radicals for photo-RAFT polymerization. Photolysis of a visible-light absorbing photocatalyst in methacrylate/DMSO mixtures results in the formation of p-MMA and polymers with well-defined molecular weights can be synthesized with the addition of a chain transfer agent. For the controlled polymerizations, PET electron and/or energy transfer RAFT polymerization was ruled out as a possible mechanism. Instead, it was shown that excited-state AQ-1 was capable of abstracting an electron from DMSO and this lead to the eventual formation of the reactive radicals necessary to initiate polymerization. This work describes an initiation system for photochemical polymerization that has not been explored previously in the literature. Additional studies are required to determine to what effect this initiation scheme plays a role in already well-known photochemical polymerizations. A small study was performed to gain insight into conditions required to oxidize DMSO for polymerization.

The viability of DMSO oxidation to initiate polymerization by a series of photocatalysts was studied. A library of photocatalysts which, using the Rehm Weller equation, were predicted to oxidize DMSO from either the excited-singlet ($\Delta G_{ET, S1}$) , or triplet state ($\Delta G_{ET, T1}$) were photolyzed in a 1:1 DMSO/MMA mixture. All samples were purged with N_2 prior to photolysis. The photocatalyst (10 mM) in DMSO/MMA was photolyzed with either 300 (12 bulb, 14.5 W broadband) or 419 nm light for 18 hours and polymerization was confirmed by precipitation of p-MMA from adding the photolysis solution to 1:1 MeOH/Petroleum ether. The results of the experiment are

compiled in Table 5.5. The photophysical parameters were compiled from the following reference[36].

Table 5.5 Photophysical parameters and polymerization of various photocatalysts

PC[b]	λ_{max} (nm)	τ (ns)	ϕ_f	ϕ_{ISC}	E_{S1}, kcal/mol	E_{T1}, kcal/mol	E_{red}, V vs SCE	$\Delta G_{ET, S1}$ kcal/mol	$\Delta G_{ET, T1}$ kcal/mol	Polymer (Y/N?)
DCA[a]	422	14.9	0.76	0.0085	66.7	41.63	-0.91	-8.8	-	N
XO	340	0		1	78.2	74.06	-1.65	-3.3	0.9	Y
TCBQ	450	-	-	1	-	56.58	0	-	-19.7	N
AQ	326	-	-	1.04	-	62.79	-0.96	-	-3.8	Y
TPT+	415	4.38	0.58	0.42	65.09	52.9	-0.32	-20.8	-8.6	Y
Mes-Acr-Me+[c]	495	6	0.035	0.38	61.41	44.62	-0.49	-13.2	3.6	N
Mes-Acr-Me+[d]	-	-	0.08	-	59.11	-	-0.57	-9.1	-	N
MB+	650	1		0.52	43.47	34.5	-0.3	0.3	9.3	N
PDI[a]	521	3.9	0.98	-	54.05	-	-0.43	-7.2	46.8	N

* The oxidation potential of DMSO used was +1.6 V vs. SCE. **Yellow areas are used to indicate exergonic electron transfer. ***Red areas are used to indicate visible polymerization was observed.
[a] samples were not soluble at 10 mM and had to be photolyzed at 1 mM
[b] abbreviations: DCA: 9,10-dicyanoanthracene; XO: xanthone; TCBQ: chloranil; AQ: 9,10-anthraquinone; TPT+: 2,4,6-triphenylpyrilium tetrafluorborate; Mes-Acr-Me+: 9-mesityl-10-methylacridinium tetrafluorborate; MB+: methylene blue; PDI: *N,N*'-bis(2,6-diisopropylphenyl)perylene-3,4,9,10-tetracarboxylic diimide
[c] locally excited [d] charge transfer

Of the compounds studied, all were expected to abstract an electron from DMSO in their excited-state. Interestingly, only those that were expected to be exergonic from the T_1 state were seen to form visible polymer while no polymerization was observed with those that were expected to be exergonic from only the S_1 state. Two exceptions are XO and TCBQ. In the case of XO, the predicted free energy change is less than 1 kcal/mol endergonic which, although unfavorable, could easily be overcome. In fact, if 1.55 V vs SCE is used as the oxidation potential of DMSO, the predicted free energy of electron transfer becomes slightly exergonic (-0.3 kcal/mol). On the other hand, electron transfer to TCBQ is predicted to be very exergonic (-19.7 kcal/mol) though no polymerization was noted. However, TCBQ is reduced at a potential of 0 V vs. SCE making it a good excited-state oxidant, but a

poor photocatalyst due to problems with turnover of the reduced $TCBQ^{\bullet-}$. Ur mechanism requires that the photocatalyst turnover to continue to initiate polymerization. In the absence of a substance, such as O_2, to regenerate the starting species, the concentration of radical species formed will be too low to result in significant polymerization. The experiments in Table 5.5 were performed under N_2 which makes the stability of the reduced photocatalyst important. Therefore, in the case of TCBQ, although electron transfer from DMSO is exergonic, it is possible that low conversions and no catalytic turnover lead to no observable polymer formation.

In each case, it was shown that although electron transfer from DMSO was predicted to be exergonic in S_1, no polymerization was observed. This leads us to believe that there is a significant solvent cage effect for the contact ion pair formed in the singlet excited-state. For the singlet state, because back electron transfer is spin allowed it is expected to out compete hydration of $DMSO^{+\bullet}$. In the absence of a quencher, the $DMSO^{+\bullet}$ is unable to react with water to form radicals capable of initiation. Future studies will aim to determine if adding water, or other quenchers, to the system results in observable polymerization with photocatalysts that react from S_1. Doing so will allow us to perform polymerizations without prior deoxygenation. This work represents an investigation into the role of DMSO in photo-initiated polymerization systems. The solvent must be considered when examining all initiation pathways and using DMSO has, under highly oxidizing conditions, been shown to produce radicals reactive enough to initiate polymerization.

5.9. References:

(1) Pan, X.; Tasdelen, M. A.; Laun, J.; Junkers, T.; Yagci, Y.; Matyjaszewski, K.

Photomediated Controlled Radical Polymerization. *Prog. Polym. Sci.* **2016**, *62*, 73–125.

(2) Hill, M. R.; Carmean, R. N.; Sumerlin, B. S. Expanding the Scope of RAFT Polymerization: Recent Advances and New Horizons. *Macromolecules*. **2015**, *48*, 5459–5469.

(3) Chen, M.; Zhong, M.; Johnson, J. A. Light-Controlled Radical Polymerization: Mechanisms, Methods, and Applications. *Chem. Rev.* **2016**, *116* (17), 10167–10211.

(4) McKenzie, T. G.; Fu, Q.; Uchiyama, M.; Satoh, K.; Xu, J.; Boyer, C.; Kamigaito, M.; Qiao, G. G. Beyond Traditional RAFT: Alternative Activation of Thiocarbonylthio Compounds for Controlled Polymerization. *Adv. Sci.* **2016**, *3* (9), 1500394.

(5) Corrigan, N.; Shanmugam, S.; Xu, J.; Boyer, C. Photocatalysis in Organic and Polymer Synthesis. *Chemical Society Reviews*. The Royal Society of Chemistry November 7, 2016, pp 6165–6212.

(6) Shanmugam, S.; Xu, J.; Boyer, C. Photocontrolled Living Polymerization Systems with Reversible Deactivations through Electron and Energy Transfer. *Macromolecular Rapid Communications*., **2017**, *38*, 1700143.

(7) McKenzie, T. G.; Fu, Q.; Wong, E. H. H.; Dunstan, D. E.; Qiao, G. G. Visible Light Mediated Controlled Radical Polymerization in the Absence of Exogenous Radical Sources or Catalysts. *Macromolecules* **2015**, *48* (12), 3864–3872.

(8) Otsu, T. Iniferter Concept and Living Radical Polymerization. *J. Polym. Sci.*

Part A Polym. Chem. **2000**, *38* (12), 2121–2136.

(9) Khan, M. Y.; Cho, M.-S.; Kwark, Y.-J. Dual Roles of a Xanthate as a Radical Source and Chain Transfer Agent in the Photoinitiated RAFT Polymerization of Vinyl Acetate. *Macromolecules* **2014**, *47* (6), 1929–1934.

(10) Shanmugam, S.; Cuthbert, J.; Kowalewski, T.; Boyer, C.; Matyjaszewski, K. Catalyst-Free Selective Photoactivation of RAFT Polymerization: A Facile Route for Preparation of Comblike and Bottlebrush Polymers. *Macromolecules* **2018**, *51* (19), 7776–7784.

(11) Quinn, J. F.; Barner, L.; Barner-Kowollik, C.; Rizzardo, E.; Davis, T. P. Reversible Addition - Fragmentation Chain Transfer Polymerization Initiated with Ultraviolet Radiation. *Macromolecules* **2002**, *35* (20), 7620–7627.

(12) You, Y.-Z.; Hong, C.-Y.; Bai, R.-K.; Pan, C.-Y.; Wang, J. Photo-Initiated Living Free Radical Polymerization in the Presence of Dibenzyl Trithiocarbonate. *Macromol. Chem. Phys.* **2002**, *203* (3), 477–483.

(13) Lu, L.; Zhang, H.; Yang, N.; Cai, Y. Toward Rapid and Well-Controlled Ambient Temperature RAFT Polymerization under UV - Vis Radiation: Effect of Radiation Wave Range. *Macromolecules* **2006**, *39* (11), 3770–3776.

(14) Xu, J.; Shanmugam, S.; Duong, H. T.; Boyer, C. Organo-Photocatalysts for Photoinduced Electron Transfer-Reversible Addition-Fragmentation Chain Transfer (PET-RAFT) Polymerization. *Polym. Chem.* **2015**, *6* (31), 5615–5624.

(15) Phommalysack-Lovan, J.; Chu, Y.; Boyer, C.; Xu, J. PET-RAFT Polymerisation: Towards Green and Precision Polymer Manufacturing. *Chem.*

Commun. **2018**, *54* (50), 6591–6606.

(16) Shanmugam, S.; Xu, J.; Boyer, C. Exploiting Metalloporphyrins for Selective Living Radical Polymerization Tunable over Visible Wavelengths. *J. Am. Chem. Soc.* **2015**, *137* (28), 9174–9185.

(17) Theriot, J. C.; Miyake, G. M.; Boyer, C. A. *N* , *N* -Diaryl Dihydrophenazines as Photoredox Catalysts for PET-RAFT and Sequential PET-RAFT/O-ATRP. *ACS Macro Lett.* **2018**, *7* (6), 662–666.

(18) Figg, C. A.; Hickman, J. D.; Scheutz, G. M.; Shanmugam, S.; Carmean, R. N.; Tucker, B. S.; Boyer, C.; Sumerlin, B. S. Color-Coding Visible Light Polymerizations To Elucidate the Activation of Trithiocarbonates Using Eosin Y. *Macromolecules* **2018**, acs.macromol.7b02533.

(19) Corrigan, N.; Rosli, D.; Jones, J. W. J.; Xu, J.; Boyer, C. Oxygen Tolerance in Living Radical Polymerization: Investigation of Mechanism and Implementation in Continuous Flow Polymerization. *Macromolecules* **2016**, *49* (18), 6779–6789.

(20) Yeow, J.; Chapman, R.; Gormley, A. J.; Boyer, C. Up in the Air: Oxygen Tolerance in Controlled/Living Radical Polymerisation. *Chemical Society Reviews*. **2018**, *47* (12), 4357–4387.

(21) Shanmugam, S.; Xu, J.; Boyer, C. Utilizing the Electron Transfer Mechanism of Chlorophyll a under Light for Controlled Radical Polymerization. *Chem. Sci.* **2015**, *6* (2), 1341–1349.

(22) Shanmugam, S.; Xu, S.; Adnan, N. N. M.; Boyer, C. Heterogeneous Photocatalysis as a Means for Improving Recyclability of Organocatalyst in

"Living" Radical Polymerization. *Macromolecules* **2018**, *51* (3), 779–790.

(23) Corrigan, N.; Xu, J.; Boyer, C. A Photoinitiation System for Conventional and Controlled Radical Polymerization at Visible and NIR Wavelengths. *Macromolecules* **2016**, *49* (9), 3274–3285.

(24) Kishore, K.; Asmus, K.-D. Radical Cations from One-Electron Oxidation of Aliphatic Sulphoxides in Aqueous Solution. A Radiation Chemical Study. *J. Chem. Soc. Perkin Trans. 2* **2004**, No. 12, 2079.

(25) Fuchigami, T.; Mahito, A.; Shinsuke, I. *Fundamentals and Applications of Organic Eletrochemistry: Synthesis, Materials, Devices*, First Edit.; John Wiley & Sons, Inc., 2015.

(26) Crean, C.; Geacintov, N. E.; Shafirovich, V. Methylation of 2′-Deoxyguanosine by a Free Radical Mechanism. *J. Phys. Chem. B* **2009**, *113* (38), 12773–12781.

(27) Thum, M. D.; Falvey, D. E. Photoreleasable Protecting Groups Triggered by Sequential Two-Photon Absorption of Visible Light: Release of Carboxylic Acids from a Linked Anthraquinone- N -Alkylpicolinium Ester Molecule. *J. Phys. Chem. A* **2018**, *122* (12), 3204–3210.

(28) Ly, D.; Kan, Y.; Armitage, B.; Schuster, G. B. Cleavage of DNA by Irradiation of Substituted Anthraquinones: Intercalation Promotes Electron Transfer and Efficent Reaction at GG Steps. *J. Am. Chem. Soc.* **1996**, *118* (36), 8747–8748.

(29) Breslin, D. T.; Schuster, G. B. Anthraquinone Photonucleases: Mechanisms for GG-Selective and Nonselective Cleavage of Double-Stranded DNA. *J. Am. Chem. Soc.* **1996**, *118* (10), 2311–2319.

(30) Görner, H. Photoreduction of 9,10-Anthraquinone Derivatives: Transient Spectroscopy and Effects of Alcohols and Amines on Reactivity in Solution¶. *Photochem. Photobiol.* **2003**, *77* (2), 171–179.

(31) Bardagi, J. I.; Ghosh, I.; Schmalzbauer, M.; Ghosh, T.; König, B. Anthraquinones as Photoredox Catalysts for the Reductive Activation of Aryl Halides. *European J. Org. Chem.* **2018**, *2018* (1), 34–40.

(32) Kuss-Petermann, M.; Wenger, O. S. Electron Transfer Rate Maxima at Large Donor-Acceptor Distances. *J. Am. Chem. Soc.* **2016**, *138* (4), 1349–1358.

(33) Kuss-Petermann, M.; Orazietti, M.; Neuburger, M.; Hamm, P.; Wenger, O. S. Intramolecular Light-Driven Accumulation of Reduction Equivalents by Proton-Coupled Electron Transfer. *J. Am. Chem. Soc.* **2017**, *139* (47), 5225–5232.

(34) Görner, H. Photoreactions of P-Quinones with Dimethyl Sulfide and Dimethyl Sulfoxide in Aqueous Acetonitrile†. *Photochem. Photobiol.* **2005**, *82* (1), 71.

(35) Shanmugam, S.; Xu, J.; Boyer, C. Photoinduced Oxygen Reduction for Dark Polymerization. *Macromolecules* **2017**, *50* (5), 1832–1846.

(36) Romero, N. A.; Nicewicz, D. A. Organic Photoredox Catalysis. *Chem. Rev.* **2016**, *116* (17), 10075–10166.

Chapter 6: Supplemental Information

General Methods And Materials:

All Chemicals and solvents were purchased from commercial suppliers and were used without further purification unless otherwise noted. All ^{1}H and ^{13}C NMR were obtained on a Bruker 400 mHz spectrometer. Chemical shifts (δ) are reported in parts per million (ppm). Ultraviolet-visible (UV/Vis) spectrum were recorded on a Shimadzu UV-1800 spectrometer using UVProbe 2.43 software. Samples were scanned from using a fast scanning speed and a sampling interval of 1.0 nm. ATR-FT-IR data was collected using a Thermo Nicolet 670 with OMNIC software package.

Gel Permeation Chromatography (GPC) was used to obtain molecular weight (Mn and Mw) and polydispersity index (PDI) of polymers using Viscotek GPCMax equipped with 4 columns (T2500, T3000, T4000, and T5000) in a column oven and differential refractometer (maintained at 40 °C). Tetrahydrofuran (THF, HPLC Grade) was used as the eluent with a flow rate of 1 mL/min). Polystyrene standards (from Polymer Laboratories Inc., 580 Da – 3,150 kDa) were used for calibration. For GPC sample preparation 6-10 mg of dry polymer sample was dissolved in 1 g of THF then filtered through a 0.2μm Nylon Target2 filter.

Mass spectra data was acquired using a JEOL AccuTOF-CS using ESI-TOF. Cyclic voltammetry experiments were performed using a glassy carbon working electrode, a platinum counter electrode, and a Ag/AgCl reference electrode.

Laser flash photolysis experiments were performed using a Nd:YAG laser pump beam source with a Continuum Surelite II-10 capable of 266, 532, or 355 nm

pulses between 4-6 ns A LeCroy 350 MHz digital oscilloscope was used to observe all waveforms. Samples were prepared so that their relative absorbance was between 0.75 and 1.5 at the excitation wavelength, 355 nm. The probe beam was a 350 W Xenon arc lamp. The samples were loaded into a 1 cm quartz cuvette and N_2 was purged for 10 minutes in the solution and an additional 5 minutes in the headspace. Samples were flowed continuously thorough out the experiment to avoid buildup of photoproducts. Fluorescence experiments were conducted on a Hitachi F-4500 fluorescence spectrophotometer.

Photolysis experiments were performed with one of the following: 100 mW 405 nm CW Diode Laser, 100 mW 532 nm CW Diode Laser, 0-1 W tunable 447 nm CW diode laser, 1 W 808 nm CW diode Laser, RPR-100 Rayonet reactor (16-bulb, 35 W, 35ºC operating temperature, 350/419 nm), RMR-600 Rayonet reactor (8-bulb, 32 watt, 37ºC operating temperature, 253.7/300/350 nm). All lasers were provided by Laserglow Technologies. The emission of the RPR-100 rayonet is given below.

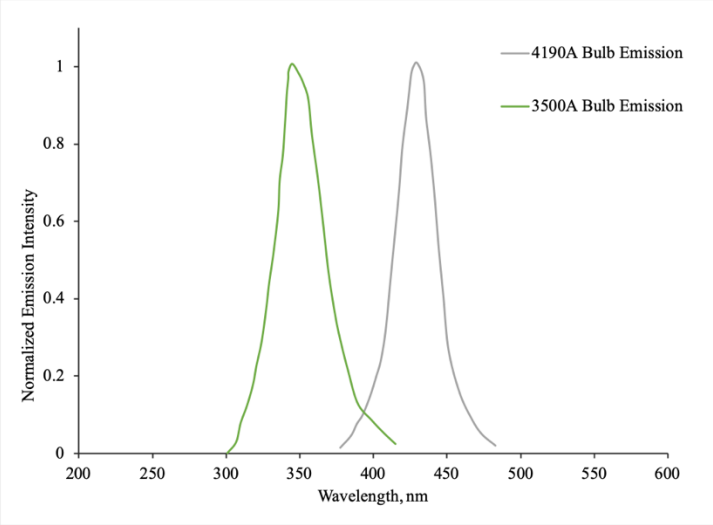

Figure 6.1. The normalized broadband emission intensity of the RPR-100 Rayonet reactor.

6.2 Chapter 2 Experimental Results:

(a) **Preparation of Alginate Hydrogels**

Stock solutions of RB (0.26 mM), Ca-EDTA (50 mM) and sodium alginate (3.75 wt%) were prepared in pH = 9.3 buffered carbonate/bicarbonate buffered water. Additionally, $CaCl_2$ standard 0.1 M (Sigma Aldrich) was used. Final solution concentration before photolysis was 0.084 mM RB, 16 mM EDTA, 19 mM Ca^{2+}, 1.21 wt% sodium alginate.

1) 350 nm photolysis

Photolysis solutions were prepared by mixing 1 mL each of RB and Ca-EDTA stock solutions with 1 mL of sodium alginate in a 5 mL vial with a stirbar. To this was added 100 μL of 0.1 M $CaCl_2$ standard. The solution was carefully mixed prior to photolysis. The sample was then irradiated for 2 hours using a 350 nm, 12-bulb, Rayonet photoreactor. The sample was continuously stirred during photolysis. After photolysis the presence of a free-standing gel was observed while the dark control showed no significant gelation.

2) 447 nm photolysis

The solution was carefully mixed prior to photolysis. The sample was then irradiated for 2 hours using a 447 nm CW diode laser. The sample was continuously stirred during photolysis. After photolysis the presence of a free-standing gel was observed while the dark control showed no significant gelation.

(b) Transient Absorption Spectroscopy

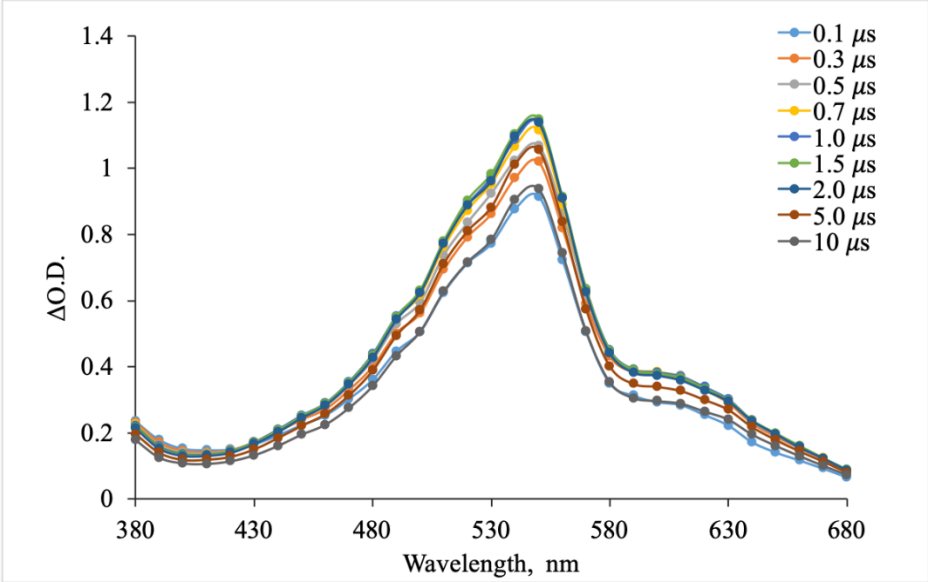

Figure 6.2. Transient absorption spectra (355 nm) of benzophenone in MeOH with TEA.

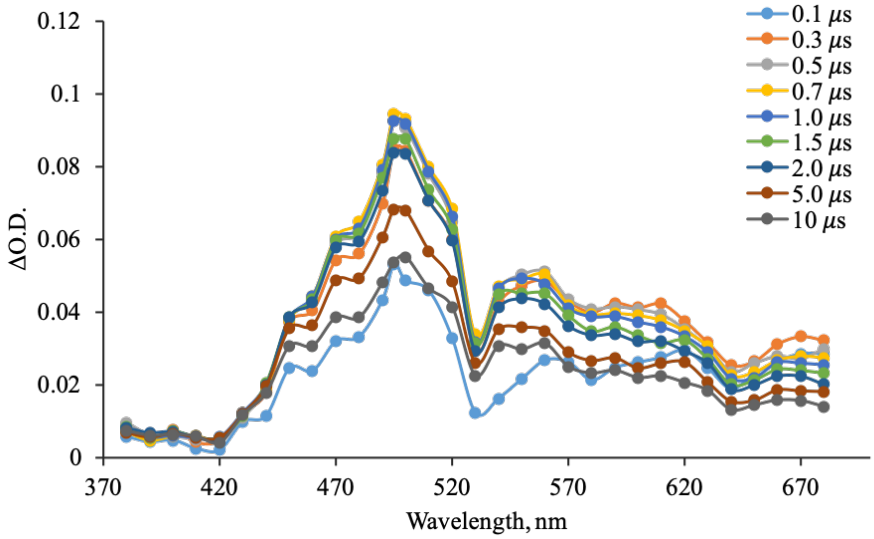

Figure 6.3. Transient absorption spectra (355 nm) of 2-aminoanthracene in MeCN.

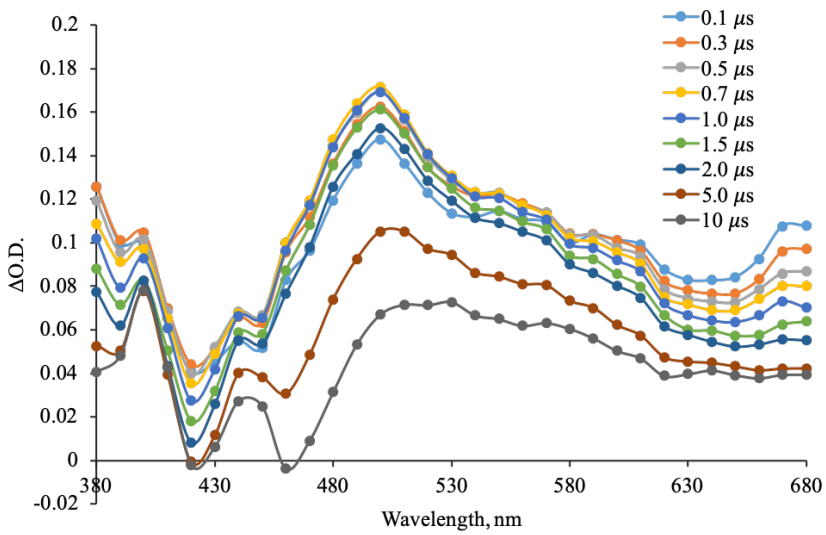

Figure 6.4. Transient absorption spectra (355 nm) of 2-aminoanthracene with NHC-CO_2 (10 eq.) in MeCN.

6.3 Chapter 3 Experimental Results:

(a) Cyclic Voltammetry

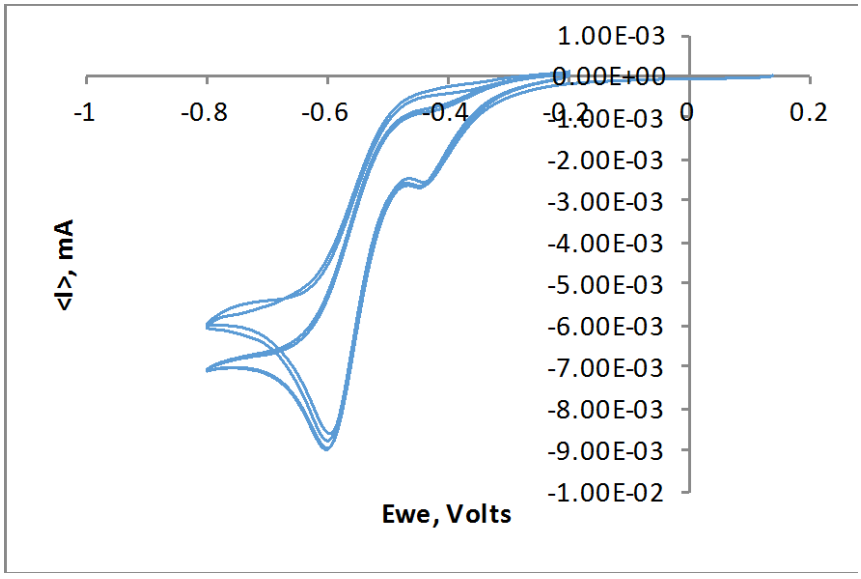

Figure 6.5. Anthraquinone-2-acetaniline, **1**, in MeOH, 0.1 M NH_4Cl 25 mV/s. All potentials measured vs. Ag/AgCl.

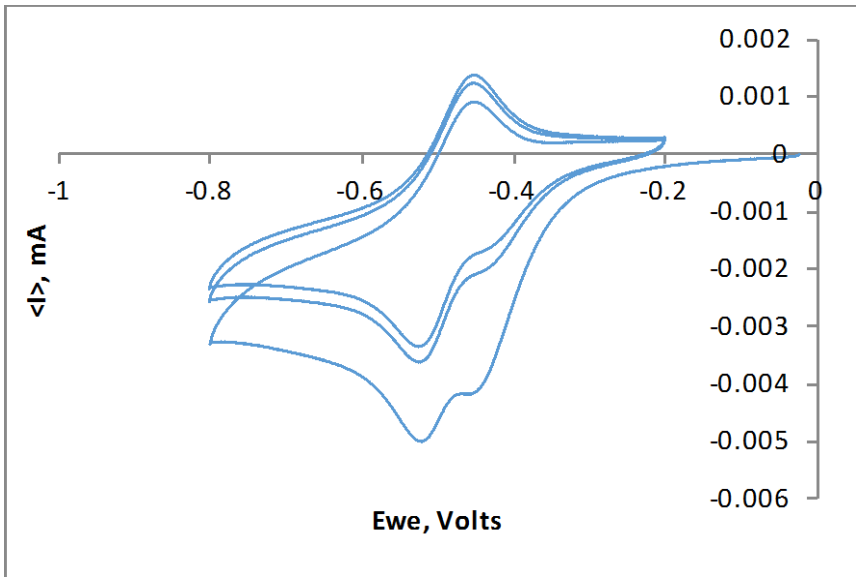

Figure 6.6. PAQ-1 in Water, 0.5 M NH_4Cl: 100 mV/s. All potentials measured vs. Ag/AgCl.

(b) Characterization and Synthesis of compounds

1-((9,10-dioxo-9,10-dihydroanthracen-2-yl)methyl)-4-((2-phenylacetoxy)methyl) pyridin-1-ium chloride. PAQ-1 A round bottom flask containing 2-chloro-*N*-(9,10-anthraquinone-2-)acetaniline (457 mg, 1.5 mmol) and picolyl phenylacetate (1.35 g, 6.0 mmol) in 25 mL freshly distilled THF was refluxed for 18 hours. The solution was vacuum filtered and the precipitate was recrystallized from hot methanol to afford 258 mg of **PAQ-1** as a dark yellow powder which crystalizes under high vacuum in 33% yield. Melting Point 112-114°C. ^{1}H NMR (400 MHz, DMSO-d_6) δ 11.60 (s, 1H), 9.05 (d, 2H), 8.52 (d, 1H), 8.26-8.05 (m, 7H), 7.94 (m, 2H), 7.32 (m, 5H), 5.74 (s, 2H), 5.53 (s, 2H), 3.93 (s, 2H); ^{13}C NMR (400 MHz, DMSO-d_6) δ 182.2, 182.1, 170.8, 144.9, 140,4, 134.7, 134.5, 133.9, 133.6, 133.4, 132.9, 129.5, 128.4, 127.8, 127.16, 127.0, 128.8, 125.4, 63.4, 62.1; IR (solid) 2947, 2360, 2340,

1741, 1704, 1671, 1645, 1589, 1576, 1546, 1495, 1467, 1422; *m/z* calcd for $C_{30}H_{33}N_2O_5$ (M^+) 491.1601, found 491.1602.

1-(2-((9,10-dioxo-9,10-dihydroanthracen-2-yl)amino)-2-oxoethyl)-4-methylpyridin-1-ium chloride. PAQ-0. A round bottom flask containing 2-chloro-*N*-(9,10-anthraquinone-2-)acetaniline (507 mg, 1.7 mmol) and 4-methyl pyridine (0.35 mL, 3.5 mmol) in 30 mL freshly distilled THF was refluxed for 48 hours. The solution was vacuum filtered and the precipitate was recrystallized from hot methanol to afford 287 mg of **PAQ-0** as a brown powder in 43% yield. Melting Point 280-283°C. ^{1}H NMR (400 MHz, DMSO(d6)) δ 11.63 (s, 1H), 8.92 (d, 2H), 8.52 (d, 1H), 8.22 (m, 3H), 8.08 (d, 3H), 7.94 (m, 2H), 5.69 (s, 2H), 2.67 (s, 3H); ^{13}C NMR (400 MHz, DMSO-d_6) δ 182.4, 181.4, 164.7, 160.0, 145.4, 143.7, 134.7, 134.4, 134.3, 133.11, 133.08, 128.7, 128.6, 127.9, 126.8, 126.7, 124.0, 116.1, 61.5, 21.6; IR (solid) 2925, 1700, 1674, 1651, 1591, 1550, 5125, 1494; *m/z* calcd for $C_{22}H_{17}N_2O_3$ (M^+) 357.1234, found 357.1232.

2-chloro-*N*-(9,10-anthraquinone-2-)acetaniline. 2-amino anthraquinone (3.04 g, 13.5 mmol) was dissolved in 150 mL of dry dichloromethane and pyridine (2.6 mL, 16.2 mmol). The solution was cooled to 0°C and 2-chloroacetyl chloride (1.8 mL, 22.4 mmol) in 15 mL dry dichloromethane was added dropwise over the course of 10 minutes. The solution was stirred at 0°C for an hour and then at room temperature overnight. The solution was acidified with 10 mL of HCl (10% v:v) and vacuum filtered. The precipitate was washed with water and dried overnight in vacuo to yield

2.84g of product as a dry brown powder in 70% yield. Melting Point 246-250 ºC (lit 250 ºC).[1] ^{1}H NMR (400 MHz, DMSO-d_6) δ 10.97 (s, 1H), 8.47 (d, 1H), 8.20 (m, 3H), 8.09 (dd, 1H), 7.93 (m, 2H), 4.36 (s, 2H). ^{13}C NMR (400 MHz, DMSO-d_6) δ 182.5, 182.4, 169.4, 144.8, 134.6, 134.2, 133.2, 128.6, 127.8, 126.8, 126.7, 123.6, 115.7, 24.27.

9,10-anthraquinone-2-acetaniline, 1. 2-amino anthraquinone (1.88 g, 8.42 mmol) was dissolved in 40 mL of dry dichloromethane and pyridine (0.75 mL, 9.31 mmol). The solution was cooled to 0ºC and acetyl chloride (1.2 mL, 16.8 mmol) in 15 mL dry dichloromethane was added dropwise over the course of 10 minutes. The solution was stirred at 0ºC for an hour and then stirred at room temperature overnight. The solution was acidified with 10 mL of HCl (10% v:v) and vacuum filtered. The precipitate was washed with water and dried overnight in vacuo to yield 1.05 g of product as a dry brown powder in 47% yield. Melting Point 244-246ºC. ^{1}H NMR (400 MHz, DMSO-d_6) δ 10.63 (s, 1H), 8.45 (d, 1H), 8.19 (m, 3H), 8.08 (dd, 1H), 7.91 (m, 2H), 2.14 (m, 3H); ^{13}C NMR (400 MHz, DMSO-d_6) δ 182.5, 182.4, 169.4, 144.8, 134.6, 134.2, 133.2, 128.6, 127.8, 126.8, 126.7, 123.6, 115.7, 24.27.; IR (solid) 3360, 1697, 1669, 1576, 1530; *m/z* calcd for $C_{16}H_{11}NO_3$ (M^+) 266.0817, found 266.0841.

(c) Deprotection photolysis

A stock solution of PAQ-1 (0.24 mM in isopropyl alcohol) was prepared and filtered through a 0.45 μm cellulose acetate syringe filter prior to photolysis. To a 1 cm quartz cuvette with a stirbar was added 1.5 mL of stock solution. This was purged with N_2 for 10 minutes in the solution and an additional 5 minutes in the headspace.

The solution was photolyzed using a 1 Watt Laserglow 447 nm CW diode laser while being kept at 25°C and stirring using a Quantum Northwest TC125 temperature controlled cuvette holder. After photolysis for the desired time, the solution was transferred to a vial and the solvent was removed under reduced pressure. To this, 0.5 mL of CD_3OD was added before being analyzed using ^1H NMR.

(d) Oxygen Dependence

A solution of PAQ-1 was prepared as described above, but was not subjected to purging with nitrogen prior to photolysis. The photolysis was carried out in air using an open-top cuvette with stirring.

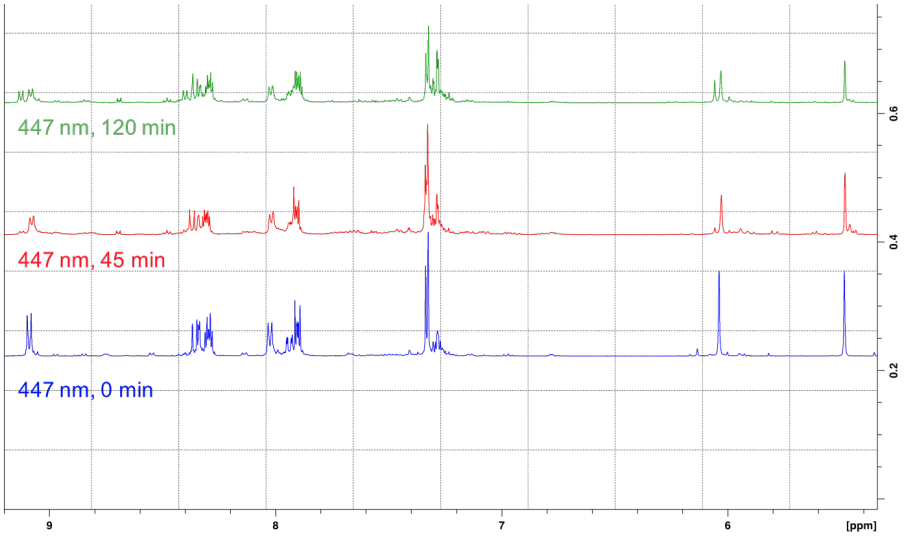

Figure 6.7. ^1H NMR showing PAQ-1 in isopropyl alcohol, photolysis at 447 nm in the presence of air.

(e) Steady-state Photolysis

A solution of PAQ-1 prepared as described above (see Deprotection photolysis, **e**) was photolyzed using a RPR-100 Rayonet reactor (16-bulb, 35 watt,

33°C operating temperature, 350 nm) Southern New England Ultraviolet. After photolysis at the desired time the UV/Vis specrum was recorded.

(e-1) Oxygen dependence on $PAQH_2$ formation

The oxygen dependence on the steady-state kinetic of the formation of $PAQH_2$ were explored. After extended irradiation times, there is no noticeable formation of the reduced species.

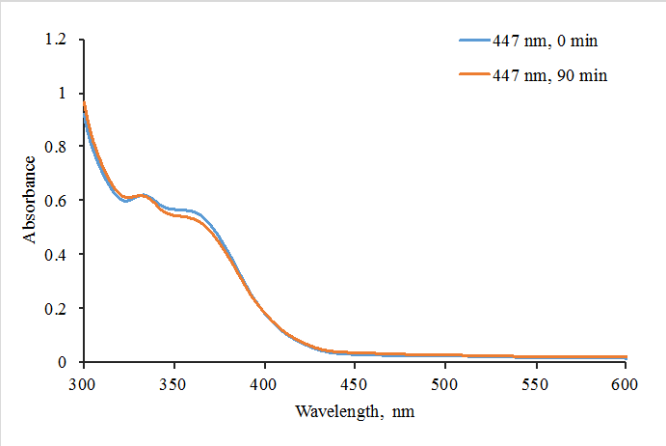

Figure 6.8. UV/Vis showing photolysis of PAQ-1 in the presence of air.

(f) Chemical Reduction of Anthraquinone with Sodium Dithionite

(f-1) Linked System, PAQ-1

In a 1 cm quartz cuvette with a stirbar, 1.5 mL of a stock solution of PAQ-1 (0.89 mM in CD_3OD) was purged with N_2 for 15 minutes. To this solution was added 0.5 mL of 0.1 M sodium dithionite (E_{red} = -0.66 V vs. SCE Powder, purified J.T. Baker) in D_2O.[3] The solution was then purged an additional 5 minutes with N_2. The appearance of a dark yellow color indicated the formation of hydroquinone. The solution was then photolyzed at 1.08 W using a 447 nm CW diode laser for one hour. An identically prepared sample was covered with aluminum foil and kept in the dark

for the entirety of the experiment. Before analyzing the sample by ^{1}H NMR, it was bubbled with molecular oxygen for 5 minutes.

(f-2) Model Unlinked System, Anthraquinone Acetamide and NAP-crotonate perchlorate

Anthraquinone-2-acetaniline, **1**, was synthesized as a model chromophore for use in unlinked experiments. Additionally, NAP-crotonate perchorate, **2**, was used as model NAP protected carboxylic acid for ease of detection of free crotonic acid by ^{1}HNMR. It was determined that, without first reducing the anthraquinone to the hydroquinone with dithionite, no release of crotonic acid was detected after photolysis at 447nm. Additionally, all solutions tested without the presence of dithionite showed no release crotonic acid. However, the sample which was first reduced with dithionite and then photolyzed at 447 nm for 60 minutes showed only free crotonic acid and no presence of protected carboxylic acid.

A stock solution of **1** was made by dissolving 3.1 mg in 5 mL (2.27 mM) of CD_3OD and sonicated for 2 hours. The solution was filtered through a 0.45 μm cellulose acetate syringe filter prior to photolysis. A stock **2** solution was made by dissolving 5.3 mg in 4 mL (4.54 mM) CD_3OD. The photolysis solution was made by adding 0.3 mL of NAP solution to 0.9mL of **1** in a 1 cm quartz cuvette with a stirbar. The sample was purged with nitrogen for 10 minutes before, while purging, 0.5 mL of sodium dithionite (39.4 mM in D_2O) was added. The solution turns a dark yellow and fluoresces brightly when irradiated conforming the formation of hydroquinone. The solution was purged with nitrogen an additional 5 minutes before photolysis while stirring at 1.08 W using a 447 nm CW diode laser for 60 minutes. An

identically prepared sample was prepared and kept wrapped in foil as a dark control. An additional control was prepared where pure D_2O without dithionite was added before photolysis.

(g) Quenching semiquinone by model NAP group

A stock solution of **1** was prepared by dissolving 9.7 mg in 250 mL isopropyl alcohol (0.15 mM, abs_{355nm} = 0.786). To 1 mL of anthraquinone acetaniline stock was added a total of 1 mL of mixtures of **2** stock (2.0 mM in isopropyl alcohol) and isopropyl alcohol to reach the desired final concentration of NAP in solution.

(h) Quantum Yield Determination

Quantum yield for the formation of $PAQH_2$ was calculated as follows. A solution of PAQ-0 in isopropyl alcohol (14.4 mM) was photolyzed at 405 nm using a CW diode laser at a power of 102 mW (Figure S-12). The formation of hydroquinone was monitored using the growth shown below at 390 nm. The fraction converted was calculated using equation 1 while the quantum yield was calculated using equations 2 and 3.

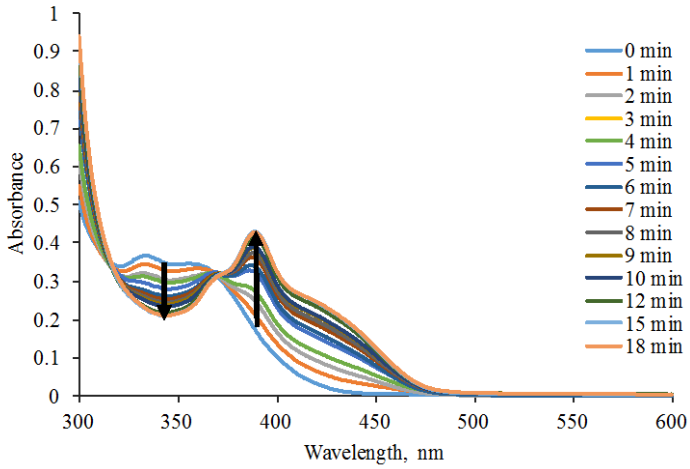

Figure 6.9. UV/Vis showing photolysis of PAQ-0 in IPrOH at 405 nm with a 102 mW CW diode laser. The formation of the hydroquinone can be seen as a peak at 390 nm.

$$1)\ f_{conv.} = \frac{\Delta A}{A_\infty - A_0}$$

$$2)\ k_{ex.} = \frac{Laser\ Power,\ W}{Photon\ Energy,\ J} * (1 - 10^{-A})$$

$$3)\ \Phi_{PAQH_2} = \frac{k_{PAQH_2}}{k_{ex.}}$$

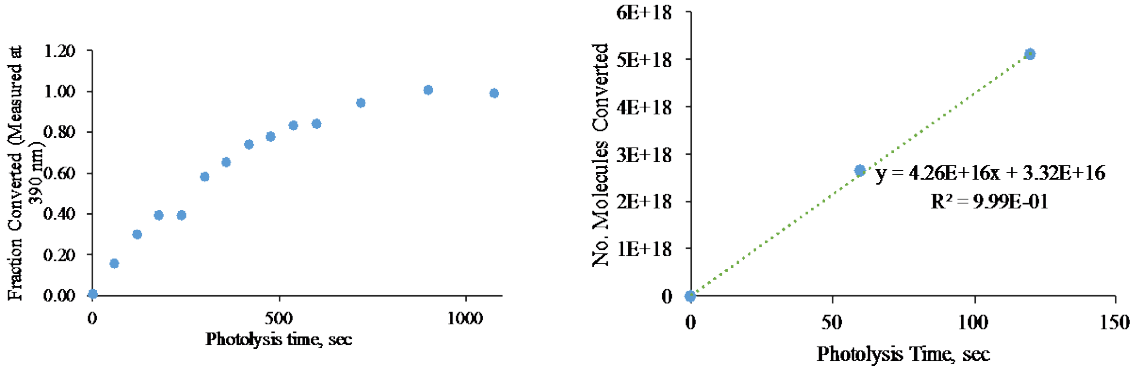

Figure 6.10. *Left*. Fraction of conversion of PAQ-0 to PAQ-0H_2 using equation 1 by measuring the absorbance change at 390 nm. *Right*. Initial rate of decomposition measured at 390 nm used to determine k_{PAQH2} in equation 3.

(i) Oxygen Dependence on triplet lifetime of PAQ-1

Waveforms taken at 410 and 510 nm respectively show that the triplet, which appears as an initial fast decay, has its lifetime decreased by purging with molecular oxygen. A solution of PAQ-1 in isopropyl alcohol was prepared as described in section (b) above, however, the samples were purged with molecular oxygen for 5

minutes in the solution and 3 minutes in the headspace prior to photolysis. The effect of the presence of oxygen is shown below.

(j) NMR spectrum of selected compounds

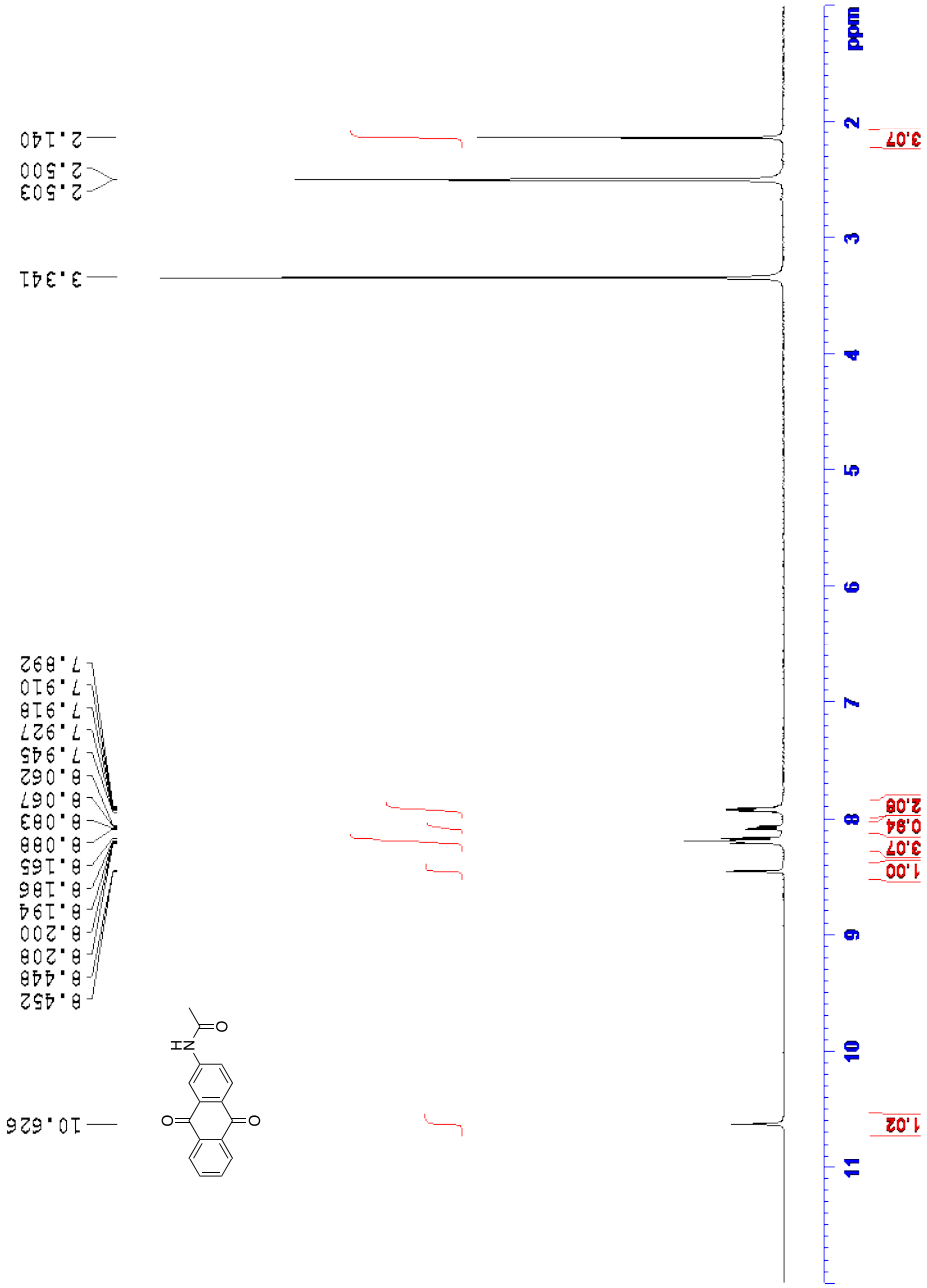

Figure 6.11. [1]HNMR Spectrum of anthraquinone-2-acetaniline.

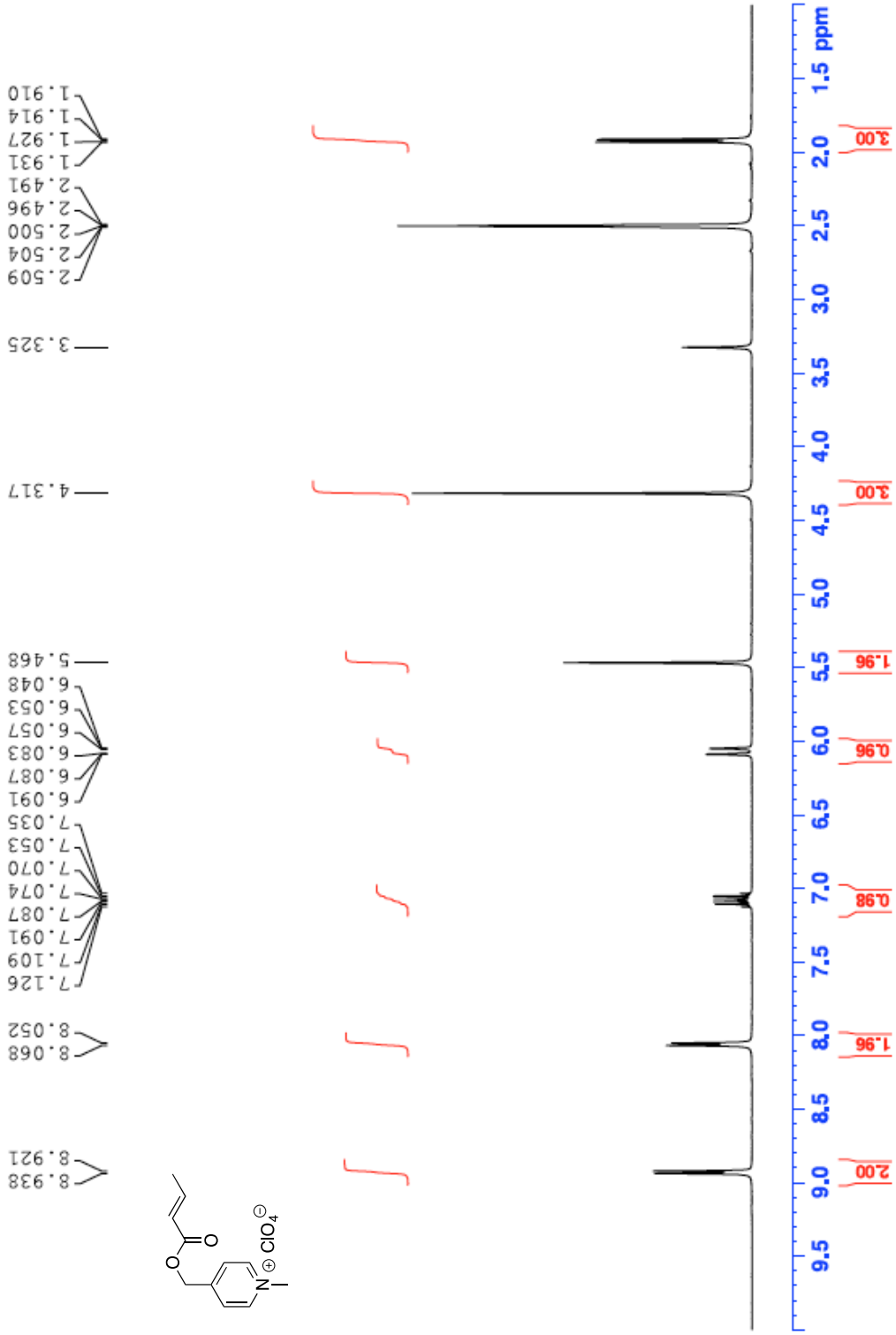

Figure 6.12. ^{1}H NMR Spectrum of NAP-Crotonate Perchlorate.

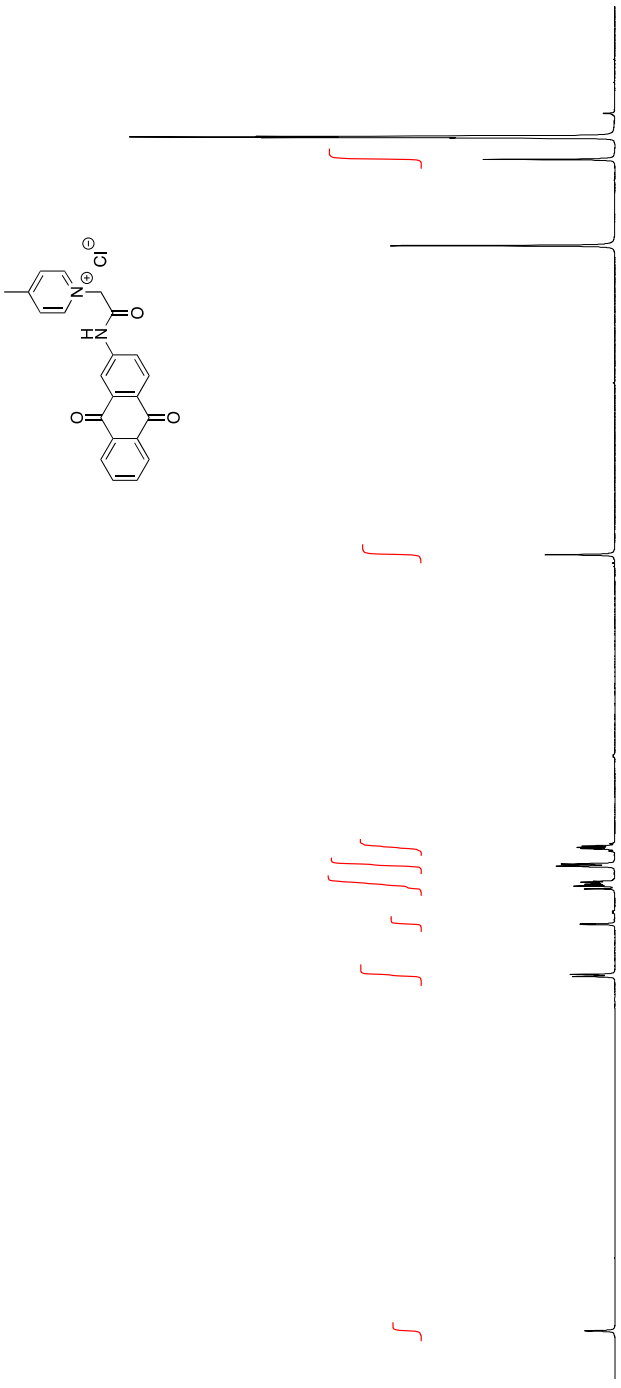

Figure 6.13. ^{1}H NMR Spectrum of PAQ-0.

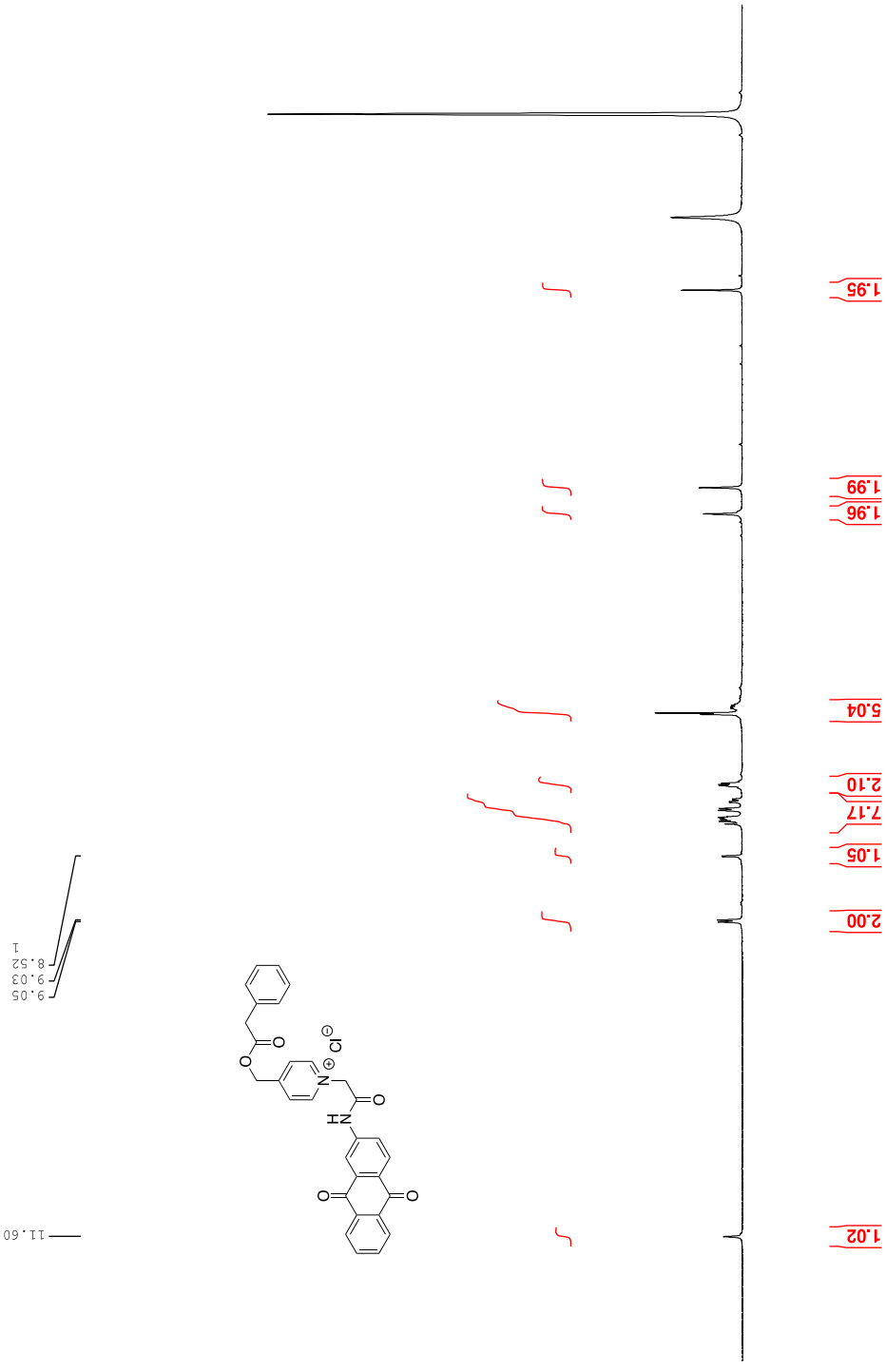

Figure 6.14. ^{1}H NMR Spectrum of PAQ-1.

6.4 Chapter 4 Experimental Results:

(a) Cyclic Voltammetry

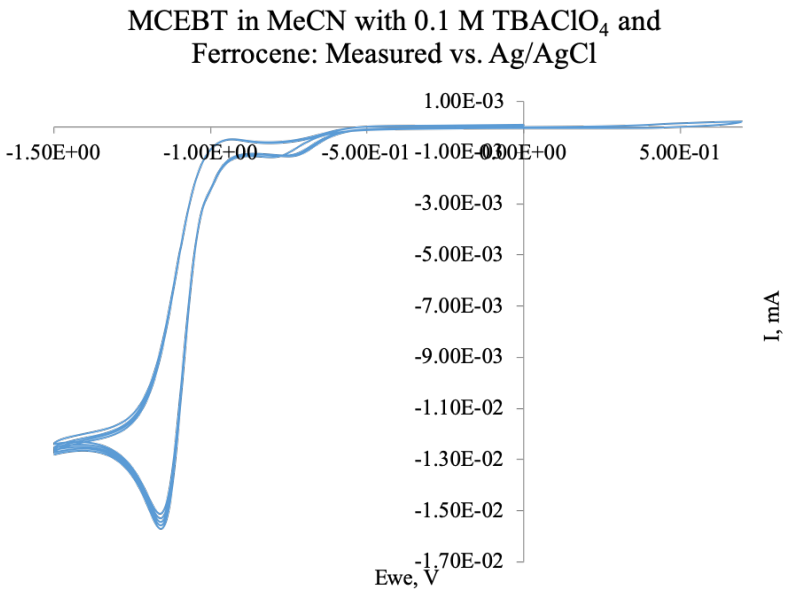

Figure 6.15. CV of MCEBT in MeCN.

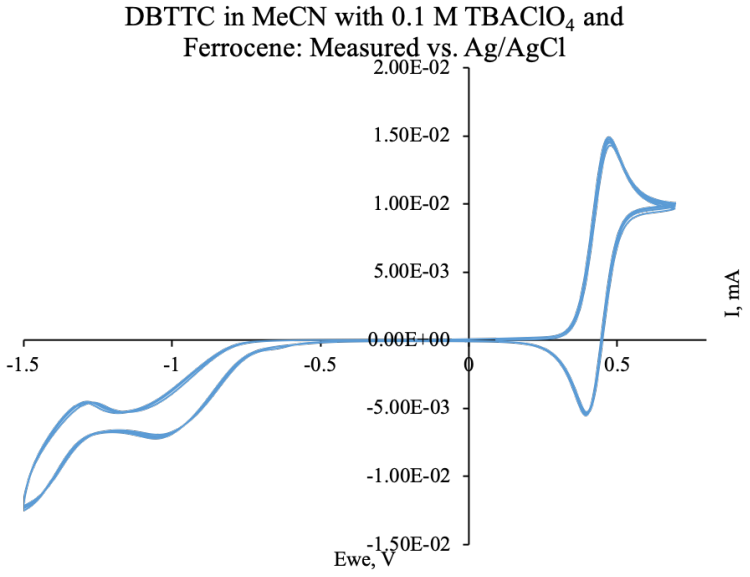

Figure 6.16. CV of DBTTC in MeCN.

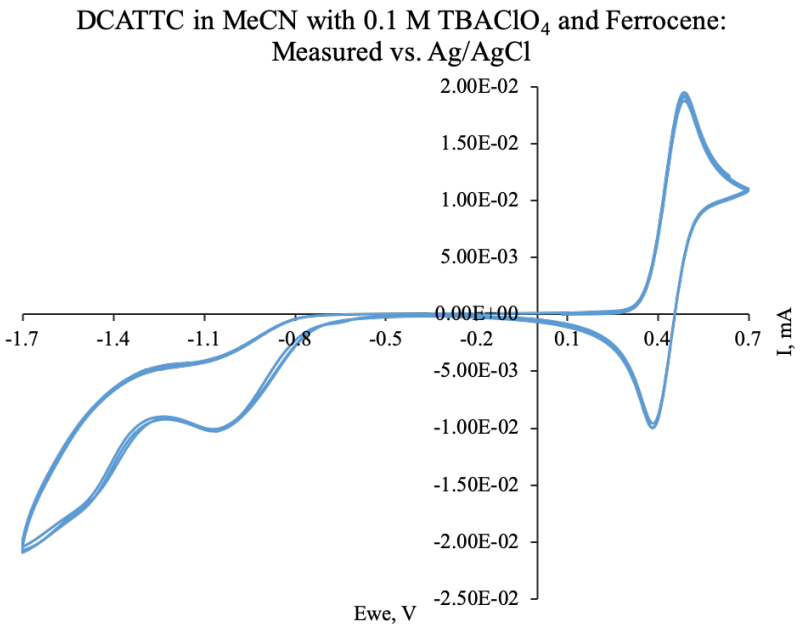

Figure 6.17. CV of DCATTC in MeCN.

(b) Transient Absorption Spectroscopy

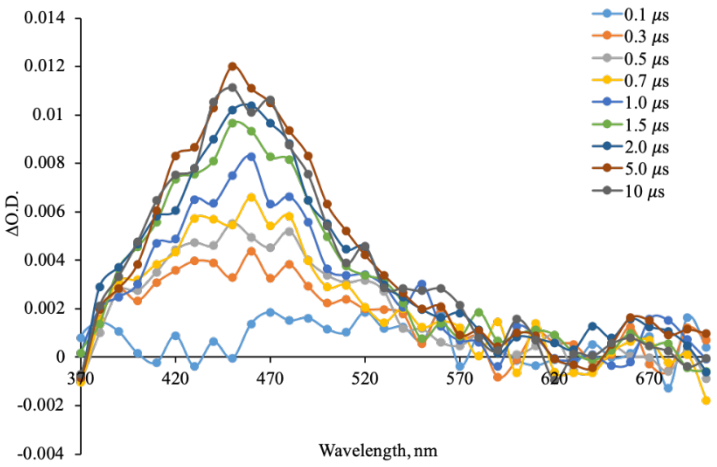

Figure 6.18. Transient absorption spectra of MCEBT in MeCN (355 nm).

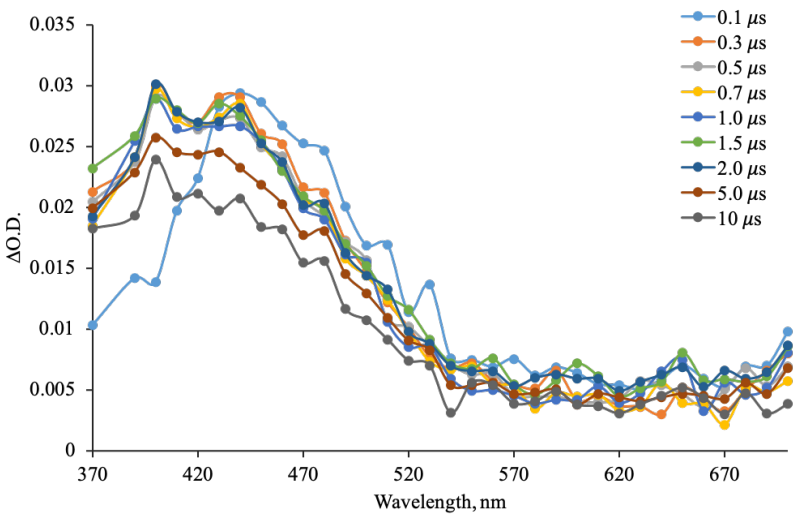

Figure 6.19. Transient absorption spectra of CPADB in MeCN (355 nm).

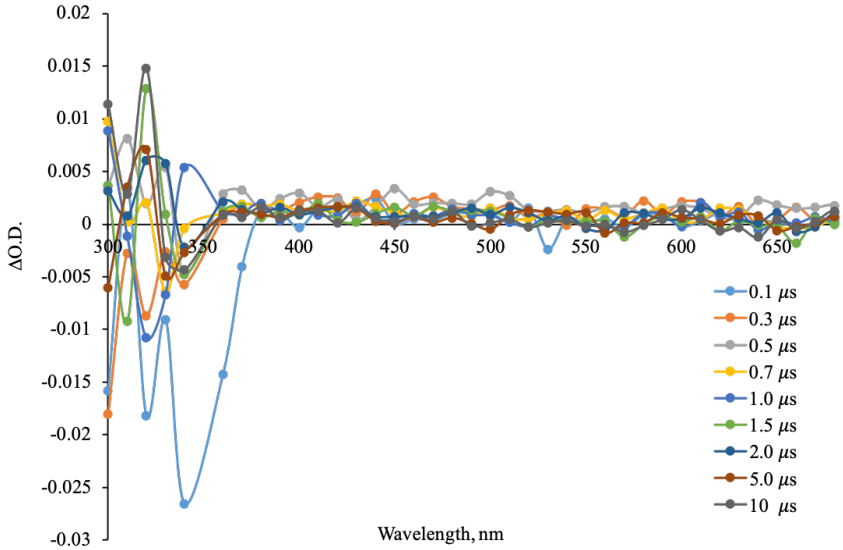

Figure 6.20. Transient absorption spectra of DBTTC in MeCN (355 nm).

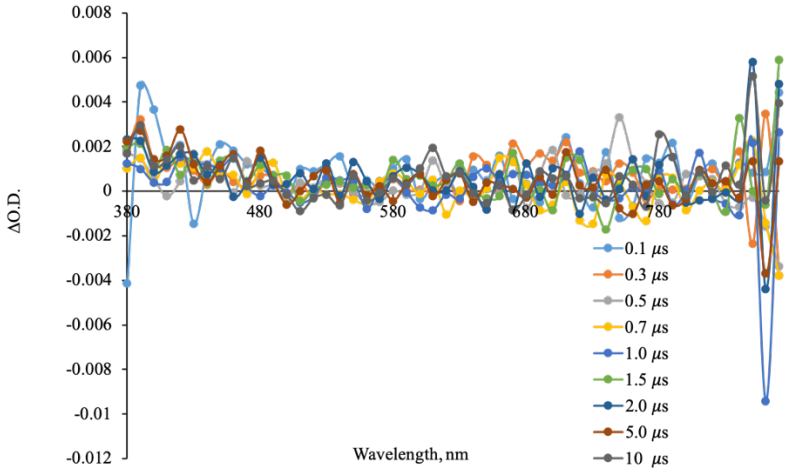

Figure 6.21. Transient absorption spectra of DCATTC in MeCN (355 nm).

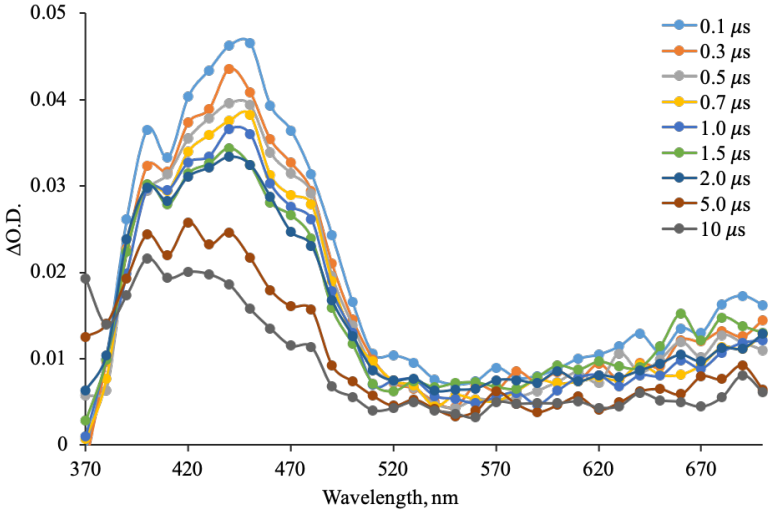

Figure 6.22. Transient absorption spectra of DTBDS in MeCN (355 nm).

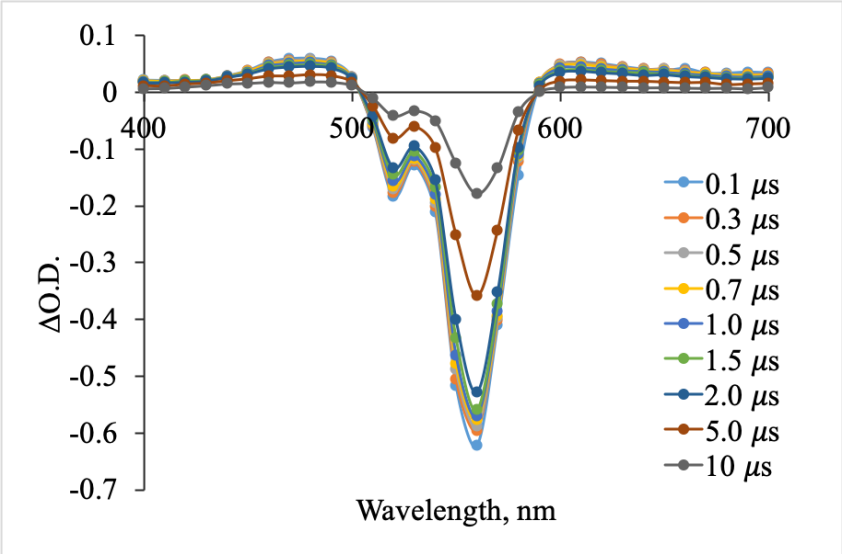

Figure 6.23. Transient absorption spectra of RB in MeCN (532 nm).

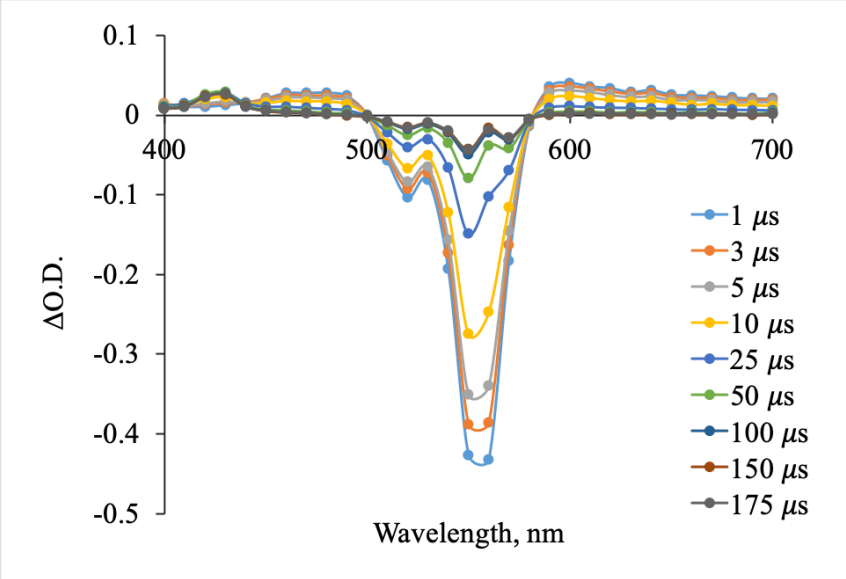

Figure 6.24. Transient absorption spectra of RB in MeCN (532 nm).

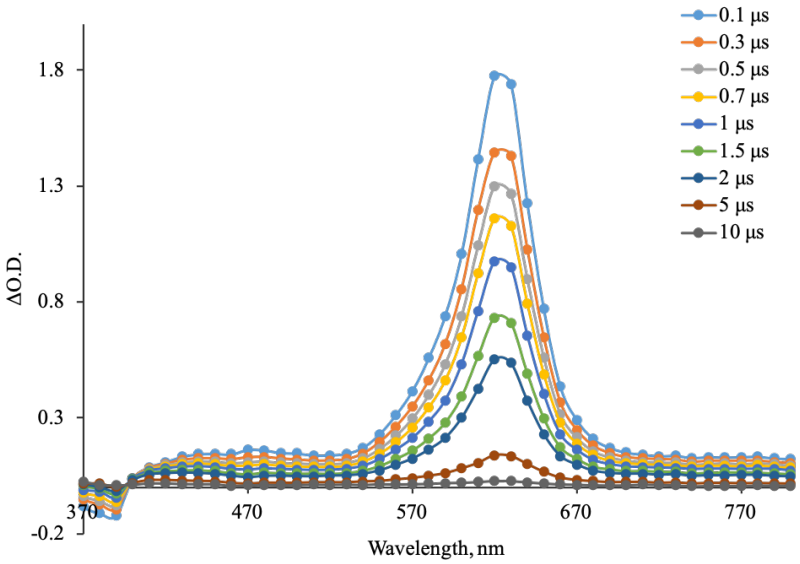

Figure 6.25. Transient absorption spectra of thioxanthone in benzene (355 nm).

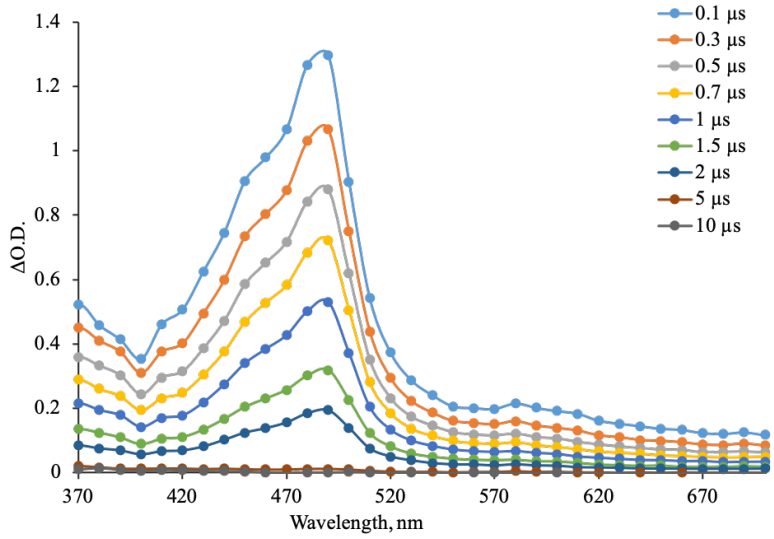

Figure 6.26. Transient absorption spectra of benzil in MeCN (355 nm).

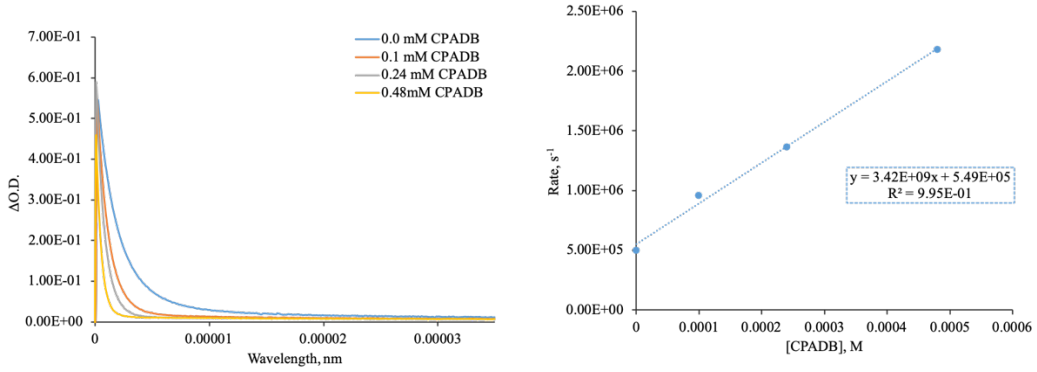

Figure 6.27. *left* Waveforms at 490 nm from pulsed photolysis (355 nm) of AQ-1 in benzene with increasing concentrations of CPADB. *Right*: rate constant from fitting the waveform to first order decay model.

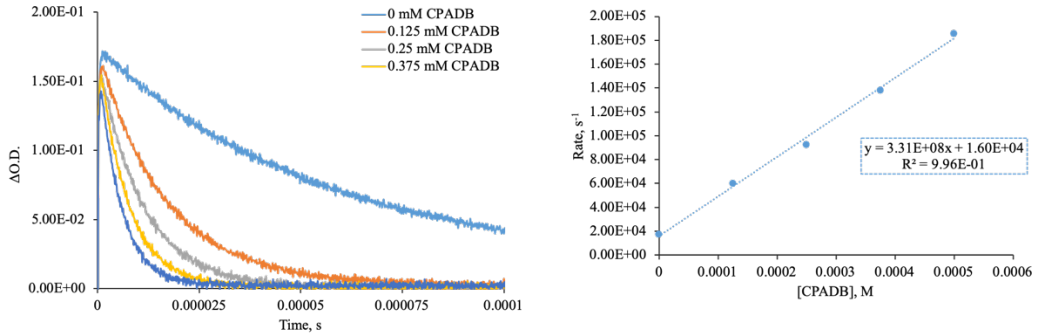

Figure 6.28. *left* Waveforms at 570 nm from pulsed photolysis (532 nm) of EY in MeCN with increasing concentrations of CPADB. *Right*: rate constant from fitting the waveform to first order decay model.

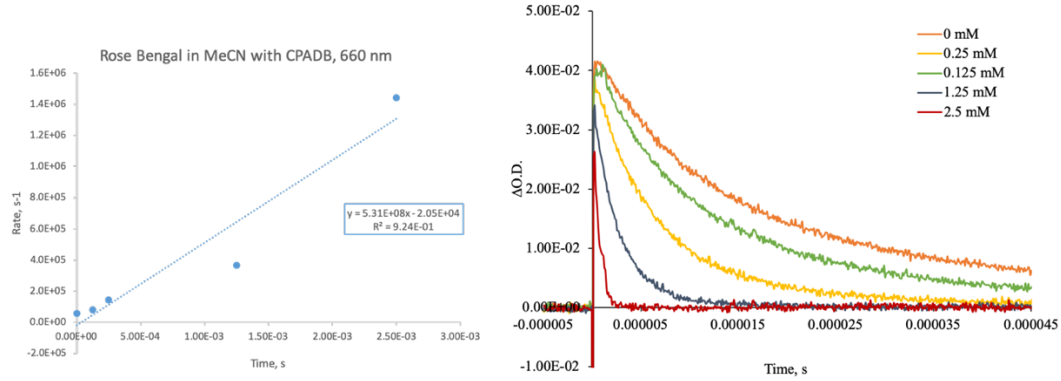

Figure 6.29. *left* Waveforms at 660 nm from pulsed photolysis (532 nm) of RB in MeCN with increasing concentrations of CPADB. *Right*: rate constant from fitting the waveform to first order decay model.

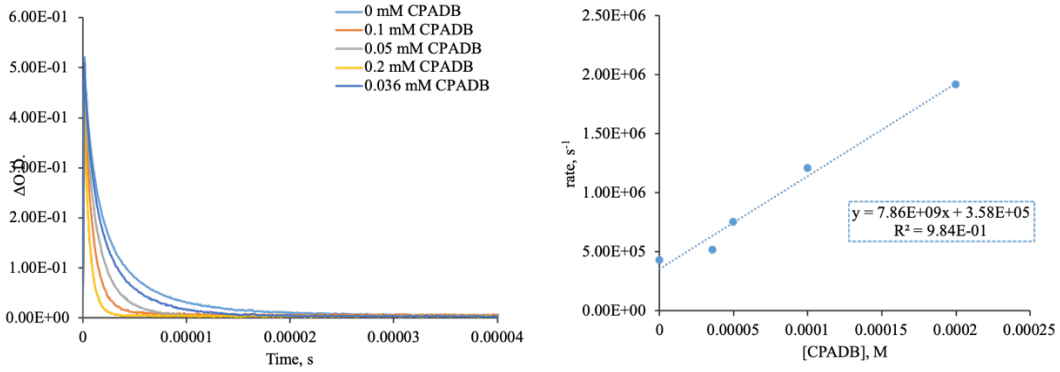

Figure 6.30. *left* Waveforms at 550 nm from pulsed photolysis of thioxanthone in benzene with increasing concentrations of CPADB. *Right*: rate constant from fitting the waveform to first order decay model.

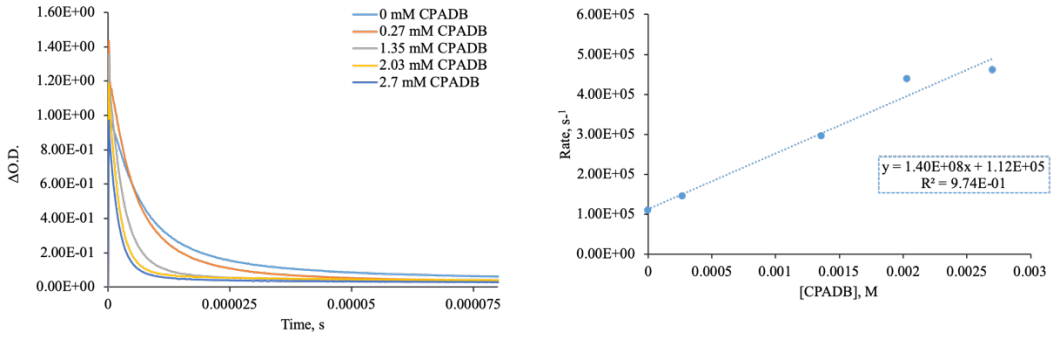

Figure 6.31. *left* Waveforms at 460 nm from pulsed photolysis (532 nm) of Zn-TPP in MeCN with increasing concentrations of CPADB. *Right*: rate constant from fitting the waveform to first order decay model.

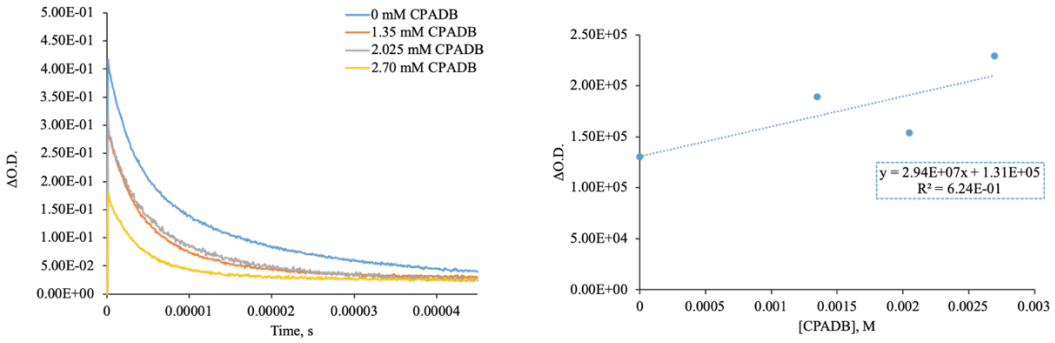

Figure 6.32. *left* Waveforms at 430 nm from pulsed photolysis (532 nm) of methylene blue in MeCN with increasing concentrations of CPADB. *Right*: rate constant from fitting the waveform to first order decay model.

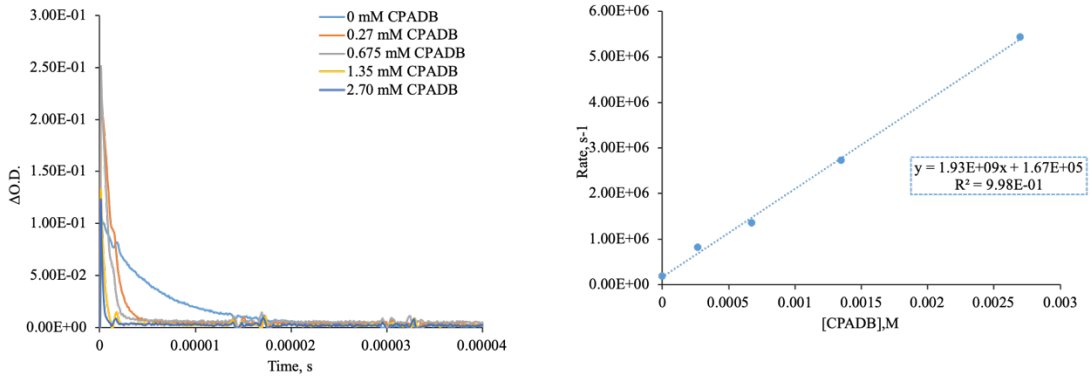

Figure 6.33. *left* Waveforms at 440 nm from pulsed photolysis (355 nm) of acridine in MeCN with increasing concentrations of CPADB. *Right*: rate constant from fitting the waveform to first order decay model.

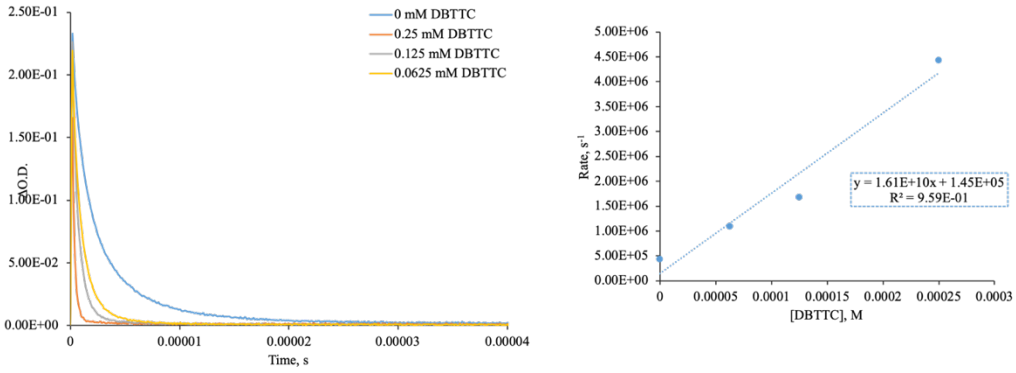

Figure 6.34. *left* Waveforms at 660 nm from pulsed photolysis (355 nm) of thioxanthone in benzene with increasing concentrations of DBTTC. *Right*: rate constant from fitting the waveform to first order decay model.

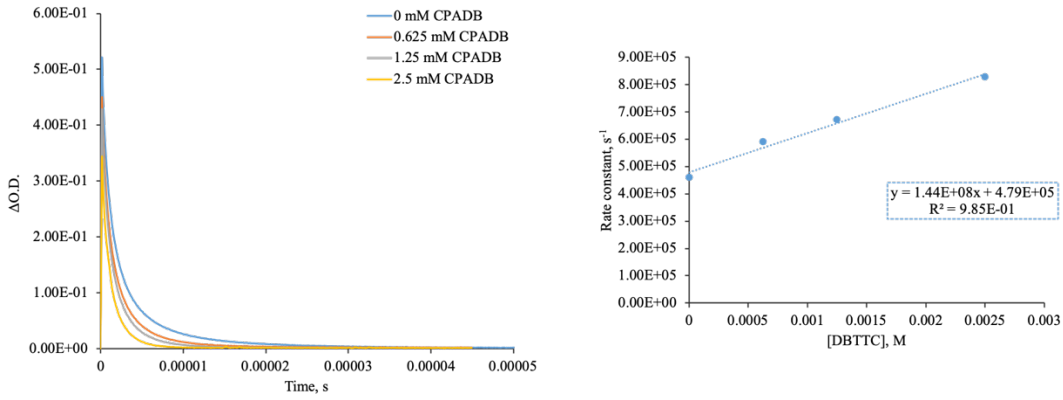

Figure 6.35. *left* Waveforms at 480 nm from pulsed photolysis (355 nm) of benzil in MeCN with increasing concentrations of DBTTC. *Right*: rate constant from fitting the waveform to first order decay model.

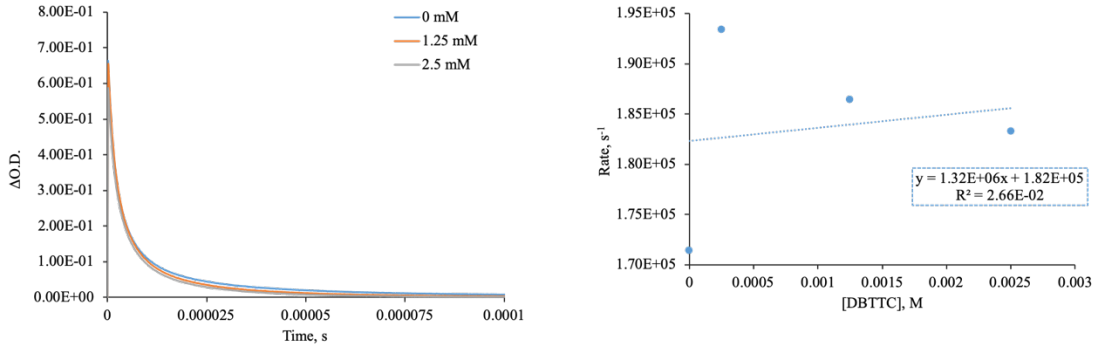

Figure 6.36. *left* Waveforms at 410 nm from pulsed photolysis (355 nm) of acridine in MeCN with increasing concentrations of DBTTC. *Right*: rate constant from fitting the waveform to first order decay model.

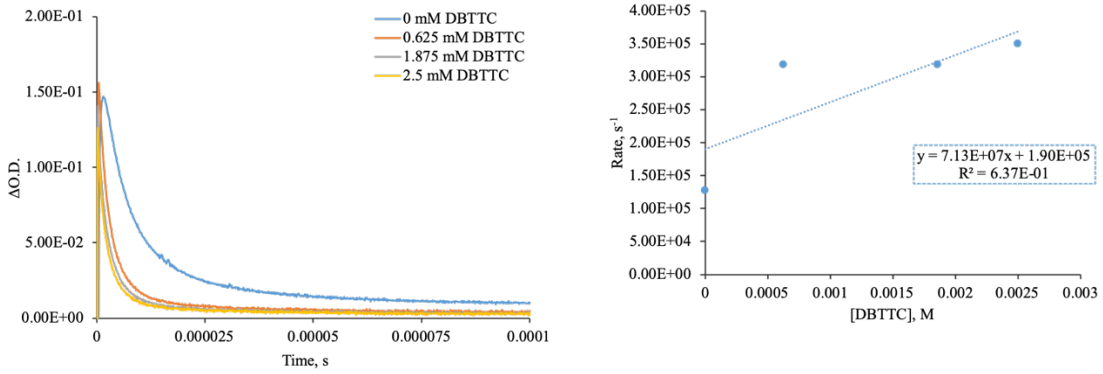

Figure 6.37. *left* Waveforms at 410 nm from pulsed photolysis (355 nm) of pyrene in MeCN with increasing concentrations of DBTTC. *Right*: rate constant from fitting the waveform to first order decay model.

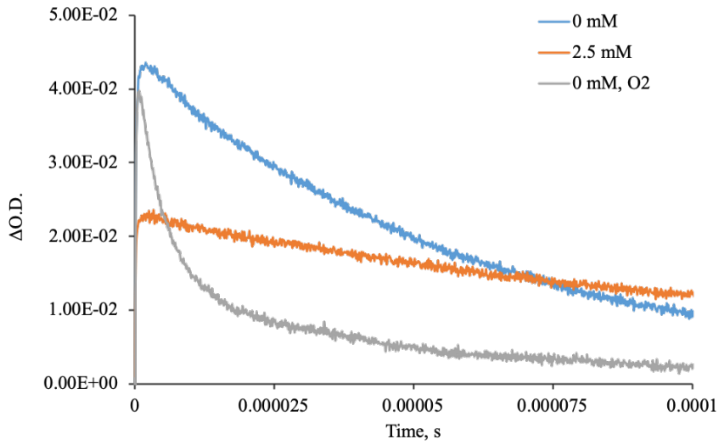

Figure 6.38. *left* Waveforms at 590 nm from pulsed photolysis (532 nm) of EY in DMSO with increasing concentrations of DBTTC.

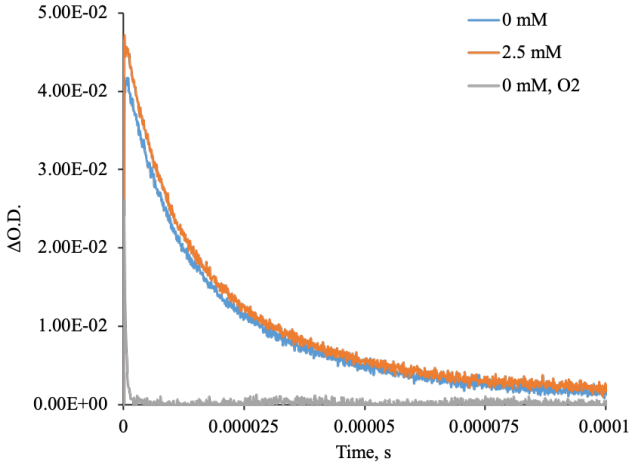

Figure 6.39. Waveforms at 660 nm from pulsed photolysis (532 nm) of Rose Bengal in MeCN with increasing concentrations of DBTTC.

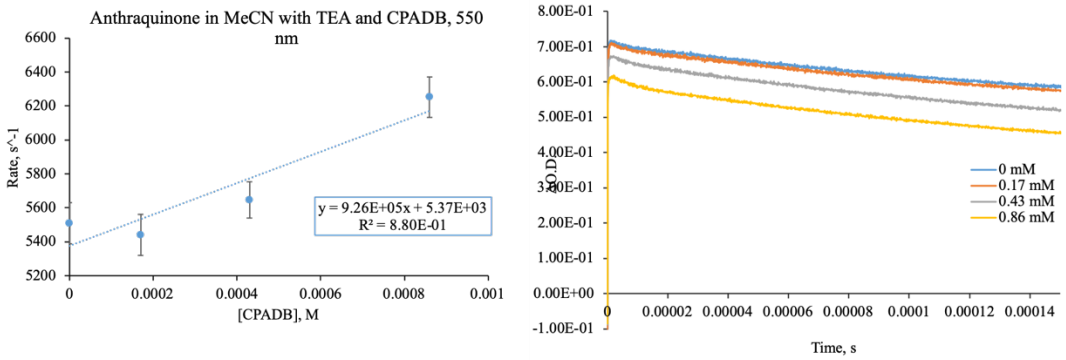

Figure 6.40. *Left:* rate constant from fitting the waveform to first order decay model. *Right*: Waveforms at 550 nm from pulsed photolysis (355 nm) of AQ in MeCN with TEA (25 mM) and increasing concentrations of CPADB.

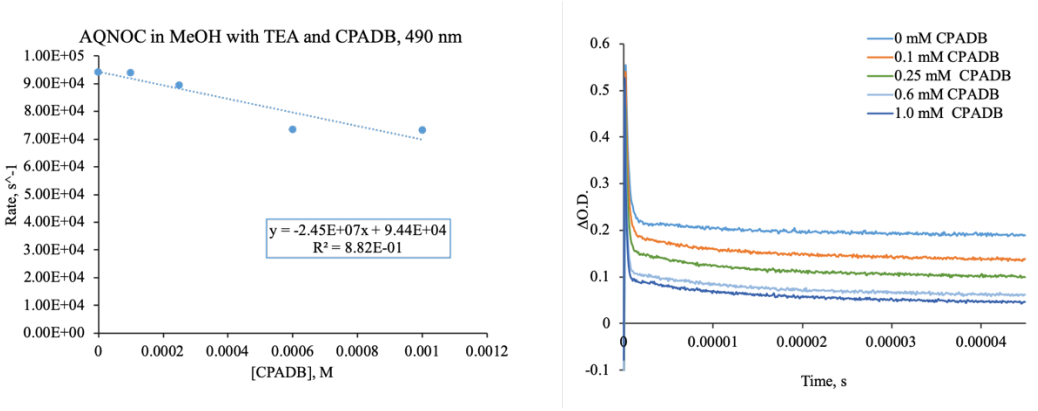

Figure 6.41. *Left:* rate constant from fitting the waveform to first order decay model. *Right*: Waveforms at 490 nm from pulsed photolysis (355 nm) of AQ-1 in MeOH with TEA (25 mM) and increasing concentrations of CPADB.

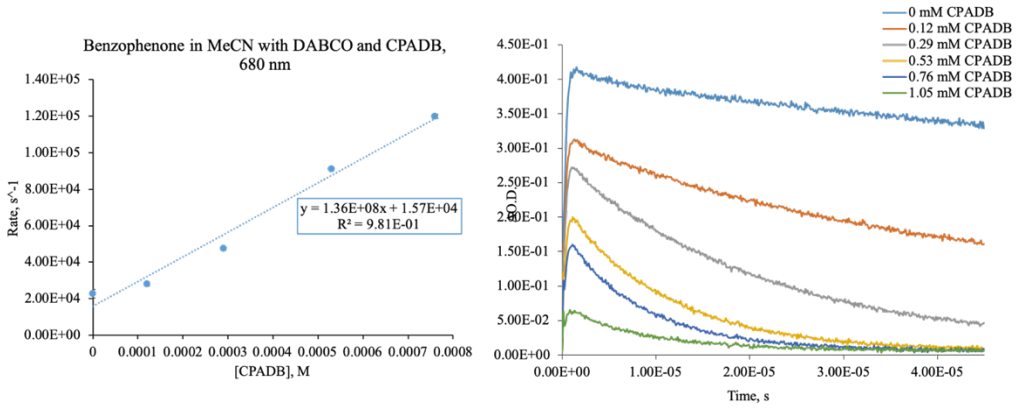

Figure 6.42. *Left:* rate constant from fitting the waveform to first order decay model. *Right*: Waveforms at 680 nm from pulsed photolysis (355 nm) of benzophenone in MeCN with DABCO (25 mM) and increasing concentrations of CPADB.

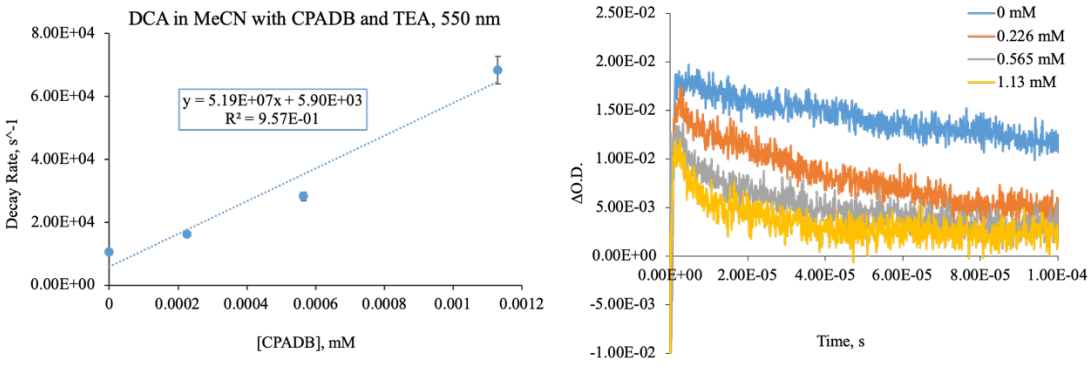

Figure 6.43. *Left:* rate constant from fitting the waveform to first order decay model. *Right*: Waveforms at 550 nm from pulsed photolysis (355 nm) of 9,10-DCA in MeCN with TEA (25 mM) and increasing concentrations of CPADB.

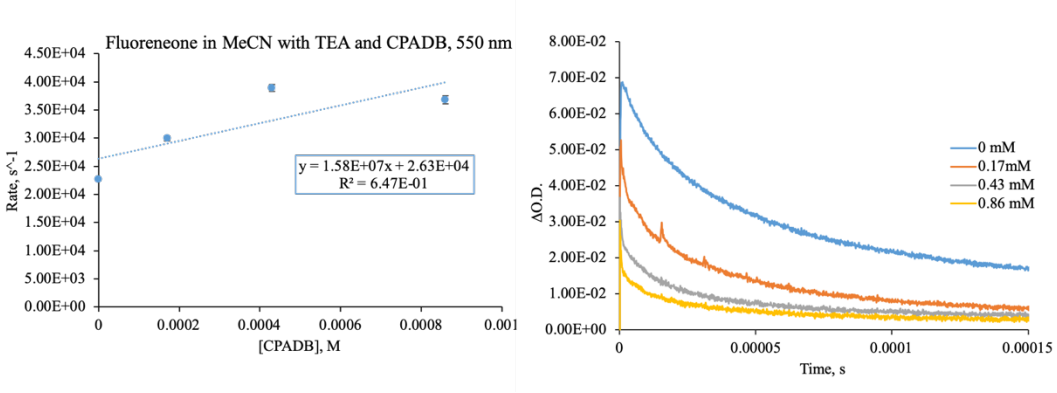

Figure 6.44. *Left:* rate constant from fitting the waveform to first order decay model. *Right*: Waveforms at 550 nm from pulsed photolysis (355 nm) of fluorenone in MeCN with TEA (25 mM) and increasing concentrations of CPADB.

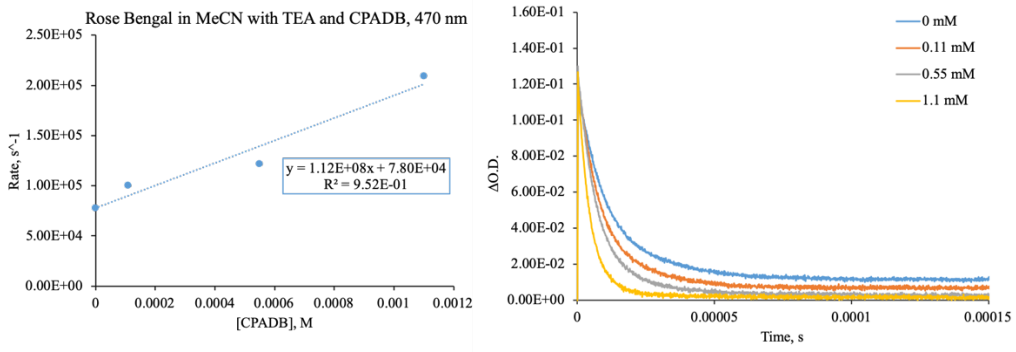

Figure 6.45. *Left:* rate constant from fitting the waveform to first order decay model. *Right*: Waveforms at 470 nm from pulsed photolysis (532 nm) of RB in MeCN with TEA (25 mM) and increasing concentrations of CPADB.

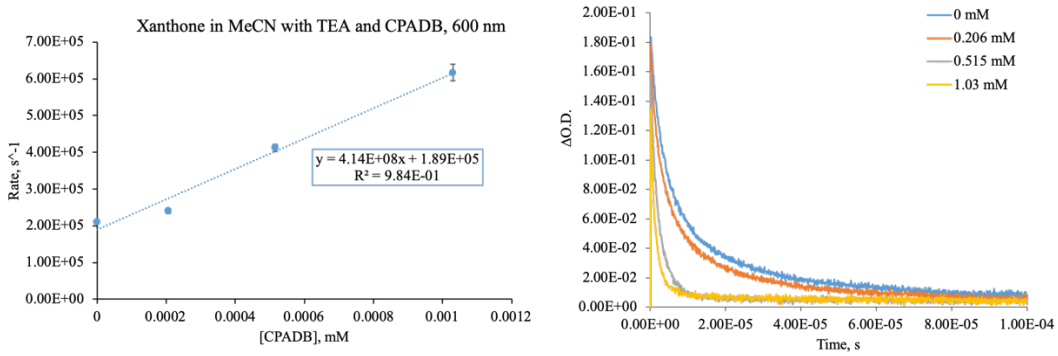

Figure 6.46. *Left:* Rate constant from fitting the waveform to a biexponential decay model. The second rate constant was used. *Right*: Waveforms at 600 nm from pulsed photolysis (355 nm) of xanthone in MeCN with TEA (25 mM) and increasing concentrations of CPADB.

(c) HPLC

High pressure liquid chromatography was performed using a Shimadzu LC-20AT with an SPD-20AV detector and a 20 microliter injection loop. An Eclipse Plus C18, 5 micrometer, 4.6 x 155 mm column was used. A flow rate of 0.8 mL/min was used with a 90/10 MeCN/H_2O solvent system was used. HPLC traces of the compounds with calibration curves are given below.

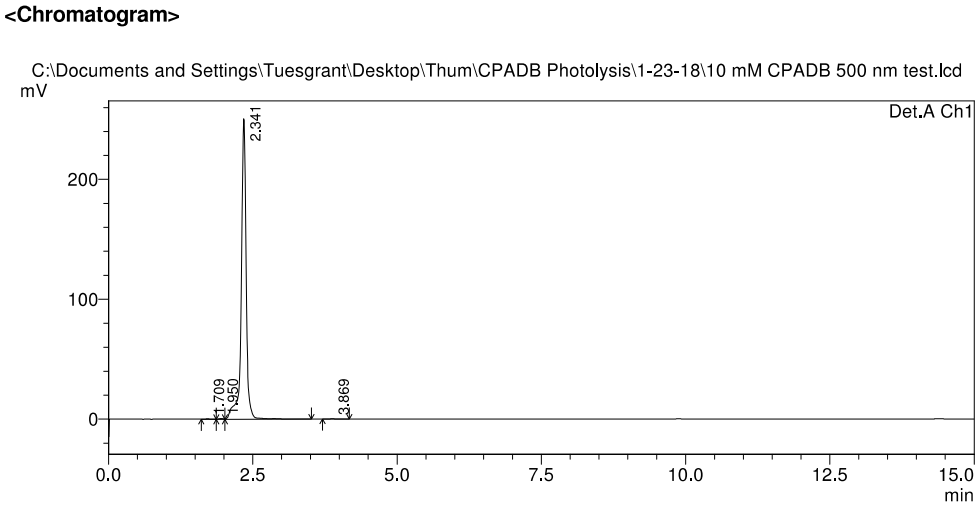

Figure 6.47. HPLC Trace of 2.84 mM CPADB in MeCN. CPADB elutes at 2.34 minutes. Detection at 500 nm.

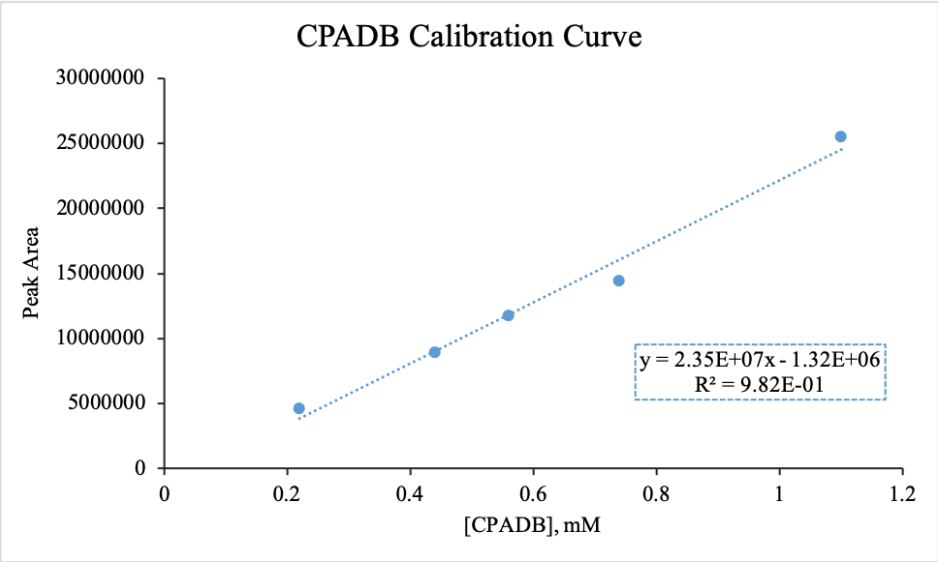

Figure 6.48. HPLC calibration curve for CPADB.

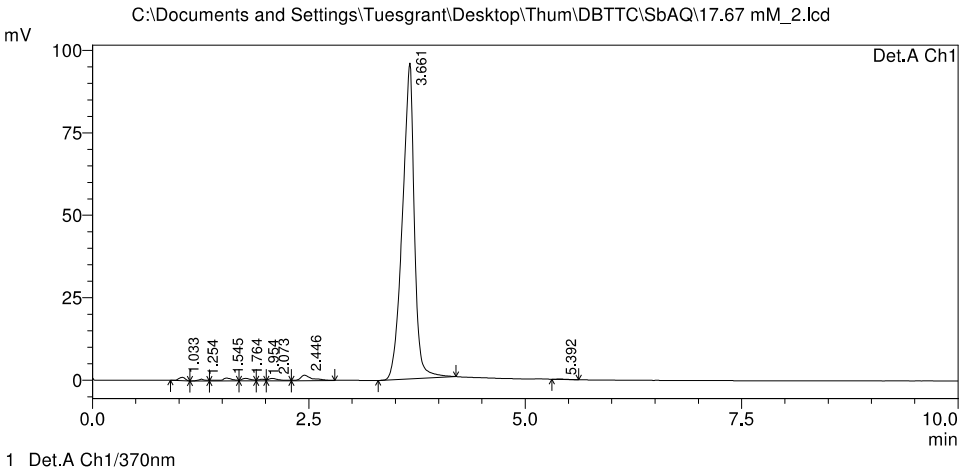

Figure 6.49. HPLC Trace of 17.67 mM DBTTC in MeCN. CPADB elutes at 3.68 minutes. Detection at 370 nm.

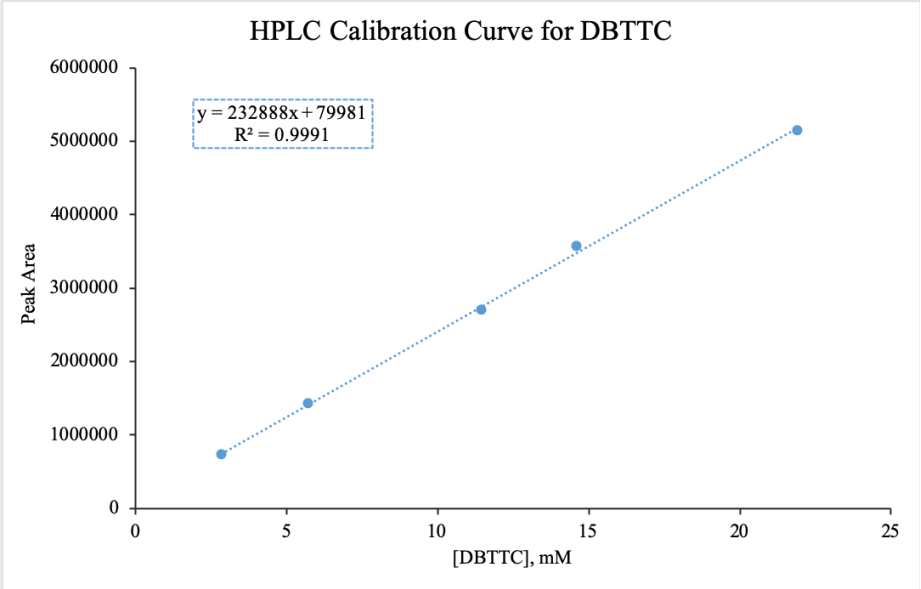

Figure 6.50. HPLC calibration curve for DBTTC.

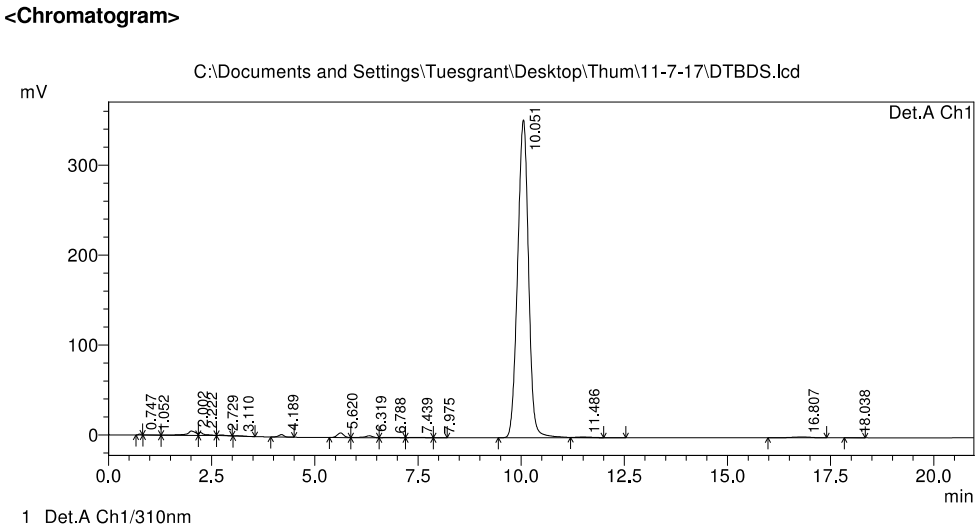

Figure 6.51. HPLC Trace of 5.68 mM DTBDS in MeCN. DTBDS elutes at 10.05 minutes. Detection at 310 nm.

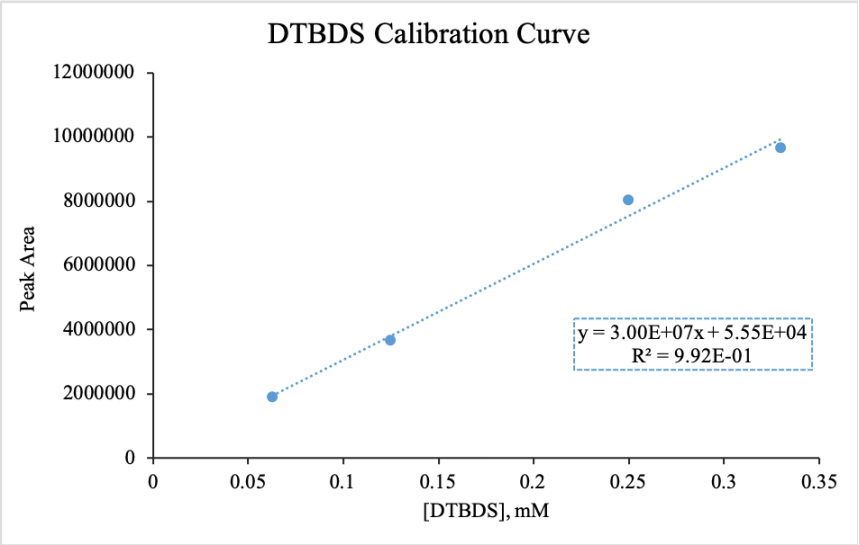

Figure 6.52. HPLC calibration curve for DTBDS.

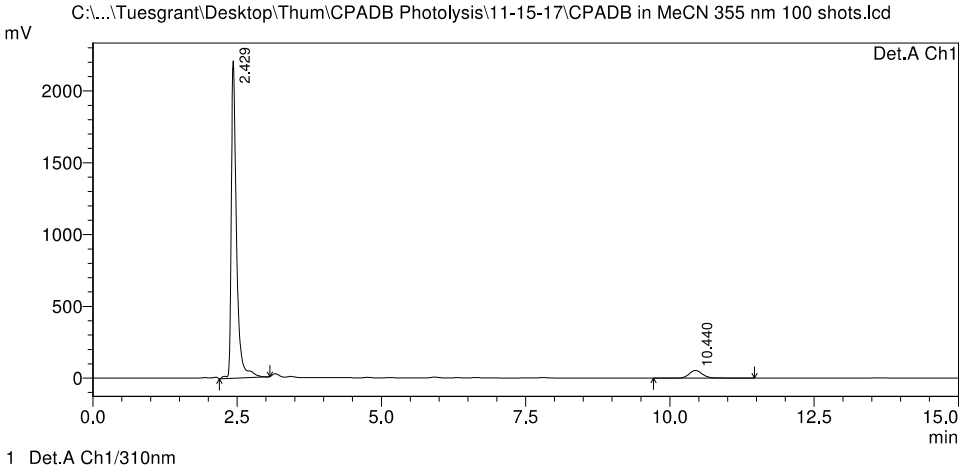

Figure 6.53. HPLC Trace of 2.84 mM of CPADB pulsed photolysis at 355 nm for 10 sec (100 shots at 10 Hz). The peak for DTBDS can be seen at 10.40 min.

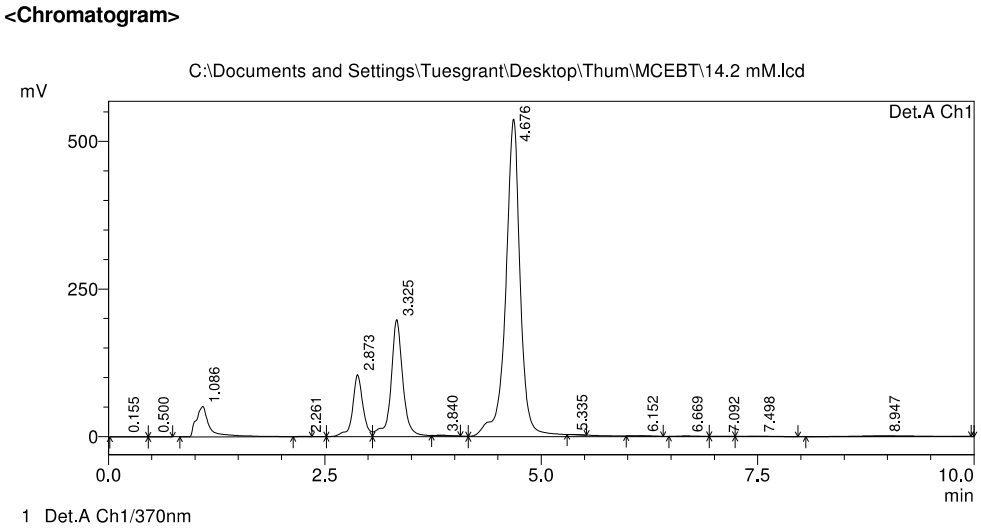

Figure 6.54. HPLC Trace of 14.2 mM MCEBT in MeCN. MCEBT elutes at 4.67 minutes. Detection at 370 nm.

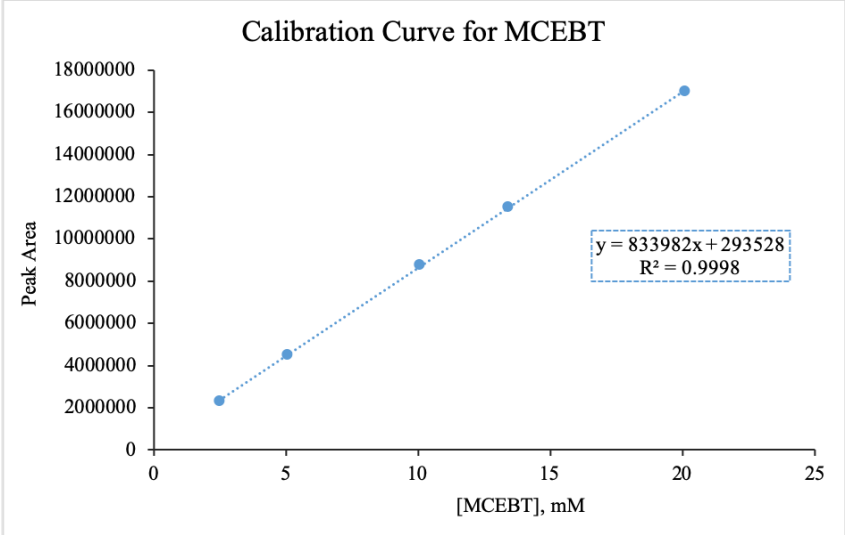

Figure 6.55. HPLC calibration curve for MCEBT.

(d) Fluorescence

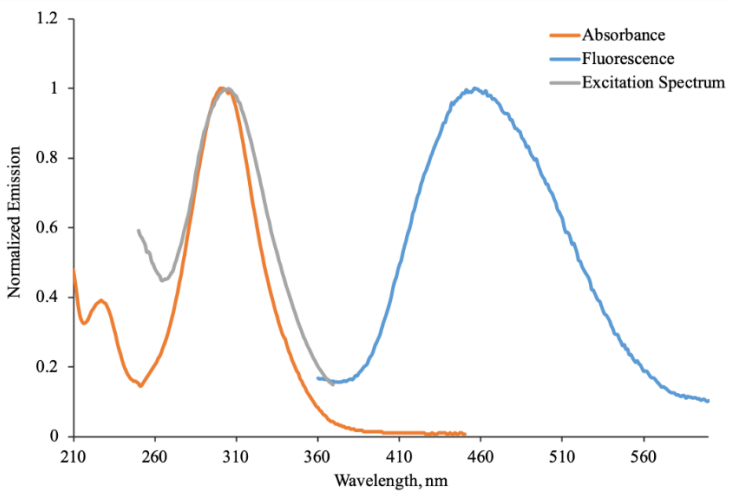

Figure 6.56. Absorption, Emission and Excitation (464 nm) spectrum.

(e) Azobenzene Actinometry

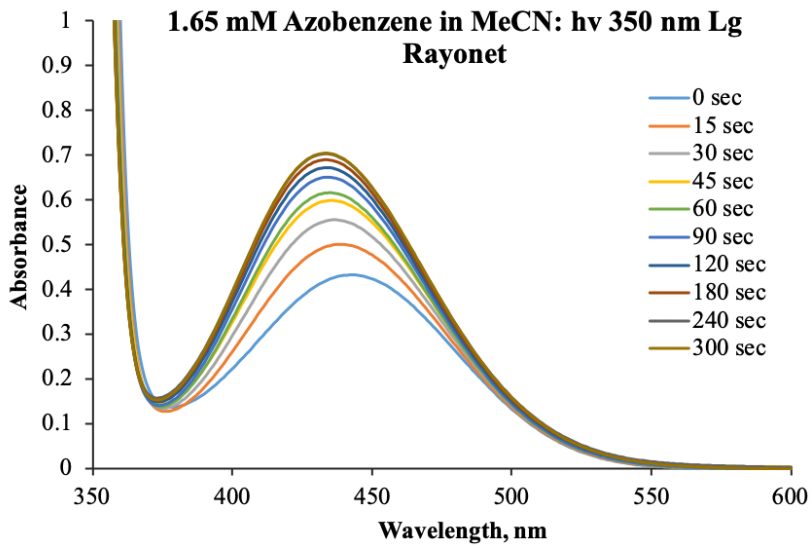

Figure 6.57. UV/Vis showing photolysis of Azobenzene in MeCN at 350 nm.

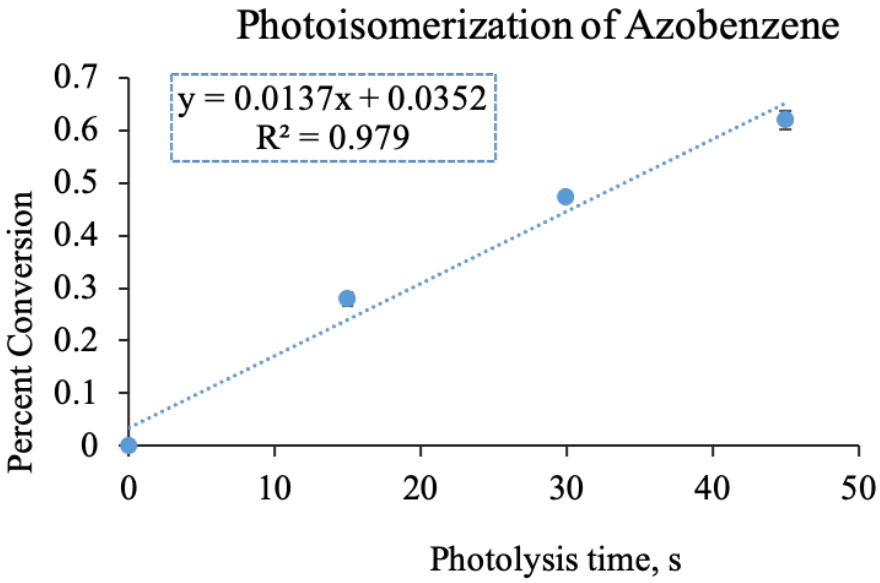

Figure 6.58. Determination of the initial rate of isomerization.

(f) ^{1}H NMR Experiments

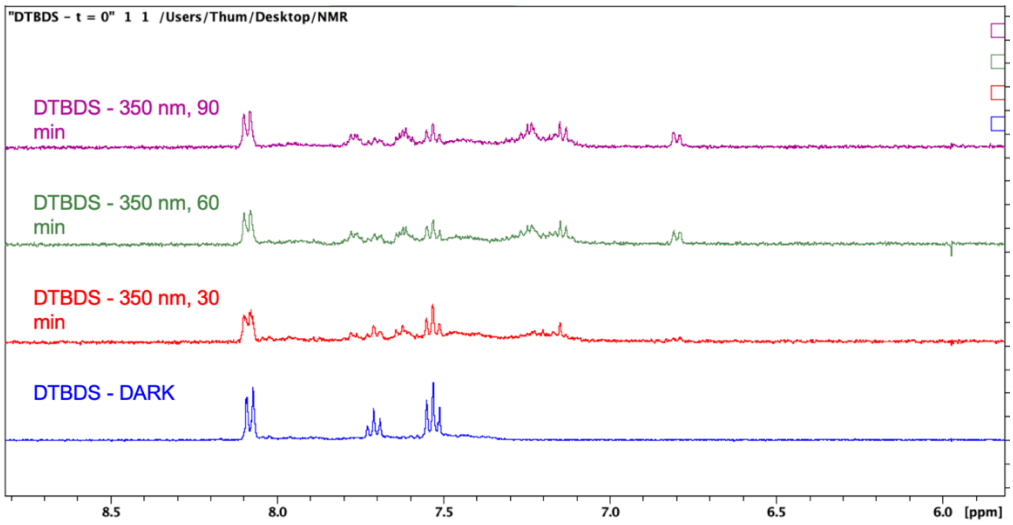

Figure 6.59. ^{1}H NMR from photolysis of DTBDS at 350 nm in MeCN for the illustrated amount of time.

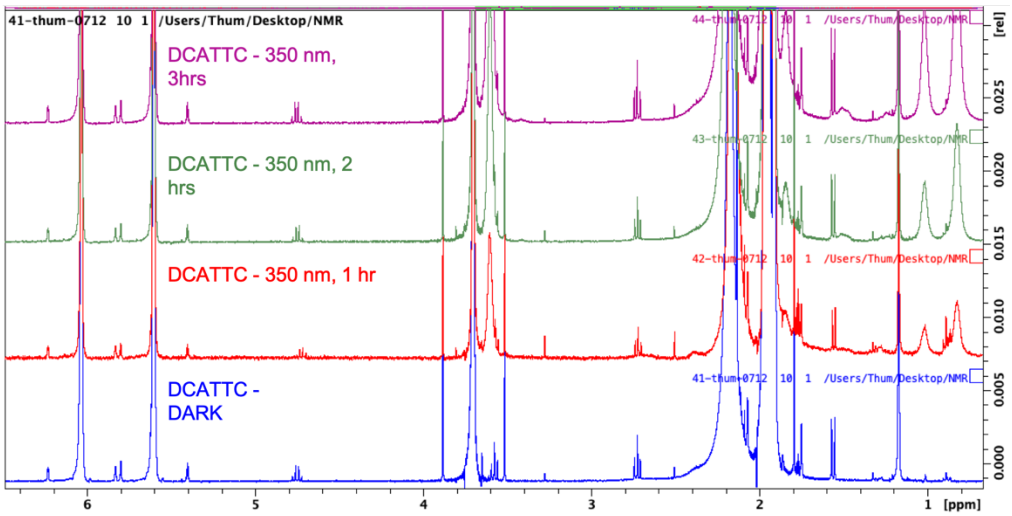

Figure 6.60. ^{1}H NMR from photolysis of DCATTC at 350 nm in MeCN/MMA for the illustrated amount of time. The DCATTC can be seen as a peak at 2.75 and 4.75 ppm respectively.

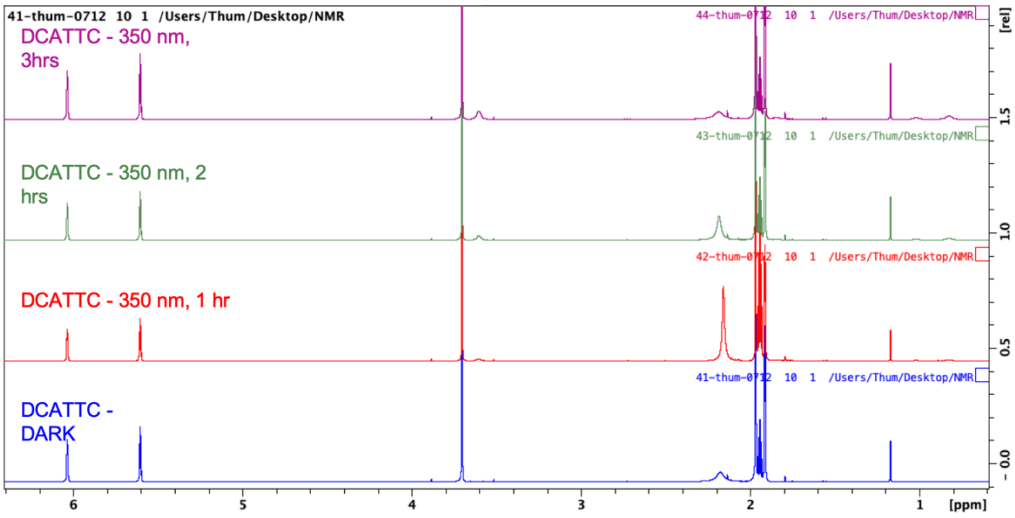

Figure 6.61. ^{1}H NMR from photolysis of DCATTC at 350 nm in MeCN/MMA for the illustrated amount of time. The conversion of MMA to p-MMA can be seen as the growth of a broad peak at 3.6 ppm.

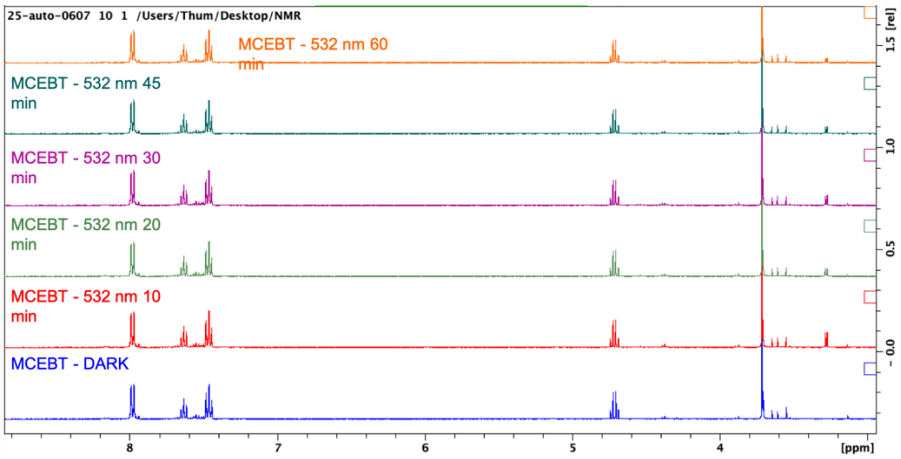

Figure 6.62. ^{1}H NMR from photolysis of MCEBT at 532 nm (100 mW) in MeCN/MMA for the illustrated amount of time. The lack of degradation illustrates the photostability of MCEBT under visible light illumination.

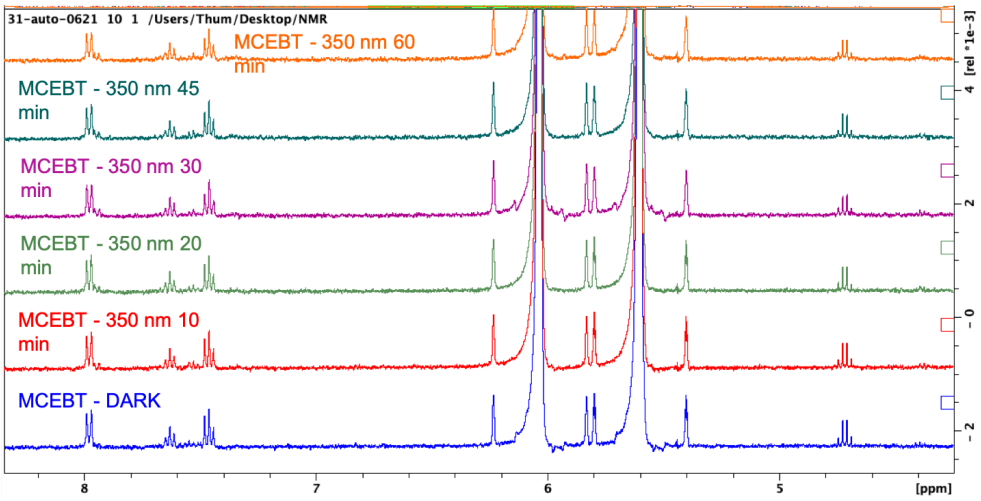

Figure 6.63. ^{1}H NMR from photolysis of MCEBT at 532 nm (100 mW) in MeCN/MMA for the illustrated amount of time. There is a slight decrease in the peaks due to degradation, and new, small, peaks are observed at 7.9 ppm with photolysis.

6.5 Chapter 5 Experimental Results:

(a) Polymerization

In a 3.5 dr vial was added the appropriate amount of AQ-1 in DMSO. To this was added 13.1 mg (46.9 mmol) of CPADB and sonicated in the absence of light until all dissolved. Methyl methacrylate (MMA), 1 mL, was added and the mixture was thoroughly mixed. If polymerizing in the presence of air, the cap was sealed and the vial was photolyzed in the Rayonet photoreactor (419 nm broadband irradiation) for the appropriate amount of time. If polymerizing under an inert atmosphere, the vial was sealed with a septum and purged with N_2 for 10 minutes in the solution and an additional 5 minutes in the headspace. Unless otherwise noted, the conversion was measured by taking a small (≈ 10 μL) amount of the mixture and adding it to 0.5 mL of CD_3CN for ^1H NMR. The amount of monomer loss was measured using the signal of DMSO, 2.5 ppm, as the internal standard and comparing it to the loss of signal at 3.7 ppm corresponding to MMA.

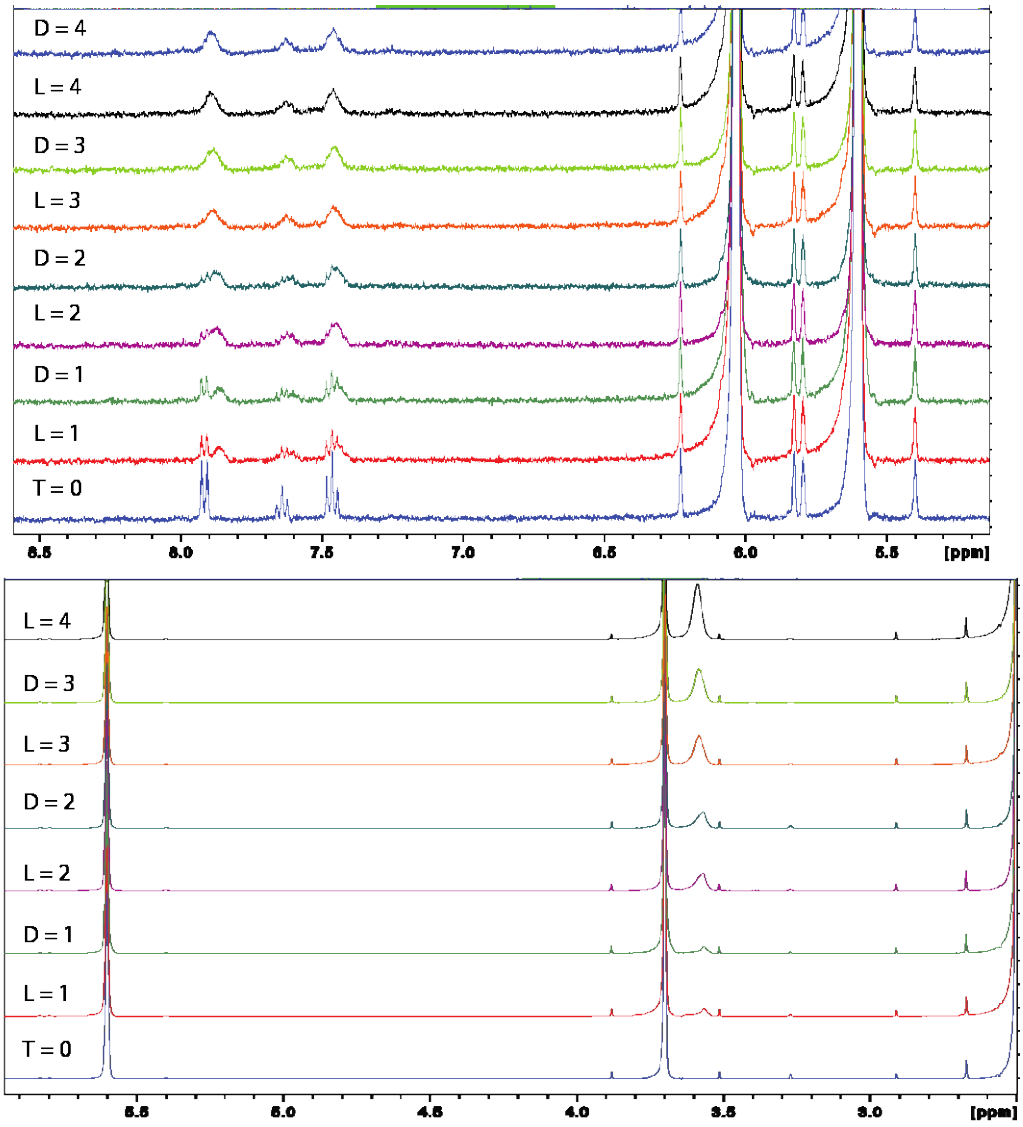

Figure 6.64. L = light, D = Dark for the number of hours shown. Photolysis performed at 419 nm. *top*: ^{1}H NMR of the photo-controlled experiments showing the incorporation of CPADB into the polymer backbone as a slight upfield shift in the aromatic peaks and a slight broadening. *bottom*: ^{1}H NMR of the photo-controlled experiments showing the formation of p-MMA as a bread peak at 3.6 ppm.

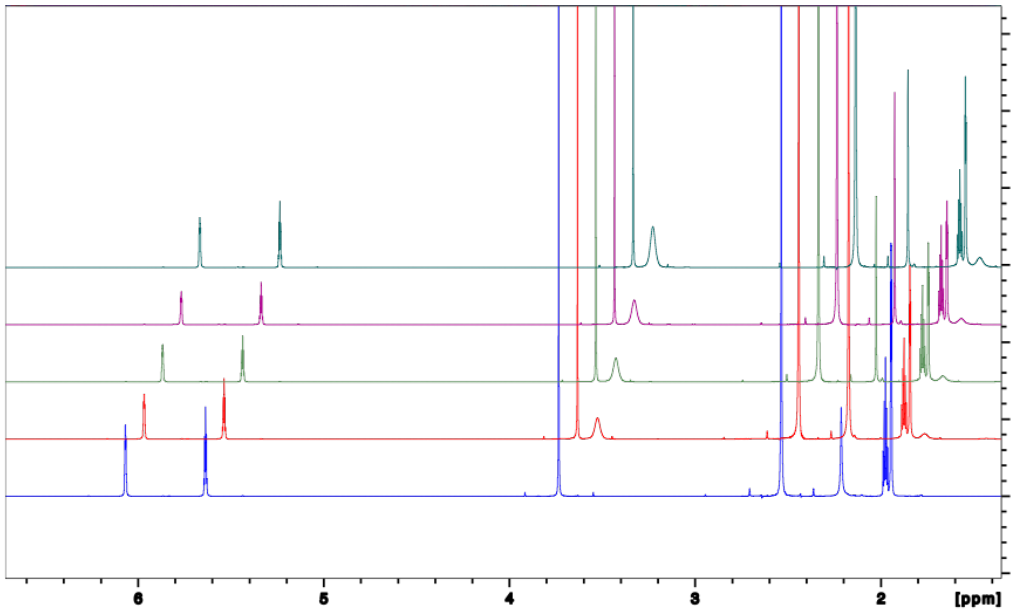

Figure 6.65. ^{1}H NMR of polymerization experiments with AQ-1. Polymerization experiments carried out with AQ-1 and CPADB in 1:1 MMA/DMSO in the presence of air. The results shows are for different concentrations of AQ-1. Photolysis performed at 419 nm. With increasing amounts of AQ-1 there is an increase in the formation of p-MMA as a peak at 3.6 ppm. *Blue*: 0.01 eq AQ-1, DARK. *Red*: 0.01 eq AQ-1, 8 hrs. *Green*: 0.02 eq. AQ-1, 8 hrs. *Purple*: 0.03 eq AQ-1, 8 hrs. *Blue-Green (top)*: 0.04 eq. AQ-1, 8 hrs.

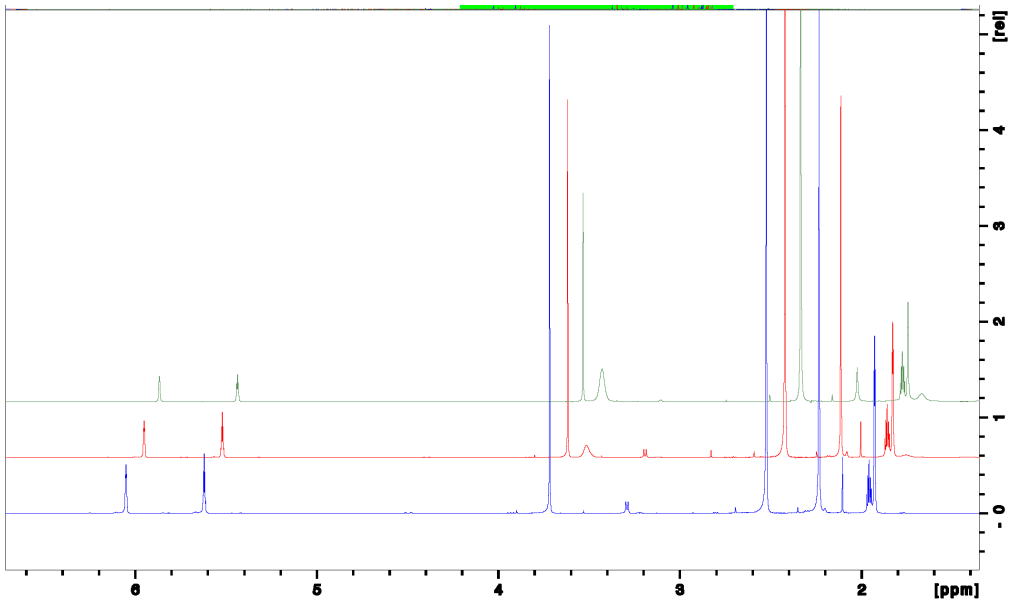

Figure 6.66. ^{1}H NMR of polymerization experiments with AQ-1. Polymerization experiments carried out with AQ-1 and CPADB in 1:1 MMA/DMSO in the presence of air. The results shows are for different concentrations of AQ-1. Photolysis performed at 419 nm. With increasing amounts of photolysis time, there is an increase in the formation of p-MMA as a peak at 3.6 ppm. *Blue*: 0.1 eq AQ-1, DARK. *Red*: 0.1 eq AQ-1, 8 hrs. *Green*: 0.1 eq. AQ-1, 16 hrs.

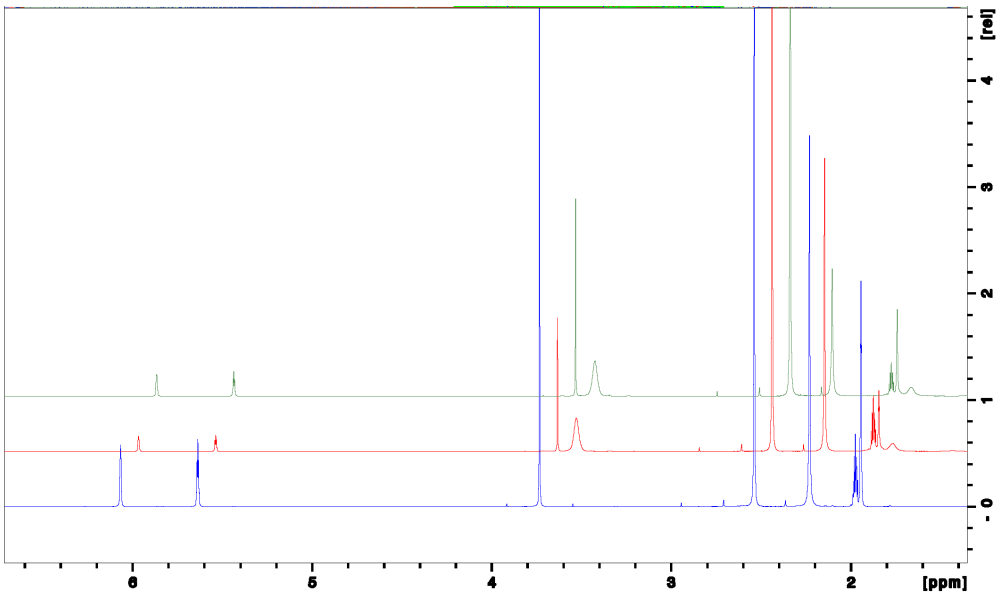

Figure 6.67. ^{1}H NMR of polymerization experiments with AQ-1. Polymerization experiments carried out with AQ-1 and CPADB in 1:1 MMA/DMSO in the presence of air (*red*) and nitrogen (*green*). Photolysis performed at 419 nm. There is little difference in the formation of polymer with prior deoxygenation with N_2. *Blue*: 0.2 eq AQ-1, DARK. *Red*: 0.2 eq AQ-1, 16 hrs, Air. *Green*: 0.2 eq. AQ-1, 16 hrs, N_2.

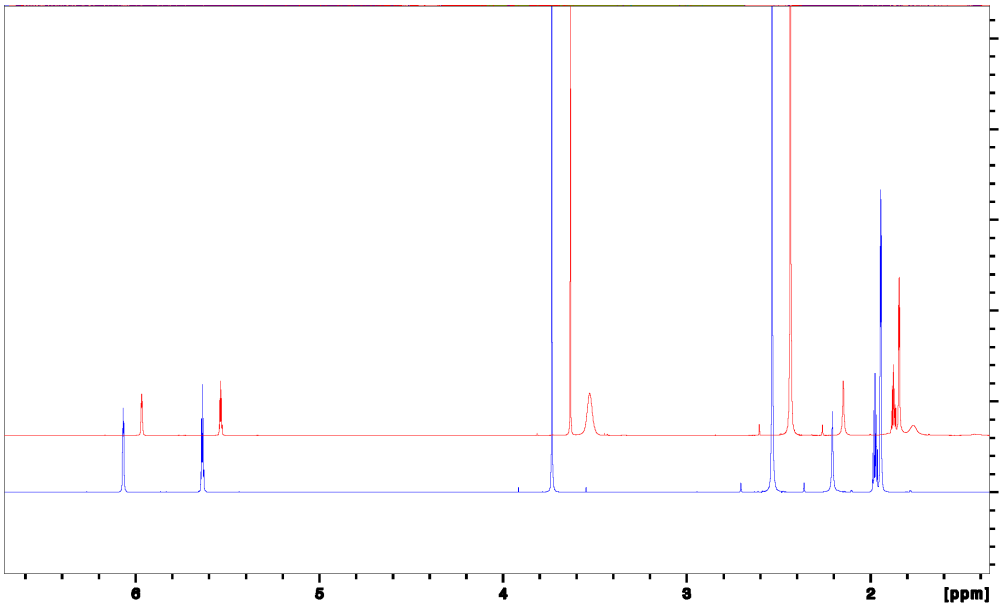

Figure 6.68. ^{1}H NMR of polymerization experiments in the absence of AQ-1. Polymerization experiments carried out with CPADB in 1:1 MMA/DMSO in the presence of air. Photolysis performed at 419 nm. *Blue*: DARK. *Red*: 16 hrs.

(b) GPC Traces for select polymer samples

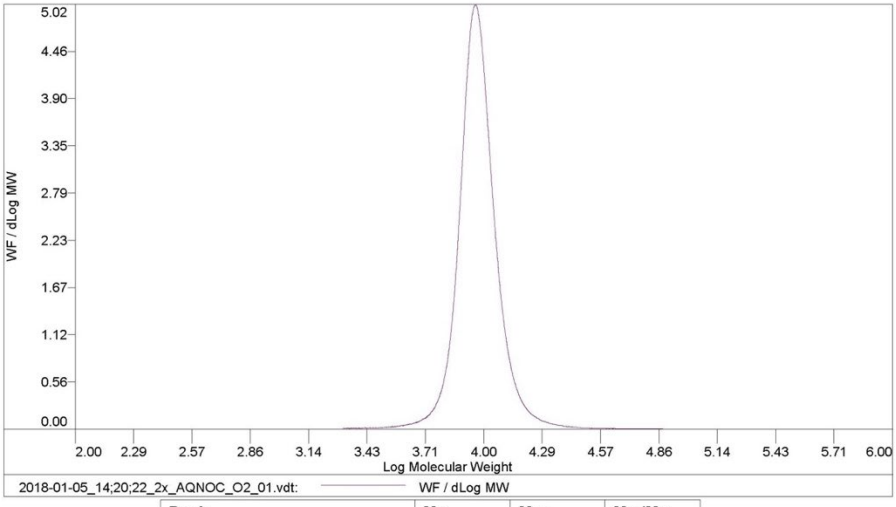

Peak	Mn	Mw	Mw/Mn
1	9,113	9,692	1.064

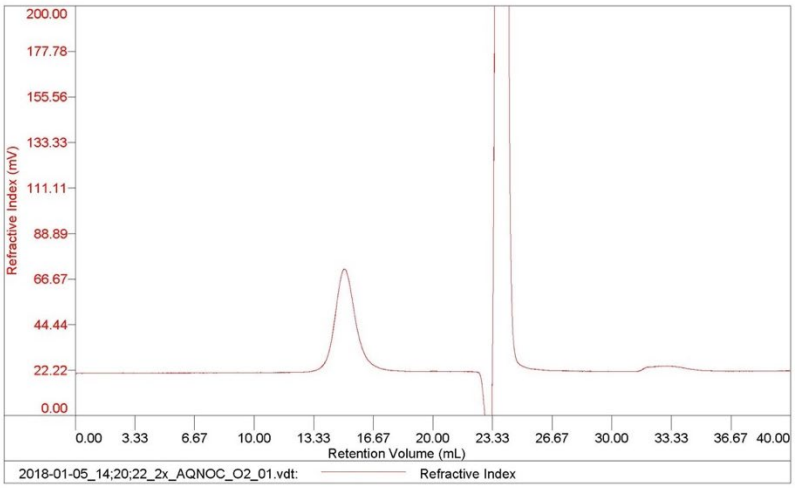

Figure 6.69. GPC trace from polymerization with 0.1 eq of AQ-1 for 8 hrs in air.

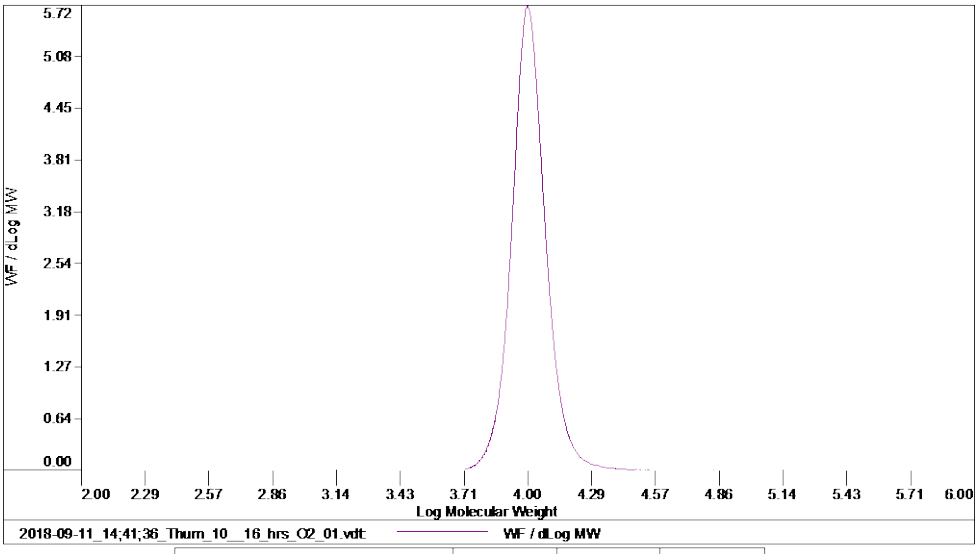

Peak	Mn	Mw	Mw/Mn
1	10,014	10,323	1.031

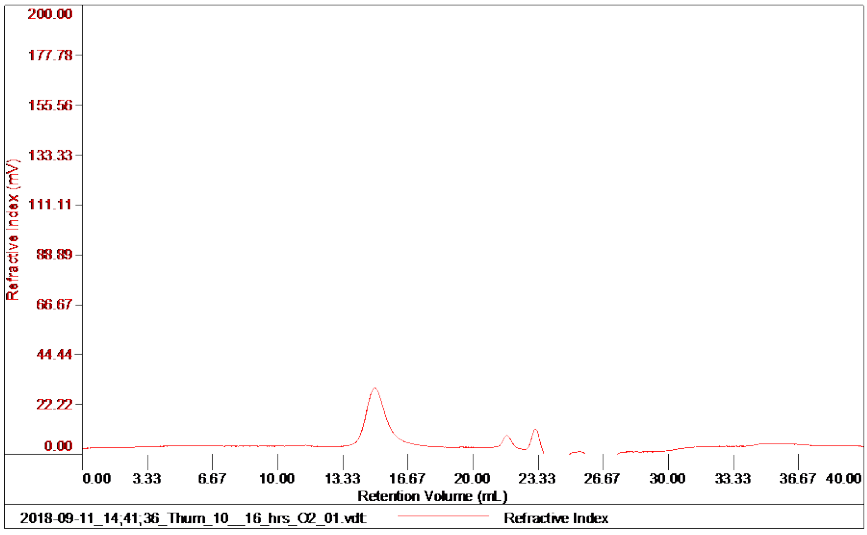

Figure 6.70. GPC trace from polymerization with 0.1 eq of AQ-1 for 16 hrs in air.

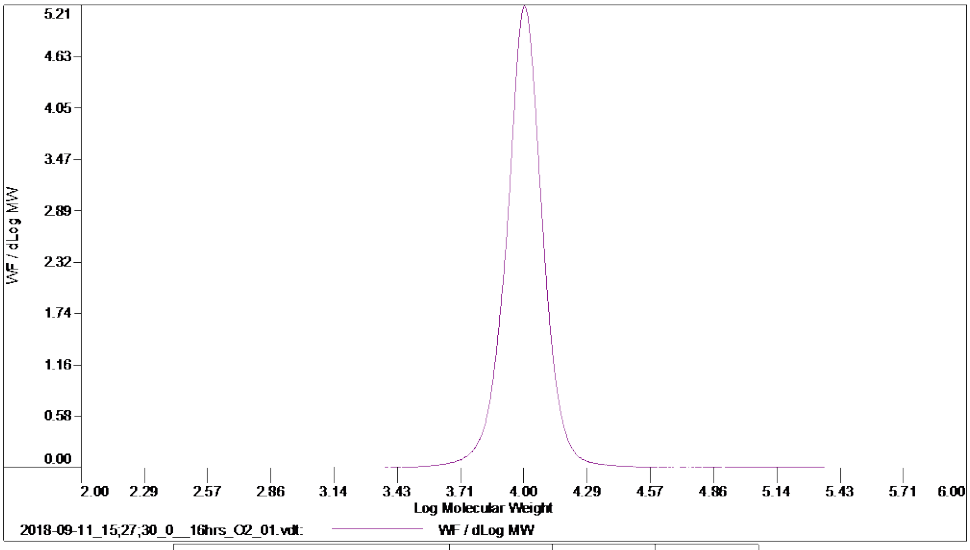

Peak	Mn	Mw	Mw/Mn
1	9,814	10,321	1.052

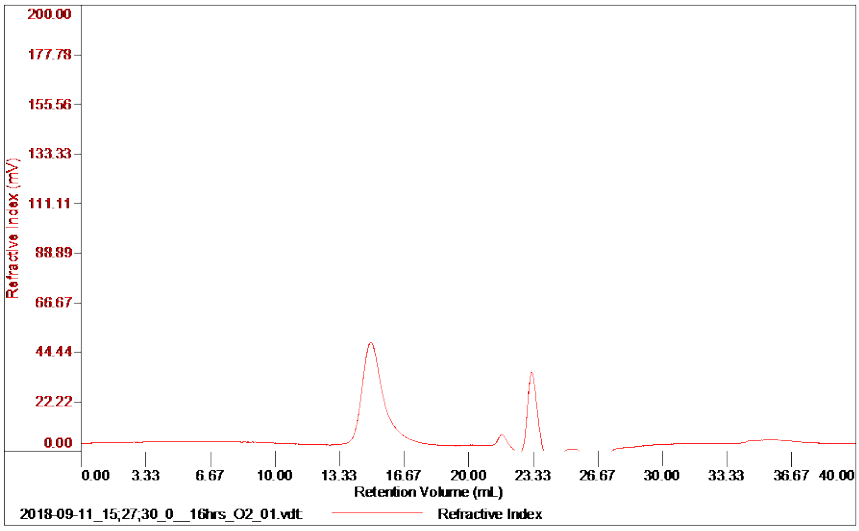

Figure 6.71. GPC trace from polymerization with 0 eq of AQ-1 for 16 hrs in air.

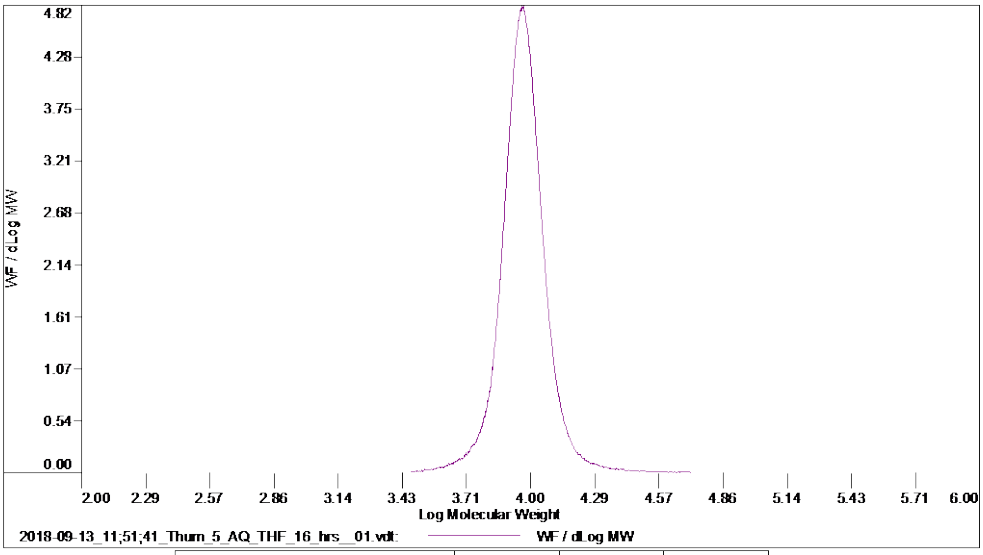

Peak	Mn	Mw	Mw/Mn
1	9,005	9,596	1.066

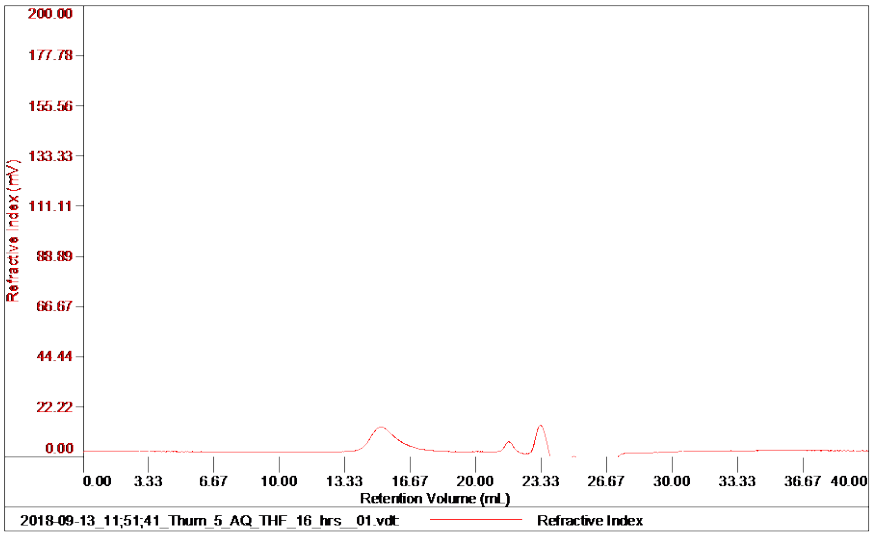

Figure 6.72. GPC trace from polymerization with 0.05 eq of AQ-1 in THF for 16 hrs in air.

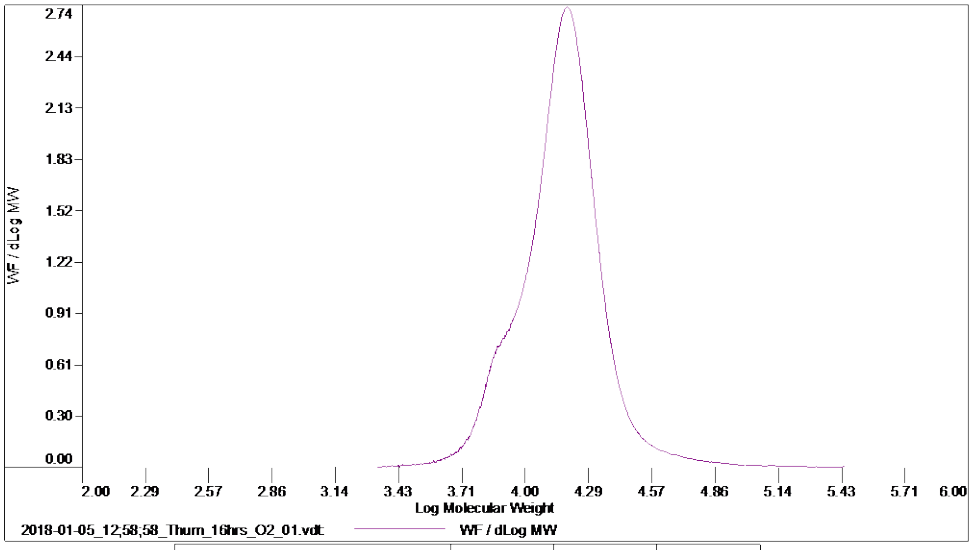

Peak	Mn	Mw	Mw/Mn
1	13,139	16,219	1.234

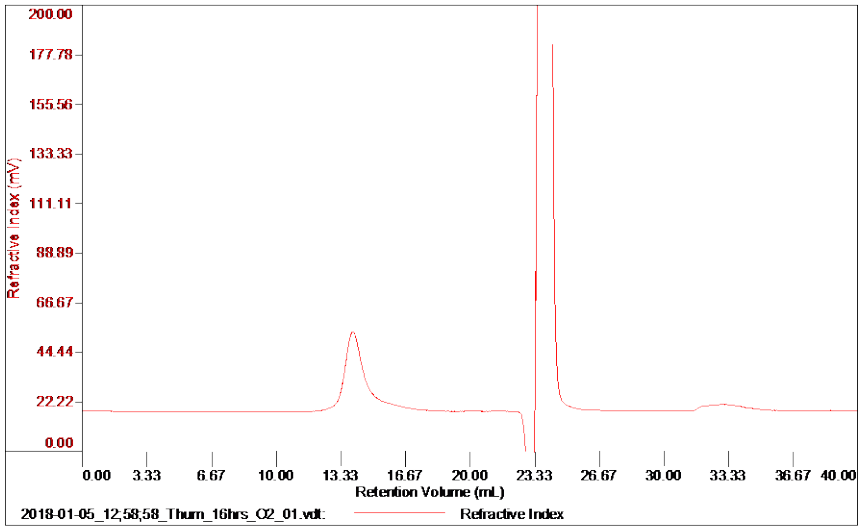

Figure 6.73. GPC trace from polymerization with 0.05 eq of AQ-1 for 16 hrs in air.

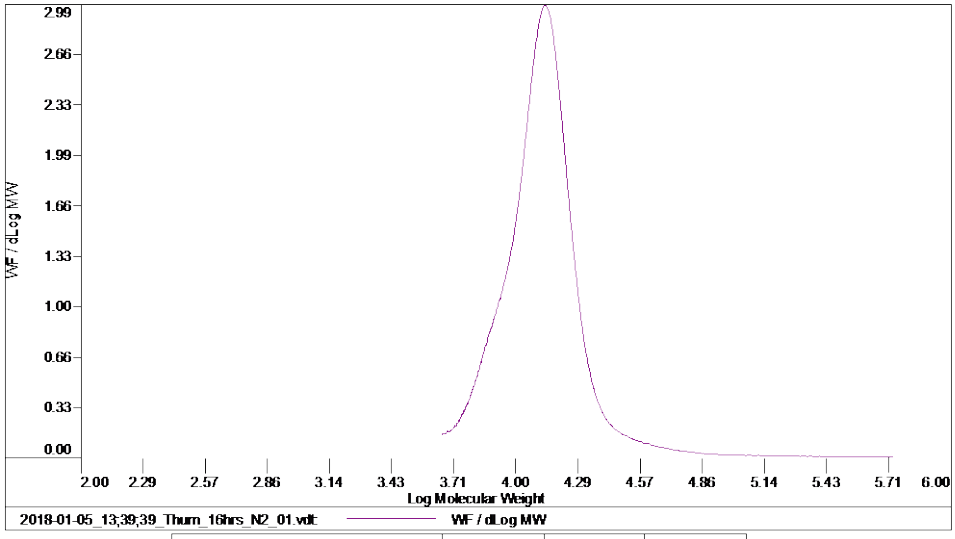

Peak	Mn	Mw	Mw/Mn
1	12,203	16,111	1.320

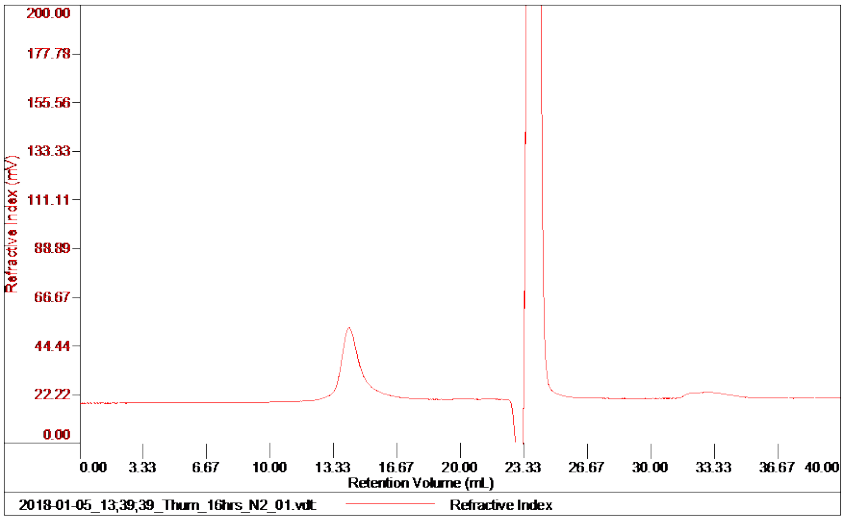

Figure 6.74. GPC trace from polymerization with 0.05 eq of AQ-1 for 16 hrs in N_2.

(c) Characterization and synthesis of compounds.

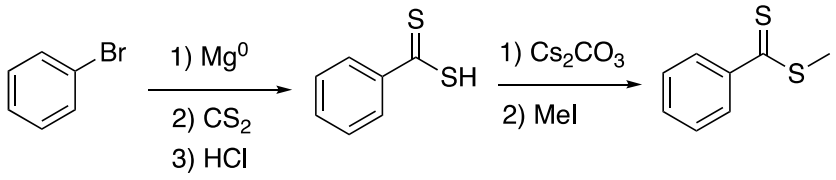

Figure 6.75. Synthesis of methyl benzodithioate.

Benzodithioic acid. Bromobenzene, 15.70 g (0.1 mmol), was added dropwise to a solution of 2.51 g ground magnesium turnings in dry THF. After cessation of the reaction, to the grey, cloudy, solution was added dropwise 7.6 g of carbon disulfide. After stirring at room temperature for two hours, the reaction was quenched by pouring over ice. Any excess magnesium was filtered off and two hundred milliliters of diethyl ether was added. With stirring, HCl (6N) was added until the aqueous layer became clear and the organic layer a deep-red. The organic layer was extracted with water, 2 x 100 mL and dried over sodium sulfate. The solvent was removed under reduced pressure to form a red oil which was used without further purification. ^{1}H NMR (400 MHz, CD_3CN) δ 8.04 (d, 2H), 7.65 (t, 1H), 7.46 (t, 2H).

Methyl benzodithioate. Benzodithioic acid, 412 mg (2.67 mmol) was dissolved in 50 mL of freshly distilled acetonitrile. To this solution, Cs_2CO_3, 4.74 g (5.45 eq), was added to form a slurry. The solution was purged with nitrogen for ten minutes and heated to 60ºC under a condenser. Methyl iodide, 0.91 mL (5.45 eq.) was added and the mixture turned cloudy, light pink. The solution was stirred at 60ºC for two hours and 50 mL of methanol was added before the solvent was removed under reduced pressure. The resulting light-red oil was chromatographed on silica using 10:1 hexanes/ethyl acetate to yield 360 mg of a clear-red oil in 84% yield. ^{1}H NMR (400 MHz, CD_3CN) δ 8.00 (dd, 2H), 7.60 (t, 1H), 7.45 (t, 2H), 2.78 (s, 3H) ^{13}C NMR (400 MHz, CD_3CN) δ 231.6, 146.1, 133.21, 129.6, 127.5, 21.28.

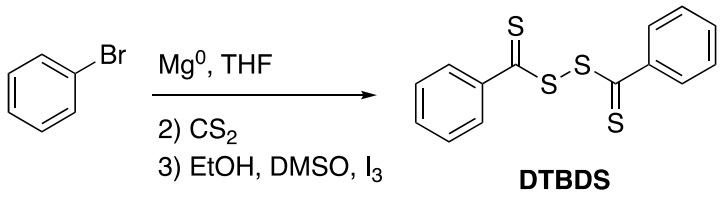

Figure 6.76. Synthesis of DTBDS.

Benzothioic dithioperoxyanhydride. (DTBDS). Bromobenzene, 15.70g (0.1 mmol) was added to a flame dried solution of freshly distilled THF containing 2.51 g Mg^0. The solution was gently heated with a heat gun, and a crystal of iodine was added to catalyze the reaction. After the gringnard reagent was formed as a light grey solution, and all of the Mg^0 was consumed, 7.6g of CS_2 (0.1 mmol) was added slowly. The solution turned deep red and was stirred at room temperature for 2 hrs. After, the solution was filtered and added to 200 mL ethyl ether. To this was added 100 mL of 10% HCl. The organic layer was extracted with portions of 10% HCl until clear. The ether layer was washed with 3 x 100 mL DI water and dried over $MgSO_4$. The solvent was removed under reduced pressure to yield the crude dithiobenzoic acid as a red oil. The oil was dissolved in 100 mL of EtOH and 7.8 mL (0.1 mmol) of DMSO and a crystal of iodine were added. The solution was stirred for one hour and put in the freezer overnight. The dimer was filtered off as a dark pink solid and recrystallized three times from EtOH to yield 13.1 g (0.04 mmol) of DTBDS in 42% yield. ^1H NMR (400 MHz, CD_3CN) δ 8.07 (dd, 2H), 7.70 (t, 1H), 7.53 (t, 2H).

(d) LFP of AQ-1 in Benzene

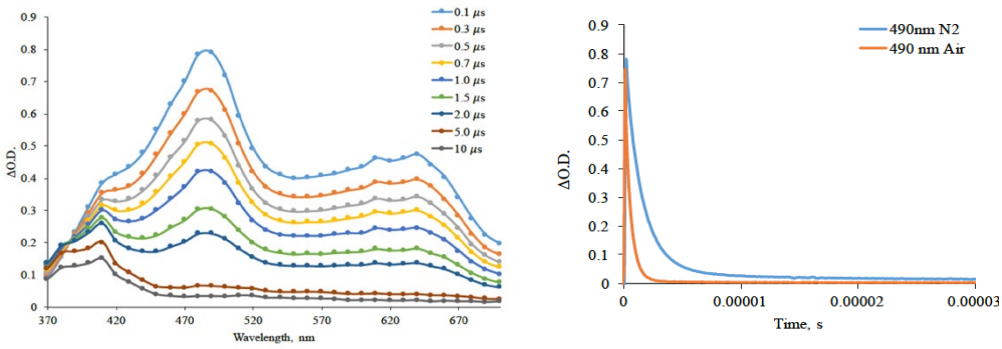

Figure 6.77. *Left*: Transient absorption spectrum of AQ-1 in benzene under N_2. The peaks corresponding to AQ-1^3* are seen at 490 and 630 nm. Small amounts of semiquinone, possibly due to self-quenching, can be seen at 410 nm. *Right*: Waveforms showing quenching of AQ-1^3* in air.

(e) NMR of Compounds

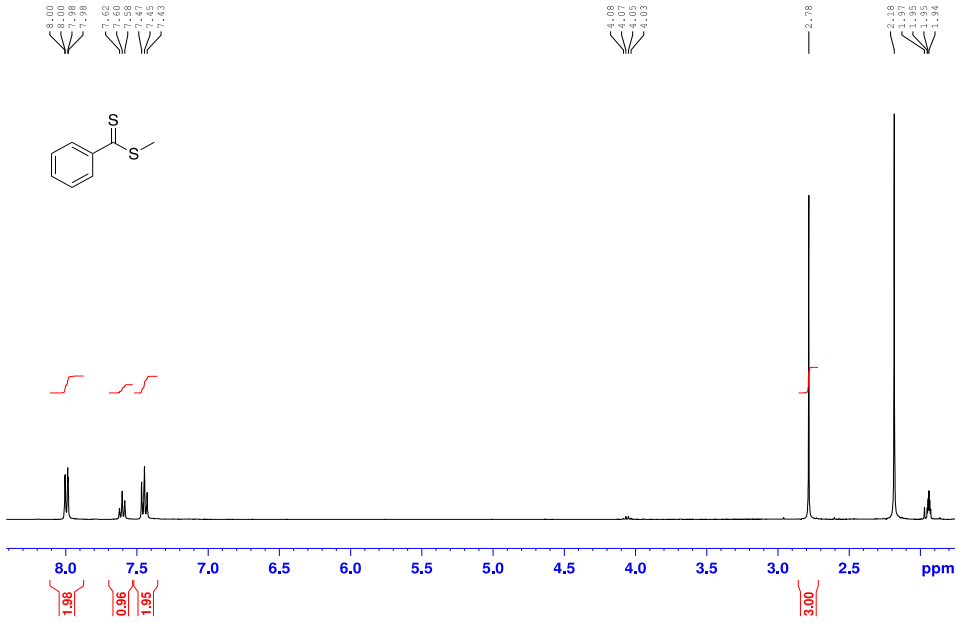

Figure 6.78. ^{1}H NMR of methyl benzodithioate.

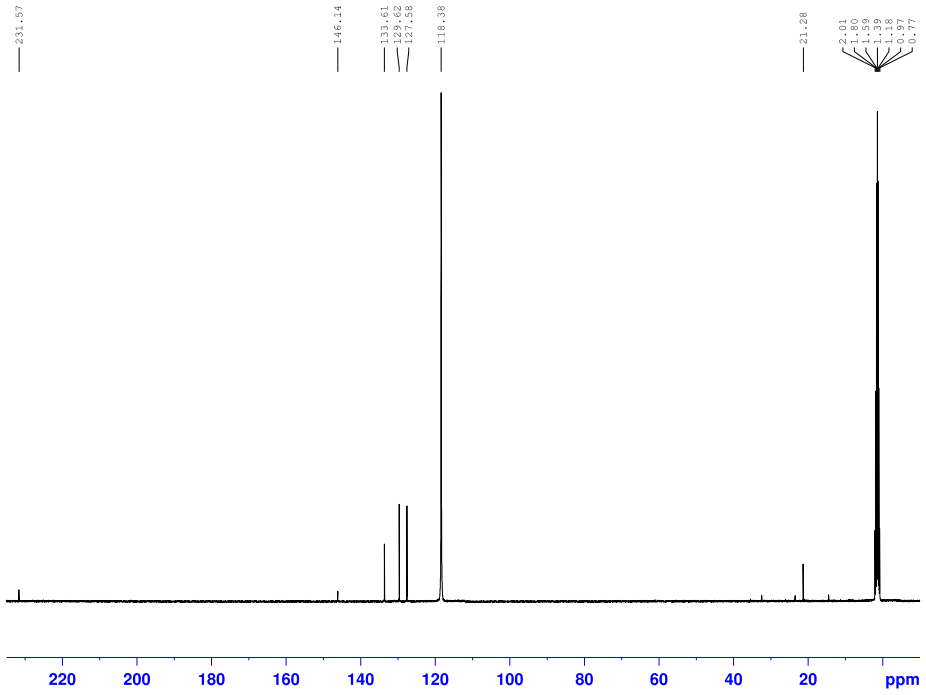

Figure 6.79. ^{13}C NMR of methyl benzodithioate.

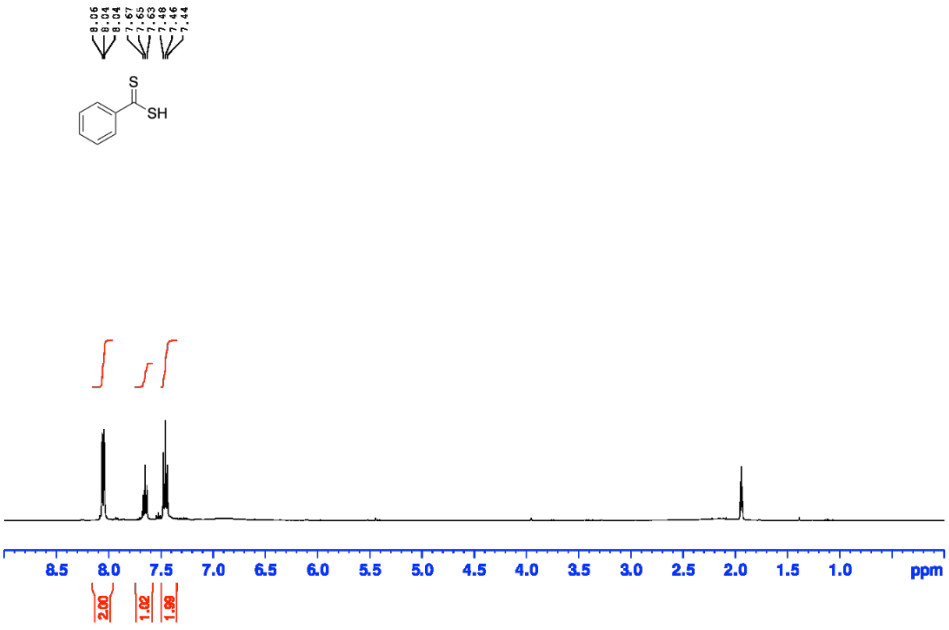

Figure 6.80. ^{1}H NMR of dithiobenzoic acid.

6.6 Synthesis of thioxanthone derivatives

The following compounds were synthesized for a collaboration in the development of photoinitiators with the Fourkas group.

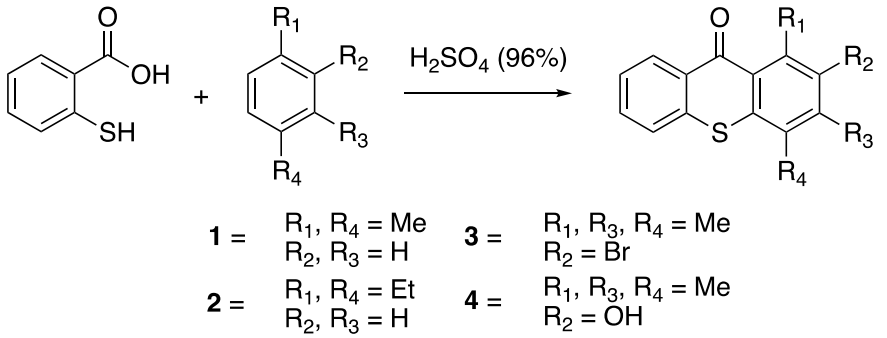

Figure 6.81. Synthesis of TX derivatives. When the aryl group is only substituted at the R_2 or R_3 positions, the final regiochemistry is difficult to predict.

(a) General Procedure for the synthesis of substituted thioxanthones.

To a 250 mL RBF was added mercaptobenzoic acid (1 eq) and substituted benzene (10 eq) in 50 mL of H_2SO_4 (96%). The solution was stirred at room temperature overnight before being poured over ice. Once melted, the solution was washed with 3 x 50 mL of chloroform. The organic layers were combined and washed with sat'd $NaHCO_3$ 2 x 50 mL and water 1 x 50 mL before being dried over Na_2SO_4. The solvent was removed under reduced pressure to yield the substituted thioxanthone.

2-bromothioxanthone, 1. ^{1}H NMR (400 MHz, CD_3CN) δ 8.04 (d, 2H), 7.65 (t, 1H), 7.46 (t, 2H).

2-hydroxythioxanthone, 2. ^{1}H NMR (400 MHz, DMSO(d6)) δ 8.45 (d, 1H), 7.9-7.65 (m, 4H), 7.55 (t, 1H), 7.35 (dd, 1H).

1,4-dimehtylthioxanthone, 3. ^{1}H NMR (400 MHz, CD_3CN) δ 8.35(d, 1H), 7.65 (m, 2H), 7.49 (t, 1H), 7.41 (d, 1H), 7.22 (d, 1H), 2.80 (s, 3H), 2.48 (s, 3H).

1,4-diethylthioxanthone, 4. ^{1}H NMR (400 MHz, $CDCl_3$) δ 8.39(d, 1H), 8.18 (d, 1H), 7.60 (m, 3H), 7.49 (m, 1H), 7.18 (t 1H), 6.64 (d, 1H), 3.41 (q, 2H), 2.90 (q, 2H), 1.37 (q, 6H).

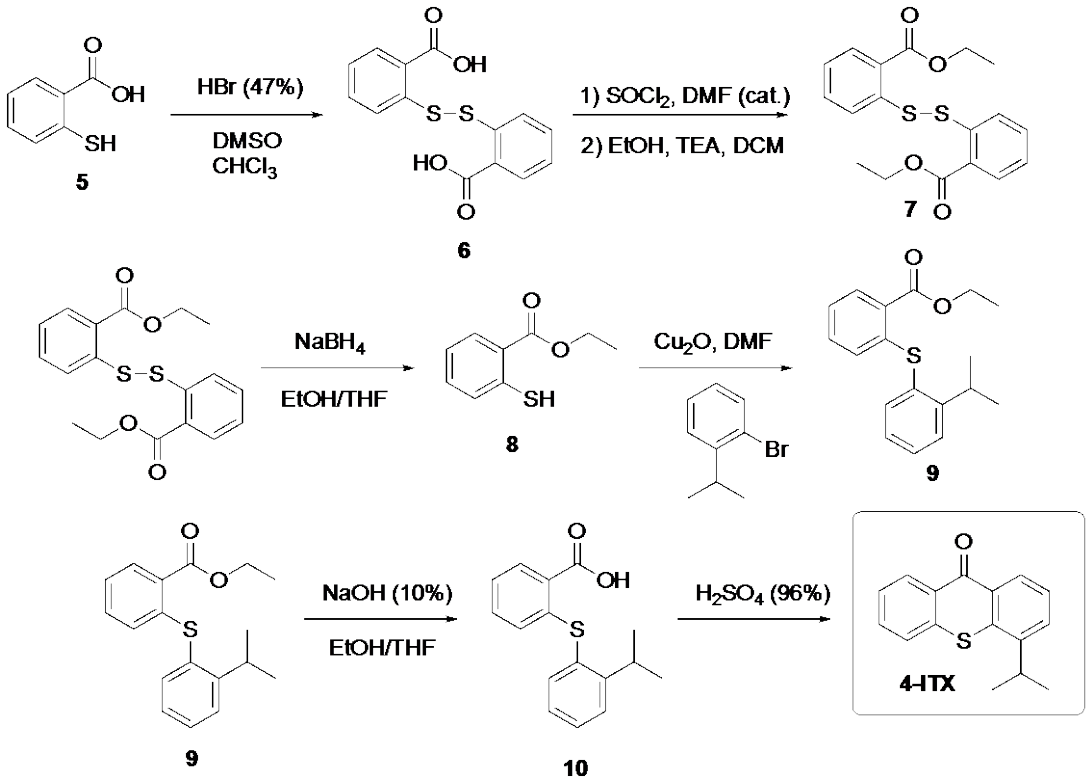

Figure 6.82. Synthesis of 4-isopropyl thioxanthone.

2,2'-disulfanediyldibenzoic acid, 6. 2-mercaptobenzoic acid (**5**), 5.103 g (33.1 mmol) was dissolved in 30 mL of $CHCl_3$ and 30 mL of DMSO. To this was added 1 mL of HBr (20%) and the solution was stirred for 2 hours. After stirring, 50 mL of water was added and a white precipitate was formed. The precipitate was filter off and the filter cake was washed multiple times with cold acetone. The filter cake was dried under reduced pressure to yield 3.314 g of **6.**

diethyl 2,2'-disulfanediyldibenzoate, 7. To 5.141g (16.8 mmol) of **6** in a 250 mL RBF was added dropwise, 30 mL of $SOCl_2$. The reaction mixture was refluxed at 80ºC at the beginning of which, 10 drops of DMF was added through the top of the condenser. The solution was refluxed for 2 hours. After reaching room temperature, the solvent was removed under reduced pressure and the excess $SOCl_2$ was quenched with and ICE/MeOH mixture. The result was a light yellow powder, which was used without further purification. The powder was dissolved in 100 mL of DCM and, to this was added slowly a solution containing 9.4 mL TEA (4 eq.), 3.9 mL EtOH (4 eq.) in 50 mL of DCM. The mixture was stirred overnight. The organic layer was washed with 2 x 20 mL of sat'd $NaHCO_3$ and 1 x 20 mL 5% H_2SO_4 and dried over Na_2SO_4. The solvent was removed to yield **7** as a light brown oil. 4.323g, 71% yield. ^{1}H NMR (400 MHz, DMSO(D6)) δ 8.05 (d, 1H), 7.61 (m, 2H), 7.37 (t, 1H), 4.39 (q, 2H), 1.37 (t, 3H).

ethyl 2-mercaptobenzoate, 8. 7, 2.103g (5.8 mmol) was dissolved in 80 mL of a 1:1 EtOH/THF mixture. To this was added slowly, $NaBH_4$, 0.884 g (4 eq.). After the bubbling ceased, the solution was stirred for 2 hrs. The solvent was removed under reduced pressure and the leftover solids were dissolved in water. Glacial acetic acid was added until pH ≈ 4. The solution was extracted with ethyl acetate and the organic layer was collected and washed with Na_2SO_4. The solvent was removed and the crude oil was purified by column chromatography on silica (10:1 Hexanes/EtOAc, R_f = 0.6). The resulting product was 581.1 mg of a light yellow oil in 55% yield. ^{1}H NMR

(400 MHz, DMSO(D6)) δ 7.92 (d, 1H), 7.56 (d, 1H), 7.41 (t, 1H), 7.22 (t, 1H), 4.30 (q, 2H), 1.31 (t, 3H).

ethyl 2-((2-isopropylphenyl)thio)benzoate, 9. In a 10 mL RBF was mixed **8**, 414.0 mg (2.27 mmol), 0.35 mL bromocumene (1 eq), and 491.3 mg Cu_2O (1.5 eq) in 4 mL of DMF. The solution was refluxed at 150°C overnight. Once cooled to room temperature, the mixture was poured into 50 mL of water and extracted with 50 mL of ethyl acetate. The organic layer was washed with brine, 2 x 20 mL and dried over Na_2SO_4. The solvent was removed to yield 757.2 mg of **9** as a light yellow oil in 90% yield. ^{1}H NMR (400 MHz, CD_3CN) δ 7.93 (d, 2H), 7.51 (m, 3H), 7.28 (m, 2H), 7.19 (t, 1H), 6.65 (d, 1H), 4.38 (q, 2H), 3.42 (m, 1H), 1.38 (t, 3H), 1.15 (d,1H).

2-((2-isopropylphenyl)thio)benzoic acid. 10. A solution of 507.1 mg of **9** (1.68 mmol) was dissolved in 30 mL of KOH (10%), 60 ml EtOH and 60 mL THF. The solution was refluxed overnight at 70°C. The majority of the solvent was removed under reduced pressure and the remaining, mostly aqueous, solution was adjusted to pH ≈ 4 with glacial acetic acid. Ethyl acetate was added and the organic layer was extracted. The organic layer was dried over Na_2SO_4 and the solvent was removed under reduced pressure to yield 451.9 mg of **10** as a light yellow oil. ^{1}H NMR (400 MHz, DMSO(D6)) δ 13.16 (s (br), 1H), 7.94 (d, 1H), 7.50 (m, 3H), 7.32 (m, 3H), 7.19 (t, 2H), 6.53 (d, 1H), 3.38 (m, 1H), 1.12 (d, 6H).

4-isopropyl thioxanthone, 4-ITX. To 20 mL of H_2SO_4 (96%) was added 504.5 mg (1.78 mmol) of **10** and the solution was stirred overnight. The mixture was poured over ice and, once the ice melted, the aqueous layer was extracted with 100 mL of chloroform. The organic layer was washed 3 x 20 mL sat'd $NaHCO_3$ and 1 x 50 mL DI water. The organic layer was dried with $MgSO_4$ as the solvent was removed under reduced pressure. The resulting yellow powder was recrystallized from $CHCl_3$/Hex resulting in 201.1 mg of 4-ITX in 44 percent yield. ^{1}H NMR (400 MHz, DMSO(D6)) δ 8.45 (d, 1H), 8.43 (d, 1H), 7.90 (d, 1H), 7.79 (m, 2H), 7.60 (m, 2H), 3.41 (m, 1H), 1.36 (d, 6H).

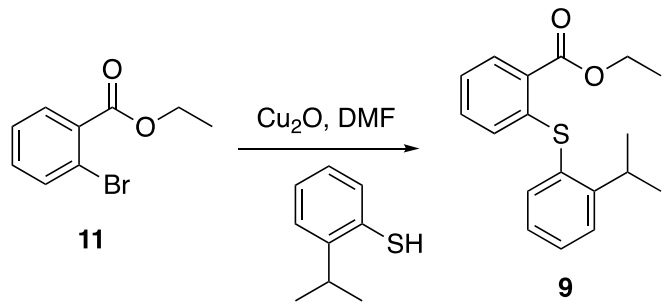

Figure 6.83. Alternate synthesis of compound **9** from commercial starting materials.

ethyl 2-((2-isopropylphenyl)thio)benzoate, 9. In a 25 mL RBF was mixed 0.56 mL of **11** (3.5 mmol), 0.53 mL of thiocumene (3.5 mmol), and 0.751 g Cu_2O (1.5 eq.) in 5 mL DMF. The mixture was refluxed at 150°C overnight and, once cooled to room temperature, poured into water. The water was extracted 3 x 25 mL with ethyl acetate and the organic layer was dried over Na_2SO_4. The solvent was removed under reduced pressure to yield 1.052 g of **9** as a light yellow oil in 90% yield.

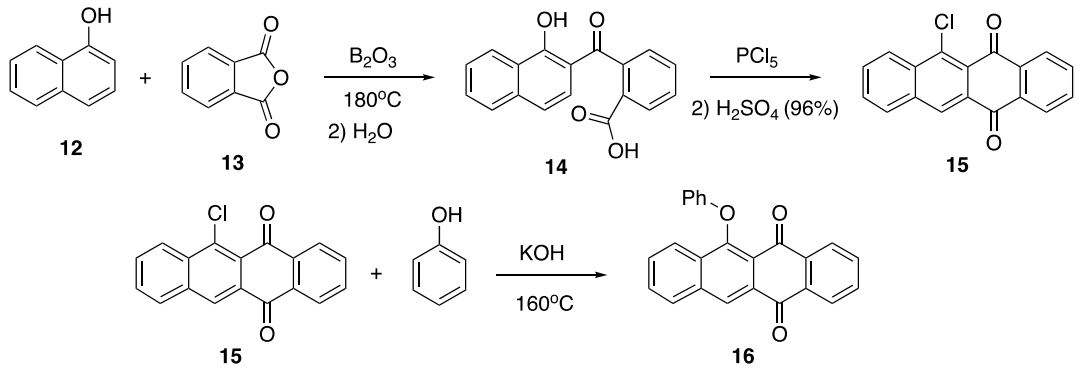

Figure 6.84. Synthesis of phenoxynapthacenequinone (PNQ, **16**).

2-(1-hydroxy-2-naphthoyl)benzoic acid, 14. Napthol, **12**, 5.0561g (35.1 mmol) and phthalic anhydride, **13**, 7.7223 g (52.1 mmol) were ground together with 3.7947g of B_2O_3 (1.5 eq). The powder was added to a 100 mL RBF and heated to 180°C under a condenser for 2 hours. After the mixture was allowed to cool to room temperature, 100 mL of water was added and the solution was refluxed for 1 hr. The solution was filtered hot and the solids were dissolved in 300 mL of chloroform. The solvent was removed down to ≈ 100 mL and the remaining solution was poured into 500 mL hexanes. The final product, **14**, was filtered off as a brown powder. 9.96 g, 90% yield. ^{1}H NMR (400 MHz, DMSO(D6)) δ 13.59 (s, 1H), 13.31 (s (br), 1H), 8.41 (d, 1H), 8.31 (s, 1H), 8.08 (d, 1H), 7.90 (d, 1H), 7.79 (t, 1H), 7.73 (q, 1H), 7.66 (t, 1H), 7.55 (d, 1H), 7.31 (d, 1H), 7.00 (d, 1H).

6-chlorotetracene-5,12-dione, 15. In a mortar and pestle, ≈ 21g of PCl_5 and ≈ 4.8g of **14** we ground together. The mixture was heated to 160°C in a 100 mL RBF for 1.5 hrs. After the solution was left to cool for 10 min, 5 mL of glacial acetic acid was added dropwise to the warm mixture. The solution was poured into 150 mL water and solution was filtered. The precipitate was collected and added slowly to 40 mL of

H_2SO_4 (96%). The mixture was heated to 60ºC for 1 hr before being poured over ice. Ethyl acetate (≈ 500 mL) was added or until the solids dissolved. The organic layer was washed with sat'd $NaHCO_3$ and DI water before the organic layer was dried over Na_2SO_4. The solution was put into the freezer overnight and, in the morning, the pure product was filtered off as an orange powder. The rest of the solvent was removed and was purified by column chromatography on silica (20% $CHCl_3$ 80% Hexanes, R_f = 0.5). ^{1}H NMR (400 MHz, DMSO(D6)) δ 8.93 (s, 1H), 8.65 (d, 1H), 8.43 (d, 1H), 8.25 (m, 2H), 7.95 (m, 4H).

6-phenoxytetracene-5,12-dione, 16. Phenol, 2.7846 (29.6 mmol), and **15**, 1.2758 (4.36 mmol), were ground together in a mortar and pestle. The mixture was added to a 100 mL RBF and heated to 160ºC with a condenser overnight. The hot solution was poured into 50 mL of KOH (10%) and it turned deep red. The mixture was refluxed for 10 min and the solids were filtered off. The solids were dissolved in chloroform and washed with 10% KOH (2 x 20 mL), sat'd $NaHCO_3$ (1 x 20 mL) and DI water (2 x 20 mL) before drying over Na_2SO_4. The solvent was removed under reduced pressure and the light orange powder was recrystallized from DMSO to yield 0.6980 g of **16** in 46% yield. ^{1}H NMR (400 MHz, DMSO(D6)) δ 8.88 (s, 1H), 8.43 (d, 1H), 8.27 (m, 1H), 8.10 (m, 2H), 7.90 (m, 2H), 7.79 (dt, 2H), 7.29 (t, 2H), 7.02 (t, 1H), 6.90 (d, 2H).

Bibliography

1.10 References

(1) Pandey, G.; Karthikeyan, M.; Murugan, A. *J. Org. Chem.* **2002**, *63* (9), 2867.

(2) Pandey, G.; Murugan, A.; Balakrishnan, M. *Chem. Commun.* **2002**, *2* (6), 624.

(3) Akaba, R.; Ohshima, K.; Kawai, Y.; Obuchi, Y.; Negishi, A.; Sakuragi, H.; Tokumaru, K. *Tetrahedron Lett.* **1991**, *32* (1), 109.

(4) Kuriyama, Y.; Arai, T.; Sakuragi, H.; Tokumaru, K. *Chem. Lett.* **2006**, *17* (7), 1193.

(5) Sundararajan, C.; Falvey, D. E. *J. Org. Chem.* **2004**, *69* (17), 5547.

(6) Sundararajan, C.; Falvey, D. E. *J. Am. Chem. Soc.* **2005**, *127* (22), 8000.

(7) Sundararajan, C.; Falvey, D. E. *Photochem. Photobiol. Sci.* **2006**, *5* (1), 116.

(8) Lee, K.; Falvey, D. E. *J. Am. Chem. Soc.* **2000**, *122* (39), 9361.

(9) Sundararajan, C.; Falvey, D. E. *Photochem. Photobiol. Sci.* **2006**, *5* (1), 116.

(10) Marcus, R. A. *Pure Appl. Chem.* **2007**, *69* (1), 13.

(11) Marcus, R. A. *Annu. Rev. Phys. Chem.* **2003**, *15* (1), 155.

(12) Marcus, R. A. *J. Chem. Phys.* **1956**, *24* (5), 966.

(13) Weller, A. *Pure Appl. Chem.* **1968**, *16* (1), 115.

(14) Rehm, D.; Weller, A. *Isr. J. Chem.* **1970**, *8* (2), 259.

(15) Romero, N. A.; Nicewicz, D. A. *Chem. Rev.* **2016**, *116* (17), 10075.

(16) Miller, J. R.; Calcaterra, L. T.; Closs, G. L. *J. Am. Chem. Soc.* **1984**, *106* (10), 3047.

(17) Miller, J. R.; Beitz, J. V.; Huddleston, R. K. *J. Am. Chem. Soc.* **1984**, *106* (18), 5057.

(18) Pan, X.; Tasdelen, M. A.; Laun, J.; Junkers, T.; Yagci, Y.; Matyjaszewski, K. *Prog. Polym. Sci.* **2016**, *62*, 73.

(19) Braunecker, W. A.; Matyjaszewski, K. *Progress in Polymer Science (Oxford)*. 2007, pp 93–146.

(20) Matyjaszewski, K. *Macromolecules* **2012**, *45* (10), 4015.

(21) Theriot, J. C.; McCarthy, B. G.; Lim, C.-H.; Miyake, G. M. *Macromol. Rapid Commun.* **2017**, *38* (13), 1700040.

(22) Ni, Y.; Zhang, L.; Cheng, Z.; Zhu, X. *Polymer Chemistry*. The Royal Society of Chemistry May 21, 2019, pp 2504–2515.

(23) Hill, M. R.; Carmean, R. N.; Sumerlin, B. S. *Macromolecules*. 2015, pp 5459–5469.

(24) Perrier, S. *Macromolecules* **2017**, *50* (19), 7433.

(25) McKenzie, T. G.; Fu, Q.; Uchiyama, M.; Satoh, K.; Xu, J.; Boyer, C.; Kamigaito, M.; Qiao, G. G. *Adv. Sci.* **2016**, *3* (9), 1500394.

(26) Otsu, T.; Yoshida, M. *Die Makromol. Chemie, Rapid Commun.* **1982**, *3* (2), 127.

(27) Otsu, T. *J. Polym. Sci. Part A Polym. Chem.* **2000**, *38* (12), 2121.

(28) Corrigan, N.; Shanmugam, S.; Xu, J.; Boyer, C. *Chemical Society Reviews*., **2016**, *45*, 6165.

(29) Phommalysack-Lovan, J.; Chu, Y.; Boyer, C.; Xu, J. *Chem. Commun.* **2018**, *54* (50), 6591.

(30) Lee, I.-H.; Discekici, E. H.; Anastasaki, A.; de Alaniz, J. R.; Hawker, C. J. *Polym. Chem.* **2017**, *8*, 3351.

(31) Xu, J.; Atme, A.; Marques Martins, A. F.; Jung, K.; Boyer, C. *Polym. Chem.* **2014**, *5* (10), 3321.

(32) Shanmugam, S.; Xu, J.; Boyer, C. *Chem. Sci.* **2015**, *6* (2), 1341.

(33) Prier, C. K.; Rankic, D. A.; MacMillan, D. W. C. *Chem. Rev.* **2013**, *113* (7), 5322.

(34) Narayanam, J. M. R.; Stephenson, C. R. J. *Chem. Soc. Rev.* ***2011****, 40 (1), 102-113.*

(35) Nicewicz, D. A.; MacMillan, D. W. C. *Science* **2008**, *322* (5898), 77.

(36) Ischay, M. A.; Anzovino, M. E.; Du, J.; Yoon, T. P. *J. Am. Chem. Soc.* **2008**, *130* (39), 12886.

(37) Narayanam, J. M. R.; Tucker, J. W.; Stephenson, C. R. J. *J. Am. Chem. Soc.* **2009**, *131* (25), 8756.

(38) Edson, J. B.; Spencer, L. P.; Boncella, J. M. *Org. Lett.* **2011**, *13* (23), 6156.

(39) Borak, J. B.; Falvey, D. E. *J. Org. Chem.* **2009**, *74* (10), 3894.

(40) Christmann, J.; Ibrahim, A.; Charlot, V.; Croutxé-Barghorn, C.; Ley, C.; Allonas, X. *ChemPhysChem* **2016**, *17* (15), 1439.

(41) Corrigan, N.; Xu, J.; Boyer, C.; Allonas, X. *ChemPhotoChem* **2019**, 3, 1.

(42) Hari, D. P.; König, B. *Chem. Commun.* **2014**, *50* (51), 6688.

(43) Redmond, R. W.; Gamlin, J. N. *Photochem. Photobiol.* **1999**, *70* (4), 391.

(44) Xu, J.; Shanmugam, S.; Duong, H. T.; Boyer, C. *Polym. Chem.* **2015**, *6* (31), 5615.

(45) Liu, Z.; Zhang, Y.; Cai, Z.; Sun, H.; Cheng, X. *Adv. Synth. Catal.* **2015**, *357* (2–3), 589.

(46) Cheng, C.; Sun, G.; Khoshdel, E.; Wooley, K. L. *J. Am. Chem. Soc.* **2007**, *129* (33), 10086.

2.12 References:

(1) Klán, P.; Šolomek, T.; Bochet, C. G.; Blanc, A.; Givens, R.; Rubina, M.; Popik, V.; Kostikov, A.; Wirz, J. *Chem. Rev.* **2013**, *113* (1), 119.

(2) Murov, S. L.; Hug, G. L.; Carmichael, I. *Handbook of photochemistry*; M. Dekker, 1993.

(3) Jasny, J.; Sepit, J.; Karpiuk, J.; Gilewski, J. *Rev. Sci. Instrum.* **1994**, *65* (12), 3646.

(4) Berera, R.; van Grondelle, R.; Kennis, J. T. M. *Photosynth. Res.* **2009**, *101* (2–3), 105.

(5) Görner, H. *Photochem. Photobiol.* **2003**, *77* (2), 171.

(6) Ellis-Davies, G. C. R. *Chem. Rev.* **2008**, *108* (5), 1603.

(7) Berridge, M. J.; Lipp, P.; Bootman, M. D. *Nat. Rev. Mol. Cell Biol.* **2000**, *1* (1), 11.

(8) Javvaji, V.; Baradwaj, A. G.; Payne, G. F.; Raghavan, S. R. *Langmuir* **2011**, *27* (20), 12591.

(9) Lee, K. Y.; Mooney, D. J. *Prog. Polym. Sci.* **2012**, *37* (1), 106.

(10) Higham, A. K.; Bonino, C. A.; Raghavan, S. R.; Khan, S. A. *Soft Matter* **2014**, *10* (27), 4990.

(11) Maleki Dizaj, S.; Sharifi, S.; Ahmadian, E.; Eftekhari, A.; Adibkia, K.; Lotfipour, F. *Expert Opin. Drug Deliv.* **2019**, *16* (4), 331.

(12) Kraly, J. R.; Holcomb, R. E.; Guan, Q.; Henry, C. S. *Anal. Chim. Acta* **2009**,

653 (1), 23.

(13) Heymann, R. R.; Thum, M. D.; Hardee, A. L.; Falvey, D. E. *Photochem. Photobiol. Sci.* **2017**, *16* (6).

(14) Bechtold, T.; Burtscher, E.; Turcanu, A. *J. Electroanal. Chem.* **1999**, *465* (1), 80.

(15) König, B. *Chemical photocatalysis*; De Gruyter: Berlin, 2013.

(16) Siliprandi, N.; Bianchi, P. *BBA - Biochim. Biophys. Acta* **1955**, *16* (C), 424.

(17) Liu, C.; Zachara, J. M.; Foster, N. S.; Strickland, J. *Environ. Sci. Technol.* **2007**, *41* (22), 7730.

(18) Loeff, I.; Trelnln, A.; Llnschltz ', H. *J. Phys. Chem* **1983**, *87*, 2536.

(19) Bernt Melø, T.; Adriana Ionescu, M.; Haggquist, G. W.; Razi Naqvi, K. *Spectrochim. Acta - Part A Mol. Biomol. Spectrosc.* **1999**, *55* (11), 2299.

(20) Su, Z.; Mariano, P. S.; Falvey, D. E.; Yoon, U. C.; Oh, S. W. *J. Am. Chem. Soc.* **1998**, *120* (41), 10676.

(21) Fife, D. J.; Moore, W. M. *Photochem. Photobiol.* **1979**, *29* (1), 43.

(22) Heelis, P. F.; Parsons, B. J.; Phillips, G. O.; McKellar, J. F. *Photochem. Photobiol.* **1979**, *30* (3), 343.

(23) Babay, P. A.; Emilio, C. A.; Ferreyra, R. E.; Gautier, E. A.; Gettar, R. T.; Litter, M. I. *Int. J. Photoenergy* **2001**, *3* (4), 193.

(24) Denning, D. M.; Pedowitz, N. J.; Thum, M. D.; Falvey, D. E. *Org. Lett.* **2015**, *17* (24), 5986.

(25) Barnett, W. E.; Needham, L. L. *J. Chem. Soc. D* **1971**, *0* (3), 170.

(26) Zeppuhar, A. N.; Hill-Byrne, K.; Falvey, D. E. *Photochem. Photobiol. Sci.*

2019.

(27) Feng, D.-M.; Zhu, Y.-P.; Chen, P.; Ma, T.-Y.; Feng, D.-M.; Zhu, Y.-P.; Chen, P.; Ma, T.-Y. *Catalysts* **2017**, *7* (12), 373.

(28) Benson, E. E.; Kubiak, C. P.; Sathrum, A. J.; Smieja, J. M. *Chem. Soc. Rev.* **2009**, *38* (1), 89.

(29) La Porte, N. T.; Martinez, J. F.; Chaudhuri, S.; Hedström, S.; Batista, V. S.; Wasielewski, M. R. *Coordination Chemistry Reviews*., **2018**, *361*, 98.

(30) Tommasi, I.; Sorrentino, F. *Tetrahedron Lett.* **2005**, *46* (12), 2141.

(31) Kayaki, Y.; Yamamoto, M.; Ikariya, T. *Angew. Chemie Int. Ed.* **2009**, *48* (23), 4194.

(32) Denning, D. M.; Thum, M. D.; Falvey, D. E. *Org. Lett.* **2015**, *17* (17), 4152.

(33) de Robillard, G.; Devillers, C. H.; Kunz, D.; Cattey, H.; Digard, E.; Andrieu, J. *Org. Lett.* **2013**, *15* (17), 4410.

(34) Sundararajan, C.; Falvey, D. E. *J. Org. Chem.* **2004**, *69* (17), 5547.

(35) Alkaitis, S. A.; Grätzel, M. *J. Am. Chem. Soc.* **1976**, *98* (12), 3549.

3.11 References:

(1) Murov, S. L.; Hug, G. L.; Carmichael, I. *Handbook of photochemistry*; M. Dekker, 1993.

(2) Huppert, D.; Jortner, J.; Rentzepis, P. M. *Chem. Phys. Lett.* **1972**, *13* (3), 225.

(3) Müller, A.; Pflüger, E. *Chem. Phys. Lett.* **1968**, *2* (3), 155.

(4) Scaiano, J. C.; Tanner, M.; Weir, D. *J. Am. Chem. Soc.* **1985**, *107* (15), 4396.

(5) Scaiano, J. C.; Johnston, L. J. *Pure Appl. Chem.* **1986**, *58* (9), 1273.

(6) McGimpsey, W. G.; Scaiano, J. C. *J. Am. Chem. Soc.* **1987**, *109* (7), 2179.

(7) Scaiano, J. C.; Johnston, L. J.; McGimpsey, W. G.; Weir, D. *Acc. Chem. Res.* **1988**, *21* (1), 22.

(8) Wintgens, V.; Johnston, L. J.; Scaiano, J. C. *J. Am. Chem. Soc.* **1988**, *110* (2), 511.

(9) Turro, N. J.; Ramamurthy, V.; Cherry, W.; Farneth, W. *Chem. Rev.* **1978**, *78* (2), 125.

(10) Kobayashi, Y.; Mutoh, K.; Abe, J. *J. of Photochem. and Photobiol. C: Photochem. Rev*. **2018**, *34*, 2.

(11) O'Connor, N. A.; Berro, A. J.; Lancaster, J. R.; Xinyu, G.; Jockusch, S.; Nagai, T.; Ogata, T.; Lee, S.; Zimmerman, P.; Willson, C. G.; Turro, N. J. *Chem. Mater.* **2008**, *20* (24), 7374.

(12) Tasdelen, M. A.; Kumbaraci, V.; Jockusch, S.; Turro, N. J.; Talinli, N.; Yagci, Y. *Macromolecules* **2008**, *41* (2), 295.

(13) Yagci, Y.; Jockusch, S.; Turro, N. J. *Macromolecules* **2010**, *43* (15), 6245.

(14) Jeudy, M. J.; Robillard, J. J. *Opt. Commun.* **1975**, *13* (1), 25.

(15) Mutoh, K.; Nakagawa, Y.; Sakamoto, A.; Kobayashi, Y.; Abe, J. *J. Am. Chem. Soc.* **2015**, *137* (17), 5674.

(16) Kobayashi, Y.; Katayama, T.; Yamane, T.; Setoura, K.; Ito, S.; Miyasaka, H.; Abe, J. *J. Am. Chem. Soc.* **2016**, *138* (18), 5930.

(17) Yamaguchi, T.; Kobayashi, Y.; Abe, J. *J. Am. Chem. Soc.* **2016**, *138* (3), 906.

(18) Kobayashi, Y.; Okajima, H.; Sotome, H.; Yanai, T.; Mutoh, K.; Yoneda, Y.; Shigeta, Y.; Sakamoto, A.; Miyasaka, H.; Abe, J. *J. Am. Chem. Soc.* **2017**, *139* (18), 6382.

(19) Inagaki, Y.; Kobayashi, Y.; Mutoh, K.; Abe, J. *J. Am. Chem. Soc.* **2017**, *139* (38), 13429.

(20) Fujita, M.; Ishida, A.; Majima, T.; Takamuku, S. *J. Phys. Chem.* **1996**, *100* (13), 5382.

(21) Sakamoto, M.; Cai, X.; Kim, S. S.; Fujitsuka, M.; Majima, T. *J. Phys. Chem. A* **2007**, *111* (2), 223.

(22) Cai, X.; Sakamoto, M.; Fujitsuka, M.; Majima, T. *J. Phys. Chem. A* **2007**, *111* (10), 1788.

(23) Breslin, D. T.; Fox, M. A. *J. Phys. Chem.* **1994**, *98* (2), 408.

(24) Marchini, M.; Gualandi, A.; Mengozzi, L.; Franchi, P.; Lucarini, M.; Cozzi, P. G.; Balzani, V.; Ceroni, P. *Phys. Chem. Chem. Phys.* **2018**, *20* (12), 8071.

(25) Ghosh, I.; Ghosh, T.; Bardagi, J. I.; König, B. *Science* **2014**, *346* (6210), 725.

(26) Bardagi, J. I.; Ghosh, I.; Schmalzbauer, M.; Ghosh, T.; König, B. *European J. Org. Chem.* **2018**, *2018* (1), 34.

(27) Eggins, B. R.; Robertson, P. K. J. *J. Chem. Soc. Faraday Trans.* **1994**, *90* (15), 2249.

(28) Nelleborg, P.; Lund, H.; Eriksen, J. *Tetrahedron Lett.* **1985**, *26* (14), 1773.

(29) Pirrung, M. C.; Pieper, W. H.; Kaliappan, K. P.; Dhananjeyan, M. R. *Proc. Natl. Acad. Sci. U. S. A.* **2003**, *100* (22), 12548.

(30) Falvey, D. E.; Sundararajan, C. *Photochem. Photobiol. Sci.* **2004**, *3* (9), 831.

(31) Falvey, D. E.; Sundararajan, C. *Photochem. Photobiol. Sci.* **2004**, *3* (9), 831.

(32) Sundararajan, C.; Falvey, D. E. *Photochem. Photobiol. Sci.* **2006**, *5* (1), 116.

(33) Kunsberg, D. J.; Kipping, A. H.; Falvey, D. E. *Org. Lett.* **2015**, *17* (14), 3454.

(34) Cape, J. L.; Edson, J. B.; Spencer, L. P.; Declue, M. S.; Ziock, H.-J.; Maurer, S.; Rasmussen, S.; Monnard, P.-A.; Boncella, J. M. *Bioconjug. Chem.* **2012**, No. 23, 2014.

(35) Edson, J. B.; Spencer, L. P.; Boncella, J. M. *Org. Lett.* **2011**, *13* (23), 6156.

(36) Borak, J. B.; Falvey, D. E. *J. Org. Chem.* **2009**, *74* (10), 3894.

(37) Borak, J. B.; Falvey, D. E. *Photochem. Photobiol. Sci.* **2010**, *9* (6), 854.

(38) Thum, M. D.; Falvey, D. E. *J. Phys. Chem. A* **2018**, *122* (12), 3204.

(39) Lee, K.; Falvey, D. E. *J. Am. Chem. Soc.* **2000**, *122* (39), 9361.

(40) Sundararajan, C.; Falvey, D. E. *Org. Lett.* **2005**, *7* (13), 2631.

(41) Kunsberg, D. J.; Kipping, A. H.; Falvey, D. E. *Org. Lett.* **2015**, *17* (14), 3454.

(42) Griesbeck, A. G.; Oelgemöller, M.; Ghetti, F. *CRC handbook of organic photochemistry and photobiology*; Taylor & Francis, 2012.

(43) Patai, S.; Rappoport, Z. *Chem. Funct. groups* **1988**, *I*, 878 blz.

(44) Kuss-Petermann, M.; Orazietti, M.; Neuburger, M.; Hamm, P.; Wenger, O. S. *J. Am. Chem. Soc.* **2017**, *139* (47), 5225.

(45) Goulet, M.-A.; Tong, L.; Pollack, D. A.; Tabor, D. P.; Kwan, E. E.; Aspuru-Guzik, A.; Gordon, R. G.; Aziz, M. J. *J. Am. Chem. Soc.* **2019**, jacs. 8b13295.

(46) Zhang, J.; Hill, N.; Lalevée, J.; Fouassier, J.-P.; Zhao, J.; Graff, B.; Schmidt, T. W.; Kable, S. H.; Stenzel, M. H.; Coote, M. L.; Xiao, P. *Macromol. Rapid Commun.* **2018**, *39* (19), 1800172.

(47) Kuss-Petermann, M.; Wenger, O. S. *J. Am. Chem. Soc.* **2016**, *138* (4), 1349.

(48) Lerch, S.; Unkel, L.-N.; Brasholz, M. *Angew. Chemie* **2014**, *126* (25), 6676.

(49) Romero, N. A.; Nicewicz, D. A. *Chem. Rev.* **2016**, *116* (17), 10075.

(50) Görner, H. *Photochem. Photobiol.* **2003**, *77* (2), 171.

(51) Ly, D.; Kan, Y.; Armitage, B.; Schuster, G. B. *J. Am. Chem. Soc.* **1996**, *118* (36), 8747.

(52) Breslin, D. T.; Schuster, G. B. *J. Am. Chem. Soc.* **1996**, *118* (10), 2311.

(53) Sundararajan, C.; Falvey, D. E. *J. Org. Chem.* **2004**, *69* (17), 5547.

4.11 References:

(1) Otsu, T.; Yoshida, M. Role of Initiator-Transfer Agent-Terminator (Iniferter) in Radical Polymerizations: Polymer Design by Organic Disulfides as Iniferters. *Die Makromol. Chemie, Rapid Commun.* **1982**, *3* (2), 127–132.

(2) McKenzie, T. G.; Fu, Q.; Wong, E. H. H.; Dunstan, D. E.; Qiao, G. G. Visible Light Mediated Controlled Radical Polymerization in the Absence of Exogenous Radical Sources or Catalysts. *Macromolecules* **2015**, *48* (12), 3864–3872.

(3) Otsu, T. Iniferter Concept and Living Radical Polymerization. *J. Polym. Sci. Part A Polym. Chem.* **2000**, *38* (12), 2121–2136.

(4) Quinn, J. F.; Barner, L.; Barner-Kowollik, C.; Rizzardo, E.; Davis, T. P. Reversible Addition - Fragmentation Chain Transfer Polymerization Initiated with Ultraviolet Radiation. *Macromolecules* **2002**, *35* (20), 7620–7627.

(5) Lu, L.; Zhang, H.; Yang, N.; Cai, Y. Toward Rapid and Well-Controlled Ambient Temperature RAFT Polymerization under UV - Vis Radiation: Effect of Radiation Wave Range. *Macromolecules* **2006**, *39* (11), 3770–3776.

(6) Khan, M. Y.; Cho, M.-S.; Kwark, Y.-J. Dual Roles of a Xanthate as a Radical Source and Chain Transfer Agent in the Photoinitiated RAFT Polymerization

of Vinyl Acetate. *Macromolecules* **2014**, *47* (6), 1929–1934.

(7) McKenzie, T. G.; Fu, Q.; Uchiyama, M.; Satoh, K.; Xu, J.; Boyer, C.; Kamigaito, M.; Qiao, G. G. Beyond Traditional RAFT: Alternative Activation of Thiocarbonylthio Compounds for Controlled Polymerization. *Adv. Sci.* **2016**, *3* (9), 1500394.

(8) Jiangtao, X.; Sivaprakash, S.; Nathaniel Alan, C.; Cyrille, B. Catalyst-Free Visible Light-Induced RAFT Photopolymerization. *Control. Radic. Polym. Mech.* **2015**, *1187* (1187), 247–267.

(9) Ding, C.; Fan, C.; Jiang, G.; Pan, X.; Zhang, Z.; Zhu, J.; Zhu, X. Photocatalyst-Free and Blue Light-Induced RAFT Polymerization of Vinyl Acetate at Ambient Temperature. *Macromol. Rapid Commun.* **2015**, *36* (24), 2181–2185.

(10) Mckenzie, T. G.; Da, L. P.; Costa, M.; Fu, Q.; Dunstan, D. E.; Qiao, G. G. Investigation into the Photolytic Stability of RAFT Agents and the Implications for Photopolymerization Reactions. *Polym. Chem.* **2016**, *7*, 4246.

(11) Huppert, D.; Jortner, J.; Rentzepis, P. M. S2 → S1 Emission of Azulene in Solution. *Chem. Phys. Lett.* **1972**, *13* (3), 225–228.

(12) Murata, S.; Iwanaga, C.; Toda, T.; Kokubun, H. Fluorescence Yields of Azulene Derivatives. *Chem. Phys. Lett.* **1972**, *13* (2), 101–104.

(13) Gillispie, G. D.; Lim, E. C. Further Results on the Triplet—Triplet Fluorescence of Anthracenes. *Chem. Phys. Lett.* **1979**, *63* (2), 355–359.

(14) Eaton, D. F.; Evans, T. R.; Leermakers, P. A. No Title. *Mol. Photochem.* **1969**, *1*, 347.

(15) Demchenko, A. P.; Tomin, V. I.; Chou, P. T. Breaking the Kasha Rule for

More Efficient Photochemistry. *Chem. Rev.* **2017**, *117* (21), 13353–13381.

(16) Wolf, S. Applied Photochemistry for Multicolor Photolithography, University of Maryland, 2018.

(17) Kitchin, A. D.; Velate, S.; Chen, M.; Ghiggino, K. P.; Smith, T. A.; Steer, R. P. Photophysics of a Dithioester RAFT Polymerization Agent and the Acenaphthenyl Model Light-Harvesting Chromophore. *Photochem. Photobiol. Sci.* **2007**, *6* (8), 853.

(18) Quinn, J. F.; Barner, L.; Barner-Kowollik, C.; Rizzardo, E.; Davis, T. P. Reversible Addition - Fragmentation Chain Transfer Polymerization Initiated with Ultraviolet Radiation. *Macromolecules* **2002**, *35* (20), 7620–7627.

(19) Degirmenci, I.; Coote, M. L. Effect of Substituents on the Stability of Sulfur-Centered Radicals. *J. Phys. Chem. A* **2016**, *120* (37), 7398–7403.

(20) Shen, T.; Zhao, Z.-G.; Yu, Q.; Xu, H.-J. Photosensitized Reduction of Benzil by Heteroatom-Containing Anthracene Dyes. *J. Photochem. Photobiol. A Chem.* **1989**, *47* (2), 203–212.

(21) Murov, S. L.; Hug, G. L.; Carmichael, I. *Handbook of Photochemistry*; M. Dekker, 1993.

(22) Romero, N. A.; Nicewicz, D. A. Organic Photoredox Catalysis. *Chem. Rev.* **2016**, *116* (17), 10075–10166.

(23) Xu, J.; Jung, K.; Boyer, C. Oxygen Tolerance Study of Photoinduced Electron Transfer-Reversible Addition-Fragmentation Chain Transfer (PET-RAFT) Polymerization Mediated by Ru(Bpy)3Cl2. *Macromolecules* **2014**, *47* (13), 4217–4229.

(24) Xu, J.; Shanmugam, S.; Duong, H. T.; Boyer, C. Organo-Photocatalysts for Photoinduced Electron Transfer-Reversible Addition-Fragmentation Chain Transfer (PET-RAFT) Polymerization. *Polym. Chem.* **2015**, *6* (31), 5615–5624.

(25) Shanmugam, S.; Xu, J.; Boyer, C. Exploiting Metalloporphyrins for Selective Living Radical Polymerization Tunable over Visible Wavelengths. *J. Am. Chem. Soc.* **2015**, *137* (28), 9174–9185.

(26) Shanmugam, S.; Xu, J.; Boyer, C. Utilizing the Electron Transfer Mechanism of Chlorophyll a under Light for Controlled Radical Polymerization. *Chem. Sci.* **2015**, *6* (2), 1341–1349.

(27) Corrigan, N.; Xu, J.; Boyer, C.; Allonas, X. Exploration of the PET-RAFT Initiation Mechanism for Two Commonly Used Photocatalysts. *ChemPhotoChem* **2019**, 3, 1.

5.9. References:

(1) Pan, X.; Tasdelen, M. A.; Laun, J.; Junkers, T.; Yagci, Y.; Matyjaszewski, K. Photomediated Controlled Radical Polymerization. *Prog. Polym. Sci.* **2016**, *62*, 73–125.

(2) Hill, M. R.; Carmean, R. N.; Sumerlin, B. S. Expanding the Scope of RAFT Polymerization: Recent Advances and New Horizons. *Macromolecules*. **2015**, *48*, 5459–5469.

(3) Chen, M.; Zhong, M.; Johnson, J. A. Light-Controlled Radical Polymerization: Mechanisms, Methods, and Applications. *Chem. Rev.* **2016**, *116* (17), 10167–10211.

(4) McKenzie, T. G.; Fu, Q.; Uchiyama, M.; Satoh, K.; Xu, J.; Boyer, C.; Kamigaito, M.; Qiao, G. G. Beyond Traditional RAFT: Alternative Activation of Thiocarbonylthio Compounds for Controlled Polymerization. *Adv. Sci.* **2016**, *3* (9), 1500394.

(5) Corrigan, N.; Shanmugam, S.; Xu, J.; Boyer, C. Photocatalysis in Organic and Polymer Synthesis. *Chemical Society Reviews*. The Royal Society of Chemistry November 7, 2016, pp 6165–6212.

(6) Shanmugam, S.; Xu, J.; Boyer, C. Photocontrolled Living Polymerization Systems with Reversible Deactivations through Electron and Energy Transfer. *Macromolecular Rapid Communications*., **2017**, *38*, 1700143.

(7) McKenzie, T. G.; Fu, Q.; Wong, E. H. H.; Dunstan, D. E.; Qiao, G. G. Visible Light Mediated Controlled Radical Polymerization in the Absence of Exogenous Radical Sources or Catalysts. *Macromolecules* **2015**, *48* (12), 3864–3872.

(8) Otsu, T. Iniferter Concept and Living Radical Polymerization. *J. Polym. Sci. Part A Polym. Chem.* **2000**, *38* (12), 2121–2136.

(9) Khan, M. Y.; Cho, M.-S.; Kwark, Y.-J. Dual Roles of a Xanthate as a Radical Source and Chain Transfer Agent in the Photoinitiated RAFT Polymerization of Vinyl Acetate. *Macromolecules* **2014**, *47* (6), 1929–1934.

(10) Shanmugam, S.; Cuthbert, J.; Kowalewski, T.; Boyer, C.; Matyjaszewski, K. Catalyst-Free Selective Photoactivation of RAFT Polymerization: A Facile Route for Preparation of Comblike and Bottlebrush Polymers. *Macromolecules* **2018**, *51* (19), 7776–7784.

(11) Quinn, J. F.; Barner, L.; Barner-Kowollik, C.; Rizzardo, E.; Davis, T. P. Reversible Addition - Fragmentation Chain Transfer Polymerization Initiated with Ultraviolet Radiation. *Macromolecules* **2002**, *35* (20), 7620–7627.

(12) You, Y.-Z.; Hong, C.-Y.; Bai, R.-K.; Pan, C.-Y.; Wang, J. Photo-Initiated Living Free Radical Polymerization in the Presence of Dibenzyl Trithiocarbonate. *Macromol. Chem. Phys.* **2002**, *203* (3), 477–483.

(13) Lu, L.; Zhang, H.; Yang, N.; Cai, Y. Toward Rapid and Well-Controlled Ambient Temperature RAFT Polymerization under UV - Vis Radiation: Effect of Radiation Wave Range. *Macromolecules* **2006**, *39* (11), 3770–3776.

(14) Xu, J.; Shanmugam, S.; Duong, H. T.; Boyer, C. Organo-Photocatalysts for Photoinduced Electron Transfer-Reversible Addition-Fragmentation Chain Transfer (PET-RAFT) Polymerization. *Polym. Chem.* **2015**, *6* (31), 5615–5624.

(15) Phommalysack-Lovan, J.; Chu, Y.; Boyer, C.; Xu, J. PET-RAFT Polymerisation: Towards Green and Precision Polymer Manufacturing. *Chem. Commun.* **2018**, *54* (50), 6591–6606.

(16) Shanmugam, S.; Xu, J.; Boyer, C. Exploiting Metalloporphyrins for Selective Living Radical Polymerization Tunable over Visible Wavelengths. *J. Am. Chem. Soc.* **2015**, *137* (28), 9174–9185.

(17) Theriot, J. C.; Miyake, G. M.; Boyer, C. A. *N* , *N* -Diaryl Dihydrophenazines as Photoredox Catalysts for PET-RAFT and Sequential PET-RAFT/O-ATRP. *ACS Macro Lett.* **2018**, *7* (6), 662–666.

(18) Figg, C. A.; Hickman, J. D.; Scheutz, G. M.; Shanmugam, S.; Carmean, R. N.;

Tucker, B. S.; Boyer, C.; Sumerlin, B. S. Color-Coding Visible Light Polymerizations To Elucidate the Activation of Trithiocarbonates Using Eosin Y. *Macromolecules* **2018**, acs.macromol.7b02533.

(19) Corrigan, N.; Rosli, D.; Jones, J. W. J.; Xu, J.; Boyer, C. Oxygen Tolerance in Living Radical Polymerization: Investigation of Mechanism and Implementation in Continuous Flow Polymerization. *Macromolecules* **2016**, *49* (18), 6779–6789.

(20) Yeow, J.; Chapman, R.; Gormley, A. J.; Boyer, C. Up in the Air: Oxygen Tolerance in Controlled/Living Radical Polymerisation. *Chemical Society Reviews*. **2018**, *47* (12), 4357–4387.

(21) Shanmugam, S.; Xu, J.; Boyer, C. Utilizing the Electron Transfer Mechanism of Chlorophyll a under Light for Controlled Radical Polymerization. *Chem. Sci.* **2015**, *6* (2), 1341–1349.

(22) Shanmugam, S.; Xu, S.; Adnan, N. N. M.; Boyer, C. Heterogeneous Photocatalysis as a Means for Improving Recyclability of Organocatalyst in "Living" Radical Polymerization. *Macromolecules* **2018**, *51* (3), 779–790.

(23) Corrigan, N.; Xu, J.; Boyer, C. A Photoinitiation System for Conventional and Controlled Radical Polymerization at Visible and NIR Wavelengths. *Macromolecules* **2016**, *49* (9), 3274–3285.

(24) Kishore, K.; Asmus, K.-D. Radical Cations from One-Electron Oxidation of Aliphatic Sulphoxides in Aqueous Solution. A Radiation Chemical Study. *J. Chem. Soc. Perkin Trans. 2* **2004**, No. 12, 2079.

(25) Fuchigami, T.; Mahito, A.; Shinsuke, I. *Fundamentals and Applications of*

Organic Eletrochemistry: Synthesis, Materials, Devices, First Edit.; John Wiley & Sons, Inc., 2015.

(26) Crean, C.; Geacintov, N. E.; Shafirovich, V. Methylation of 2′-Deoxyguanosine by a Free Radical Mechanism. *J. Phys. Chem. B* **2009**, *113* (38), 12773–12781.

(27) Thum, M. D.; Falvey, D. E. Photoreleasable Protecting Groups Triggered by Sequential Two-Photon Absorption of Visible Light: Release of Carboxylic Acids from a Linked Anthraquinone- N -Alkylpicolinium Ester Molecule. *J. Phys. Chem. A* **2018**, *122* (12), 3204–3210.

(28) Ly, D.; Kan, Y.; Armitage, B.; Schuster, G. B. Cleavage of DNA by Irradiation of Substituted Anthraquinones: Intercalation Promotes Electron Transfer and Efficent Reaction at GG Steps. *J. Am. Chem. Soc.* **1996**, *118* (36), 8747–8748.

(29) Breslin, D. T.; Schuster, G. B. Anthraquinone Photonucleases: Mechanisms for GG-Selective and Nonselective Cleavage of Double-Stranded DNA. *J. Am. Chem. Soc.* **1996**, *118* (10), 2311–2319.

(30) Görner, H. Photoreduction of 9,10-Anthraquinone Derivatives: Transient Spectroscopy and Effects of Alcohols and Amines on Reactivity in Solution¶. *Photochem. Photobiol.* **2003**, *77* (2), 171–179.

(31) Bardagi, J. I.; Ghosh, I.; Schmalzbauer, M.; Ghosh, T.; König, B. Anthraquinones as Photoredox Catalysts for the Reductive Activation of Aryl Halides. *European J. Org. Chem.* **2018**, *2018* (1), 34–40.

(32) Kuss-Petermann, M.; Wenger, O. S. Electron Transfer Rate Maxima at Large Donor-Acceptor Distances. *J. Am. Chem. Soc.* **2016**, *138* (4), 1349–1358.

(33) Kuss-Petermann, M.; Orazietti, M.; Neuburger, M.; Hamm, P.; Wenger, O. S. Intramolecular Light-Driven Accumulation of Reduction Equivalents by Proton-Coupled Electron Transfer. *J. Am. Chem. Soc.* **2017**, *139* (47), 5225–5232.

(34) Görner, H. Photoreactions of P-Quinones with Dimethyl Sulfide and Dimethyl Sulfoxide in Aqueous Acetonitrile. *Photochem. Photobiol.* **2005**, *82* (1), 71.

(35) Shanmugam, S.; Xu, J.; Boyer, C. Photoinduced Oxygen Reduction for Dark Polymerization. *Macromolecules* **2017**, *50* (5), 1832–1846.

(36) Romero, N. A.; Nicewicz, D. A. Organic Photoredox Catalysis. *Chem. Rev.* **2016**, *116* (17), 10075–10166.